HETEROCYCLES FOR LIFE-SCIENCES APPLICATIONS AND INFORMATION STORAGE

by

TEJ BAHADUR SHRESTHA

B. S., Tribhuvan University, Kathmandu, Nepal 1992
M. S., Tribhuvan University, Kathmandu, Nepal 1995

AN ABSTRACT OF A DISSERTATION

submitted in partial fulfillment of the requirements for the degree

DOCTOR OF PHILOSOPHY

Department of Chemistry
College of Arts and Sciences

KANSAS STATE UNIVERSITY
Manhattan, Kansas

2010

Abstract

The photochromic spirodihydroindolizine/betaine (DHI/B) system has been reinvestigated applying picosecond, microsecond, stationary absorption measurements, and NMR-kinetics. The first surprise was that the electronic structure of the betaines is quite different than commonly assumed. The photochemical ring-opening of DHIs to betaines is a conrotatory 1,5 electrocyclic reaction, as picosecond absorption spectroscopy confirms. The (disrotatory) thermal ring-closing occurs from the *cisoid* betaine. The lifetime of the *transoid* betaine is 60 s at 300 K, whereas the lifetime of the *cisoid* isomer is of the order of 250 microseconds. According to these results, the electrocyclic back reaction of the betaines to the DHI is NOT rate determining, as previously thought, but the *cisoid*-*transoid*-isomerization of the betaine.

Although the presence of a second nitrogen atom increases the photostability of the spirodihydroindolizine-pyridazine/betaine-system remarkably, the photochemical reaction mechanism appears to be exactly the same for spirodihydroindolizine-pyridazine/betaine-system.

A nondestructive photoswitch or an information recording systems has been explored using styryl-quinolyldihydroindolizines. Both isomers DHI and betaine are fluorescent. When the blue betaine is stabilized in a thin polymethyl methacrylate (PMMA) matrix, it is stable for several hours even in room temperature and very stable at 77K. Although irradiation of visible light λ = 532 nm allows the photo-induced reaction of the Betaine back to the DHI, a nondestructive read-out can be performed at λ = 645 nm upon excitation with λ = 580 nm. Image recording (write) and read-out, as well as information storage (at 77K) have been demonstrated.

A charged and maleimide-functionalized DHI/B system was synthesized for use as photochemical gates of the mycobacterial channel porin MspA. Positively charged and maleimide functionalized DHI groups that were attached to the DHI/B-system permit the binding of the photoswitch to selective positions in the channel proteins due to the presence of a cysteine moiety.

An inexpensive new method for the large scale synthesis of coelenterazine is developed. A modified Negishi coupling reaction is used to make pyrazine intermediates from

aminopyrazine as an economical starting material. This method permits the use of up to 1g coelenterazine per kg body weight and day, which turns the renilla transfected stem cells into powerful light sources.

HETEROCYCLES FOR LIFE-SCIENCES APPLICATIONS AND INFORMATION STORAGE

by

TEJ BAHADUR SHRESTHA

B. S., Tribhuvan University Kathmandu, Nepal 1992
M. S., Tribhuvan University Kathmandu, Nepal 1995

A DISSERTATION

submitted in partial fulfillment of the requirements for the degree

DOCTOR OF PHILOSOPHY

Department of Chemistry
College of Arts and Sciences

KANSAS STATE UNIVERSITY
Manhattan, Kansas

2010

Approved by:

Major Professor
Stefan H. Bossmann

Abstract

The photochromic spirodihydroindolizine/betaine (DHI/B) system has been reinvestigated applying picosecond, microsecond, stationary absorption measurements, and NMR-kinetics. The first surprise was that the electronic structure of the betaines is quite different than commonly assumed. The photochemical ring-opening of DHIs to betaines is a conrotatory 1,5 electrocyclic reaction, as picosecond absorption spectroscopy confirms. The (disrotatory) thermal ring-closing occurs from the *cisoid* betaine. The lifetime of the *transoid* betaine is 60 s at 300 K, whereas the lifetime of the *cisoid* isomer is of the order of 250 microseconds. According to these results, the electrocyclic back reaction of the betaines to the DHI is NOT rate determining, as previously thought, but the *cisoid*-*transoid*-isomerization of the betaine.

Although the presence of a second nitrogen atom increases the photostability of the spirodihydroindolizine-pyridazine/betaine-system remarkably, the photochemical reaction mechanism appears to be exactly the same for spirodihydroindolizine-pyridazine/betaine-system.

A nondestructive photoswitch or an information recording systems has been explored using styryl-quinolyldihydroindolizines. Both isomers DHI and betaine are fluorescent. When the blue betaine is stabilized in a thin polymethyl methacrylate (PMMA) matrix, it is stable for several hours even in room temperature and very stable at 77K. Although irradiation of visible light λ = 532 nm allows the photo-induced reaction of the Betaine back to the DHI, a nondestructive read-out can be performed at λ = 645 nm upon excitation with λ = 580 nm. Image recording (write) and read-out, as well as information storage (at 77K) have been demonstrated.

Charged and maleimide-functionalized DHI/B systems have beed synthesized for use as photochemical gates of the mycobacterial channel porin MspA. Positively charged and maleimide functionalized DHI groups that were attached to the DHI/B-system permit the binding of the photoswitch to selective positions in the channel proteins due to the presence of a cysteine moiety.

An inexpensive new method for the large scale synthesis of coelenterazine is developed. A modified Negishi coupling reaction is used to make pyrazine intermediates from

aminopyrazine as an economical starting material. This method permits the use of up to 1g coelenterazine per kg body weight and day, which turns the renilla transfected stem cells into powerful light sources.

Table of Contents

List of Figures

List of Tables

Acknowledgements

First and foremost, I would like to thank to my advisor professor Dr. Bossmann for his endless help and support. He always encourages me to be positive and look forward to things, which has developed my confidence and helped me become a better person. He always respects new ideas and allows me to follow those ideas, which eventually made me self-motivated and an independent researcher. His door is always open for me not only for academic discussions but also for talking about a career in chemistry and life beyond the university chemistry lab. My Ph.D thesis would not have been possible without his support.

I would like to greatly acknowledge Katharine Bossmann for her help. She has helped me a lot to improve my written and oral presentation. She always gives me feedback, input and suggestions how to present results and hypotheses in the scientific community.

I would like to thank all my Ph.D committee members: Dr. Hua, Dr. Aakeröy, Dr. Tomich and Dr. Chang for their time and input.

Thanks to members of Bossmann group, present and past. I had a good time working in the lab and attending conferences with you.

I would like to thank Dr. Higgins for letting us using his photophysical instruments and Dr Aakeröy and his group for the recording of the IR spectra. I would also like to thank Dr. Desper for collecting X-ray crystallographic data and resolving structures of my compounds. I would also like to extend my thanks to Alvaro Herrera and Dr. Leila Maurmann for keeping the NMR-facility running, Jim Hodgson for designing and making glassware, Tobe Eggers for fixing electrical and electronic problems and Richard Bachamp and Ron Jackson for their constructive work.

I would like to extend my sincere thanks to all collaborators: Dr. Deryl Troyer, KSU; Dr. Claudia, Turró Ohio State University, OH; Dr. Joseph V. Ortiz, Auburn University, Auburn, AL; Dr. Heinz Dürr, University of Saarland, Germany; Dr. Michael Niederweis University of Alabama at Birmingham, AL; and Dr. Megh Raj Pokhrel, Tribhuvan University, Nepal for their experimental help and useful discussions. I would also like to thank their post-docs and students for all photophysical measurements.

Finally, I would like to thank everyone who was involved and contributed to my life here at K-state and back home. Most importantly is the contribution of my family: their love, care and support throughout my life are greatly acknowledged.

Dedication

I dedicate this dissertation to my family: father, mother, wife, son and daughter.

Father and mother- Thank you so much for your inspiration and support to bring me to this level. Without your support it would not be possible. I will never be able to pay you back for everything you have done for me, but I have made both of you proud!

My wife Sunila is a strong lady who helped me in every way to make this dissertation possible. We have gone through ups and down in our lives, but she is very optimistic and always encourages me to look forward and open a new door to the future. Without her I would not be the scientist I am.

My son Saubhagya and my daughter Tejaswi are my future. Both of them are also part of this success. They helped me a lot during the writing of my dissertation by being quiet and behaving as model kids.

Finally, my Grandfather and Grandmother are not here with us, but their contribution in my early age is never forgotten.

Preface

This dissertation carried out at Kansas State University has led to the publication of the following research articles in scientific journals.

- Thomas Hartmann, Tej. B. Shrestha, Stefan H. Bossmann, Christian Hübner, Alois Renn and Heinz Dürr, A Light-Induced Photochromic Nanoswitch Capable of Non-Destructive Readout via Fluorescence Emission: Cluster *vs*. Single-Molecule Excitation of Dihydroindolizines. *Photochem. Photobiol. Sci.*, **2009**, *8*, 1172-1178.
- Tej B. Shrestha, Junia Melin, Yao Liu, Olga Dolgounitcheva, Viatcheslav G. Zakrzewski, Megh Raj Pokhrel, Eliso Gogritchiani, Joseph Vincent Ortiz, Claudia Turró and Stefan H. Bossmann, New insights in the photochromic *spiro*-dihydroindolizine/betaine-system *Photochem. Photobiol. Sci.*, **2008**, ***7***, 1449.

CHAPTER 1 - Photochromism of Spirodihydroindilizines and Application

1.1 Introduction

1.1.1 Photochromism

"Photochromism is a reversible transformation of a chemical species induced in one or both directions by the absorption of electromagnetic radiation, between two forms, **A** and **B**, having different absorption spectra (**Figure 1.1**)."[1] These compounds, **A** and **B**, are called photochromic compounds or photochromic switches.[1] Upon UV or visible (blue) light irradiation, the thermodynamically stable compound **A**, colorless or weakly colored, converts into the colored compound **B**, which reverts back into **A** thermally and/or photochemically (usually with visible light).[1] Photochromism can be achieved by very different approaches. To date, the following physical and chemical properties have been used for the generation of photochromic systems:[1] triplet-triplet absorption, tautomerization, *cis-trans* isomerization, dissociation, electron transfer/reduction and pericyclic reactions.

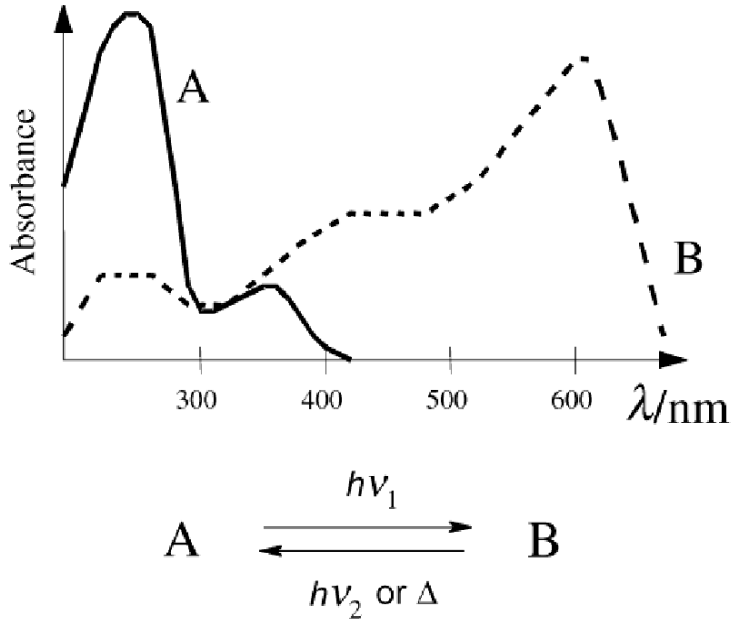

Figure 1.1 Photochromism between the constitutional isomers A and B.[1]

So far, there are two types of photochromic reactions, unimolecular and bimolecular which are summarized in **Table 1.1** and **Table 1.2**.[1-12] From the literature, it has been found that the unimolecular reaction is the most prevalent reaction.[1-12] This type of reaction is often called *positive* ***photochromism***.[1] The molecular basis of *positive* ***photochromism*** involves either ring closing/opening or *cis-trans/trans-cis* isomerization.[1-12] On the other hand, bimolecular photochromic reactions, often called *negative* ***photochromism***, involve photocycloadditions, electron transfer processes, hydrogen transfer reactions or more complex reactions (including decomposition).[1-12]

Table 1.1: Ring closing and ring opening of various photochromic compounds[2-7]

Diarylethenes[2]

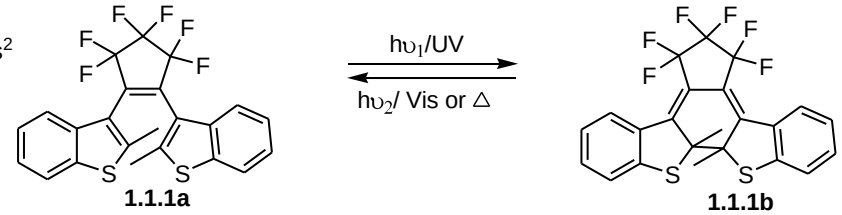

1.1.1a **1.1.1b**

Spiropyrans[3]

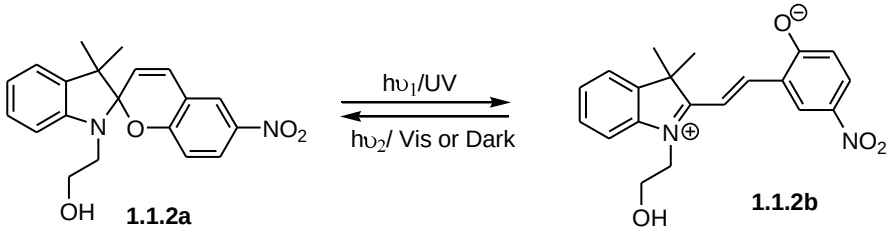

1.1.2a **1.1.2b**

Oxazines[4]

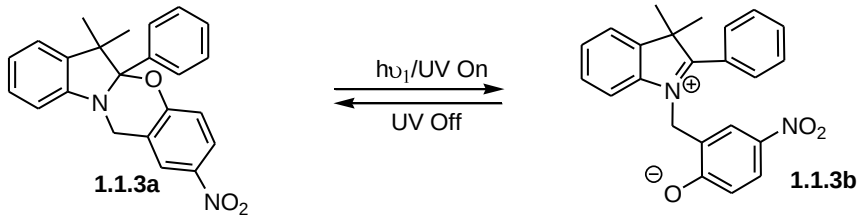

1.1.3a **1.1.3b**

Spirodihydroindolizines[5]

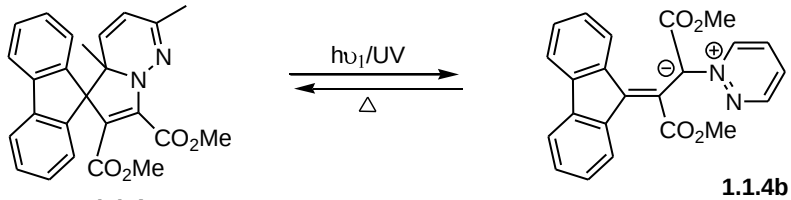

1.1.4a **1.1.4b**

Fulgides[6]

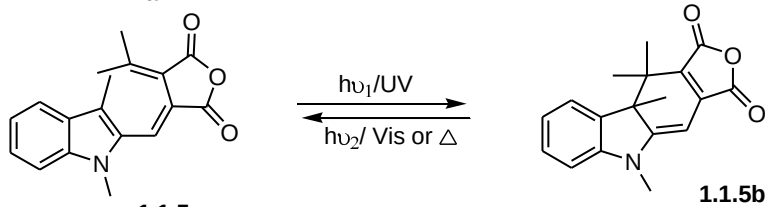

1.1.5a **1.1.5b**

Fulgimides[7]

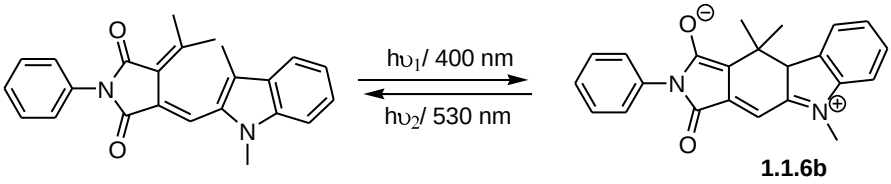

1.1.6a **1.1.6b**

Table 1.2: Ring closing and opening, *Cis/Trans* isomerization, chemical and hydrogen transfer photochromic compounds.[8-12]

Spironapthoxazines[8]

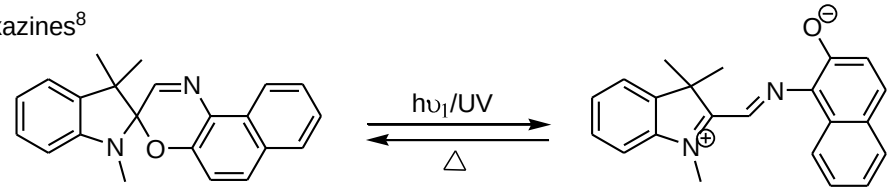

1.7a **1.7b**

Dimethyldihydropyrenes[9]

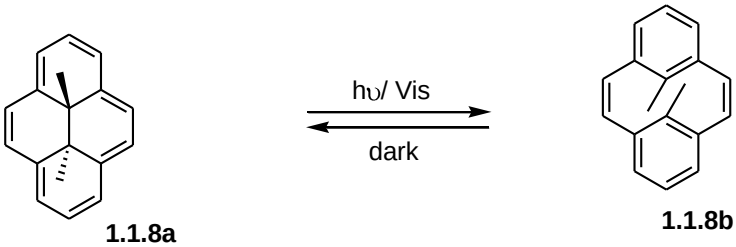

1.1.8a **1.1.8b**

Azo compounds[10]

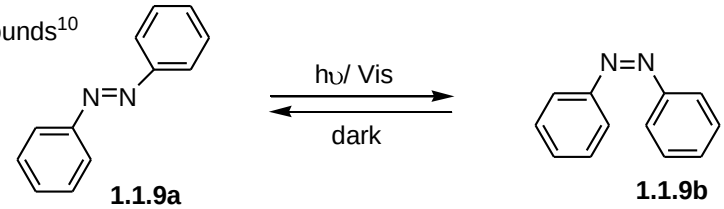

1.1.9a **1.1.9b**

Perimidinespirocyclohexadienones[11]

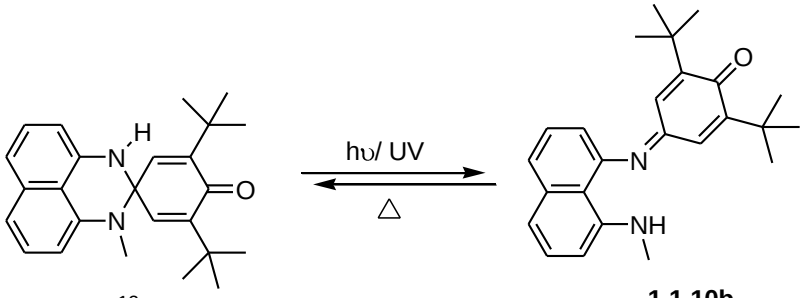

Heterocoerdianthrone[12]

1.1.10a **1.1.10b**

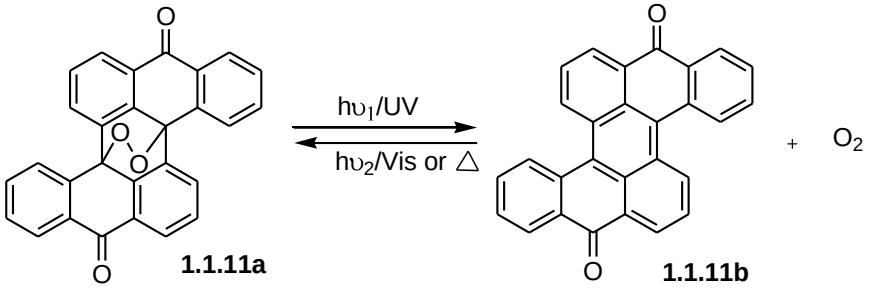

1.1.11a **1.1.11b**

1.1.2 Photochromic Spirodihydroindolizines/Betaine Systems

Following the pioneering work of Dürr and coworkers,[13] numerous photochromic spirodihydroindolizines (DHI)[14] and the related photochromic spirotetrahydroindolizines (THI)[15,16], dihydropyrazolopyridines[17] and 1H-benzo[c]pyrazolo[1,2-a]cinnolines[18] have been developed. Spirodihydroindolizines (DHI's) operate based on photoinduced electrocyclic reactions and are extremely versatile with respect to the observed lifetimes and UV/Vis-absorption spectra of their colored (betaine) forms. The working principles of photochromic DHI's are summarized in **Figure 1.2**:[19] The first step consists of the absorption of a UV-photon by a DHI, which reaches its electronically excited state. From the excited state, a pericyclic ring-opening reaction occurs, followed by a *cis-trans*-isomerization. Resulting from this sequence of reactions is the formation of a zwitterionic betaine, which shows a strongly bathochromic UV/Vis-absorption, compared to the DHI. From the ground state of the betaine, a pericyclic ring-closure to form the DHI is observed which obeys a typical Arrhenius-dependence on the reaction temperature.[1,20] The photochemical switching from the betaine to the DHI is possible as well.[1,20]

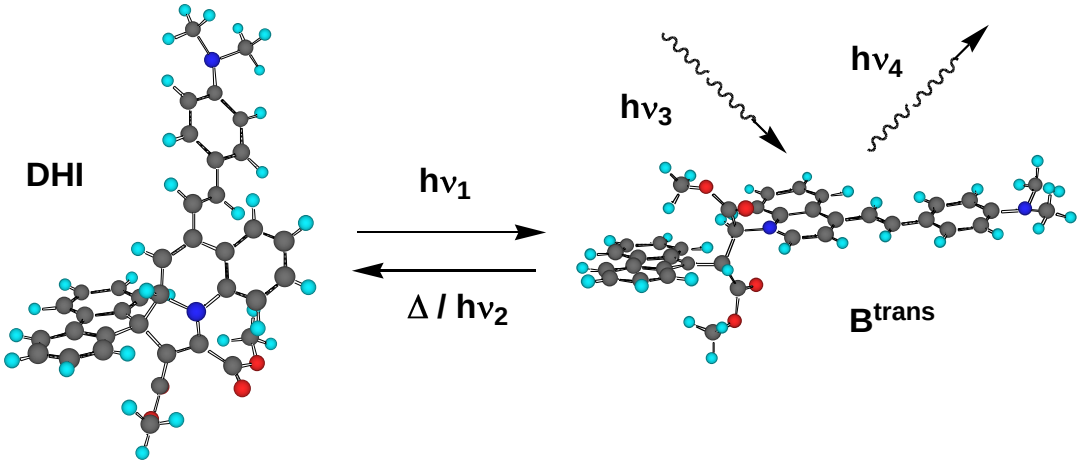

Figure 1.2 Light-induced ring-opening and photochemical or thermal closure of the photochromic *spiro*-dihydroindolizine/ betaine system. The Arrhenius parameters for the thermal ring closure are: $\Delta G^{\#}$ = 72 K J mol^{-1}, $\Delta H^{\#}$ = 33 KJ mol^{-1}, $\Delta S^{\#}$ = 131 J K^{-1} mol^{-1}. The betaine shows fluorescence at 630 nm when excited with 575 nm.[19] C: black, N: dark blue, H: light blue, O: red

The DHI molecule can be divided into five regions:[20,21,22] the *spiro*- or fluorine part (A), the heterocycle or (di)azine part (B), the part of the double bond (C), the steric hindrance (D, optional), and the linker (E, optional). The photochromic properties of the DHI/betaine-systems can be tailored according to the following rules, which are summarized in **Figure 1.3.**[20,21,22]

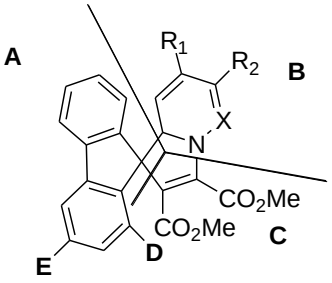

A: *spiro- or fluorene part*. Electron withdrawing substituents: $\tau_{1/2}$ increases; electronic donor groups: $\tau_{1/2}$ decreases.

B: *heterocycle or azine part*. Electron withdrawing substituents: stability against photodecomposition decreases.

C: *double bond part.* Methylester-groups: increased stability; cyano-groups (not shown): bathochromic shifts of the VIS-absorption of the betaine-forms, decreased stability against photodecomposition.

D: *steric hindrance*. $\tau_{1/2}$ decreases drastically

E: *linker to the protein structure.* Is of no profound consequence for

X=N: Greatly enhanced photochemical stability

In general, the *spiro*-DHI/betaine systems can be divided into five different categories, which permit very different applications of these photochromic substances:[1]

Very slow systems	$\tau_{1/2} > 1\ h$
Slow systems	$\tau_{1/2} > 1\ min$
Medium systems	$1\ s < \tau_{1/2} < 1\ min$
Fast systems	$1\ \mu s < \tau_{1/2} < 1\ s$
Ultra-fast systems	$\tau_{1/2} < 1\ \mu s$

Figure 1.3 Three characteristic regions of a *spiro*-DHI and influences of typical changes in the photo-physical properties of the *spiro*-DHI/betaine system.[1,20,21,22]

1.1.3 Electronic Structure of Dihydroindolizines/Betaines

Since their discovery in 1979,[13] the electronic structures of the photochromic *spiro*-dihydroindolizine forms and especially the corresponding betaines (Bs), formed by reverse electrocyclization from photoexcited (^{1}S)-states, have been under discussion. Betaines undergo thermal back reaction to their corresponding *spiro*-DHI-isomers via 1,5-electro-cyclization **(Scheme 1.1).**[13,20] Only if the electronic and also the geometric structures of the DHIs and especially the betaines can be predicted accurately, could possible applications be designed and optimized beforehand. Without that particular knowledge, it is virtually

impossible to design optical switches and/or molecular machines. One example of a potential use is the disruption of cell membranes, but because it is not precisely known what change of shape and charge distribution can be expected upon the photoexcitation of a DHI, the design of an optimal DHI/Betaine system still depends on optimization experimentals rather than prediction via calculation.

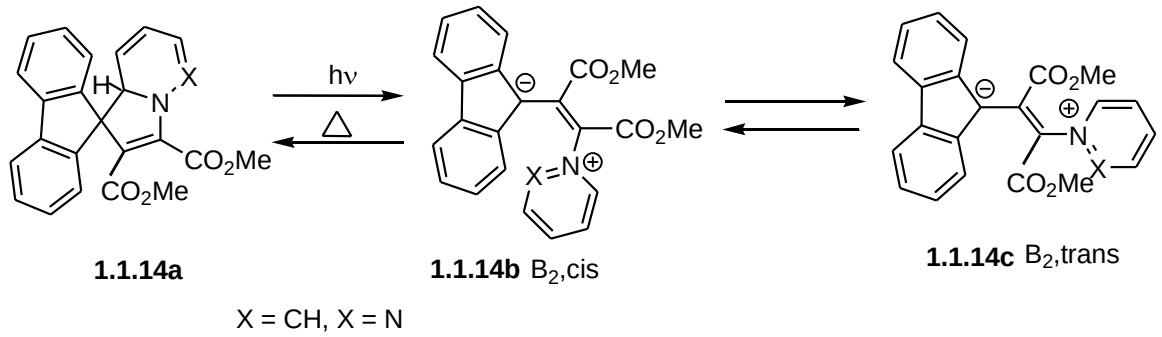

Scheme 1. 1: Reaction scheme for *spiro*[9,1'(8'aH)-indolizine]-2',3'-dicarboxylic acid, dimethyl ester (X= CH) the "classic" betaine-structures, which were postulated in numerous mechanistic discussions, are $B_{2,cis}$ and $B_{2,trans}$.

1.1.4 Potential Applications of the DHI/Betaine System

Although DHIs are known since 1979, applications other than for photochromic glasses have only slowly been developed, because the required hardware/technical instrumentation has become available only in this millenium. Photochromic dihydroindolizines and related photochromic switches have been successfully used in prototypes of the photosynthetic process[23]; as a photo-logical device[24], in high-density data storage polymer films[25], as molecular machines[26], and in prototypes for advanced nucleic acid sequencing.[27] The application in high-density data storage films is especially intriguing, because the material is very inexpensive and very high storage densities, comparable to the most modern conventional data storage devices, are attainable. All that is required is a PMMA-film containing a DHI, which can form a thermally stable betaine that is highly fluorescent and a suitable optical write/read device.

Beside the photophysical parameters: absorption wavelengths of the opened and closed forms, half-life ($\tau_{1/2}$) of the colored betaine forms, cyclization kinetics and reaction

quantum yields of the pericyclic ring-opening reaction, the stability of especially the betaines against photodecomposition is also of great importance with respect to their applications. Longer lifetime in the minute-range are required for the photo-switching of the biochemical activity of channel porins, such as the very stable porin MspA from *Mycobacterium smegmatis*, whereas the betaines designed for electron-transfer between electrode and nanoparticle should live only microseconds in order to perform quickly. The presence of a sterically hindering group (e.g. a methyl group) in the D-position of the DHI is known to cause a drastic shortening of the lifetime of the corresponding betaine.[28] In contrast, linking the DHI to the aspartates in the constriction zone of MspA via amide bonds in position E only changes the photophysical properties of the DHI/betaine marginally (**Figure 1.3**).

1.1.5 Main Goals

The wealth of photochromic compounds that have been synthesized has permitted the development of empirical rules relating the observed absorption and emission properties of both, the photochromic compounds and the corresponding isomeric betaines, to their structural features. However, without a detailed molecular understanding of the functional principles of the photochromic DHI/betaine reaction and its thermal back reaction (**Scheme 1.1**), the ability to design new systems with tailored optical and structural properties remained severely limited. My main goals of this first chapter are: 1. Assigning of the electronic structures of DHI/Betaine systems using both experimental and theoretical calculation methods, 2. Exploring the potential application of the DHI/Betaine system in information storage device and photogating of the channel porin MspA to modulate the flow of cations in biological systems.

1.1.6 References

1. Bouas-Laurent, H.; Duerr, H.; Organic Photochromism *Pure and Appl. Chem.* **2001**, *73*, 639–665.
2. Knag, J.; Kim, J.; Kim, E. *Appl. Phys. Lett.* **2002**, *80*, 1710-1712.
3. Raymo, F. M.; Giordani, S. *Org. Lett*. **2001**, *12*, 1834-1836.

4. Tomasulo, M.; Sortino, S.; Raymo, F. M. Org. Lett. **2005**, *7*, 1109-1112.
5. (a) Weber, C.; Rustemeyer, E.; Duerr, H. *Adv. Mater*. **1998**, *10*, 1348-1351. (b) Duerr, H.; Schommer, C.; Muenzmay, T. *Angewandte Chemie* **1986**, *98*, 565-7.
6. Grishin, Y.; Chunaev, Y. M.; Przhiyalgovskaya, N. M.; Metelitsa, A. V. *Chemistry of Heterocyclic Compounds* **1992**, *Is 3*, 422-423.
7. Dvornikov, A. S.; Liang, Y.; Curse, C. S.; Rentzepis, P. M. *J. Phys. Chem. B* **2004**, *108*, 8652-8658.
8. Crano, J. C.; Flood, T.; Knowles, D.; Kumar, A.; Gement,B. V. *Pure and Appl. Chem*. **1996,** *68,* 1395-1398.
9. Blattmann, H. R.; Meuche, D.; Heilbronner, E.; Molyneux, R. J.; Boekelheide, V. *J. Am. Chem. Soc.* **1965**, *87*, 130-131.
10. Hegedus, L. S.; Lundmark, B. R. *J. Am. Chem. Soc*. **1989,** *111*, 9194-9198.
11. Minkin, V. I.; Komissarov, V. N. *Mol. Cryst. Liq. Cryst*. **1997**, *297*, 205-212.
12. Brauer, H. D.; Schmidt, R. *Photochemistry and Photobiology* **1983**, *37*, 587-591.
13. Hauck, G.; Duerr, H. *Angewandte Chemie*, **1979**, *91*, 1010–11.
14. Duerr, H. *Angewandte Chemie* **1989**, *101*, 427–45.
15. Duerr, H.; Gross, H.; Zils, K. D.; Hauck, G.; Klauck G.; Hermann, H. *Chemische Berichte* **1983**,*116*, 3915–25;
16. Ahmed, S. A.; Abdel-Wahab, A.-M. A.; Durr, H. *J. Photochem. Photobiol. A: Chem.* **2003**, *154*, 131–144.
17. Duerr, H.; Schommer, C.; Muenzmay, T. *Angewandte Chemie* **1986**, *98*, 565–7.
18. Duerr, H.; Thome, A.; Steiner, U.; Ulrich, T.; Kruger, C.; Raabe, E. *J. Chem. Soc. Chem. Commun.* **1988**, 338–40.
19. Gross, H.; Duerr, H. Photochromic System. Part 4. *Angewandte Chemie.***1982**, *94*, 204-5
20. Duerr, H. *Pure Appl.d Chem.* **1990**, *62*, 1477-1482.
21. Duerr, H. *Organic Photochromic and Thermochromic Compounds* **1999**, 223-266.
22. Duerr, H. 4n+2 Systems Based on 1,5-Electrocyclization. *Photochromism: molecules and systems* **2003**, 210-269.
23. Straight, S. D.; Andreasson, J.; Kodis, G.; Moore, A. L.; Moore, T. A.; Gust, D. *J. Am. Chem. Soc.* **2005**, *127*, 2717-2724.

24. Straight, S. D.; Andreasson, J.; Kodis, G.; Bandyopadhyay, S.; Mitchell, R. H.; Moore, T. A.; Moore, A. L.; Gust, D. *J. Am. Chem. Soc.* **2005**, *127*, 9403-9409.
25. Weitzel, T.; Wild, U.; Amlung, M.; Duerr, H.; Irie, M. *Molecular Crystals and Liquid Crystals Science and Technology, Section A: Molecular Crystals and Liquid Crystals* **2000**, *344*, 191-198.
26. (a) Masson, J.-F.; Hartmann, T.; Duerr, H.; Booksh, S. K. *Optical Materials (Amsterdam, Netherlands)*, **2005**, *27*, 435-439. (b) Weber, C.; Rustemeyer, F.; Duerr, H. *Advanced Materials* **1998**, *10*, 1348-1351.
27. Gogritchiani, E.; Hartmann, T.; Palm, B. S.; Samsoniya, S.; Durr, H. *J. Photochem. Photobiol. B: Biol* **2002**, *67*, 18-22.
28. Fromm, R. Synthese, *Ph. D. thesis*, University of Saarland: Saarbruecken, Germany, **1996**.

1.2 Photochromic *Spiro*-dihydroindolizine/betaine-system of Pyridine

The majority of this chapter is taken from the publisher with permission: Shrestha, T. B.; Melin, J.; Liu, Y.; Dolgounitcheva, O.; Zakrzewski, V. G.; Pokhrel, M. R.; Gogritchiani, E.; Ortiz, J. V.; Turró, C.; Bossmann, S. H. New insights in the photochromic *spiro*-dihydroindolizine/betaine-system. *Photochem. Photobiol. Sci.* **2008**, 7, 1449-1456.

1.2.1 Introduction

Counter to most other photochromic systems, such as spiropyrans, spirooxazines, chromenes, fulgides and diarylethenes[1], no uncharged resonance structure of the betaine-isomers is possible. Virtually all studies have assigned the negative charge to the bridging carbon of the fluorenyl-system ($B_{2,cis}$ and $B_{2,trans}$, **Scheme 1.2**).[1-3] This assignment was originally inspired by the very broad absorption band in the visible region of the betaine spectrum, which seemed to arise from a high degree of delocalization and/or intramolecular charge transfer.[2,3] Since the positions of the charges determine the location of the single and double bonds of the betaines, they also determine their molecular structure (and therefore geometric shape), as well as their absorption and emission of light and also their redox properties. The occurrence of *cisoid vs. transoid* betaine isomers is also of great interest, because without this exact knowledge the DHI $\rightarrow$ betaine $\rightarrow$ DHI cycle cannot be properly understood.

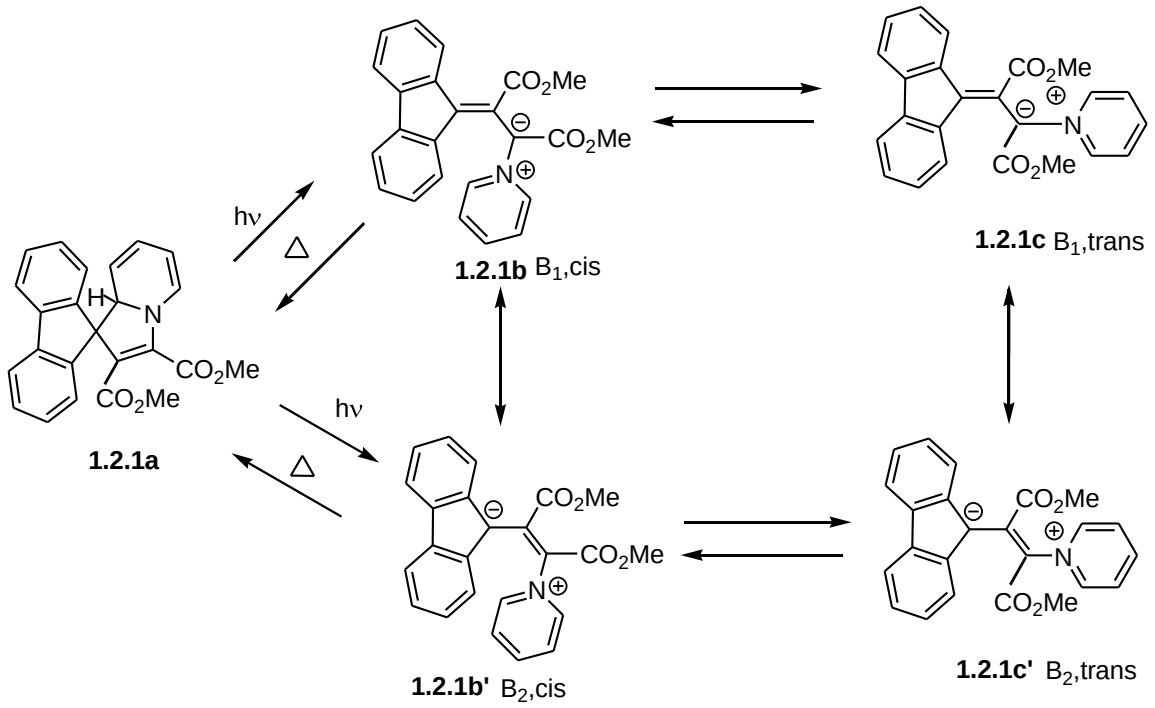

Scheme 1. 2: Reaction scheme for *spiro*[9,1'(8'aH)-indolizine]-2',3'-dicarboxylic acid, dimethyl ester. The "classic" betaine-structures, which were postulated in numerous mechanistic discussions, are $B_{2,cis}$ and $B_{2,trans}$.

Before this study, the thermal back reaction, which is a disrotatory 1,5-electrocyclization, was regarded as the rate-limiting step. However, we will present evidence for the *trans/cis* isomerization k_{-2} to be rate-determining in this chapter **(Scheme 1.3)**: Empirically it was assigned that k_{-1} is bigger than k_{-2}: k_{-2} would be then the rate determining step.[3]

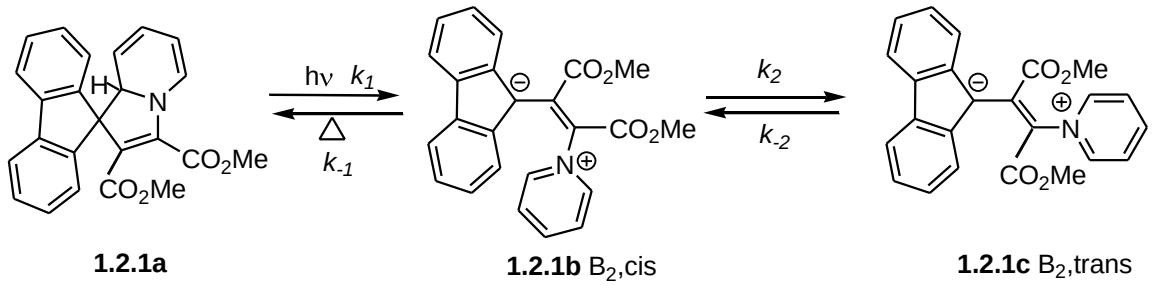

Scheme 1. 3: Thermal back reaction (1,5-electrocyclization reaction of *spiro*[9,1'(8'aH)-indolizine]-2',3'-dicarboxylic acid, dimethyl ester.

It must be noted that molecular shape, dielectric and redox properties are also dependant on the population of the *cisoid vs*. *transoid* betaine isomers. This is of importance when spiro-dihydroindolizines/betaines are used as moleculat switches or molecular machines.

1.2.2 Experimental

1.2.2.1 Chemical and Instruments

All chemicals were obtained from Acros Organics, unless noted otherwise. 400 MHz and 200 MHz Varian NMR-spectrometer and a Nicolet Protégé 460 FT-IR spectrometer were used in this study. I would like to thank the Analytical Laboratory of Dr. Ruth Welti at KSU for recording the mass spectra of compounds employing an Applied Biosystems API-4000 triple quadrupole mass spectrometer with electrospray and APCI sources.

1.2.2.2 Calculations

I would like to thank Prof. Dr. Joshep V. Ortiz, Dr. Junia Melin, Dr. Olga Dolgounitcheva and Dr. Viatcheslav G. Zakrzewski, Auburn University, Alabama, for performing the density function calculations on these compounds.

All calculations were performed with the Gaussian03 suite of programs.[4] B3LYP hybrid functional was used for geometry optimization [4,5] which is a standard DFT method for studying organic molecules. [6-9] The B3LYP functional was chosen in combination with the 6-31G(d) basis set, since it is a good compromise between accuracy and computational cost for the this type of systems.[10,11] B3LYP/6-31G(d) optimizations[5,12] and harmonic frequency analysis revealed minima for *cis*- and *trans*-betaine and *spiro*- configurations. MP2/6-31G(d) optimizations were performed as well. Subsequent single-point calculations with the 6-311G(d,p) basis set were done at the geometries obtained.

1.2.2.3 Kinetic ^{1}H NMR Experiments and Identification of the trans-Betaine

Stock solutions of pyridine (**1.2.7**) and *spiro*[2-cyclopropene-1,9'-[9H]fluorene]-2,3-dicarboxylic acid, 2,3-dimethyl ester (**1.2.6**) in $CDCl_3$ (1 mmol each) were prepared and stored in a water bath at 283 K, 293 K, 303 K or 313 K. 2.0 mL of each stock solution were mixed using an Eppendorf pipette and then filled in a pyrex NMR tube. ^{1}H-NMR

measurements were performed using a 400 MHz Varian-NMR-spectrometer. The precision of its temperature units was ±0.5 K. Integration of the characteristic methylester peaks of the spirocyclopropene (**1.2.6**) as a function of reaction time permitted the determination of the kinetics and the Eyring-activation parameters.

1.2.2.4 Steady-State Absorption and Photolysis

Acetonitrile was used as solvent. The irradiation wavelength is 355 nm. The laser intensity was tuned from 1 mW to 150 mW by combination of neutral density filter and laser output. The absorption spectra of the DHI/Betaine mixture (**1.2.1/1.2.9**)) at different irradiation times were recorded using a HP 8543A UV-Vis spectrometer. During the photolysis, the solution was constantly stirred.

1.2.2.5 Laser Flash Photolysis

Transient absorption spectra and lifetimes were measured on a home-built instrument pumped by a frequency tripled (355 nm) Spectra-Physics GCR-150 Nd: YAG laser (fwhm 8 ns, 5 mJ per pulse unless indicated otherwise). The output from a 150W Xe arc lamp (USHIO) powered by a PTI PS-220 power supply, pulsed with electronics built in-house, was focused onto the sample at 90° with respect to the laser beam. The white light transmitted by the sample was collimated and focused onto the entrance slit of a Spex HR-20 single monochromator (1200 gr/mm) and was detected utilizing a Hamamatsu R928 photomultiplier tube and processed by a Tektronics 400 MHz oscilloscope (TDS 380).[13,14]

1.2.2.6 Synthesis of Spiro[9H-fluorene-9,1'(8'aH)-indolizine]-2',3'-dicarboxylic acid, dimethyl ester (1.2.1a) The synthesis had been previously reported in:
Shrestha, T. B.; Melin, J.; Liu, Y.; Dolgounitcheva, O.; Zakrzewski, V. G.; Pokhrel, M. R.; Gogritchiani, E.; Ortiz, J.V.; Turro, C.; Bossmann, S. H. New insights in the photochromic *spiro*-dihydroindolizine/betaine-system. *Photochem. Photobiol. Sci.* **2008,** *7*, 1449-1456.

Fluorenone-9-hydrazone (1.2.2)

Synthetic procedure: Hydrazine hydrate (6.024g, 0.12 mol of H_4N_2) was added drop-wise to a suspension of 9-fluorenone (20.0 g, 0.11 mol) in ethanol (200 mL) at room temperature (RT). An exothermic reaction was observed, which subsided after 15 min. The reaction mixture

was heated under reflux overnight and then allowed to cool down to RT. After 12 h, the precipitate (yellow needles) was separated by filtration and recrystallized from anhydrous ethanol. Yield: 15.5 g, 72.2%. The purity of compound (**1.2.2**) was confirmed by using TLC (silica, mobile phase: *n*-hexane/ethyl acetate 4/1, v/v, R_f = 0.14). Melting point 152 ºC (reference 15: 152-153 °C)[15] IR ν_{max} (KBr pellets) cm^{-1} 710, 773, 1198, 1449, 1577, 1600, 3060, 3201,3313, 3385; ^{1}H NMR ($CDCl_3$, 200 MHz), δ [ppm] 6.3 (s, 2H, -NH_2), 7.2-7.4 (m, 4H), 7.5-7.6 (dd, *J* = 5.5 Hz, *J* = 2.2 Hz,1H,), 7.6-7.7(2H m), 7.9(d, *J* = 7 Hz,1H); ^{13}C NMR ($CDCl_3$, 200 MHz) δ [ppm] 119.7, 120.6, 120.9, 125.6, 127.8, 128.1, 128.6, 129.8, 130.2, 138, 138.6 141.7 145.9

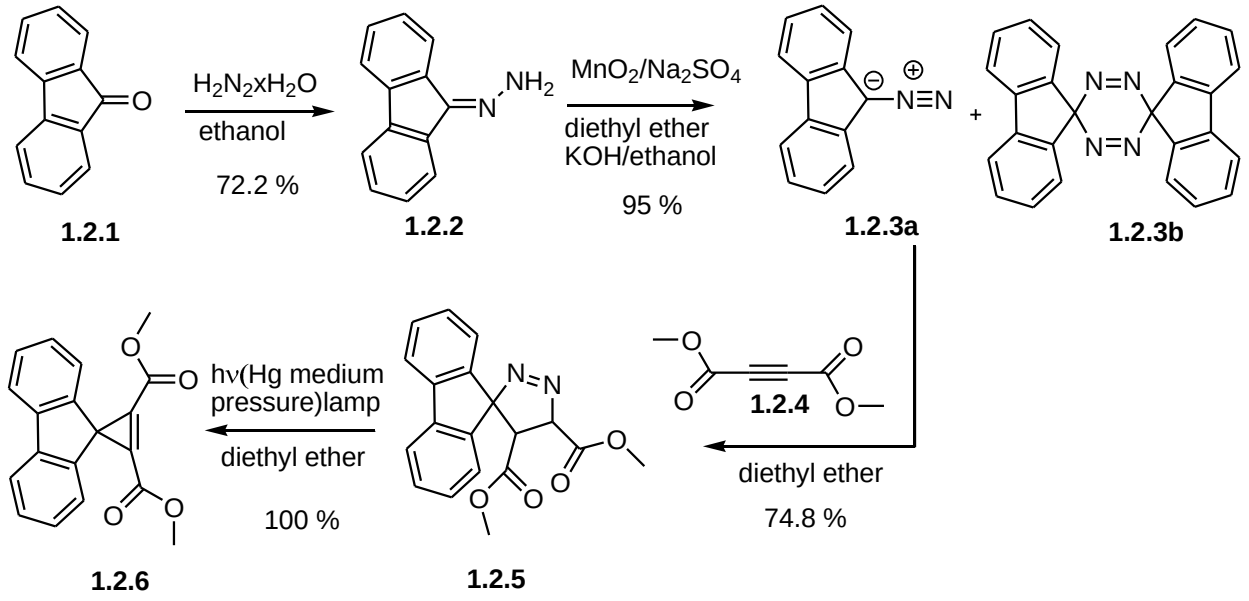

Scheme 1. 4: Reaction sequence from 9-fluorenone (1.2.1) to *spiro*[2-cyclo-propene-1,9'-[9H]fluorene]-2,3-dicarboxylic acid, 2,3-dimethyl ester (1.2.6)

9-Diazofluorenone (1.2.3a)

Synthetic procedure: A suspension of **1.2.2** (8.57g, 0.044 mol) in anhydrous diethyl ether (100 mL) was cooled to 0 ºC using an ice bath. Then, a thorough mixture of manganese dioxide (MnO_2, 10.2g, 0.117 mol, Aldrich) and anhydrous sodium sulfate (2.91g, 0.0205 mol, Fisher Scientific) was added in small amounts. The reaction mixture was allowed to warm up to RT during 30 min. Then, a mixture of 1.0 mL of saturated KOH in water and 25 mL of anhydrous

ethanol was added at once and the reaction mixture stirred vigorously. (Note that it is important to wait until the KOH/H_2O mixture has cooled down to RT after mixing to avoid over-concentrating the KOH. The mixture was stirred at RT for 15 h and filtered. The solid phase was washed twice with 25 mL of anhydrous diethyl ether and then discarded. The combined liquid phases were concentrated to 60 mL and kept at 4 °C overnight. The precipitate (red needles) of 9- diazofluorenone was filtered off, washed twice with diethyl ether (4 ºC) and then dried in high vacuum at RT. Yield: 8.11g, 95.0%. Melting point 90 ºC (dec.) (reference 16: 94-95 ºC)[16] IR ν_{max} (KBr pellets) cm^{-1} 712, 743, 1229, 1326, 1372, 1439, 1600, 2069, 3032; ^{1}H NMR ($CDCl_3$ 400 MHz) δ [ppm] 7.28- 7.38 (td, *J* = 7.3 and 1.5 Hz, 2H), 7.37 (td, *J* = 7.7 and 1.5 Hz, 2H), 7.5 (dt, *J* = 7.7 and 0.7 Hz, 2H), 7.9 (dt, *J* =7.7 and 0.7 Hz, 2H); ^{13}C NMR ($CDCl_3$, 400 MHz) δ [ppm] 119.5, 121.1, 124.7, 126.5, 131.7, 133.2.

1,2,4,5-tetrazine, 3,6-dihydro-3,6-di-(*spiro*-1,9'-[9H]fluorene] (1.2.3b)

Seperation: The filtrate after separation of ***1.2.3a*** contained a yellow compound **(1.2.3b)** (45 mg, 0.5%), which was separated by descending column chromatography (SiO_2/ethyl acetate). Both, ^{1}H- and ^{13}C-NMR were very similar to compound **(1.2.3a)**. Electrospray-MS indicated that this is the dimer of 9-diazofluorenone. Melting point 89 ºC (dec.) IR ν_{max} (KBr pellets) cm^{-1} 717, 748, 1425, 1650, 2059, 2331, 2356, 2842, 2924, 3042; ^{1}H NMR ($CDCl_3$, 400 MHz) δ [ppm] 7.30 (td, *J* = 7.7 and 1.4 Hz, 2H), 7.37 (td, *J* = 7.7 and 1.4 Hz, 2H), 7.50 (dd, *J* = 7.7 and 1 Hz, 2H), 7.93 (dt, *J* =7.4 and 0.7 Hz, 2H); ^{13}C NMR ($CDCl_3$, 200 MHz) δ [ppm] 119.5 121.1 124.7, 126.5, 131.6, 133.1, 152.5 MS: $C_{26}H_{16}N_4$, m/z 387 (M)

***Spiro*[9H-fluorene-9,3'-[3H]pyrazole]-4',5'-dicarboxylic acid, dimethyl ester (1.2.5)**

Synthetic procedure: A solution of **(1.2.3a)** (5.07g, 0.026 mol) in 75 mL of anhydrous diethyl ether was cooled to 0 ºC using an ice bath. Then a solution of 2-butynedioic acid dimethyl ester in 30 mL of anhydrous diethyl ether was added drop-wise to the continuously stirred solution. After all 2-butynedioic acid dimethyl ester was added, the ice bath was removed and the reaction mixture was allowed to stir for 24 h. The yellow reaction mixture was concentrated to half of its original volume and kept at 4 ºC overnight. Yellow crystals were obtained, separated from the mother liquor by filtration, and recrystallized from diethyl ether/ethanol (1:1 v/v). Yield: 6.59 g, 74.8% Melting point (dec.): 107-108 ºC (reference 17: 114-117 °C)[17] IR ν_{max} (KBr pellets) cm^{-1} 748, 1147, 1250, 1316, 1434,1639, 1741, 2945, 2990,

3062; ^{1}H NMR δ [ppm] ($CDCl_3$, 400 MHz) δ 3.5 (s, -CO_2Me, 3H), 4.09 (s, -CO_2Me, 3H), 6.83 (dt, *J* = 7.1and 0.8 Hz, 2H), 7.27 (td, *J* = 7.5 and 1.1 Hz, 2H), 7.49 (td, *J* = 7.5and 1.1 Hz, 2H), 7.8 (d, *J* = 7.3 Hz, 2H); ^{13}C NMR ($CDCl_3$, 400 MHz) δ [ppm] 53.2, 53.4, 66, 121.4, 124.06, 128.5, 130.7, 132.8, 143.8, 149, 160.5, 162, MS $C_{19}H_{14}N_2O_4$ m/z 335.2 and 357.1 (M+1 and M+Na)

***Spiro*[2-cyclopropene-1,9'-[9H]fluorene]-2,3-dicarboxylic acid, 2,3-dimethyl ester (1.2.5)**

Synthetic procedure: In a photochemical bench reactor, compound **(1.2.5)** (3.9g, 0.012 mol) in 350 mL of anhydrous diethyl ether was purged with N_2 for 30min and then irradiated employing a mercury medium pressure lamp (Hanovia 150W (608A0360)). N_2 was released vigorously at the beginning of the irradiation. The formation of bubbles stopped after 2.5h. A TLC check (SiO_2, hexane/ethyl acetate, 3/1, v/v) confirmed that compound**(1.2.5)** had indeed completely reacted. The yellow solution was then concentrated to one third of its original volume and kept overnight at 4ºC. Yellow needles of pure compound **(1.2.6)** were obtained. Yield: 3.57g, 100% Melting point: 147-149 ºC (dec.) (reference 18: 149 ºC)[18] IR ν_{max} (KBr pellets) cm^{-1} 737, 1050, 1250, 1429, 1721, 1854, 2950, 3073; ^{1}H NMR ($CDCl_3$, 400 MHz) δ [ppm] 3.83 (s, 6H, 2-CO_2Me), 7.26 (d, *J* = 7 Hz, 2H), 7.34 (td, *J* = 7.3 and 0.7 Hz, 2H), 7.4 (td, *J* = 7.4 and 1.1Hz, 2H), 7.8 (d, *J* = 7.3 Hz, 2H); ^{13}C NMR ($CDCl_3$, 400 MHz) δ [ppm] 53.3, 120.3, 121.07, 121,6, 127.3, 128.1, 141.7, 144.5,158.3; MS $C_{19}H_{14}O_4$, 307.1 and 329.2(M+1 and M+ Na)

***Spiro*[9H-fluorene-9,1'(8'aH)-indolizine]-2',3'-dicarboxylic acid, dimethyl ester (1.2.1a)**

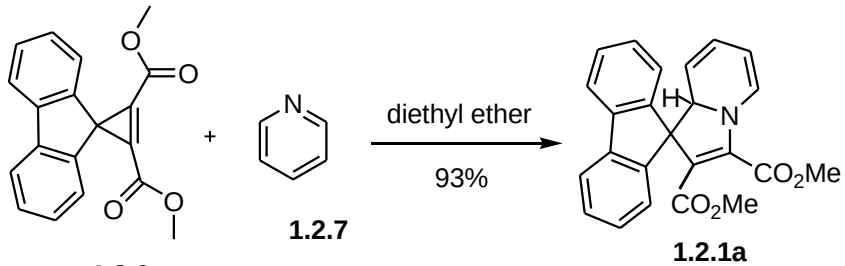

Scheme 1. 5: Synthesis of *Spiro*[9H-fluorene-9,1'(8'aH)-indolizine]-2',3'-dicarboxylic acid, dimethyl ester (1.2.1a)

Synthetic procedure: The spirene **(1.2.6)**, (0.50 g, 1.6 mmol) was dissolved in 50 mL of anhydrous diethyl ether (dried over CaH_2 and distilled prior to use) at RT. A solution of pyridine

(dried over KOH and distilled prior to use) (0.1266 g, 1.6 mmol) in 5.0 mL of anhydrous diethyl ether was added drop-wise under vigorous stirring. The color of the mixture changed from light yellow to deep blue-green upon addition of pyridine indicating the formation of the betaine. The reaction mixture was continuously stirred in the dark at RT for 20h. TLC-control was used to check for the presence of non-reacted spirene (silica, n-hexane/ethyl acetate, 4/1, v/v). In the case that unreacted spirene was found, pyridine in diethyl ether (see above) was added (rate: 1 drop/h) and the reaction mixture was repeatedly checked by TLC until no more spirene was present. The volume of the reaction was decreased to 25 percent using a rotavap and the kept at 4 ºC overnight. Yellow crystals, which turn to green under irradiation and back to yellow in the dark, were obtained. Traces of pyridine were removed in high vacuum. Yield: 574 mg, 93%. The observed losses are caused by the crystallization procedure. Melting point: 133-134 ºC (reference 19: 132-133 ºC)[19] IR ν_{max} (KBr pellets) cm^{-1} 743, 1122, 1224, 1255, 1444, 1552, 1588, 1675, 1746, 2786, 2945, 3032; ^{1}H NMR ($CDCl_3$, 400 MHz) δ [ppm] 3.25 (s,3H), 3.98 (s, 3H), 4.4 (d, *J* = 9.8 Hz, 1H), 5.1 (t, *J* = 6.6 Hz, 1H), 5.4 (s, 1H), 5.64 – 5.69 (m, 1H), 6.4 (d, *J* = 7.4, 1H), 7.2 (td, *J* = 7.4 and 1 Hz, 1H), 7.28 – 7.39 (m, 3H), 7.4 (d, *J* = 7.4 Hz, 1H), 7.5 (1H d, *J* = 7.6 Hz), 7.7 (2H dd, *J* = 7.4 and 0.8 Hz); ^{13}C NMR ($CDCl_3$, 400 MHz) δ [ppm] 51.1, 53.4, 68.8, 69.9, 104.8, 117.7, 119.8, 120.1, 123.4, 123.6, 124.6, 124.8, 127.2, 127.7, 128.2, 128.4, 141.8, 142.5, 160.5, 164.1 MS $C_{24}H_{19}NO_4$ m/z 384.3, 385.3, 386.2 (M-1, M+, M+1)

1.2.3 Results and Discussion

1.2.3.1 "Greener" synthesis of spiro[2-cyclopropene-1,9'-[9H] fluorene]-2,3-dicarboxylic acid, 2,3-dimethyl ester (1.2.6) reported synthesis was modified

The goal was to synthesize the purest photochromic compounds possible to obtain clear mechanistic results. This included avoiding any mercury contamination of the compounds. The first step was the classic synthesis of fluorenone-9-monohydrazone.[20] The hydrazone **(1.2.2)** was then oxidized by using manganese dioxide (MnO_2) [21], as shown in **Scheme 1.4**. This procedure, which avoids the use of the environmentally incorrect mercury oxide (HgO), yielded 95% of 9-diazofluorenone **(1.2.3a)**. It is noteworthy that the dimerization by-product of 9-diazofluorenone was isolated **(1.2.3b)** in very small yields

(<1 %) by descending column chromatography. This is the first study in which it has been isolated. However, the formation of this product may result from the changes in the oxidation procedure. The formation of this by-product increased remarkably (to approx. 5-10%) if excess water was present during oxidation. The classic 1,3-dipolar cycloaddition reaction was used to convert 9-diazafluorenone to *spiro*[9H-fluorene-9,3'-[3H]pyrazole]-4',5'-dicarboxylic acid dimethyl ester **(1.2.5).** Photolysis of **(1.2.5)** in a bench-reactor (medium pressure Hg-lamp, emission lines: λ = 254 nm and 313 nm) led to **(1.2.6)** in quantitative yield.

1.2.3.2 Kinetics of the spirodihydroindolizine (DHI) formation.

^{1}H-NMR spectroscopy was used to study the kinetics of the electrocyclic addition of pyridine **(1.2.7)** to *spiro*[2-cyclopropene-1,9'-[9H]fluorene]-2,3-dicarboxylic acid, 2,3-dimethyl ester **(1.2.6)** in $CDCl_3$. The integration of the typical methylester peak of **(1.2.6)** and of pyridine **(1.2.7)** permitted the observation of the reactants' concentrations as a function of time. The data on the consumption of **(2.6)** was used to determine the reaction order of the addition reaction. Surprisingly, the result was a first order reaction in the temperature range from 283 to 313 K, although the addition reaction requires two reactants (*spiro*[2-cyclopropene-1,9'-[9H]fluorene]-2,3-dicarboxylic acid, 2,3-dimethyl ester and pyridine), which were added in the same concentration! ^{1}H- and ^{13}C-NMR, as well as MS, have confirmed that the DHI is formed by the addition of one molecule pyridine to one molecule of **(1.2.6)** . In **Scheme 1.6**, the mechanistic paradigm developed by Dürr and coworkers is shown.[2] The observed kinetics indicates that k_1 must be faster than k_2 = 2.23 x 10^{-3} s^{-1} (at 293 K) , thus making the latter rate-determining.

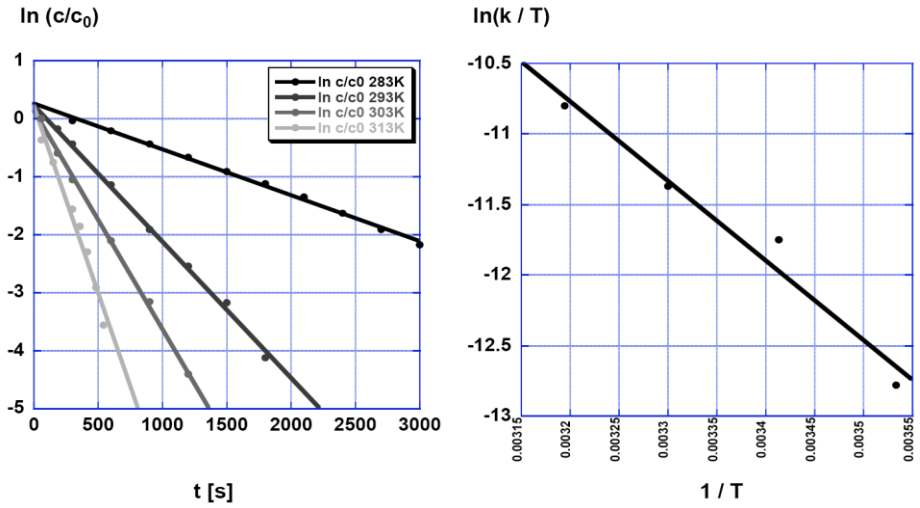

Figure 1.4 right: The plot ln(c/c$_0$) *vs.* t is perfectly linear (r > 0.99 at all four temperatures). It indicates that the reaction is first order. left: The Eyring-plot is sufficiently linear (r = 0.992) to determine $\Delta H^{\#}$ and $\Delta S^{\#}$.

The Eyring equation is given as eq 1,

$$\ln\left(\frac{k}{T}\right) = \frac{-\Delta H^{\#}}{RT} + \frac{\Delta S^{\#}}{R} + \ln\frac{k_b}{h} \qquad (1)$$

Where *k* represents the rate constant of the reaction, T is the temperature, $\Delta H^{\#}$ the enthalpy of activation, and $\Delta S^{\#}$ the entropy of activation. Eq 1 was used to calculate $\Delta H^{\#}$ = 46.8 kJ mol^{-1}, $\Delta S^{\#}$ = -1.98 J mol^{-1} K^{-1} and (at 300 K) $\Delta G^{\#}$ = 47.4 kJ mol^{-1}. The relatively low enthalpy of activation and the entropy of activation being close to zero are in agreement with the electrocyclic ring-opening reaction from the strained three-membered ring intermediate to the betaine.[21]

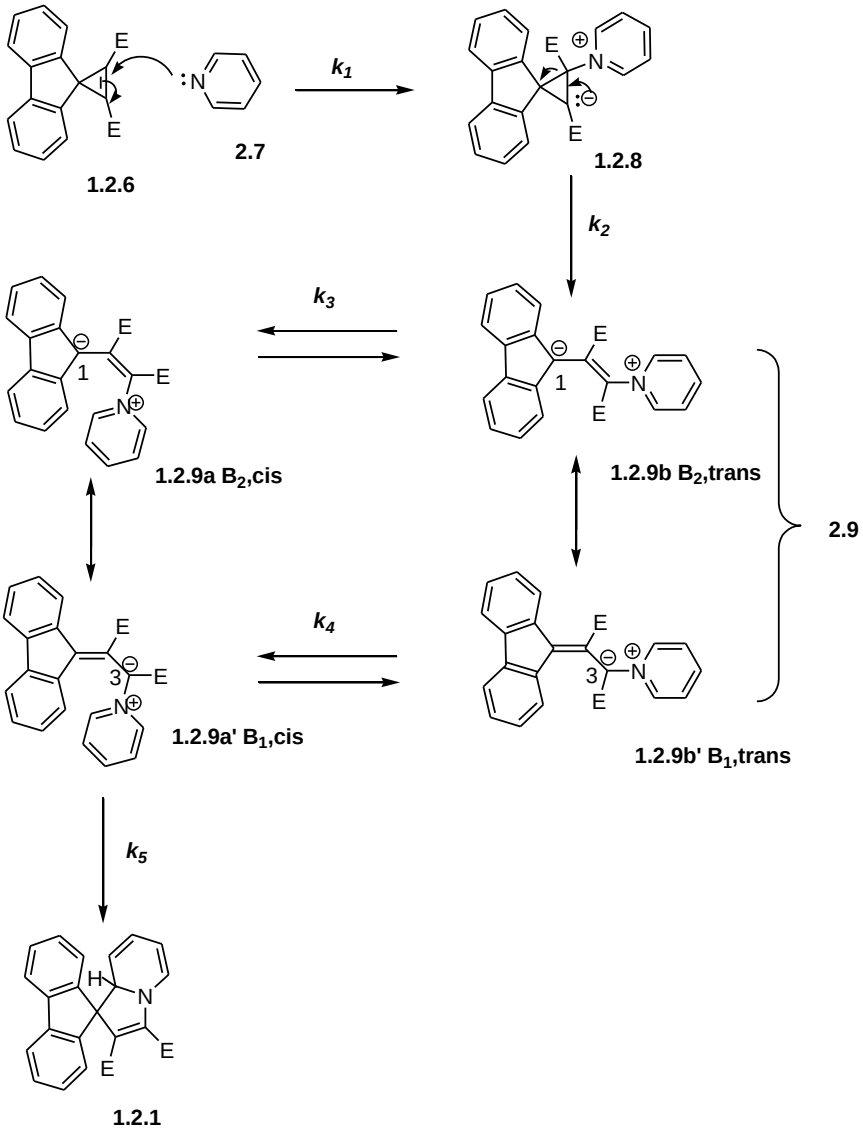

Scheme 1. 6: Nucleophilic addition of pyridine (1.2.7) to *spiro*[2-cyclopropene-1,9'-[9H]fluorene]-2,3-dicarboxylic acid, 2,3-dimethyl ester (1.2.6): The reaction proceeds in three steps: 1) Addition of pyridine to the highly strained cyclopropene intermediate 1.2.8) (1,5-electrocyclic) ring-opening to the *trans*-betaine $B_{2,trans}$. 1.2.9b) Isomerization to $B_{1,trans}$ and $B_{1,cis}$ and 1,5-electrocylic ring closure to the DHI (1.2.1a). E = -*C(O)OCH*$_3$.

1.2.3.3 Betaine Structure Determined by NMR Spectroscopy

The kinetics of the addition of pyridine **(1.2.7)** to *spiro*[2-cyclopropene-1,9'-[9H]fluorene]-2,3-dicarboxylic acid, 2,3-dimethyl ester **(1.2.6)** do not permit the recording of pure betaine ^{1}H- and ^{13}C-NMR-spectra **(1.2.9)**, because at any time, either the starting

materials and/or the DHI **(1.2.1a)** were also present. Therefore, attention was directed to the methyl-ester peaks of compounds **(1.2.6)**, **(1.2.1a)** and **(1.2.1c)** (**Figure 1.5**). Whereas the methyl ester peaks of **(1.2.6)** appear at the same ^{1}H-NMR-frequency (δ=3.83 ppm), two singlets can be discerned for the DHI (**1.2.1a**, δ = 3.25 and 3.98 ppm). At all times, there is only one set of signals for the betaine (**1.2.7c**, δ = 3.29 and 3.88 ppm) discernible, indicating that indeed only one betaine is stable between 283 K and 313 K. Using the ^{13}C-NMR-signals and the ACD/CNMR Predictor (^{13}C NMR Prediction Software)[22], it was determined that the *transoid* betaine ($B_{1,trans}$) is the only detectable isomer (or, rather, resonance structure) in the temperature interval investigated.

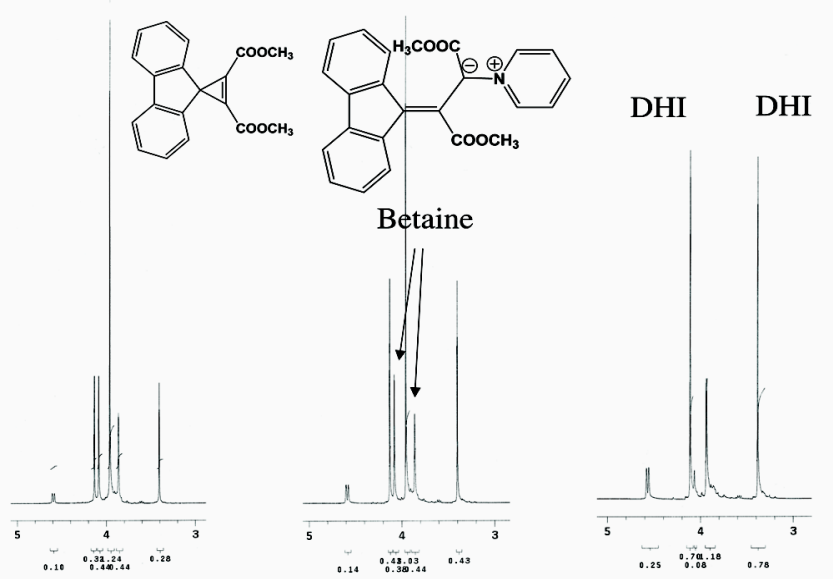

Figure 1.5 Methylester-peaks of the reaction mixture between *spiro*[2-cyclo-propene-1,9'-[9H]fluorene]-2,3-dicarboxylic acid, 2,3-dimethyl ester (1.2.6) and pyridine in $CDCl_3$ at T=20°C: left t=120s, middle: t=900 s, right: t=1,500 s. It is clearly discernible that the ester peak or the starting material (1.2.6) decreases and one set of betaine methylester signals are formed. Ring closure of the betaine leads to the appearance of one set of DHI-ester signals (1.2.9).

1.2.3.4 DFT Calculations

The computational method was applied for the determination of geometry configuration, electronic structures, and the relative stabilities of DHI and the *cisoid*,

transoid isomers of betaines. The DFT results, that have been obtained by the Ortiz´s group at Auburn University in Alabama, clearly indicate that the long-standing hypothesis concerning the most stable Lewis structures of the zwitterionic betaines, formed upon photoexcitation of the photochromic dihydroindolizines, has to be corrected.

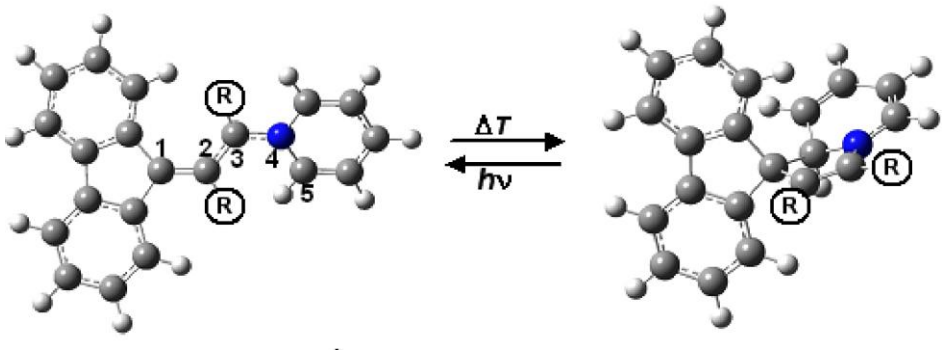

Figure 1.6 Interconversion of "*spiro*" and "betaine" forms of *spiro*[9,1'(8'aH)-indolizine]-2',3'-dicarboxylic acid, dimethyl ester (R=C(O)OCH$_3$).

In looking for possible zwitterionic character of the betaine systems, all starting geometries assumed single C_1C_2 and C_3N_4 bonds and a double C_2C_3 bond (**Figure 1. 6** for numbering), as illustrated in **Scheme 1.2** for the open-chain forms, $B_{2,cis}$ and $B_{2,trans}$. However, the optimized geometries in none of the cases have retained the suggested single-double-single bond character. On the contrary, significant delocalization can be deduced from optimized bond lengths. **Table 1.3** summarized the geometry analysis for these critical bonds.

Table 1.3: Bond lengths (Å)

	Betaine		DHI
	Trans	*Cis*	*Spiro*
C_1C_2	1.38	1.38	1.53
C_2C_3	1.46	1.44	1.36
C_3N_4	1.41	1.42	1.37

It is noteworthy that in all *cis/trans*-configurations of the betaines, the C_1C_2 bond length is closer to a double than a standard single CC bond length (which are 1.33 Å and 1.57 Å respectively). In contrast, the C_2C_3 bonds have more single than double bond character, with distances about 1.45 Å. The C_3N_4 bonds are typically in the range of a single CN bond (1.40-1.42 Å). Thus, the classical zwitterionic picture of betaine is not consistent with the *ab-initio* results. This was confirmed by performing a charge distribution analysis of the $C_1C_2C_3N_4$ betaine fragment. Condensed charges on each atom of this fragment, shown in **Table1.4**, were estimated by two reliable methods. The Merz-Singh- Kollman (MSK) population analysis [23] assigns the charges so as to reproduce the molecule's electrostatic potential. In the Atomic Polar Tensor (APT) method, the atomic charge is related to the corresponding tensor of derivatives of the dipole moment with respect to Cartesian coordinates of this atom.[24] No partitioning of the basis set is implicit in either scheme.

Table 1.4: Charge distribution in the $C_1C_2C_3N_4C_5$ fragment

	MSK			**APT**		
	$I_{Betaine}$		I_{DHI}	$I_{Betaine}$		I_{DHI}
	Trans	*Cis*	*Spiro*	*Trans*	*Cis*	*Spiro*
C_1	-0.13	-0.28	-0.22	0.04	-0.35	0.11
C_2	-0.07	-0.09	-0.22	0.16	0.47	-0.62
C_3	-0.96	-0.48	-0.28	-0.99	-0.96	0.62
N_4	0.73	0.26	0.08	0.76	0.41	-0.89
C_5	-0.21	-0.04	0.70	-0.20	-0.07	0.26

Both analyses predict the largest negative charge to be localized on C_3 and the largest positive charge to be localized on N_4 for the *cis*- and *trans*- betaine configurations. Although none of the classic Lewis structures shown in **Scheme 1.2** are able to describe the structure and charge distribution correctly, B1*cis,trans* better describes the structure and charge distribution from the calculations than B2*cis,trans*. In accordance with our calculation results, the terms *cisoid* and *transoid* will be used hereafter.

1.2.3.4.1 Relative Stabilities of the DHI and its corresponding betaines.

The relative stabilities of isomers were estimated from their total energies and schematically presented in **Figure 1.7**. According our results, the stability order is: *cis* < *trans* < *spiro*. The energy difference between *cis*-*trans* betaine isomers is small: 2.41 kcal/mol with B3LYP/6-31G(d) and 1.197 kcal/mol for the single-points calculated with 6-311(d,p) basis set. A larger difference is predicted for *cis* and *spiro* energy gap. With the small bases set, the *cis*-*spiro* ΔE = 5.87 kcal/mol, whereas for the larger basis the energy difference is ΔE = 5.49 kcal/mol.

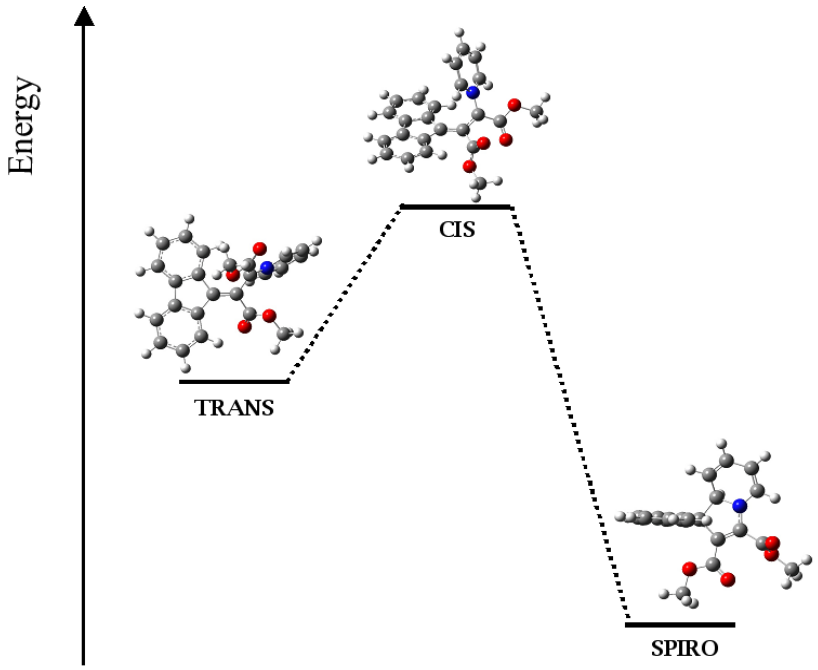

Figure 1.7 Relative energies for R= -*C(O)OCH$_3$* (schematic drawing)

Overall, our calculations show that the energy gaps between open forms of betaine are only slightly larger than the kinetic energy of the molecules at room temperature (1.5RT is approximately 1 kcal/mol). These results also indicate that small but distinct driving forces for the thermal 1,5-electrocyclizations of the betaines to the *spiro*-DHIs exist. However, we did not attempt to calculate Arrhenius-parameters for the thermal cyclization at this early

stage of our computation efforts. Instead, we have studied the implications of our findings with respect to the interpretation of (photo)physical measurements.

1.2.3.5 Photophysical Measurements

To date, there is no commonly accepted paradigm that is able to describe all mechanistic phenomena, which are observed studying photochromic dihydro-indolizine/betaine systems. It is well known that impurities and decomposition products can have a great impact on the measurements' results. Furthermore, it must be noted that most betaines are oxygen sensitive. This is what we know about the photophysical properties of the simplest DHI (**1.2.1**):

The photoexcited singlet state of DHI undergoes a 1,5-electrocyclic ring-opening reaction to the betaine singlet excited state (**1.2.9***). Whereas the absorption maxima of DHIs are typically in the UVA and blue spectral regions, betaines are highly colored and possess unusually broad absorption spectra. The back reaction of our model DHI proceeds thermally.

Both DHI and betaines are weakly fluorescent. The identity of DHI and betaine singlet states has been confirmed by the use of singlet quenchers. There are small (approx. 3 nm) hypsochromic shifts observed for the position of the DHI-fluorescence when the polarity of the solvent is increased (e.g. from dichloromethane to acetonitrile).[26] This is indicative of a slightly more polar excited state than the ground state. The fluorescence occurring from betaines can be more strongly influenced by a change in solvent due to its higher degree of charge delocalization.[3,27,28]

All efforts to triplet-sensitize a photochromic ring-opening or ring-closure reaction failed.[28,29]

Because the fluorescence occurring from the DHI ($\tau_F << 0.4$ns) and the kinetics of the photochemical 1,5-electrocyclization ($\tau_R > 0.5$ns) cannot occur from the same singlet state, the co-existence of at least two different singlet states that are relatively close in their respective energies, but separated by a rather large activation barrier must be concluded. It is also concluded that both are populated upon excitation with UV light. Otherwise, the rate constant for cyclization would have to compete with the rate of fluorescence.[28,30]

1.2.3.5.1 Light Absorption Studies

The laser absorption spectroscopy studies were performed at the department of Chemistry, Ohio State University by Dr. Yao Liu and Prof. Dr. Claudia Turró. Time-resolved laser absorption of *spiro*[9H-fluorene-9,5'(4'aH)-pyrrolo[1,2-b]pyridazine]-6',7'-dicarboxylic acid, dimethyl ester and derived bis-photochromes indicated[31] that the excitation from the DHI to the betaine is a one-photon process. Based on a literature survey, this has never been shown for the basic *spiro*-dihydroindolizine molecule. The photoinitiated formation of betaine from DHI and the subsequent thermal regeneration of the starting material can be written as equations 2 and 3.

$$DHI + nh\nu \xrightarrow{k_1} Betaine \qquad (2)$$

$$Betaine \xrightarrow{k_2} DHI \qquad (3)$$

The reaction rate can be described as eq. 4,

$$\frac{d[Betaine]}{dt} = k_1[DHI]I - k_2[Betaine] \qquad (4)$$

Where k_1 is the rate constant of the forward reaction, k_2 is the rate constant of back reaction, I represents the light intensity, n is the number of photons, and [Betaine] and [DHI] represent the concentrations of the ring-open and ring-closed forms, respectively. In addition, the relation [Betaine] + [DHI] = C_0 was used, where C_0 is the starting concentration of DHI, resulting in eq 5.

$$\frac{d[Betaine]}{dt} = k_1 C_0 I - (k_1 I + k_2)[Betaine] \qquad (5)$$

Solving the differential equation results in eq 6, which shows the relationship between the concentration of the products and the irradiation time.

$$[Betaine] = \frac{k_1 C_0 I}{k_1 I + k_2}(1 - e^{-(k_1 I + k_2)t}) \qquad (6)$$

In the case of DHI, the absorption spectrum of the ring-closed form show absorption peak at 387 nm. After laser irradiation, the 387 nm absorption peak decreases and new

absorption bands at ~ 450 nm and 582 nm appear. **Figure 1.8** shows the absorbance at 582 nm at different irradiation times under different laser intensities. The color change of the solution is faster with increasing laser intensity. At each laser power, the absorbance change reaches a plateau after long irradiation times. The value of the absorbance at 582 nm also increases with the laser intensity.

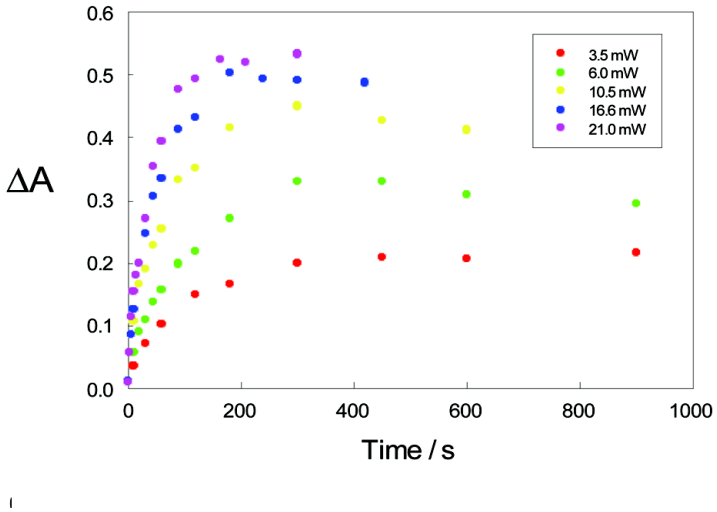

Figure 1.8 Change in the absorbance at 582 nm of DHI solution at different irradiation time and under different laser intensities.

At each laser intensity, the absorbance reaches a plateau beyond a certain irradiation time, which means the reaction can reach equilibrium. Therefore, equations 7 and 8 can be written,

$$\frac{[Betaine]_e}{C_0 - [Betaine]_e} = \frac{k_1}{k_2} I \qquad 7)$$

$$\ln\left(\frac{[Betaine]_e}{C_0 - [Betaine]_e}\right) = \ln\left(\frac{k_1}{k_2}\right) + n\ln(I) \qquad (8)$$

where $[Betaine]_e$ is the concentration of the ring-open form at the equilibrium. To determine the absorbance corresponding to C_0, the laser power was slowly increased up to 150 mW. The value of the absorbance was monitored until no further changes were observed, indicative that the plateau was reached. It should be noted that the electronic absorption

spectrum of the solution measured before after the experiment was the same (once all the Betaine was transformed into the DHI again), indicating that all the DHI was recovered without decomposition of the sample.

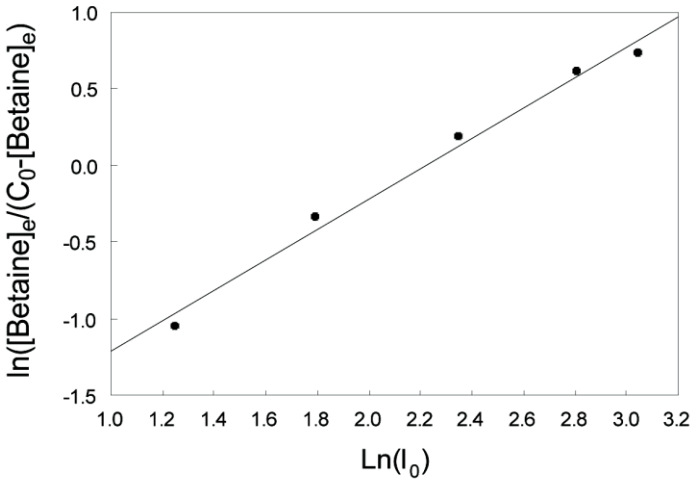

Figure 1.9 ln([Betaine]$_e$/(C$_0$-[Betaine]$_e$) *vs.* ln(I)shows the plot of ln([Betaine]$_e$/(C$_0$-[Betaine]$_e$) *vs.* ln(I). The slope for DHI is 0.99 (r=0.957), which clearly indicates that the ring-open processes require one photon.

1.2.3.5.2 Time-Resolved Absorption Spectroscopy of the Betaines

The transient absorption spectra measured following excitation 0.10 mmol DHI in acetonitrile with a laser pulse (355 nm, fwhm ~ 8 ns) are shown in **Figure 1.10**, collected immediately and 300 μs after excitation. The spectra are characterized by a peak at 440 nm and a broad absorption with maximum at 600 nm (immediately after excitation) and 585 nm (after 300 μs). These maxima are known to correspond to betaine **(1.2.1b)**. The changes in the absorbance as a function of time decay monoexponentially with lifetime of 239 μs at 440 nm.

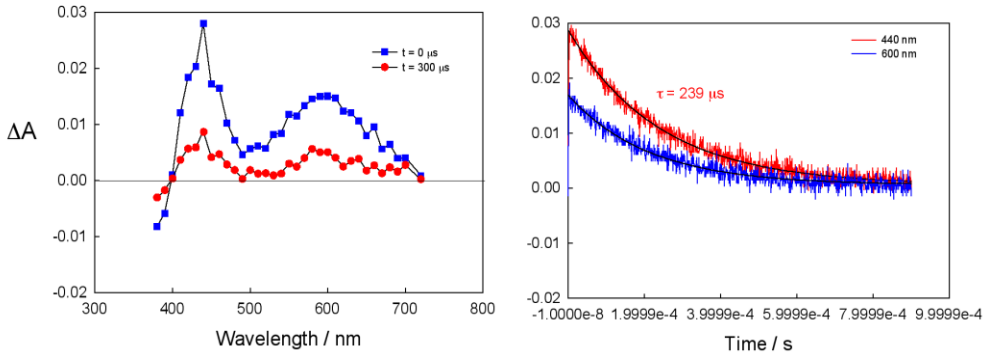

Figure 1.10 Transient absorption spectroscopy of the betaine (1.2.1b,c)

It is noteworthy that the ratio of the absorbance at 440 nm and 600 nm ($\Delta A_{440/600}$) is greater immediately following the laser pulse than after 300 ms, indicating that two different species may be present in solution, with different concentrations at these two times. A possible explanation for this observation is the coexistence of the *cisoid* and the *transoid* betaine in this time domain. Since it was already established by ^{1}H NMR that on the minute timescale only the *transoid* betaine isomer is present, it may be concluded that the *cisoid* species decays with life-time (τ) = 239 μs to regenerate DHI. Based on the spectra shown in **Figure 1.10**, it appears that the *cisoid* species, representing most of the sample at t = 0, absorbs more strongly at 440 nm than the *transoid* isomer. It should also be noted that the absorption signals at 440 nm and 585–600 nm do not completely return to zero after 900 μs, with ~5% absorbance from the initial ΔA remaining. Assuming similar molar extinction coefficients for the *cisoid* and *transoid* species at 440 nm, it may be concluded that both the *cisoid* and *transoid* betaine are being formed in the photochemical electrocyclic ring opening reaction, resulting in production ~95% *cisoid* and ~5% *transoid* species. Whereas the *cisoid* betaine quickly reacts *via* electrocyclization back the DHI, the *transoid* betaine appears to bemetastable. Therefore, the optical absorption at t > 1 ms can be attributed to *transoid* betaine. The life-time of the electrocyclization process at 293 K is 239 ± 10 μs. Our findings are supported by an earlier result obtained by Dűrr and Kossanyi,[31] where betaines with fixed *cisoid* geometry show rapid back reactions in the nanosecond time window.

1.2.3.5.3 The Kinetics of the Thermal Back Reaction

Table 1.5 summarizes the relevant photophysical parameters of DHI and betaine. The

spectral features of *transoid* betaine are observed following photolysis of a DHI (**1.2.1a**) solution with laser light (355 nm) for 3 min, and are shown in the spectrum at t = 0 in **Figure 1.11**. It is widely accepted that the fluorescence of DHI occurs from an S_2 state.[3,28]

Table 1.5: Photophysical Data for DHI 1.2.1 and *transoid* Betaine (1.)[2,27]

DHI					Betaine	
λ_{max} [nm]	lg ε	λ_{em} [nm]	ϕ_{EM}	τ_{EM} [ns]	λ_{max} [nm]	λ_{em} [nm]
384	4.02	460	0.024	8.1	586	492

After this initial spectrum, the changes to the absorption were monitored as a function of time while the sample was kept in the dark at 293 K. It is evident from **Figure 1.11** that spectral changes correspond to the regeneration of DHI **(1.2.1a)** from betaine **(1.2.1c)** through its thermal electrocyclization. In CH_3CN at 293 K, the unimolecular thermal back reaction has a rate constant of 4.90×10^{-3} s^{-1}, which is in excellent agreement with the literature.[2] Note that this value corresponds to k_4 in **Scheme 1.8**. The Eyring-plot derived from these data is also shown in **Figure 1.11**. From the plot shown in **Figure 1.11**, the activation parameters were calculated to be $\Delta H^{\#}$ = 106 J mol^{-1}, $\Delta S^{\#}$ = -256 J $K^{-1}mol^{-1}$, and $\Delta G^{\#}$ = 76,900 J mol^{-1}(298 K) (**Scheme 1.8**).

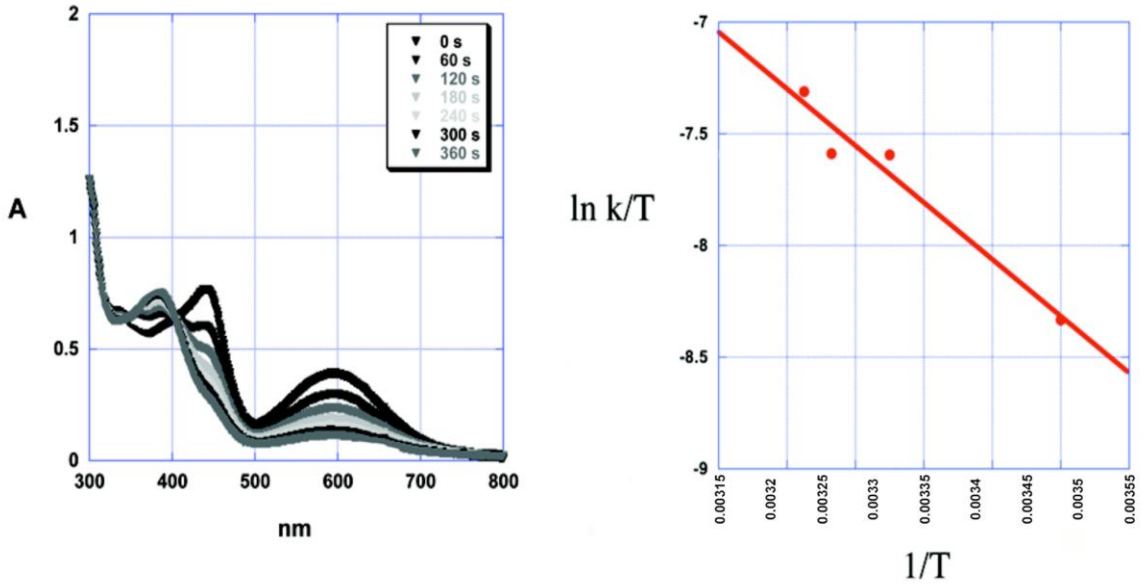

Figure 1.11: left: Changes to the UV/Vis spectrum of Betaine (t = 0) as a function of time regenerating DHI at 293 K. Note that the conversion from DHI to betaine is ~ 40 %, therefore the spectrum at t = 0 has contributions from DHI in the region from 300 nm to 480 nm. right: Eyring-plot derived from data obtained in the temperature interval 283 – 313 K.

1.2.4 Conclusions

The results presented here permit the development of a new paradigm describing the photochemical reactivity of the DHI/Betaine system. Upon photoexcitation of DHI an adiabatic photoreaction occurs. The excited state-reaction finds the lowest point of the potential-energy surface, which acts as a "sinkhole". As this is the case in many photoreactions[31], the deactivation leads to a mound, which is the ground-state activation barrier between the *cisoid* and the *transoid* betaine.

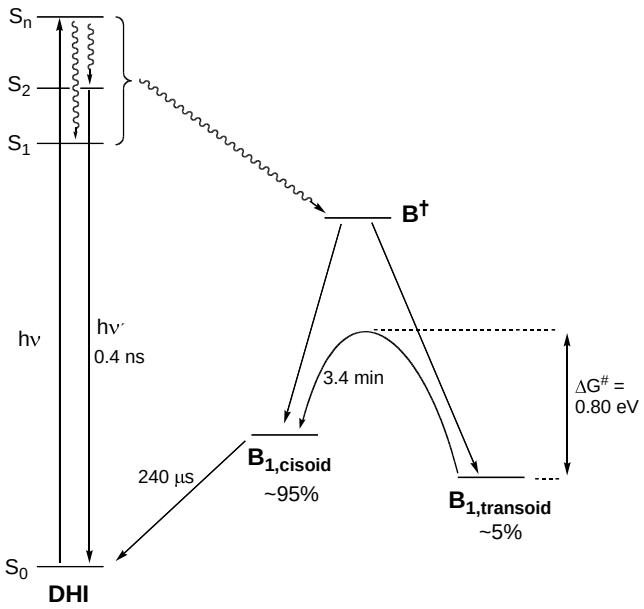

Scheme 1. 7: Simplified photochemical reaction scheme for the DHI/Betaine system showing the generation of *cisoid* and *transoid* betaine following excitation of DHI. The thermal back reaction is fast for *cisoid* betaine, while that for the *transoid* species is slower owing to a large activation barrier to isomerization.

The exact position of the point where the deactivation funnel hits the mound determines, which fraction of the molecules become *cisoid* and *transoid* Betaines. Whereas the *cisoid* betaine reacts within several hundred microseconds (depending on the temperature) to the DHI, the *transoid* betaine is stable for seconds to hours. The Eyring activation parameters that have been attributed to the electrocyclic ring closure in basically all mechanistic papers dealing with the DHI/Betaine system are in reality for the *transoid*/*cisoid* isomerization of the betaine!

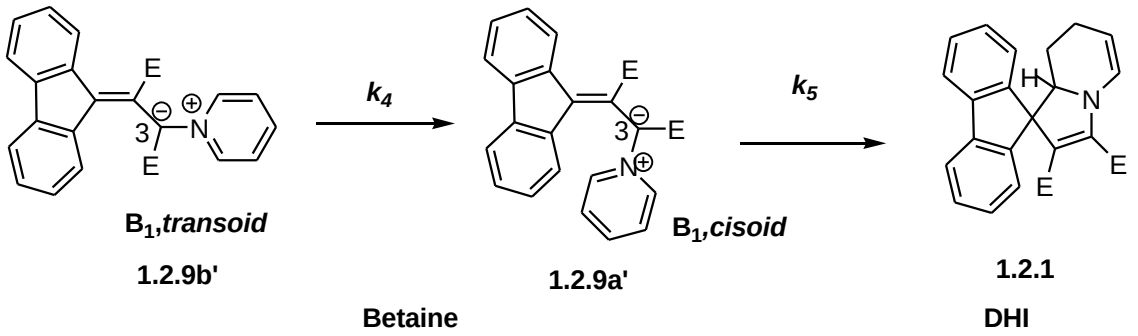

Scheme 1. 8: The thermal back reaction is slow for the *transoid* → *cisoid* isomerization. Once the *cisoid* betaine is formed, 1,5-electrocyclization to the betaine is relatively fast.

1.2.5 References

1. Bouas-Laurent, H. and Duerr, H *Pure Appl. Chem*. **2001**, *73*, 639–665.
2. G. Hauck and H. Duerr, *Angewandte Chemie* **1979**, *91*, 1010– 11.
3. Duerr, H. *Angewandte Chemie* **1989**, *101*, 427–45.
4. Frisch, M. J.; Trucks, G.W.; Schlegel, H. B.; Scuseria, G. E.; Robb, M. A.; Cheeseman, J. R.; Montgomery, Jr., J. A.; Vreven, T.; Kudin, K. N.; Burant, J. C.; Millam, J. M.; Iyengar, S. S.; Tomasi, J.; Barone, V.; Mennucci, B.; Cossi, M.; Scalmani, G.; Rega, N.; Petersson, G. A.; Nakatsuji, H.; Hada, M.; Ehara, M.; Toyota, K.; Fukuda, R.; Hasegawa, J.; Ishida, M.; Nakajima, T.; Honda, Y.; Kitao, O.; Nakai, H.; Klene, M.; Li, X.; Knox, J. E.; Hratchian, H. P.; Cross, J. B.; Bakken, V.; Adamo, C.; Jaramillo, J.; Gomperts, R.; Stratmann, R. E.; Yazyev, O.; Austin, A. J.; Cammi, R.; Pomelli, C.; Ochterski, J.; Ayala, P. Y.; Morokuma, K.; Voth, G. A. Salvador, P.; Dannenberg, J. J.; Zakrzewski, V. G.; Dapprich, S.; Daniels, A. D.; Strain, M. C.; Farkas, O.; Malick, D. K.; Rabuck, A. D.; Raghavachari, K.; Foresman, J. B.; Ortiz, J. V.; Cui, Q.; Baboul, A. G.; Clifford, S.; Cioslowski, J.; Stefanov, B. B.; Liu, G.; Liashenko, A.; Piskorz, P.; Komaromi, I.; Martin, R. L.; Fox, D. J.; Keith, T.; Al-Laham, M. A.; Peng, C. Y.; Nanayakkara, A.; Challacombe, M.; Gill, P. M. W.; Johnson, B. G.; Chen, W.; Wong, M. W.; Gonzalez C.; Pople, J. A. *GAUSSIAN 03 (Revision C.02)*, Gaussian, Inc., Wallingford, CT, **2004**.

5. (a) Becke, A. D. *Phys. Rev. A* **1988**, *38*, 3098–100; (b) Lee, C.; Yang, W. and Parr, R.G. *Phys. Rev. B* **1988**, *37*, 785–9.
6. Alajarin, M.; Sanchez-Andrada, P.; Vidal, A.; Tovar, F. *J. Org. Chem.* **2005**, *70*, 1340–1349.
7. Robiette, R. *J. Org. Chem.* **2006**, *71*, 2726–2734.
8. Karzazi, Y.; Vergoten, G.; Surpateanu, G. *Journal of Molecular Structure* **1998**, *417*, 83–93.
9. Karzazi, Y.; Lungu, C. N.; Surpateanu, G.; Vergoten, G. *Journal of Molecular Structure* **1997**, *406*, 45–49.
10. Niewodniczanski, W.; Bartkowiak, W.; Leszcynski, J. *J. Mol. Model.* **2005**, *11*, 392–397.
11. Robiette, R.; Aggarwal, V. K.; Harvey, J. N. *J. Am. Chem. Soc.* **2007**, *129*, 15513–15525.
12. Krishnan, R.; Binkley, J. S.; Seeger, R.; Pople, J. A. *J. Chem. Phys.* **1980**, *72*, 650–4.
13. Bradley, P. M.; Bursten, B. E.; Turro, C. *Inorg. Chem.* **2001**, *40*, 1376–1379.
14. Warren, J. T.; Chen, W.; Johnston, D. H.; Turró, C. *Inorg. Chem*. **1999**, *38*, 6187–6192.
15. Heydt, H. *Science of Synthesis*, **2004**, *27*, 843-935.
16. McDowell, L. J.; Khodaei, M. M.; Bethell, D. *Organic & Biomolecular Chemistry* **2003**, *1*, 995-1003.
17. Duerr, H.; Kober, H.; Sergio, R.; Formacek, V. *ChemischeBerichte* **1974**, *107*, 2037-49.
18. Mataka, S.; Tashiro, M. *J. Org. Chem.* **1981**, *46*, 1929-31.
19. Duerr, H.; Hauck, G. Photochromic *spiro*[1,8-a-dihydroindolizines] and their use in radiation-sensitive materials., *Ger. Offen.* **1980**, *DE 2906193*, 29.
20. Creary, X. and Butchko, M. A. *J. Org. Chem.* **2002**, *67*, 112–118.
21. Caroll, F. A. *Perspectives on Structure and Mechanism in Organic Chemistry*, Brooks/Cole Publishing Company, Pacific Grove, Washington, **1998**, chapter *11*: Concerted Reactions.
22. http://www.acdlabs.com/products/spec_lab/predict_nmr/cnmr/.
23. (a) Besler, B. H. Merz Jr., K. M. and Kollman, P. A. *J. Comp. Chem.* **1990**, *11*, 431–9. (b) Singh, U. C. and Kollman, P. A. *J. Comp. Chem.*, **1984**, *5*,129–45.
24. Cioslowski, J. *J. Am. Chem. Soc.* **1989**, *111*, 8333–6.

25. Sueishi, Y.; Danjo, K.; Yamamoto, S. and Nishimura, N. *Chemistry Express* **1991**, *6*, 459–62.
26. Duerr, H., *Pure and Applied Chemistry* **1990**, *62*, 1477–82.
27. Gross, H. and Duerr, H. *Angewandte Chemie*. **1982**, *94*, 204–5.
28. Duerr, H. and Bouas-Laurent, H. *Photochromism: Molecules and Systems*, Revised Edition, Elsevier Science B.V, Amsterdam, **2003**, pp. 1074.
29. Turro, N. J. *Modern Molecular Photochemistry*, Addison-Wesley Publishing Co., Reading, Mass. **1978,** pp 628.
30. Bleisinger, H.; Scheidhauer, P.; Duerr, H.; Wintgens, V.; Valat, P. and Kossanyi, J. *J. Org. Chem.* **1998**, *63*, 990–1000.
31. Fromm, R.; Born, R.; Durr, H.; Kannengiesser, J.; Breuer, H. D.; Valat, P. and Kossanyi, J. *J. Photochem. Photobiol. A: Chem.* **2000**, *135*, 85–89.

1.3 Photochromic Spirodihydroindolizine/Betaine-System (II): *Spiro*[9H-fluorene-9,5'(4'aH)-pyrrolo[1,2-b]pyridazine]-6',7'-dicarboxylic acid, 6',7'-dimethyl ester

1.3.1 Introduction

Following the pioneering work of Dürr and coworkers,[1] numerous photochromic dihydroindolizines (DHI)[2,3] and the related photochromic *spiro*-tetrahydro-indolizines (THI)[4], dihydropyrazolopyridines[5] and 1H-benzo[c]pyrazolo [1,2-a]cinnolines[6] have been synthesized. In spite of the multitude of new and exciting chemical structures, a quantitative understanding of the dependence of the photophysical properties of DHIs and their corresponding isomeric betaines on the chemical structures is only slowly emerging.[7] Recently, the Bossmann group reported the results from the studies of the simplest DHI/betaine-system (*spiro* [9,1'(8'aH)-indolizine]-2',3'-dicarboxylic acid, dimethyl ester, "pyridine DHI/betaine" ($1^{DHI}/1^{B}$)) applying state-of-the-art density functional theory (DFT) calculations in combination with stationary and time-resolved absorption measurements which is discussed in earlier subchapter **1.2**.[8]

Since their discovery in 1979,[1] the electronic structures of the photochromic *spiro*-dihydroindolizine forms and especially the corresponding betaines (Bs), formed by reverse electrocyclization from photoexcited (^{1}S)-states, have been under discussion. Betaines undergo thermal back reaction to their corresponding *spiro*-DHI-isomers via 1,5-electrocyclization.[1,2] According to our previous findings, the charges in the "pyridine-betaine" are delocalized and the bond lengths are neither typical single- nor typical double bonds, but in-between.[8] However, as depicted in **Scheme 1.9**, the most classic resonant structures for "pyridine-betaine", which resemble our findings from DFT-calculations most closely, are $B_{1,cis}$ and $B_{1,trans}$ and not $B_{2,cis}$ and $B_{2,trans}$ as discussed in virtually all mechanistic publications on this subject.

Correctly calculating the charge-distribution in betaines is of importance for our understanding of their structure, reactivity, and stability, because, counter to most other photochromic systems, such as spiropyrans, spirooxazines, chromenes, fulgides and diarylethenes[9], no uncharged resonance structures of the betaine-isomer is possible. Our understanding of the mechanisms of the occurrence of *cisoid vs. transoid* betaine isomers is

equally important, because without this knowledge the DHI → betaine → DHI cycle cannot be properly understood.

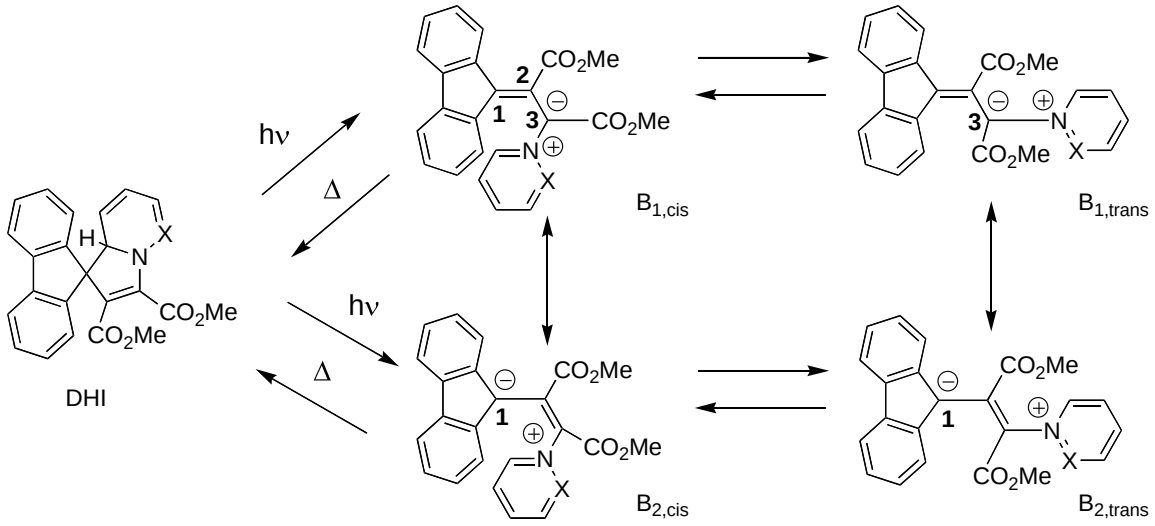

Scheme 1. 9: Reaction scheme for the most simple DBI/betaine-systems: X=CH, *spiro*[9,1'(8'aH)-indolizine]-2',3'-dicarboxylic acid, dimethyl ester, number, X=N, *spiro*[9H-fluorene-9,5'(4'aH)-pyrrolo[1,2-b]pyridazine]-6',7'-dicarboxylic acid, 6',7'-dimethyl ester, number The betaine-structures, which were postulated in numerous mechanistic discussions (e.g. 2,4,5), are $B_{2,cis}$ and $B_{2,trans}$.

The most important finding of this recent study[8] was that the electrocyclic back reaction of the betaines to the DHI is not rate determining, as previously thought, but instead the kinetics are dictated by the *cis*-*trans*-isomerization of the betaine, which features a ground-state barrier. After the photochemical ring opening of DHI's to betaines in an adiabatic photoreaction, the excited state-reaction proceeds to the lowest point of the potential-energy surface, which acts as a "sinkhole". As this is the case in many photoreactions[10], the deactivation leads to a "mound" which is the ground-state activation barrier between the *cisoid* and the *transoid* betaine. The exact position of the point where the deactivation funnel hits the mound determines, which fraction of the molecules become *cisoid* and *transoid* betaines.

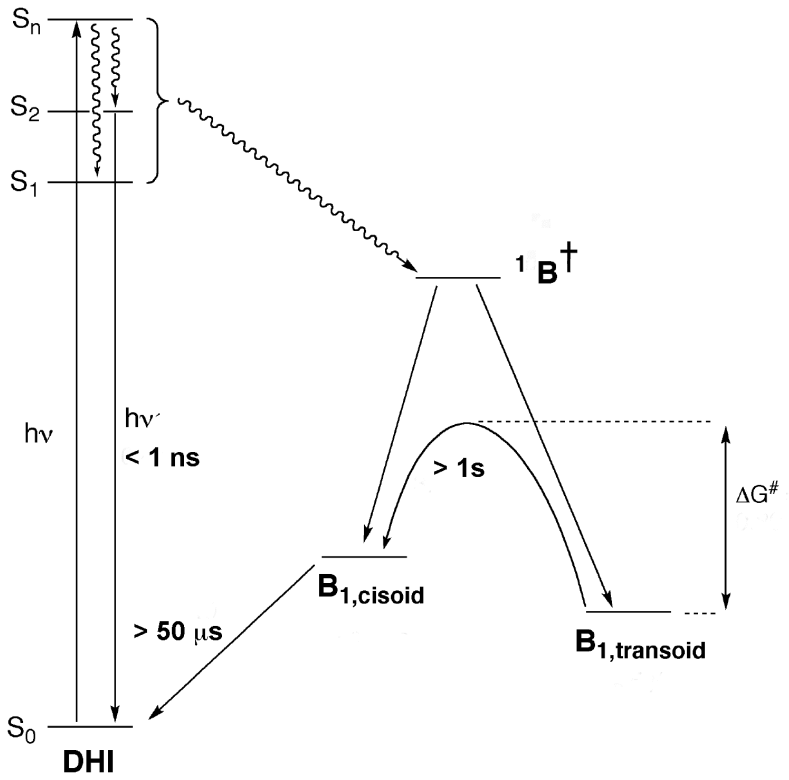

Scheme 1. 10: Simplified photochemical reaction scheme for the DHI/Betaine system showing the generation of *cisoid* and *transoid* betaine following excitation of DHI. The thermal back reaction is fast for *cisoid* betaine, while that for the *transoid* species is slower owing to a large activation barrier to isomerization. A thermal barrier[10] exists between the *cisoid* and *transoid* betaine conformations.

In the research reported here, I have selected *spiro*[9H-fluorene-9,5'(4'aH)-pyrrolo[1,2-b]pyridazine]-6',7'-dicarboxylic acid, 6',7'-dimethyl ester ("pyridazine-DHI/betaine", ($2^{DHI}/2^{B}$) studying the influence of the additional sp^2-nitrogen present in the (4'aH)-pyrrolo[1,2-b]pyridazine-subunit. This compound was chosen so that the influences of any substituents as a part of the heterocycle or aromatic system would be eliminated. This was then compared to the results for this DHI with the previously re-investigated simplest DHI-structure, *spiro*[9,1'(8'aH)-indolizine]-2',3'-dicarboxylic acid, dimethyl ester (($\mathbf{1^{DHI}/1^{B}}$) **Scheme 1.9**). The studies reported here comprise A) the investigation of the kinetics and mechanism of the addition of pyridazine to *spiro*[2-cyclopropene-1,9'-[9H]fluorene]-2,3-dicarboxylic acid, 2,3-dimethyl ester, B) state-of-the-art density functional theory (DFT) calculations of the DHI/betaine pair ($2^{DHI}/2^{B}$) to

determine their geometries and charge distributions, C) steady-state and time-resolved photophysical experiments of the DHI/betaine pair ($2^{DHI}/2^{B}$). D) It was also confirmed, using ^{1}H-NMR, that the predictions from the DFT calculations about the structure of the betaines were correct. This study shows that the "pyridazine DHI" (2^{DHI}) and its corresponding betaine (2^{B}) follow the mechanistic paradigm described in **Scheme 1.10**. This is an important step towards the tailored design of functional DHI/betaine systems.

This research was carried out with collaboration with Prof. Dr. Joshep V. Ortiz, Auburn University, AL and Claudia Turró, Ohio State University, OH.

1.3.2 Experimental

1.3.2.1 Chemical and Instruments

All chemicals were obtained from Acros Organics, unless noted otherwise. 400 MHz and 200 MHz Varian NMR-spectrometer and a Nicolet Protégé 460 FT-IR spectrometer were used in this study. I would like to thank the Analytical Laboratory of Dr. Ruth Welti at KSU for recording the mass spectra of compounds employing an Applied Biosystems API-4000 triple quadrupole mass spectrometer with electrospray and APCI sources.

1.3.2.2 DFT Calculations

All calculations were performed with the Gaussian*03* suite of programs.[12] B3LYP/6-31G(d) optimizations[13,14] and harmonic frequency analysis revealed minima for *cis*- and *trans*-betaine and *spiro*- configurations. MP2/6-31G(d) optimizations were performed as well. Subsequent single-point calculations with the 6-311G(d,p) basis set were done at the geometries obtained.

1.3.2.3 Synthesis of spiro[9H-fluorene-9,5'(4'aH)-pyrrolo[1,2-b]pyridazine]-6',7'-dicarboxylic acid, 6',7'-dimethyl ester (1.3.1a (2^{DHI}))

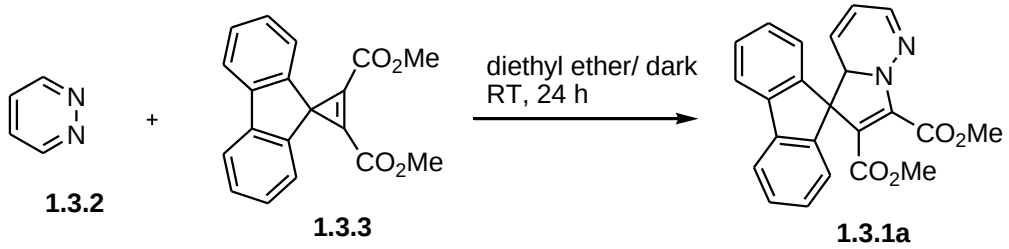

1.3.2 **1.3.3** **1.3.1a**

Scheme 1. 11: Synthesis of *spiro*[9H-fluorene-9,5'(4'aH)-pyrrolo[1,2-b]pyridazine]-6',7'-dicarboxylic acid, 6',7'-dimethyl ester (1.3.1a (2^{DHI}))[4,5]

Synthetic procedure: *Spiro*[2-cyclopropene-1,9'-[9H]fluorene]-2,3-dicarboxylic acid, 2,3-dimethyl ester **1.3.3** (0.5 g, 1.6 mmol) was dissolved in 50 mL of dry diethyl ether and 116 μL (0.138 g, 1.6 mmol) of pyridazine in 5 mL of dry diethyl ether was added drop wisely in the solution. The mixture was kept stirring for overnight at RT under argon atmosphere and dark. The reaction was monitored by TLC. The reaction was completed on next day (24 hours) and the solution was concentrated up to half via rotary evaporation. The concentrated solution was kept in refrigerator for overnight which gave yellow crystalline compound **1.3.1a** *spiro*[9H-fluorene-9,5'(4'aH)-pyrrolo[1,2-b]pyridazine]-6',7'-dicarboxylic acid, 6',7'-dimethyl ester and separated by filtration. The yield of reaction is quantitative as monitored by TLC and NMR. R_f: 0.2 TLC Silica, 4/1 (*n*-hexane/EtOAc, v/v). mp 142-143 ºC; IR (KBr) wavenumbers cm^{-1} 737, 1122, 1188, 1255, 1439, 1593, 1696, 1751, 2950, 3016; ^{1}H NMR ($CDCl_3$, 400 MHz) δ [ppm] 3.3 (s, 3H), 4 (s, 3H), 4.9 (dt, *J* = 9.9 and 2.2 Hz, 1H), 5.2 (t, *J* = 2.6 Hz, 1H), 5.6 (dt, *J* = 9 and 0.7 Hz, 1H), 6.9 (dd, *J* = 3.3 and 1.5 Hz, 1H), 7.2 (t, *J* = 7.3Hz, 1H), 7.3-7.4 (m,3H), 7.46 (d, *J* = 7.1Hz, 1H), 7.55 (d, *J* = 7.3, 1H), 7.7 (d, *J* = 7.1 Hz, 2H); ^{13}C NMR ($CDCl_3$, 400 MHz) δ [ppm] 51.35, 53.54, 63.66, 65.68, 106.30, 118.61, 120.06, 120.40, 123.73, 124.89, 126.21, 127.38, 128.05, 128.48, 128.81, 138.66, 140.68, 141.10, 141.77 146.71, 149.65, 162.02 163.61; Mass, ESI $C_{23}H_{18}N_2O_4$ calculated m/z 386.12, found 387.3(M+1) and 409.2 (M+Na)

1.3.2.4 Kinetic ^{1}H NMR Experiments and Identification of the trans-Betaine

Stock solutions of pyridazine (**1.3.2**) and *spiro*[2-cyclopropene-1,9'-[9H]fluorene]-2,3-dicarboxylic acid, 2,3-dimethyl ester (**1.3.3**) in $CDCl_3$ (1 mmol each) were prepared and stored in a water bath at 283K, 293K, 303K or 313K. 2.0 mL of each stock solution were mixed using an Eppendorf pipette and then filled in a pyrex NMR tube. ^{1}H-NMR measurements were performed using a 400 MHz Varian-NMR-spectrometer. The precision of its temperature units was ±0.5 K. Integration of the characteristic methylester peaks of the spirocyclopropene (**1.3.3**) as a function of reaction time permitted the determination of the kinetics and the Eyring-activation parameters.[10]

1.3.2.5 Steady-State Absorption and Photolysis

Acetonitrile was used as solvent. The irradiation wavelength was 355 nm. The laser intensity was tuned from 1 mW to 150 mW by combination of neutral density filter and laser output. The absorption spectra of the DHI/betaine system ($2^{DHI}/2^{betaine}$) at the different irradiation time were recorded using a HP 8543A UV-Vis spectrometer. During the photolysis, the solution was constantly stirred.

1.3.2.6 Laser Flash Photolysis

Transient absorption spectra and lifetimes were measured on a home-built instrument pumped by a frequency tripled (355 nm) Spectra-Physics GCR-150 Nd: YAG laser (fwhm 8 ns, 5 mJ per pulse unless indicated otherwise). The output from a 150W Xe arc lamp (USHIO) powered by a PTI PS-220 power supply, pulsed with electronics built in-house, was focused onto the sample at 90° with respect to the laser beam. The white light transmitted by the sample was collimated and focused onto the entrance slit of a Spex HR-20 single monochromator (1200 gr/mm) and was detected utilizing a Hamamatsu R928 photomultiplier tube and processed by a Tektronics 400 MHz oscilloscope (TDS 380).[14,16]

1.3.3 Results and Discussion

1.3.3.1 Kinetics of the spirodihydroindolizine (DHI) formation.

^{1}H-NMR spectroscopy was used to study the kinetics of the electrocyclic addition of pyridazine **(1.3.2)** to *spiro*[2-cyclopropene-1,9'-[9H]fluorene]-2,3-dicarboxylic acid, 2,3-dimethyl ester **(1.2.3)** in $CDCl_3$. The integration of the typical methylester peak of (**1.2.3**) and of pyridazine **(1.3.2)** was used to measure the concentrations of the reactants as a function of time. We used our data on the consumption of **(1.2.3)** to determine the reaction order of the addition reaction. The general reaction scheme of the nucleophilic addition reaction is shown in **Scheme 1.11**. The addition of pyridazine **(1.3.2)** to *spiro*[2-cyclopropene-1,9'-[9H]fluorene]-2,3-dicarboxylic acid 2,3-dimethyl ester (**1.2.3**) is a bimolecular reaction, as the plot of the inverse concentration of (**1.2.3**) *vs*. time indicates (**Figure 1.12**). This finding is in contrast to the addition of pyridine to (**1.2.3**)[8], which did result in a pseudo first order reaction ($k_2 > k_1$) in the temperature range from 283 to 313 K, although the two reactants ((**1.2.3**) and pyridine)) were added in the same concentration. For the addition of pyridazine, which is reported here, k_1 is larger than k_2, thus making the first step of the reaction rate determining (at 283 K, $k_1 = 1.17 \pm 0.2 \times 10^{-3}$ [l M^{-1} s^{-1}]).

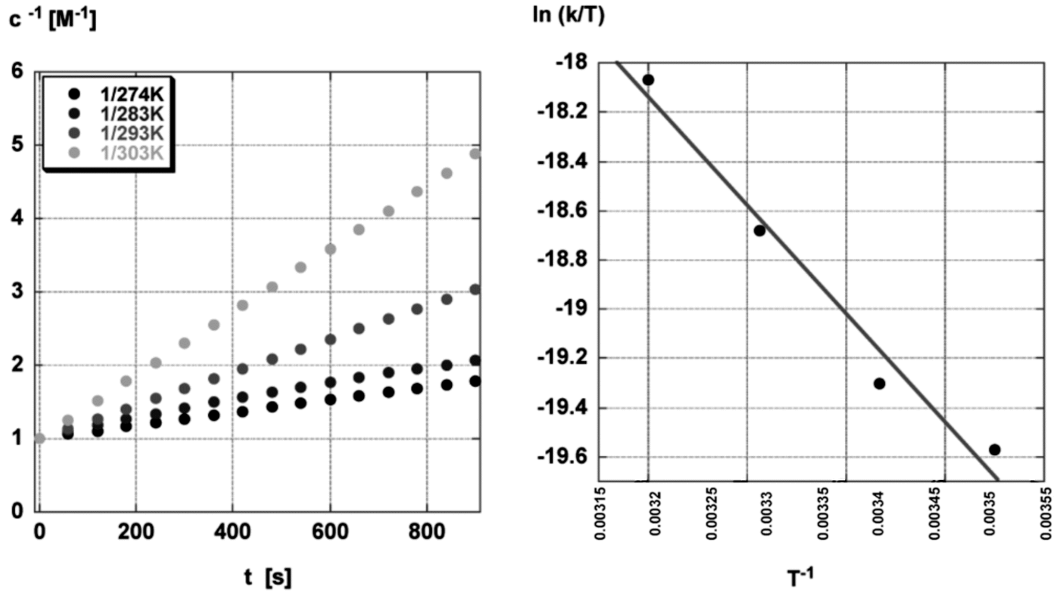

Figure 1.12: Right: The plot of c^{-1} *vs.* t is linear (r > 0.995 at all four temperatures). It indicates that the reaction is second order. The rate constants k [l M^{-1} s^{-1}] can be obtained from the negative linear slopes. Left: The Eyring-plot of the unimolecular rate constants, which have been obtained from the bimolecular rate constants k [l M^{-1} s^{-1}] by multiplication with the concentration of compound (1.3.2) (c = 1.0 x 10^{-3} M) is sufficiently linear (r = 0.995) to determine $\Delta H^{\#}$ and $\Delta S^{\#}$.

The Eyring equation is given as eq 1,

$$\ln\left(\frac{k}{T}\right) = \frac{-\Delta H^{\#}}{RT} + \frac{\Delta S^{\#}}{R} + \ln\frac{k_b}{h} \qquad (1)$$

Where k represents the rate constant of the reaction, T is the temperature, $\Delta H^{\#}$ the enthalpy of activation, $\Delta S^{\#}$ the entropy of activation, k_b the Boltzmann constant (1.3806504 x 10^{-23} in J K^{-1}) and *h* the Planck constant (6.626068 × 10^{-34} m^2 kg s^{-1}).[10]

Eq 1 was used to calculate $\Delta H^{\#}$ = 528±32 J mol^{-1}, $\Delta S^{\#}$ -228±11 J mol^{-1} K^{-1} and (at 300 K) $\Delta G^{\#}$ = 69±4 kJ mol^{-1}. The very low enthalpy of activation in combination with the rather

large entropy of activation are in agreement with the nucleophilic addition of aromatic heterocycle pyridazine (**1.3.2**) to *spiro*[2-cyclopropene-1,9'-[9H]fluorene]-2,3-dicarboxylic acid 2,3-dimethyl ester (**1.2.3**).

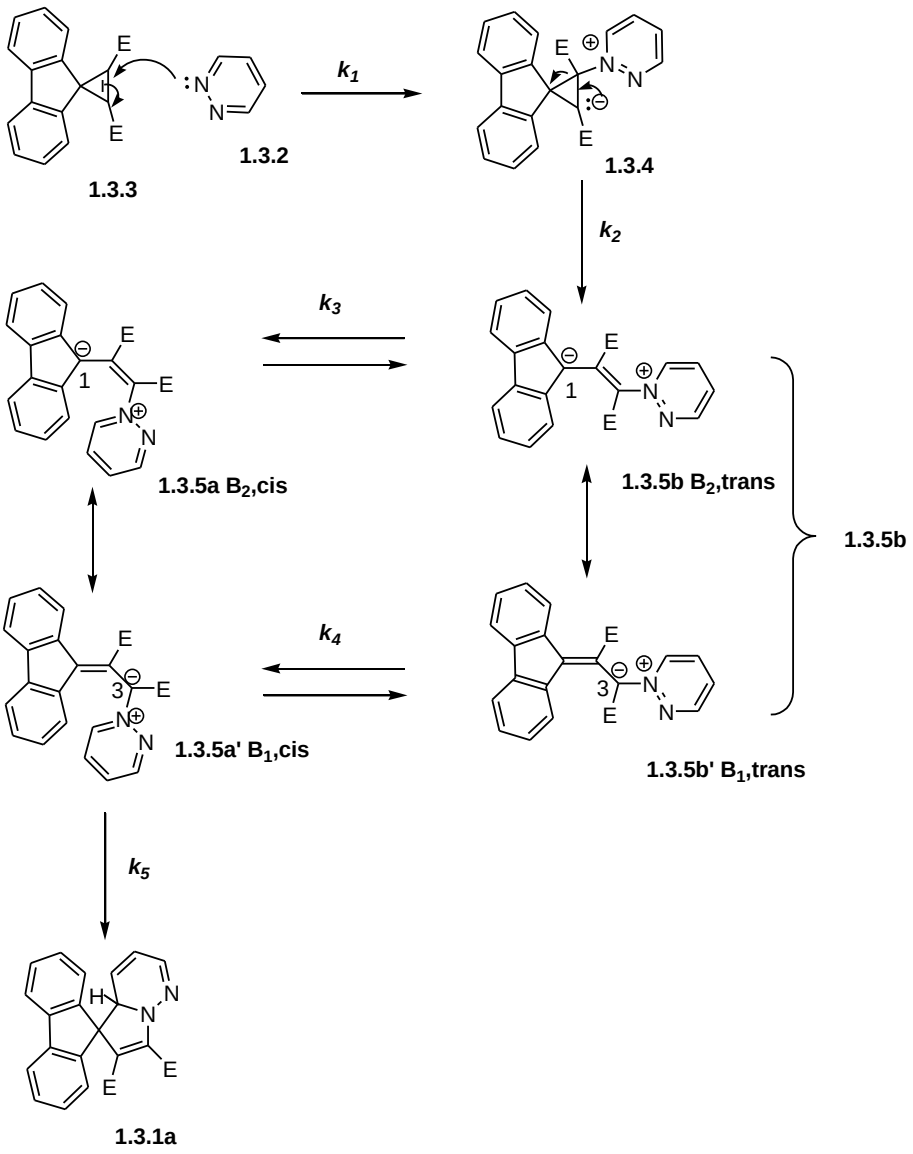

Scheme 1. 12: Nucleophilic addition of pyridazine (1.3.2) to *spiro*[2-cyclopropene-1,9'-[9H]fluorene]-2,3-dicarboxylic acid, 2,3-dimethyl ester (1.3.3): The reaction proceeds in three steps: 1) Addition of pyridine to the highly strained cyclopropene intermediate 2) (1,5-electrocyclic) ring-opening to the *trans*-betaine $B_{2,trans}$ (2^{B}, 1.3.5b). 3) Isomerization to $B_{1,trans}$ and $B_{1,cis}$ and 1,5-electrocylic ring closure to the DHI (2^{DHI}, 1.3.1a).

1.3.3.2 Analysis of the ^{1}H-NMR spectra during the nucleophilic addition of heterocyclic bases to spiro[2-cyclopropene-1,9'-[9H]fluorene]-2,3-dicar-boxylic acid, 2,3-dimethyl ester (1.3.3)

The kinetic findings have been corroborated by the analysis of the ^{1}H-NMR spectra during the addition of pyridine and pyridazine to c *spiro*[2-cyclopropene-1,9'-[9H]fluorene]-2,3-dicarboxylic acid, 2,3-dimethyl ester (**1.2.3**). Stacked ^{1}H NMR spectra in were recorded at 303 K **(Figures 1.13** and **1.14**).

The kinetics of the addition of pyridine to *spiro*[2-cyclopropene-1,9'-[9H]fluorene]-2,3-dicarboxylic acid, 2,3-dimethyl ester **(1.2.3)** do not permit discerning the spectrum of the pure betaine due to overlapping peaks with the DHI. However, both methyl ester peaks of (**1.2.3**) appear at the same ^{1}H-NMR-frequency (δ = 3.83 ppm), two singlets can be discerned for the "pyridine-DHI" (1^{DHI}) (δ = 3.25 and 3.98 ppm). At all times, there is only one set of signals for the "pyridine-betaine" (1^{B}) (δ = 3.29 and 3.88 ppm) discernible, indicating that indeed only one betaine is stable between 283 K and 313 K (**Figure 1.13**). This betaine had been assigned to $B_{1,trans}$ (**Scheme 1.12**).[8]

It is noteworthy that the addition of pyridine to *spiro*[2-cyclopropene-1,9'-[9H]fluorene]-2,3-dicarboxylic acid, 2,3-dimethyl ester **(1.2.3)** was completed after 13 min. at 303 K, whereas the addition of pyridazine took several hours to completion. This is in agreement with the observed kinetics: pseudo-first order for the addition of pyridine (k_2 = 2.23 x 10^{-3} s^{-1} (at 283 K)) and bimolecular for the addition of pyridazine (k_1 = 1.17$\pm$0.2 x 10^{-3} [l M^{-1} s^{-1}]), (**Scheme 1.12**). A mechanistic reason for the much faster reactivity of pyridine compared to pyridazine can be found in the electron densities of the sp^2-hybridized aromatic ring nitrogen atoms: according to *Gaussian 03*, an atomic net charge of -0.088 is calculated for pyridine, whereas the neighboring nitrogen in pyridazine bear significantly smaller negative partial charges (-0.021 and -0.025). A successful nucleophilic attack of a heterocyclic base on compound (**1.2.3**) requires a high electron density in the lone pair of the nitrogen, which is a part of an aromatic heterocyclic ring. The atomic net charge is a simple measure for a relative comparison of these electron densities in pyridine and pyridazine. The former is a much better nucleophile and, therefore, k_2 and not k_1 is

rate-determining. The latter is an inferior nucleophile. Therefore, the addition process itself (k_1) is rate-determining.

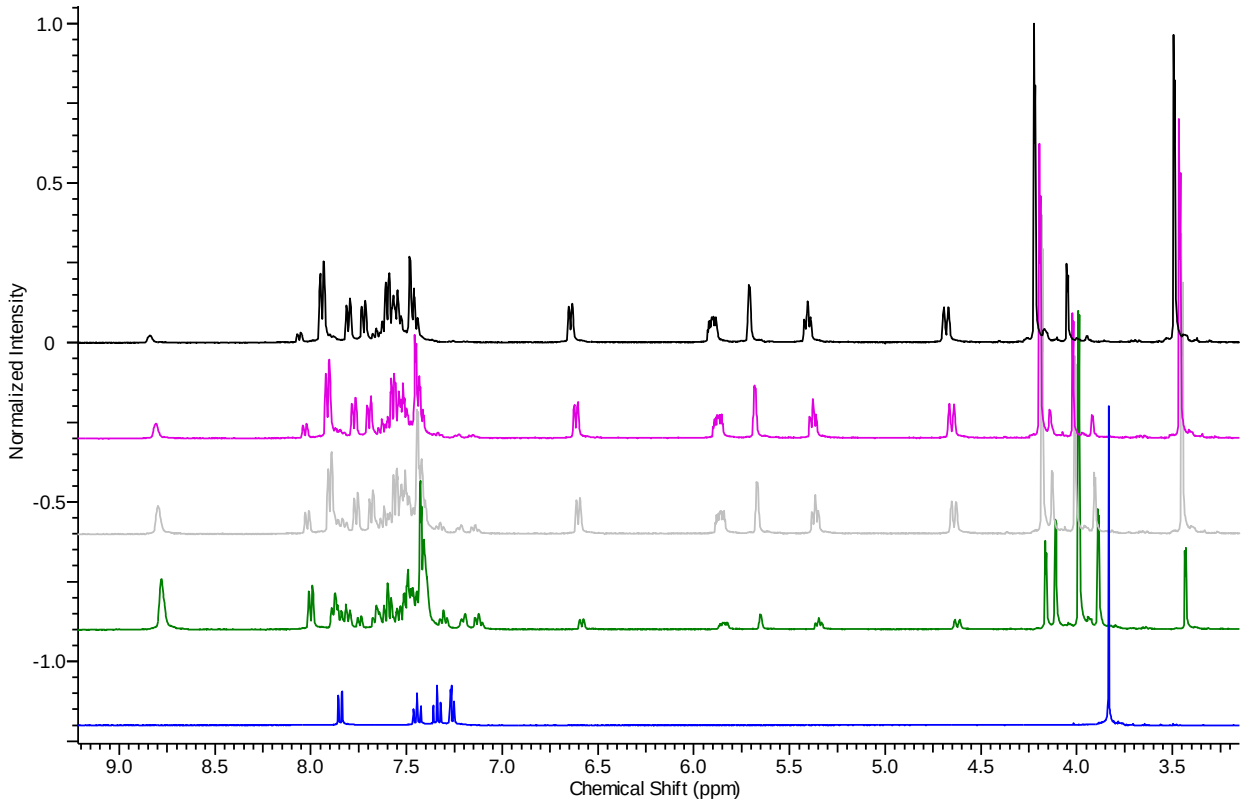

Figure 1.13 ^{1}H-NMR spectra of the reaction mixture between *spiro*[2-cyclo-propene-1,9'-[9H]fluorene]-2,3-dicarboxylic acid, 2,3-dimethyl ester (1.2.3) and pyridine in $CDCl_3$ at T = 303 K, t = 1,4,7,13 min. in increasing order

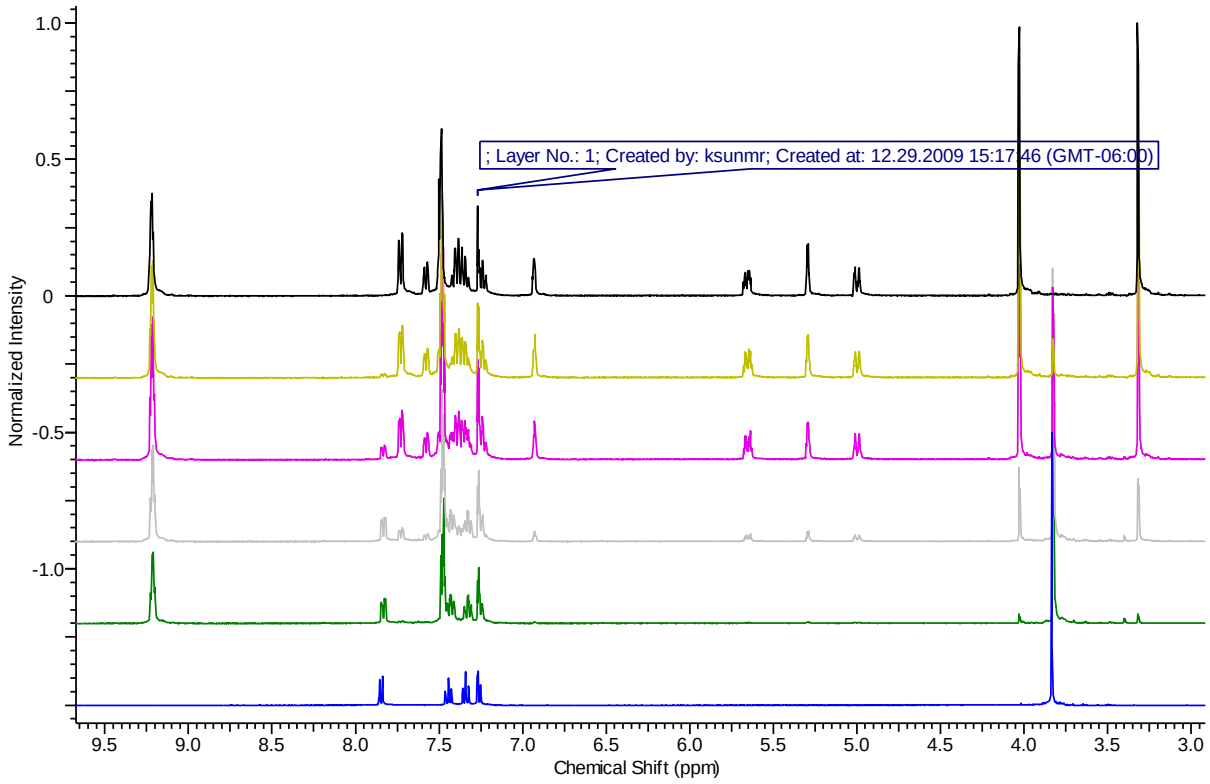

Figure 1.14 **^{1}H-NMR spectra of the reaction mixture between *spiro*[2-cyclo-propene-1,9'-[9H]fluorene]-2,3-dicarboxylic acid, 2,3-dimethyl ester (1.2.3) and pyridazine (1.3.2) in $CDCl_3$ at T = 303 K, t = 1,10,45, 95 min. and 15 h. in increasing order.**

It is noteworthy that virtually no (betaine-) intermediate is visible in the ^{1}H-NMR during the progress of the addition reaction of pyridazine to compound (**1.2.3**) under these experimental conditions. This demonstrates nicely that $k_1 << k_2$.

1.3.3.3 DFT Calculations

This report discusses the application of computational methods for the determination of the exact electronic structures and the relative stabilities of the DHIs and the *cisoid*, *transoid* isomers of the corresponding betaines. The DFT calculation results clearly indicate that the long-standing hypothesis concerning the most stable Lewis structures of the zwitterionic betaines, which are formed upon photoexcitation of the photochromic dihydroindolizines, has to be corrected.

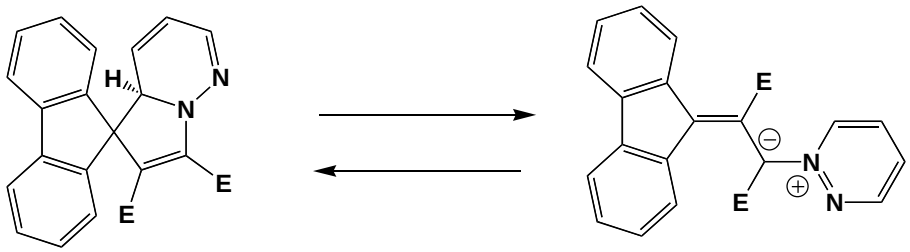

Figure 1.15*:* Interconversion of "*spiro*" and "betaine" forms of *spiro*[9,1'(8'aH)-indolizine]-2',3'-dicarboxylic acid, dimethyl ester (E=C(O)OCH$_3$) (1.3.1).

In looking for possible zwitterionic character of the betaine systems, all starting geometries assumed single C_1C_2 and C_3N_4 bonds and a double C_2C_3 bond for the open-chain forms (see $B_{2,cis}$ and $B_{2,trans}$ in **Scheme 1.9**). However, the optimized geometries in none of the cases have retained the suggested single-double-single bond character.[17,18] On the contrary, significant delocalization can be deduced from optimized bond lengths discussed in chapter **1.2**.

1.3.3.4 Photophysical Measurements

According to our reaction paradigm[8,19], the conrotatory ring-opening reaction of *spiro*-dihydroindolizines to their isomeric betaines is an adiabatic photoreaction. Whereas the absorption maxima of DHIs are typically in the UVA and blue spectral regions, betaines are highly colored and possess unusually broad absorption spectra, in spite of the fact that this absorption arises from a singlet state. The disrotatory back reaction proceeds thermally from the *cisoid* betaine ($B_{1,cis}$ in **Scheme 1.9**) to the DHI. This reaction proceeds much faster than the thermal isomerization between the *transoid* ($B_{1,trans}$) and the *cisoid* ($B_{1,cis}$) betaine-isomer, which appears to be the rate-limiting step for the back-reaction.

Table 1.6*:* Photophysical Data for DHI (2^{DHI}) and *transoid* Betaine (2^{B})

DHI					*Transoid* Betaine[20]			
λ_{abs} [nm]	log ε^{20}	λ_{em} [nm]	Φ_{EM}	λ_{em} [nm]	λ_{max} [nm]	λ_{em} [nm]	log ε	Φ_{EM}
389	3.92	462	0.0017	460	514	484	.29	0.0038

1.3.3.4.1 Steady-state Fluorescence of the "pyridazine-DHI" (2^{DHI})

It is known from the literature that the "pyridazine-DHI" (2^{DHI}) is weakly fluorescent.[8] Excitation and fluorescence spectra were recorded in a temperature interval between 283 K and 323K. It is noteworthy that the observed systematic shifts of both the excitation and emission maxima happen as a function of temperature (283 K: λ_{EX} = 345 nm, λ_{EM} = 465 nm; 293 K: λ_{EX} = 342 nm, λ_{EM} = 468 nm; 303 K: λ_{EX} = 341 nm, λ_{EM} = 466 nm; 313 K: λ_{EX} = 340 nm, λ_{EM} = 473 nm; 323 K: λ_{EX} = 337 nm, λ_{EM} = 477 nm). The maximum of excitation is blueshifted, whereas the maximum of emission is red-shifted (**Figure 1.16**). This may be indicative of more than one fluorescent state of the DHI and the existence of a small thermal activation barrier between at least two states.

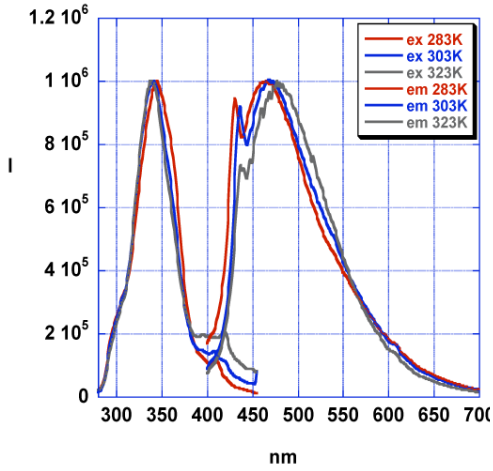

Figure 1.16 Excitation and fluorescence spectra of 2^{DHI} (5.0 x 10^{-5} M in acetonitrile) at T = 283, 303 and 323 K.

Note that the fluorescence occurring from the DHI (τ_F << 0.4ns) and the kinetics of the photochemical 1,5-electrocyclization (τ_R > 0.5ns) cannot occur from the same singlet state.[21] Otherwise, the rate constant for cyclization would have to compete with the rate of fluorescence. Therefore, the state that reacts under electrocyclic ring-opening must be separated by a rather large activation barrier from the fluorescent states.

1.3.3.4.2 Time-Resolved Absorption Spectroscopy of the Betaines

The transient absorption spectra measured following excitation 0.10 mM DHI in acetonitrile with a laser pulse (355 nm, fwhm ~ 8 ns) are shown in **Figure 1.17**. Spectra were collected immediately and 300 μs after excitation. The spectra are characterized by a peak at 460 nm and a broad absorption with maximum in the range of 540 to 580 nm immediately after excitation. After 300μs, the peak at 460 nm is still discernible (although it has considerably decayed. The broad peak has become even broader (500 to 580 nm) with an emerging maximum at 510 nm, which corresponds to the *transoid* form of the betaine (514 nm, **Figure 1.17**). The changes in the absorbance as a function of time decay monoexponentially with lifetime of 254 μs at 460 nm and 228 μs at 600 nm.

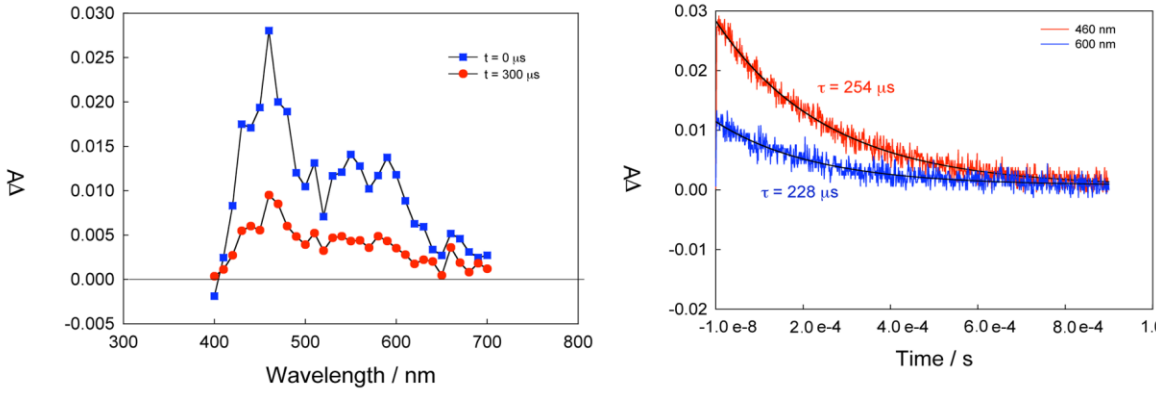

Figure 1.17 Transient absorption spectroscopy of the "pyridazine-betaine" (2^B)

It is noteworthy that the ratio of the absorbance at 460 nm and 600 nm ($\Delta A_{460/600}$) is greater immediately following the laser pulse than after 300 μs, indicating that two different species may be present in solution, with different concentrations at these two times. A possible explanation for this observation is the coexistence of the *cisoid* and the *transoid* betaine in this time domain.[8] On the minute timescale only the *transoid* betaine isomer is present. Only *cisoid* betaine possesses the right geometry for the disrotatory back reaction and decays with τ = 254 μs to regenerate the DHI. Based on the spectra shown in **Figure 1.17**, it appears that the *cisoid* species, representing most of the sample at t = 0, absorbs more strongly at 460 nm than the

transoid isomer. It should also be noted that the absorption signals at 460 nm and 600 nm do not completely return to zero after 900 ms, with ~5% absorbance from the initial ΔA remaining. We attribute this finding to the residual *transoid* betaine that does not decay within the window of observation. The life-time of the electrocyclization process from the *cisoid* betaine to the DHI at 293 K is 254 ± 10 μs, whereas the life-time of the back reaction from the *transoid* betaine to the DHI is 216±5 s (**Figure 1.17**).

The photophysical behavior of the "pyridazine-DHI/betaine system ($2^{DHI}/2^{B}$) is very similar to the previously reported photochemical reactivity of the "pyridine-DHI/betaine system ($1^{DHI}/1^{B}$) (chapter **1.2**), indicating that an additional ring-nitrogen in the neighboring position to the attached nitrogen does not alter the photochemical reactivity completely. Furthermore, the presence of two ring-nitrogens significantly decreases the reactivity of the betaine with triplet oxygen.[8,19] We estimate that the "pyridazine-betaine" is approximately 50 times more stable than the "pyridine-betaine". It should be noted that the reaction of *spiro*[2-cyclopropene-1,9'-[9H]fluorene]-2,3-dicarboxylic acid, 2,3-dimethyl ester (**1.3.3**) with pyrimidine and pyrazine does not lead to stable and photochromic *spiro*-dihydroindolizines.

1.3.3.4.3 The Kinetics of the Thermal Back Reaction

Table 1.6 summarizes the relevant photophysical parameters of DHI and betaine. The spectral features of *transoid* betaine are observed following photolysis of a DHI ($\mathbf{2^{DHI}}$) solution with laser light (355 nm) for 3 min, and are shown in the spectrum at t = 0 in **Figure 1.17**. The changes to the absorption were monitored as a function of time while the sample was kept in the dark at 283 K. The observed spectral changes correspond to the thermal back reaction from betaine ($\mathbf{2^{B}}$) to DHI ($\mathbf{2^{DHI}}$). The unimolecular thermal back reaction in acetonitrile at 283 K has a rate constant of 1.98 x 10^{-3} s^{-1}, which is in excellent agreement with the literature.[21] Note that this value corresponds to k_4 in **Scheme 1.13**.

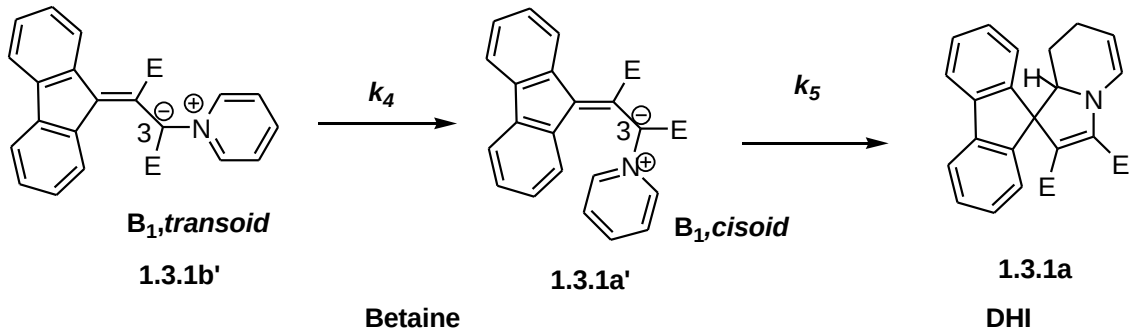

Scheme 1. 13: The thermal back reaction is slow for the transoid→ cisoid isomerization.

The Eyring-plot derived from these data is also shown in **Figure 1.18**. The thermal activation parameters were calculated to be $\Delta H^{\#}$ = 839±14 J mol^{-1}, $\Delta S^{\#}$ = -303±12 J $K^{-1}mol^{-1}$, and $\Delta G^{\#}$ = 89,600 J mol^{-1} (at 293 K). A positive activation enthalpy and negative activation entropy indicate the reaction from the *transoid* betaine towards the DHI passes through an ordered transition state. However, our time-resolved data indicate that not the DHI but the *cisoid* betaine is formed in this thermal *transoid*/*cisoid* isomerization reaction. The Eyring-parameters that we have determined are for the hindered rotation between both betaines and not for the disrotatory 1,5-electrocyclization. The latter reaction occurs from the *cisoid* betaine to the DHI. Whereas the *transoid*/*cisoid* isomerization reaction for the "pyridazine-betaine" has a lifetime of 216 s at 293 K, the electrocyclic reaction from the *cisoid* betaine to the DHI has a lifetime of 254 μs. This means it occurs approximately one million times faster!

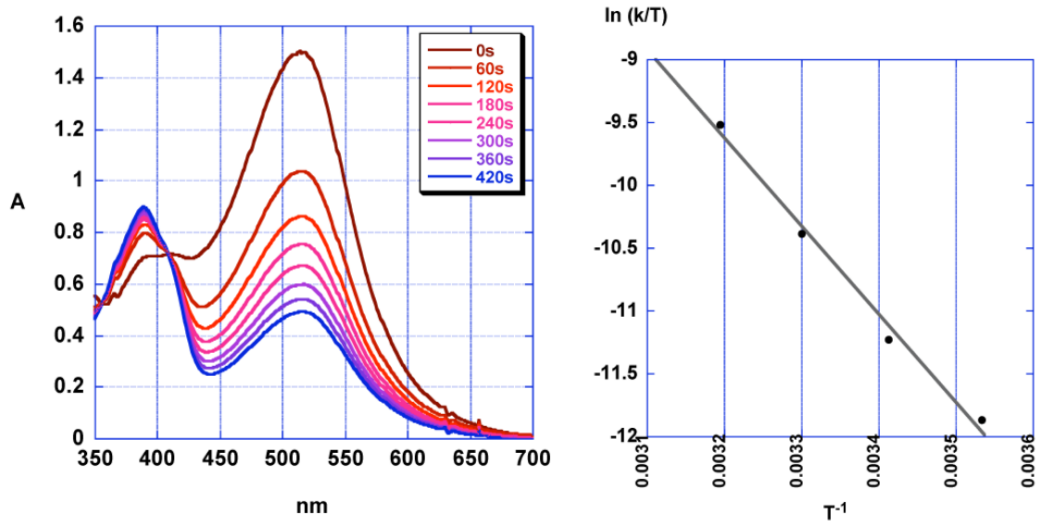

Figure 1.18 left: Changes to the UV/Vis spectrum of Betaine (t = 0) as a function of time regenerating DHI at 283 K in acetonirile. Note that the conversion from DHI to betaine is ~ 60 %, therefore the spectrum at t = 0 has contributions from DHI in the region from 300 nm to 460 nm. The presence of two isosbestic points at 356 nm and 409 nm indicates a clean photochemical transition. right: Eyring-plot derived from data obtained in the temperature interval 283 - 313K.

1.3.4 Conclusions

The experimental results obtained in this study permit the conclusion that the "pyridazine-DHI (*spiro*[9H-fluorene-9,5'(4'aH)-pyrrolo[1,2-b]pyridazine]-6',7'-dicarboxylic acid, 6',7'-dimethyl ester, $\mathbf{2}^{\mathbf{DHI}}$) and its *cisoid* and *transoid* betaines ($\mathbf{2}^{\mathbf{B}}$) react according to the new paradigm describing the photochemical reactivity of the DHI/Betaine system that has been developed studying the most simple "pyridine-DHI" ($\mathbf{1}^{\mathbf{DHI}}$) (**Scheme 1.10**).[8] Upon photoexcitation of DHI an adiabatic photoreaction occurs. The excited state-reaction finds the lowest point of the potential-energy surface, which acts as a "sinkhole".[10] The deactivation leads to a "mound", which is the ground-state activation barrier between the *cisoid* and the *transoid* betaine.[10] The position of the funnel in the case of the DHI/betaine system studied here is very similar the previously investigated system. Consequently, approximately 95 percent of *cisoid* betaine and 5 percent of *transoid* betaine are formed here as well. The 1,5-electrocyclic ring-closure to the DHI occurs from the *cisoid* betaine with a lifetime of 254 μs at 293 K. In sharp

contrast, the lifetime of the *transoid* betaine is 216 s. It reacts in a thermal *cisoid*/*transoid* isomerization reaction to the *cisoid* betaine, which then proceeds to the DHI. It is of importance for the mechanistic discussion of photochromic spirodihydroindolizine/betaine systems that the Eyring activation parameters that have been attributed to the electrocyclic ring closure in basically all mechanistic papers are in reality for the *transoid*/*cisoid* isomerization of the betaine!

1.3.5 References

1. (a) Hauck, G.; Duerr, H. *Angewandte Chemie* **1979**, *91,* 1010-11, Gross, H.; Duerr, H. (b) *Angewandte Chemie* **1982**, *94*, 204-5.
2. Duerr, H. *Angewandte Chemie* **1989,** *101*, 427-45.
3. (a) Ahmed, S. A.; Moussa, Z.; Al-Raqa, S. Y.; Alamry, S. N. *J. Phys. Org. Chem.* **2009**, *22*, 593-606. (b) Ahmed, S. A. *Tetrahedron* **2009**, *65*, 1373-1388. (c) Straight, S. D.; Andreasson, J.; Kodis, G.; Moore, A. L.; Moore, T. A.; Gust, D. *J. Am. Chem. Soc.* **2005**, *127*, 2717-2724. (d) Kodis, G.; Terazono, Y.; Liddell, P. A.; Andreasson, J.; Garg, V.; Hambourger, M.; Moore, T. A.; Moore, A. L.; Gust, D. *J. Am. Chem. Soc.* **2006**, *128*, 1818-1827. (e) Straight, S. D.; Andreasson, J.; Kodis, G.; Bandyopadhyay, S.; Mitchell, R. H.; Moore, T. A.; Moore, A. L.; Gust, D. *J. Am. Chem. Soc.* **2005**, *127*, 9403-9409. (f) Andreasson, J.; Terazono, Y.; Albinsson, B.; Moore, T. A.; Moore, A. L.; Gust, D. *Angew. Chem. Int. Ed.* **2005**, *44*, 7591-7594.(g) Andreasson, J. Straight, S. D.; Kodis, G.; Park, C.-D.; Hambourger, M.; Gervaldo, M.; Albinsson, B.; Moore, T.; Moore, A. L.; Gust, D. *J. Am. Chem. Soc*. **2006**, *128*, 16259-16265. ; (i) Andreasson, J.; Straight, S. D.; Bandyopadhyay, S.; Mitchell, R. H.; Moore, T. A.; Moore, A. L.; Gust, D. *Angew. Chem. Int. Ed.* **2007**, *46*, 958-961. (j) Andreasson, J.; Straight, S. D.; Moore, T. A.; Moore, A. L.; Gust, D. *J. Am. Chem. Soc.* **2008**, *130*, 11122-11128.
4. (a) Duerr, H.; Gross, H.; Zils, K. D.; Hauck, G.; Klauck, G.; Hermann, H. *Chemische Berichte **1983**, 116,* 3915-25. (b) Ahmed, S. A.; Abdel-Wahab, A.-M. A.; Duerr, H. *J. Photochem. Photobiol. A: Chem*. **2003**, *154*, 131-144.
5. Duerr, H.; Schommer, C.; Muenzmay, T. *Angewandte Chemie **1986**, 98,* 565-7.

6. Duerr, H.; Thome, A.; Steiner, U.; Ulrich, T.; Kruger, C.; Raabe, E. *J. Chem. Soc. Chem. Commun.* **1988**, 338-40.
7. Crano, J. C.; Guglielmetti, R. J. *Organic Photochromic and Thermochromic Compounds Volume 1: Main Photochromic Families.* Plenum Press, New York, **1999**, pp 378.
8. Shrestha, T. B.; Melin, J.; Liu, Y.; Dolgounitcheva, O.; Zakrzewski, V. G.; Pokhrel, M. R.; Gogritchiani, E.; Ortiz, J.V.; Turro, C.; Bossmann, S. H. *Photochem. Photobiol. Sci.* **2008,** *7*, 1449-1456.
9. Bouas-Laurent, H.; Durr, H. Organic photochromism. *Pure Appl. Chem.* **2001**, *73*, 639-665.
10. Turro, N. J. *Modern Molecular Photochemistry*, Addison-Wesley Publishing Co., Reading, Mass, **1978**, pp 628.
11. Bradley, P. M.; Bursten, B. E.; Turro, C. *Inorg. Chem.* **2001**, *40*, 1376-1379.
12. GAUSSIAN *03*, (Revision C.02): Gaussian, Inc, Wallingford, CT, **2004**.
13. (a) Becke, A. D. *Phys. Rev. A* 1988, *38*, 3098-100. (b) Lee, C.; Yang, W.; Parr, R. G. *Phys. Rev. B* **1988**, *37*, 785-9.
14. Krishnan, R.; Binkley, J. S.; Seeger, R.; Pople, J. A. *J. Chem. Phys.* **1980**, *72*, 650-4.
15. Warren, J. T.; Chen, W.; Johnston, D. H.; Turro, C. *Inorg. Chem.* **1999**, *38*, 6187-6192.
16. Caroll, F. A. *Perspectives on Structure and Mechanism in Organic Chemistry*, Brooks/Cole Publishing Company, Pacific Grove, Washington, *chapter 11*: *Concerted Reactions* **1998**.
17. (a) Besler, B. H.; Merz Jr., K. M.; Kollman, P. A., *J. Comp. Chem.* **1990**, *11*, 431-9. (b) Singh, U. C.; Kollman, P. A. *J. Comp. Chem.* **1984**, *5*, 129-145.
18. Cioslowski, J. *J. Am. Chem. Soc.* **1989**, *111*, 8333-6.
19. Hartmann, T.; Shrestha, T. B.; Bossmann, S. H.; Huebner, C; Renn, A; Duerr, H. *Photochem. Photobil. Sci.* **2009**, *8*, 1172-1178.
20. Bleisinger, H.; Scheidhauer, P.; Duerr, H.; Wintgens, V.; Valat, P.; Kossanyi, J. *J. Org. Chem.* **1998**, *63*, 990-1000.
21. Duerr, H. *Pure Appl. Chem.* **1990**, *62*, 1477-82.

1.4 Laser Femtosecond Absorption Spectroscopy of Spirodihydroindolizines

1.4.1 Laser sub-Picosecond Absorption Spectroscopy

Laser femtosecond absorption spectroscopy studies of *spiro*[9,1'(8'aH)-indolizine]-2',3'-dicarboxylic acid, dimethyl ester ("pyridine-DHI/betaine" ($1^{DHI}/1^{B}$) and *spiro*[9H-fluorene-9,5'(4'aH)-pyrrolo[1,2-b]pyridazine]-6',7'-dicarboxylic acid, 6',7'-dimethyl ester ($2^{DHI}/2^{B}$)were performed by Dr. Yao Liu in the research laboratories of Dr. Claudia Turro, Department of Chemistry, Ohio State University, Columbus Ohio. Femtosecond measurements permit the observation of the very first events, which take place after the absorption of a photon, which requires approximately 1 x 10^{-15} s to complete. The femtosecond absorption spectra were recorded by an instrument, which is described in detail in the literature (**Scheme 1.14**).[1] Syntheses of these two DHIs are described in chapter **1.2** and **1.3**.

1.4.2 Femtosecond Broadband UV-Vis Transient Absorption Spectrometer.

The laser system consists of a short pulse titanium-sapphire oscillator (Coherent, Mira) generating 30 fs pulses at 800 nm that seeds a high energy titanium-sapphire regenerative amplifier (Coherent/Positive Light, Legend HE USP). The regenerative amplifier produces 2.5 mJ, 40 fs pulses at 1 kHz. The main part of the beam is used to generate a pump pulse tunable from 240 to 800 nm. A small portion of the fundamental is used for white light generation in the range 320-700 nm by focusing a small portion of the fundamental output (800 nm, 1.5 μJ) into a 1 mm thick CaF_2 plate.

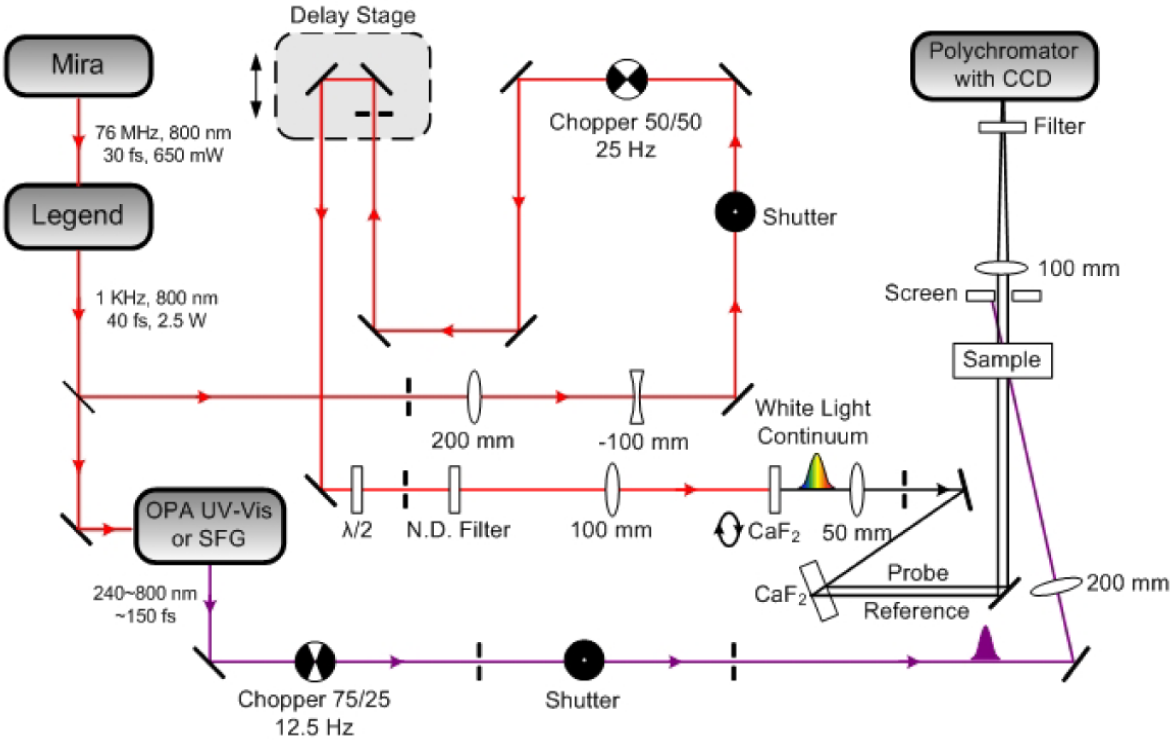

Scheme 1. 14: Femtosecond broadband UV-Vis transient absorption spectrometer (this figure is taken with permission from the supplemental information of reference 1)

A 50 mm lens collimates the white light continuum beam, which then passes through an iris to select the central, uniform region of the beam profile. The white light continuum is split into two parts, probe and reference, of nearly equal intensity by using reflection from the front (probe) and back (reference) surfaces of a 6 mm thick CaF_2 plate. Both beams pass through the sample, but only the probe overlaps with the pump beam in the sample. The detection system consists of an imaging polychromator (Triax 550 Jobin Yvon, equipped with holographic grating operating in 250-800 nm, 150 gr/mm) and thermoelectrically cooled, back illuminated CCD camera (Symphony Jobin Yvon, chip 2048, 512 pixels). Transient absorption spectra are recorded at different pump-probe delay times using an optical delay line consisting of computer-controlled, motorized translation stage mounted with a retroreflector. The entire set of pump-probe delay positions (cycle) is repeated at least three times, to observe data reproducibility from cycle to cycle. Spectra are recorded using home-developed software, written in Labview 7.0,

which also controls the optical delay line, shutters, CaF_2 rotation, and CCD acquisition. The instrument response fwhm is approximately 300 fs. All experiments are performed at room temperature (293 K).

1.4.3 Selection of Photochromic Spiro-Dihydroindolizine/Betaine Systems

Contrary to the approach chosen in the recent literature, in which a DHI/betaine featuring a methylcarboxylate-substituent has been studied (**3^{DHI}/3^{B}**, **Figure 1.19**) by femtosecond absorption and infrared spectroscopy[2], we have again investigated the unsubstituted "pyridine-system" (**1^{DHI}/1^{B}**), as well as the "pyridazine-system" (**2^{DHI}/2^{B}**), because their photochemical reactivities are not changed by the electronic and/or steric influence of substituents. The main result from reference 2 is that an electronically excited transient state ($B^{\dagger}$) has been observed. This is agreement with the novel paradigm for the photochemical DHI/betaine reactivity that has been published by our research group in 2008.[3] The second very important finding was that $B^{\dagger}$ also deactivates to the ground-state DHI. This finding is in agreement with the previously determined quantum yields for betaine-formation, which are in all cases distinctly smaller than 1.0.[4] The electronically excited transient state ($B^{\dagger}$) deactivates through a "funnel" reaching a "mound" (thermal activation barrier), which separates the *cisoid* and the *transoid* isomers of the betaine.[3,5] We will revisit this paradigm after discussing our experimental findings.

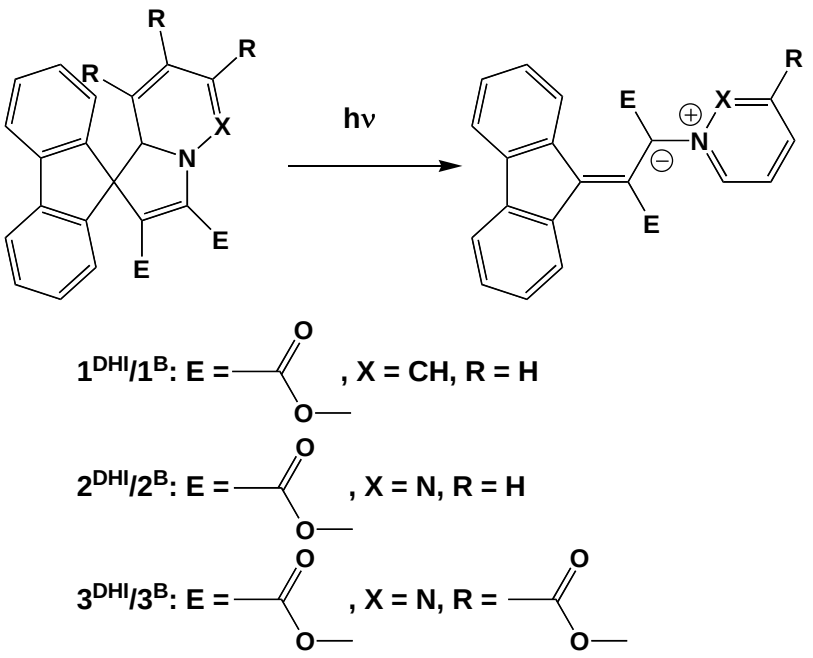

Figure 1.19 DHI/betaine – systems studied here (1^{DHI}: *spiro*[9,1'(8'aH)-indolizine]-2',3'-dicarboxylic acid, "pyridine-DHI"), 2^{DHI}: *spiro*[9H-fluorene-9,5'(4'aH)-pyrrolo[1,2-b]pyridazine]-6',7'-dicarboxylic acid, 6',7'-dimethyl ester, "pyridazine-DHI"), and in the literature 3^{DHI} (trimethyl-1'H-*spiro*[9H-fluorene-9,5'(4'aH)-pyrrolo[1,2-b]pyridazine]-2,3,6'-tricarboxylate, "methylcarboxylate-pyridazine-DHI").[2]

1.4.4 Spiro[9,1'(8'aH)-indolizine]-2',3'-dicarboxylic acid: Early Photochemical Events

After photoexcitation by one photon[3] of 310 nm wavelength, a very broad UV/Vis-absorption band between 400 nm and 600 nm rises leading to a maximum of absorption after 0.60 ps (λ_{max} = 455 nm). This band is neither consistent with the absorption spectra of the *cisoid* or the *transoid* betaine, which occur at a much later time scale.[3,6] It is noteworthy that in the high energy region of the spectrum big changes in absorption are observable, whereas we cannot discern such changes in the mid- and low-energy regions. This finding is consistent with the postulation of several states in a photoexcited DHI: After the absorption of a UV-photon (λ = 310 nm), at least two singlet states exist: one is reactive and the other (or quite possibly, several others) deactivate(s) under emission of a photon (fluorescence).[6] Note that the fluorescence occurring from the DHI (τ_F > 400 ps) and the kinetics of the photochemical 1,5-electrocyclization

(τ_R = 70-80 ps, see below) cannot occur from the same singlet state, because their time-scales do not match. Otherwise, the rate constant for cyclization would have to compete with the rate of fluorescence. Therefore, the state that reacts under electrocyclic ring-opening must be separated by a rather large activation barrier from the fluorescent state.

After the maximum intensity of the UV/Vis-absorption band has been reached after 0.6 ps, its absorbance decreases and a consecutive red-shift is observed: 0.7 ps, λ_{max} = 440 nm; 0.9 ps, λ_{max} = 445 nm; 1.2 ps, λ_{max} =455 nm). The absorption-spectra at 1.2 ps, 1.4 ps, and 1.6 ps are nearly identical in the wavelength region between 400 nm and 600 nm. In agreement with reference 2, we interpret these spectral shifts and intensity changes as vibrational deactivation of the transient state $B^{\dagger}$. After 1.2 ps, the vibrational deactivation of $B^{\dagger}$ is completed and the system remains in that state for up to 2 ps (**Figure 1.20**) before it further reacts. Note that the maximum of the "pyridine-DHI" absorption occurs at 382 nm (log ε = 4.02). At the very first delays of 0.2 ps and 0.4 ps no distinct bleach in the spectral region between 380 nm and 400 nm can be discerned, indicating that the DHI/betaine-system is on the reaction trajectory toward $B^{\dagger}$, but not there yet. It is our mechanistic assumption that we are looking at a transition that can be described by the Eyring theory of reacting states.[7] It is noteworthy that the negative intensity of the DHI-maximum remains constant in a time range between 0.6 ps and 2.0 ps. This is a strong indication that during that time period no back-reaction from $B^{\dagger}$ to the DHI can be observed. This is a strong argument for the assignment of $B^{\dagger}$ as a possible intermediate and not as a transition state![8]

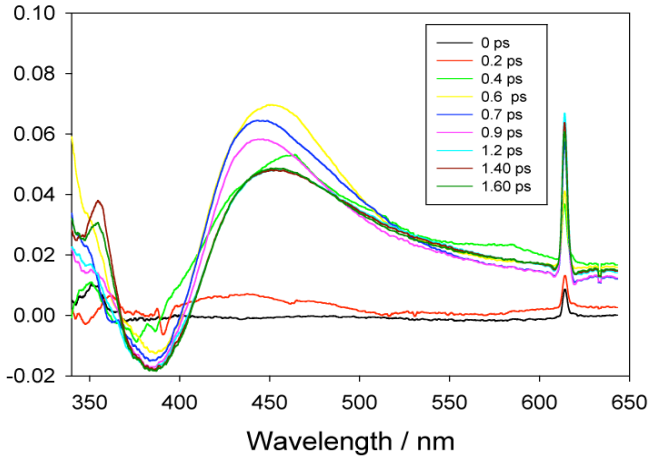

Figure 1.20 UV/Vis-absorption spectra of the *spiro*[9,1'(8'aH)-indolizine]-2',3'-dicarboxylic acid, "pyridine-DHI/betaine system" ($1^{DHI}/1^{B}$) in acetonitrile, λ_{EX} = 310 nm, observation window: 0 – 1.60 ps.

1.4.5 Spiro[9,1'(8'aH)-indolizine]-2',3'-dicarboxylic acid: Deactivation of $B^{\dagger}$ and Formation of a Mixture of Cisoid and Transoid Betaine

Whereas the UV/Vis-absorption spectra obtained after a delay of 1.2 ps to 2 ps are essentially identical, distinct spectra changes occur between 3 ps and 150 ps (**Figure 1.21**). The spectrum recorded after 150 ps is essentially identical with the mixture of approx. 95% of the *cisoid* betaine and 5% of the *transoid* betaine that can be found at much larger delay times. **Figure 1.22** shows the results from μs spectroscopy (described in detail in chapter 1.2 and 1.3). Note that virtually no decay occurs in the observation window between 0 and 2μs. It is known from our previous studies of the "pyridine-DHI/betaine system" that the disrotatory reaction from the *cisoid* betaine to the DHI has a lifetime of 239 μs (at 293 K). Accordingly, the *transoid* betaine requires several hundred seconds for its isomerization to the *cisoid* betaine (τ = 311 s at 283 K).

Apparently, we are looking at the deactivation of $B^{\dagger}$, which leads to a mixture of two reaction products, the *cisoid* and *transoid* betaine. This reaction behavior can be classically described as deactivation through a "tunnel", which leads onto a "mound" (thermal activation barrier) between the *cisoid* and *transoid* betaine.[3,8]

A second deactivation pathway also exists, which leads back to the DHI, as the decrease of the bleach between 380 nm and 400 nm indicates. This finding is in agreement with the behavior of the "methylcarboxylate-pyridazine-DHI/betaine –system" ($\mathbf{3^{DHI}/3^{B}}$)).[2]

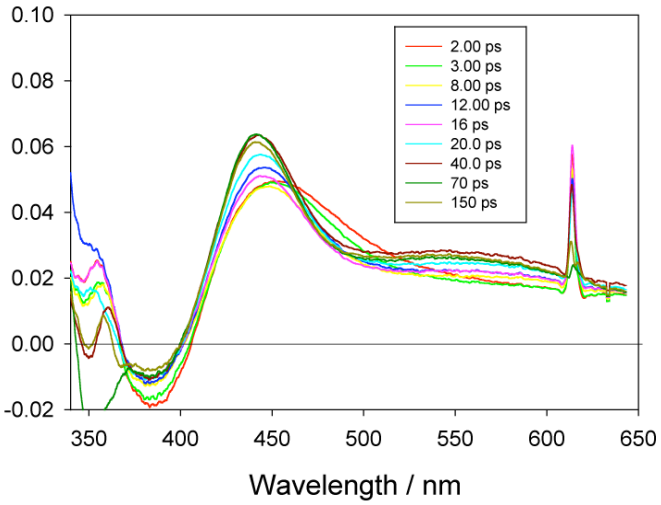

Figure 1.21 UV/Vis-absorption spectra of the *spiro*[9,1'(8'aH)-indolizine]-2',3'-dicarboxylic acid, "pyridine-DHI/betaine system" ($\mathbf{1^{DHI}/1^{B}}$) in acetonitrile, λ_{EX} = 310 nm, observation window: 2 – 150 ps.

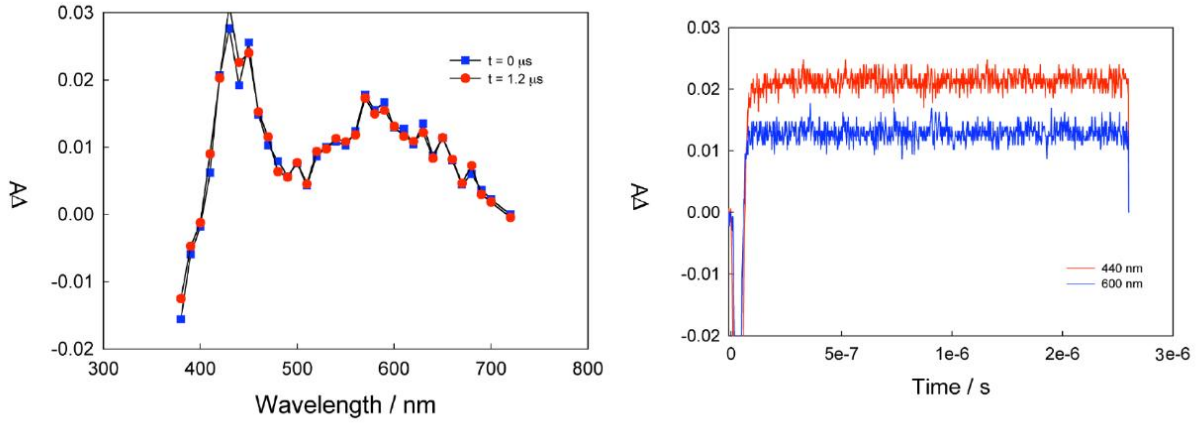

Figure 1.22 UV/Vis-absorption spectra and kinetic traces (red: 440 nm, blue: 600 nm) of the: *spiro*[9,1'(8'aH)-indolizine]-2',3'-dicarboxylic acid, "pyridine-DHI/betaine system" ($\mathbf{1^{DHI}/1^{B}}$) in acetonitrile, λ_{EX} = 310 nm, observation window: 0 - 2 μs.

1.4.5 Reaction Kinetics of the "Pyridine-DHI/betaine – System"

Figure 1.23 shows the transient absorptions at 440 nm and 540 nm of the "pyridine-DHI/betaine – system" in dependence on the delay time. 440 nm has been selected, because it is near the absorption maxima of $B^{\dagger}$ and the *cisoid* betaine. 540 nm is near the second maximum of the growing *cisoid* and *transoid* betaine absorption. The kinetics observed at 440 nm and 540 nm are essentially the same: Immediately after laser excitation, we observe a very rapid growth τ_1 = 0.5 ps. This is the lifetime for the transition from the excited singlet S^n* state of the DHI to $B^{\dagger}$. The second lifetime τ_2 = 1.2 ps is for the vibrational deactivation of $B^{\dagger}$ to its lowest vibrational level. The third lifetime τ_3 = 75.8 ps is for the deactivation of $B^{\dagger}$ through the "tunnel" and the formation of the *cisoid*/*transoid* betaine (approx. 95%/5%). As already stated, the lifetime for the reaction of the *cisoid* betaine to the DHI is τ_4 = 239 μs at 293 K. The lifetime for the thermal *transoid* betaine to *cisoid* betaine conversion is τ_5 = 311 s at 283 K). It is obvious that all lifetimes that are longer than 0.5 ns cannot be accurately measured with the femtosecond setup used here.

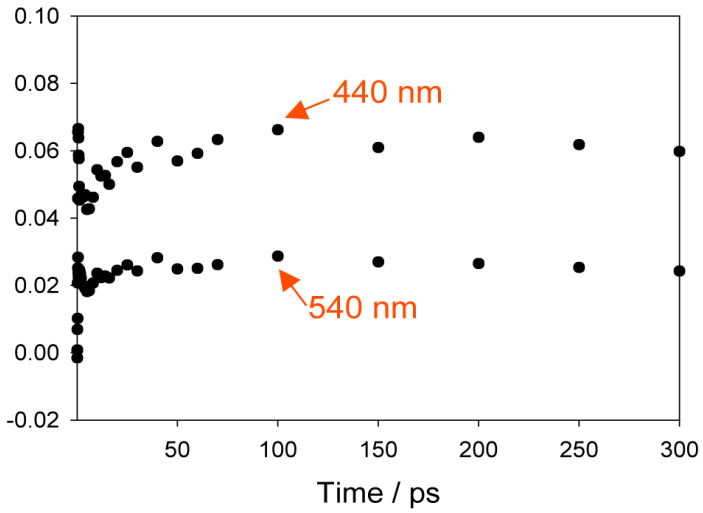

Figure 1.23 UV/Vis-absorption intensity of the *spiro*[9,1'(8'aH)-indolizine]-2',3'-dicarboxylic acid, "pyridine-DHI/betaine system" ($1^{DHI}/1^{B}$) in acetonitrile, λ_{EX} = 310 nm) *vs.* delay time.

1.4.6 Spiro[9H-fluorene-9,5'(4'aH)-pyrrolo[1,2-b]pyridazine]-6',7'-dicarboxylic acid, 6',7'-dimethyl ester

The early events for the "pyridazine-DHI/betaine- system" ($2^{DHI}/2^{B}$) are very similar to the "pyridine-DHI/betaine- system" ($1^{DHI}/1^{B}$)(**Figure 1.24**). The UV/Vis-absorption spectra recorded 0.2 ps, 0.4 ps and 0.6 ps after excitation at λ = 310 nm show the very rapid (τ_1 = 0.5 ps) population of the corresponding transient electronic state $B^{\dagger}$. We assume that $B^{\dagger}$ is in an upper vibrational state, as this was the case in the previously studied $1^{DHI}/1^{B}$ - system. Interestingly, this state deactivates bi-exponentially to a mixture of *cisoid* and *transoid* betaine. Again, the distribution is approximately 95% *cisoid* and 5% *transoid*. The corresponding lifetimes are τ_2 = 21.8 ps and τ_3 = 70.9 ps. Because of the absence of distinct spectral features, we cannot distinguish between a bifurcated pathway, which leads principally to the same mixture of products (probably with varying degrees of *cisoid vs*. *transoid* betaines) or a stepwise reaction. It is noteworthy that we did not observe an intermittent halt of the reaction when studying the "pyridazine-DHI/betaine-system, in contrast to the "pyridine-DHI/betaine-system". It is our mechanistic interpretation of this finding that there is no vibrational state in the former system, which would permit "resting" for a very short time, because there is no kinetic barrier. This means that the "funnel" is more rugged in the case of $1^{DHI}/1^{B}$, whereas it may be bifurcated in the $2^{DHI}/2^{B}$-system.

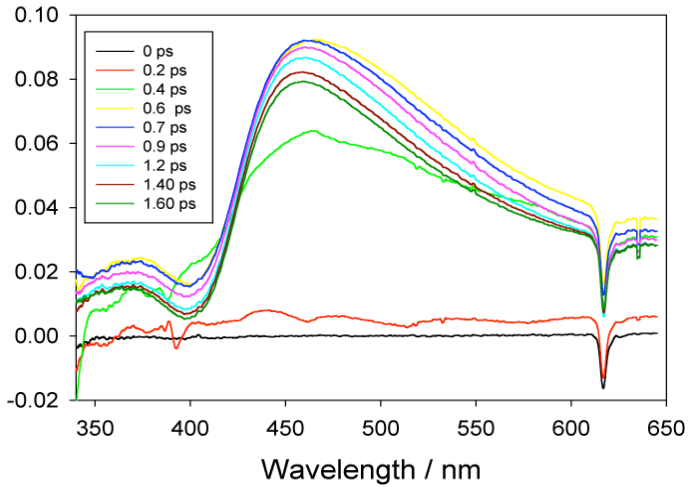

Figure 1.24 UV/Vis-absorption spectra of *spiro*[9H-fluorene-9,5'(4'aH)-pyrrolo[1,2-b]pyridazine]-6',7'-dicarboxylic acid, 6',7'-dimethyl ester, "pyridazine-DHI/betaine system" ($2^{DHI}/2^{B}$) in acetonitrile, λ_{EX} = 310 nm, observation window: 0 - 1.60 ps.

Another possible explanation for the occurrence of a bi-exponential decay from $B^{\dagger}$ to the *cisoid*/*transoid* betaine mixture may be the existence of more than two (meta)stable betaines. If the rotation along the C_3-N_4 axis (**Scheme 1.15**) leads to more than two relative minima, then their relative population will change when the total energy of the $2^{DHI}/2^{B}$-system is decreasing during deactivation. Note that the UV/Vis-absorption spectrum of each betaine-isomer will be different, because the charge-distribution in a betaine is the determining factor for the occurrence of the (very broad) absorption band.

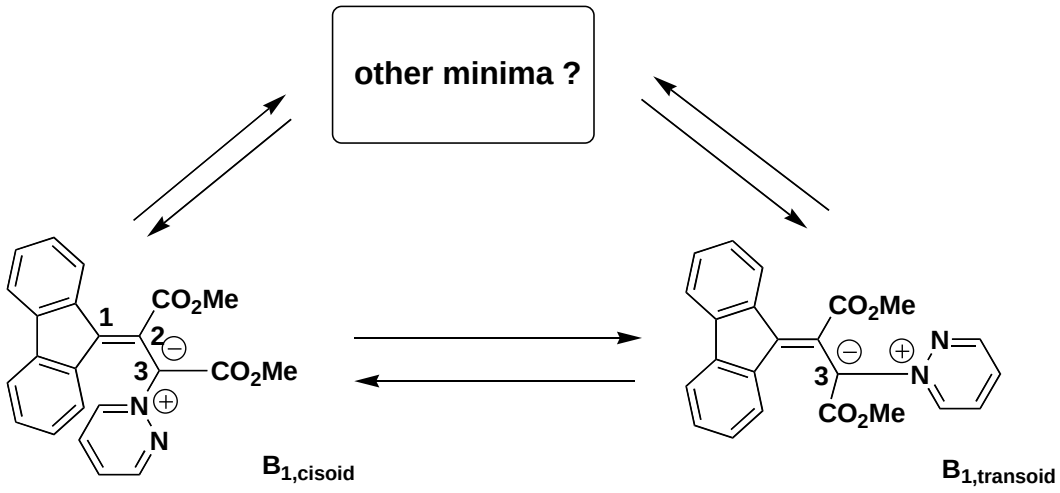

Scheme 1. 15: Cisoid and *transoid* rotamers of the investigated betaine. Are there other relative minima occurring during the rotation along the C3-N axis?

We were unable to determine, whether in the "pyridazine-DHI/betaine-system" a direct reaction pathway from $B^{\dagger}$ to the DHI exists, because the absorption of the betaine 2^{B} between 380 nm and 410 nm is larger than of the DHI (λ_{max} = 389 nm, log ε = 3.92) and the molar absorption coefficients of $B^{\dagger}$, *cisoid* and *transoid* betaine, as well as potentially formed other rotamers, are not known.

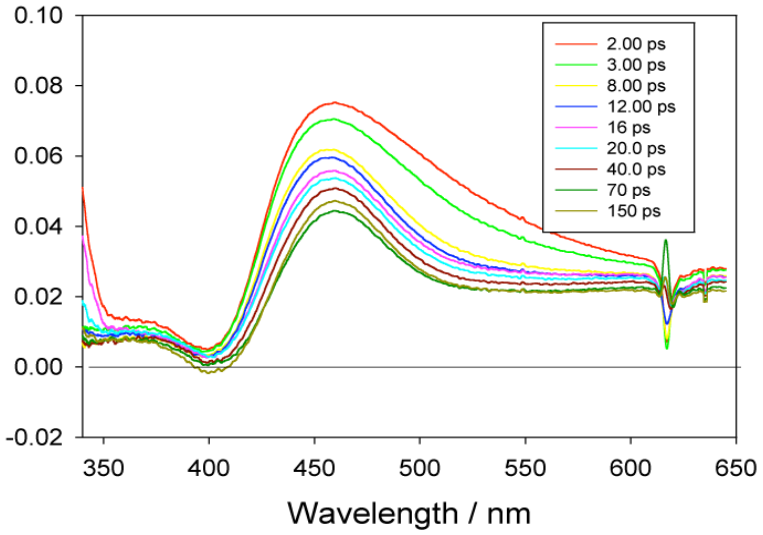

Figure 1.25 UV/Vis-absorption spectra of *spiro*[9H-fluorene-9,5'(4'aH)-pyrrolo[1,2-b]pyridazine]-6',7'-dicarboxylic acid, 6',7'-dimethyl ester, "pyridazine-DHI/betaine system" ($2^{DHI}/2^{B}$) in acetonitrile, λ_{EX} = 310 nm, observation window: 2 - 150 ps.

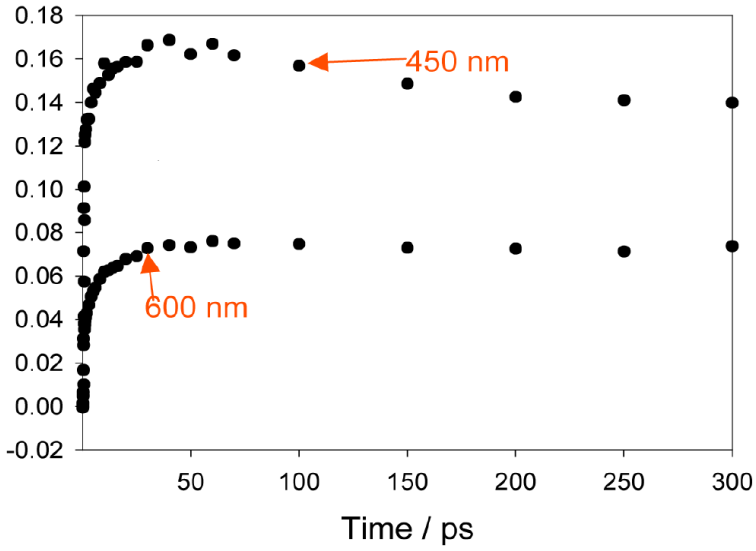

Figure 1.26 UV/Vis-absorption intensity of the *spiro*[9H-fluorene-9,5'(4'aH)-pyrrolo[1,2-b]pyridazine]-6',7'-dicarboxylic acid, 6',7'-dimethyl ester, "pyridazine-DHI/betaine system" ($2^{DHI}/2^{B}$) in acetonitrile, λ_{EX} = 310 nm) *vs*. delay time.

The kinetic information has been obtained by fitting the signal at λ = 450 nm. The biggest observed changes in the time-resolved spectra occur at or near that wavelength. The

signal at λ = 600 nm is where the greatest changes were observed in the observation window between 0 and 2 μs. However, in the femtosecond to pico-second range, the observed spectral changes were minor.

1.4.7 Are There Other Experimental Indications for the Existence of More Than Two Betaines in the "Pyridazine-DHI/Betaine-System"?

In contrast to the "pyridine-DHI/betaine-system" ($1^{DHI}/1^{B}$), which no distinct spectral changes were observed during the first two microseconds after laser-excitation (**Figure 1.22**), remarkable changes have been detected in the "pyridazine-DHI/betaine-system" ($2^{DHI}/2^{B}$) (**Figure 1.27**). At λ = 440 nm virtually no spectral changes were observed (after the dead-time of the employed laser system, see chapter **1.3**). At λ = 500 nm a signal increase with a transient rise-time of 220 ns was detected, whereas at λ = 650 nm a signal decrease featuring a lifetime of 291 ns was recorded. The corresponding absorption spectra, which were recorded point-by-point differ greatly at t = 0 ns and t = 200 ns. Whereas the absorption band between 440 nm and 480 nm, which is typical for the *cisoid* betaine, but of a lesser intensity in the *transoid* DHI[6], does not change significantly, large spectral changes were observed in the spectral range between 480 nm and 800 nm. After a delay of 200 ns an increase in absorption was measured between 480 nm and 580 nm and a decrease was found in the region between 580 nm and 800 nm. It is our hypothesis that these spectral changes are caused by the existence of more than two betaine-isomers (other than *cisoid* or *transoid*), which have sufficiently small thermal activation barriers that they permit rapid interconversion processes. The relative fractions of these betaine-isomers change on their pathway through the "funnel". Once they arrive in the electronic ground-state, only a mixture of *cisoid* and *transoid* betaine isomers can be found.

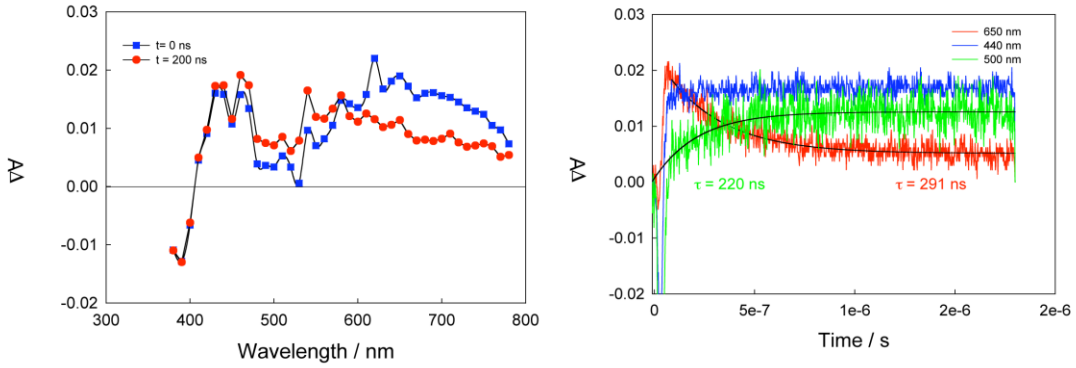

Figure 1.27 UV/Vis-absorption spectra and kinetic traces (blue: 440 nm, green: 500 nm, red: 650 nm) of the: *spiro*[9H-fluorene-9,5'(4'aH)-pyrrolo[1,2-b]pyridazine]-6',7'-dicarboxylic acid, 6',7'-dimethyl ester, "pyridazine-DHI/betaine system" ($2^{DHI}/2^{B}$) in acetonitrile, λ_{EX} = 310 nm, observation window: 0 - 2 μs.

1.4.8 Conclusions

Upon photoexcitation of the both, the "pyridine- and pyridazine-DHIs", adiabatic photoreactions occur. The excited state-reactions find the lowest point of the potential-energy surface, which acts as a "funnel". Both funnels appear to be at least bifurcated. In the case of the "pyridine-DHI/betaine-system" ($\mathbf{1}^{DHI}/\mathbf{1}^{B}$), one pathway leads back to the DHI ($\mathbf{1}^{DHI}$), whereas the other leads to a mixture of *cisoid* and *transoid* betaine isomers. For the "pyridazine-DHI/betaine-system ($\mathbf{2}^{DHI}/\mathbf{2}^{B}$), at least two pathways through the "funnel" exist as well. Both are leading to a mixture of *cisoid* and *transoid* betaine isomers, but they appear to require different reaction times. There may be a third pathway, which leads in analogy to ($\mathbf{1}^{DHI}/\mathbf{1}^{B}$) directly to the ground-state DHI, but the absorption properties of $\mathbf{2}^{DHI}$ and $\mathbf{2}^{B}$ do not permit is observation by UV/Vis-absorption spectroscopy.

In the case of the pyridine-DHI, the "funnel" may feature an intermediate state with a very small activation barrier. Deactivation through the "funnel" leads to a "mound", which is the ground-state activation barrier between the *cisoid* and the *transoid* betaine. The exact position of the point where the deactivation funnel hits the "mound" determines which fraction of the molecules become *cisoid* and *transoid* betaines. For "pyridazine-betaine", more than two isomers may exist. We assume that they are separated by low thermal barriers, as this can be expected for rotamers. Whereas the *cisoid* betaines react within several hundred microseconds (depending on

the temperature) to the DHI, the *transoid* betaines are stable for several minutes. Schematic explanation is given in chapter **1.2** and **1.3**.

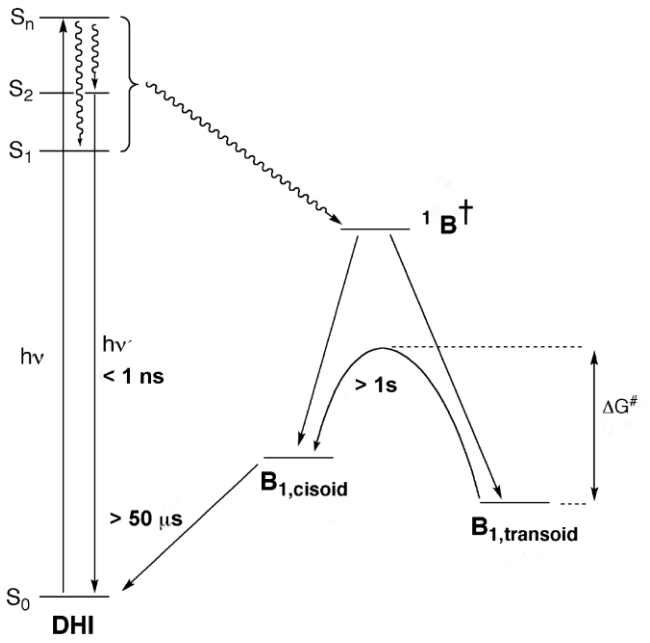

Scheme 1. 16: **Simplified photochemical reaction scheme for the DHI/Betaine system showing the generation of *cisoid* and *transoid* betaine following excitation of DHI and the formation of a transient state $B^{\dagger}$.[3] The thermal back reaction is fast for *cisoid* betaine, while that for the *transoid* species is slower owing to a large activation barrier to isomerization. A thermal barrier[9] exists between the *cisoid* and *transoid* betaine conformation**

1.4.9 References:

1. Burdzinski, G.; Hackett, J. C.; Wang, J.; Gustafson, T. L.; Hadad, C. M.; Platz, M. S., *J. Am. Chem. Soc.* **2006**, *128*, 13402-13411.
2. Mohammad, O. F.; Ahmed, S. A.; Vauthey, E.; Nibbering, E. T. J. *J. Phys. Chem. A* **2009**, *113*, 5061-5065.

3. Shrestha, T. B.; Melin, J.; Liu, Y.; Dolgounitcheva, O.; Zakrzewski, V. G.; Pokhrel, M. R.; Gogritchiani, E.; Ortiz, J.V.; Turro, C.; Bossmann, S. H. *Photochem. Photobiol. Sci.* **2008,** *7*, 1449-1456.
4. H. Duerr, H. Bouas-Laurent, *Photochromism: Molecules and Systems: Revised Edition.*, Elsevier Science B.V, Amsterdam, **2003**, 1074
5. Hartmann, T.; Shrestha, T. B.; Bossmann, S. H.; Huebner, C; Renn, A; Duerr, H. *Photochem. Photobiol. Sci.* **2009**, *8*, 1172-1178.
6. Bleisinger, H.; Scheidhauer, P.; Duerr, H.; Wintgens, V.; Valat, P. and Kossanyi, J. *J. Org. Chem.* **1998**, *63*, 990–1000.
7. Nye, M. Jo. *J. Comp. Chem.* **2007**, *28*, 98-108.
8. Turro, N. J. *Modern Molecular Photochemistry*, Addison-Wesley Publishing Co., Reading, Mass, **1978**, pp 628.
9. Chapter 1.2 and 1.3 of this Dissertation.

1.5 A Light-Induced Photochromic Nanoswitch Capable of Non-Destructive Readout via Fluorescence Emission: Cluster *vs*. Single-Molecule Excitation of Dihydroindolizines.

Most contents of this part are taken with permission from the published paper Thomas Hartmann, Tej. B. Shrestha, Stefan H. Bossmann, Christian Hübner, Alois Renn and Heinz Dürr, *Photochem. Photobiol. Sci.*, **2009**, 8, 1172-1178. My contributions to this paper are the synthesis of photochromic compound and the development of the mechanistic paradigm.

1.5.1 Introduction

Information storage using photochromic compounds has received a lot of attention in recent years.[1–4] Most of the breakthroughs, such as 3D-memory systems[5], logical elements [6–7], and highly efficient (room temperature) data storage [8–12] have been achieved using the spiropyrane/merocyanine systems, because these systems were synthetically available.

Only a limited number of photochromic molecules of the type **DHI(A)** $\rightarrow$ **betaine(B)** are known in which the fluorescence of the photoproduct B can be selectively excited without triggering the back-reaction **B**$\rightarrow$**A**.[13-18] Whereas λ_1 is able to switch **A** $\rightarrow$ **B** and λ_2 initiates the reverse reaction **B** $\rightarrow$ **A**, the photoproduct B can be selectively excited by λ_3 enabling its non-destructive fluorescence readout.

This chapter described a new application of a photochromic system comprised of a styrylquinolyl-dihydroindolizine (**Scheme 1.17)** in a PMMA matrix.[19] The photochromic reaction from **A** (DHI) to **B** (betaine) is thermally and photo-reversible in the "single mode". A non-destructive read-out of the fluorescence occurring from **B** is possible in the "dual mode". When embedded in PMMA, the system **A**$\rightarrow$**B** shows cluster and single molecule fluorescence. The study reported here was conducted in collaboration with Prof. Dr. Heinz Dürr and Dr. Thomas Hartmann (University of Saarland) and with Prof. Dr. Urs Wild and Dr. Alois Renn from the Eidgenössische Technische Hochschule (ETH) in Zürich.

As described in chapters **1.2** and **1.3**, the combination of DFT-calculations, NMR- and UV/Vis-kinetics and microsecond laser absorption spectroscopy led to the reassignment of the most likely positions of the double- and single bonds in the betaines and, consequently, also the

positions of the negative and positive charges.[20] This new mechanistic paradigm is shown in **Scheme 1.17.** [19]

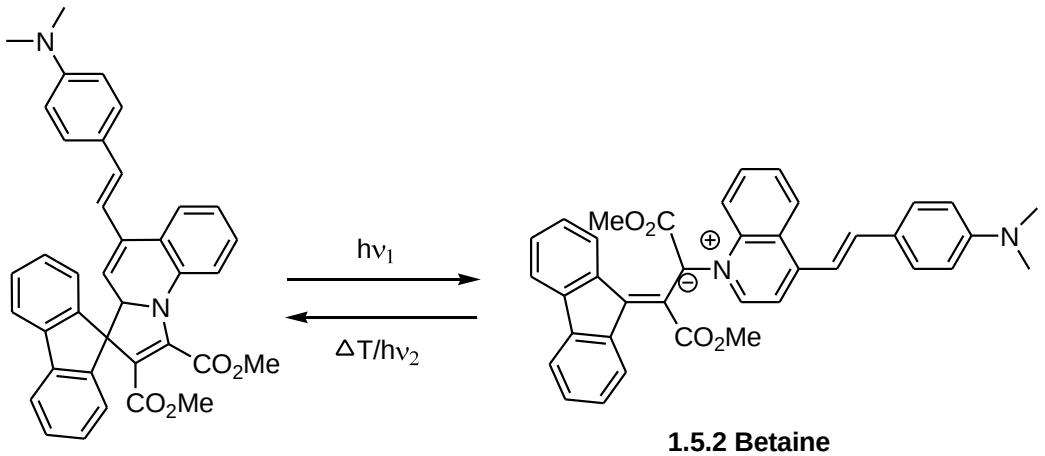

1.5.1 DHI **1.5.2 Betaine**

Scheme 1. 17: Photochromism if dimethyl-1',10'a-dihydro-9'(*trans*-2-[4''N,N-dimethylphenyl)-ethenyl]-*spiro*[9-H-fluorene-9,1'-pyrrolo-[1,2-a]quinoline]-2',3-dicarboxylate ((DHI (1.5.1)).[19]

Light microscopy permits non-invasive imaging of synthetic materials and samples of biological origin with single-molecule (single-photon-emission) sensitivity, but diffraction limits the spatial resolution to approx. 200 nm when using visible light for excitation. Recently, the method of fluorescence photoactivation localization microscopy has been developed, which permits nanometer-resolution while using optical excitation.[21] This method makes use of the enhanced fluorescence anisotropy of fluorophores, which are embedded in a high viscosity matrix.[22,23] Fluorescent DHI/betaine systems can be used for achieving this desirable, very high resolution in future optical memory devices. Described here are the first single-molecule experiments that indicate the efficacy of this photochromic system when embedded in PMMA films (**Scheme 1.18**).[19]

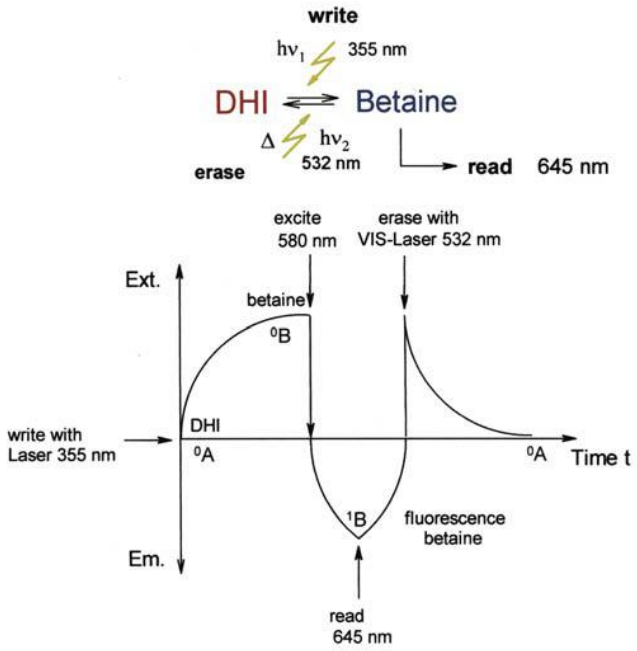

Scheme 1. 18: A system for long-term stable information storage and read-out.[19]

1.5.2 Experimental

1.5.2.1 Chemicals and Instrumentation

UV/Vis spectra: FT-UV Diodearray HP 6543, IR: Beckman Spectrometer, IR 4230, NMR: 400 MHz and 200 MHz Varian NMR-spectrometer, Flash spectrometer: 12V (50W) halogen lamp (Osram), pulse length; 10 ms, METZ 32 Z-1, Time resolved spectroscopy: Nd-YAG Laser, B. M. industries, time resolution: 30 ps (full width half maximum), lamp: pulsed Xe-high pressure lamp, Applied Photophysics and Apple microcomputer, Fluorescence spectrometer; F-3000, Hitachi LTD/SLM-Aminco 8000 C*, Force field microscopy: AFM Nanoscope III (Digital Instruments), Tunnel microscopy: JSM 6400 F (H-REM, resolution 1.5 nm) with energy dispersive microanalyzer for detection of x-rays, Single molecule spectroscopy: computer aided optical confocal raster microscope with avalanche-photodiode-point-detector; irradiation by means of a frequency-doubled Nd/YAG Laser, B. M. industries.

*1.5.2.2 Synthesis Dimethyl-1',10'a-dihydro-9'(trans-2-[4''N,N-*dimethylphenyl*)-ethenyl]-spiro[9-H-fluorene-9,1'-pyrrolo-[1,2-a]quinoline]-2',3-dicarboxylate ((DHI (1.5.1))*

Benzenamine, N,N-dimethyl-4-[(1E)-2-(4-quinolinyl)ethenyl]-) (1.4.4)

Synthetic procedure: 4-(N,N-dimethylamino) benzaldehyde **(**0.569 g, 3.82 mmol, Acros Organic) and lipidine (500 μL, 3.82 mmol) was dissolved in a 50 mL 2 necked flask under argon. 25 mL of dry methanol was added by means of a syringe. Then solid sodium methoxide (206 mg, 3.82 mmol) was added at once. The reaction mixture was heated under reflux for 24 hours. After the completion of reaction (TLC-control), the solvent was removed using a rotavap and the product was purified by descending silica gel column chromatography using 1:1 ethyl acetate/*n*-hexane as eluent. A brown crystalline compound was obtained (400 mg, 1.45 mmol, 38% yield). ^{1}H NMR (400 MHz, $CDCl_3$) δ [ppm] 2.96 (s, 6H, N-CH_3), 6.68(d, *J* = 8.4 Hz, 2H), 7.21 (d, *J* =13. 1 Hz, 1H), 7.46 (d, *J* = 8.4 Hz, 2H), 7.52 (m, 3H), 7.65 (t, *J* = 7.2 Hz, 1H), 8.05 (d, *J* = 8.4 Hz, 1H), 8.18 (d, *J* = 8.4 Hz, 1H), 8.78, (d, *J* = 5.4 Hz, 1H); ^{13}C NMR ($CDCl_3$, 400 MHz) δ [ppm] 40.51, 112.40, 116.36, 117.82, 121.00, 123.727, 124,92, 126.31, 126.62, 128.64, 129.31, 130.13, 131.54, 135.49, 143.95, 148.88, 150.29, 151.02

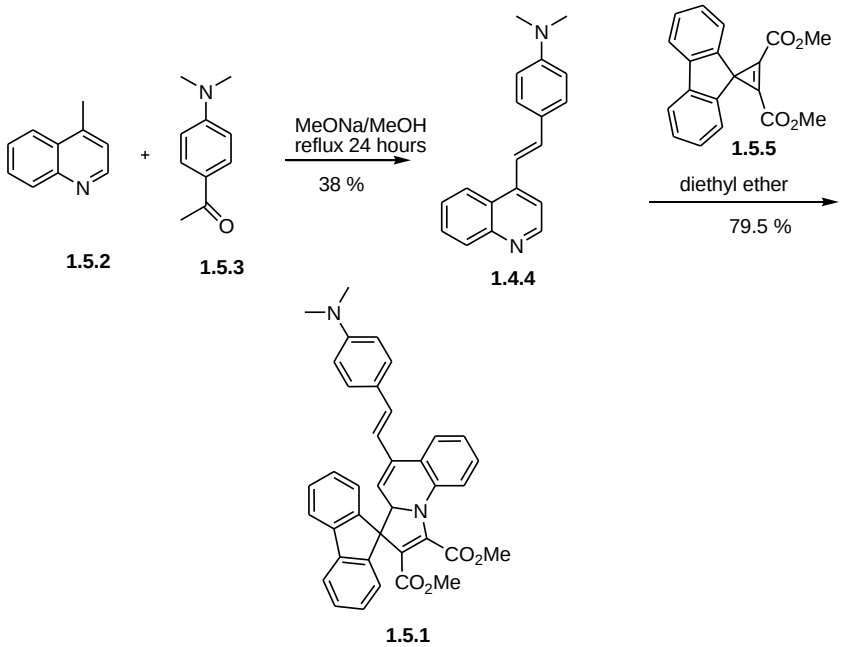

1.5.2 **1.5.3** **1.4.4** **1.5.5** **1.5.1**

Scheme 1. 19: Synthesis of dimethyl-1',10'a-dihydro-9'(*trans*-2-[4''N,N-dimethylphenyl)-ethenyl]-*spiro*[9-H-fluorene-9,1'-pyrrolo-[1,2-a]quinoline]-2',3-dicarboxylate ((DHI (1.5.1)).

Dimethyl-1',10'a-dihydro-9'(trans-2-[4''N,N-dimethylphenyl)-ethenyl]-spiro[9-H-fluorene-9,1'-pyrrolo-[1,2-a]quinoline]-2',3-dicarboxylate ((DHI (1.5.1)).

Synthetic procedure: Dimethyl-cyclopropeno-fluorene-dicarboxylate **1.5.5** (0.029 g, 0.091 mmol) [20] was dissolved in 50 mL of anhydrous diethyl ether. To this mixture, dimethyl-styryl-quinoline (CAS: Benzenamine, N,N-dimethyl-4-[(1E)-2-(4-quinolinyl)ethenyl]-)[24] (25 mg, 0.091 mmol) was added as a quickly dissolving solid. The mixture was stirred in the dark and under argon for 48 h at RT. Reaction progress was monitored by thin layer chromatography (SiO_2/CH_2Cl_2, R_f ((DHI **(1.5.1)**) = 0.21). After the completion of the addition reaction, the solvent was removed in vacuum at RT. The yellowish reaction mixture was separated by descending column chromatography in the dark (eluent: CH_2Cl_2, stationary phase: silica gel). The reaction product was further purified by recrystallization from diethyl ether. Yield: 42 mg (0.0724 mmol, 79.57 % yield) of yellow crystals mp: 167 ^oC; IR: ν cm^{-1} 725, 820, 1015, 1100, 1155, 1210, 1265, 1445, 1495, 1590, 1685,1735, 2825,, 2980, 3010, 3055; ^1H NMR ($CDCl_3$, 400 MHz) δ [ppm] 2.94 (s, 6H), 3.23 (s, 3H, -CO_2Me), 4.04 (s, 3H, -CO_2Me), 5.01 (s, 1H), 5.49, (s, 1H), 6.37 (d, *J* = 15.9 Hz, 1H) 6.58 (d, *J* = 16 Hz, 1H), 6.62 (d, *J* = 8.5 Hz, 2H), 7.02 (t, *J* = 7.4 Hz, 1H), 7.08(d, *J* = 7.4 Hz, 1H), 7.16-7.22 (m, 4H), 7.32-7.43 (m,4H) 7.46-7.47 (d, *J* = 7.4 Hz, 1H), 7.62 (d, *J* = 7.4 Hz, 1H), 7.73 (t, *J* = 6.5 Hz); ^{13}C NMR ($CDCl_3$, 400 M Hz) δ [ppm] 40.64, 51.14, 53.71, 63.06, 69.82, 109.24, 112.50, 115.44, 119.88, 120.11, 120.14, 120.44, 123.31, 124.08, 125.41, 125.44, 125.95, 126.51, 127.50, 127.84, 127.96, 128.22, 128.52, 128.86, 132.46, 134.40, 136.14, 140.54, 141.82, 144.18, 148.64, 148.83, 150.50, 164.14, 164.42

MS: (120 eV, CI, CH_4): m/z (%) = 581 (7.4) (M^++1), 580 (52.3) (M^+), 273 (3.7)

Elemental Analysis: $C_{38}H_{32}N_2O_4$, calc. C 78.60 H 5.55 N 4.82; found C 78.51 H 5.51 N 4.73

UV/Vis:

DHI **(1.5.1)** c = 1.65 x 10^{-4} M, T = 283 K

in PMMA: λ_{max} (log ε): 262 nm (4.72), 354 nm (4.12)

in CH_2Cl_2: λ_{max} (log ε): 265 nm (4.87), 355 nm (4.22)

in EtOH: λ_{max} (log ε): 269 nm (4.94), 354 nm (4.18)

Note that the solvent effects on the UV-absorption of the DHI **(1.5.1)** are minimal.

betaine **(1.5.2)** $c_{(DHI + betaine)}$ = c=1.65 x 10^{-4} M, photostationary state at 283K: approx. 45 %

PMMA: λ_{max} (log ε): 620 nm (4.32)

CH_2Cl_2: λ_{max} (log ε): 473 nm (4.21), 540 nm (4.22), 745 (3.97)

EtOH: λ_{max} (log ε): 465 nm (4.16), 527 nm (4.32), 730 (3.94)

The absorption coefficients (M^{-1} cm^{-1}) were calculated based on the conversion efficiency when reaching the photostationary state. The DHI **(1.5.1)** does not show any absorption beyond 460 nm (**Figure 1.28**).[19]

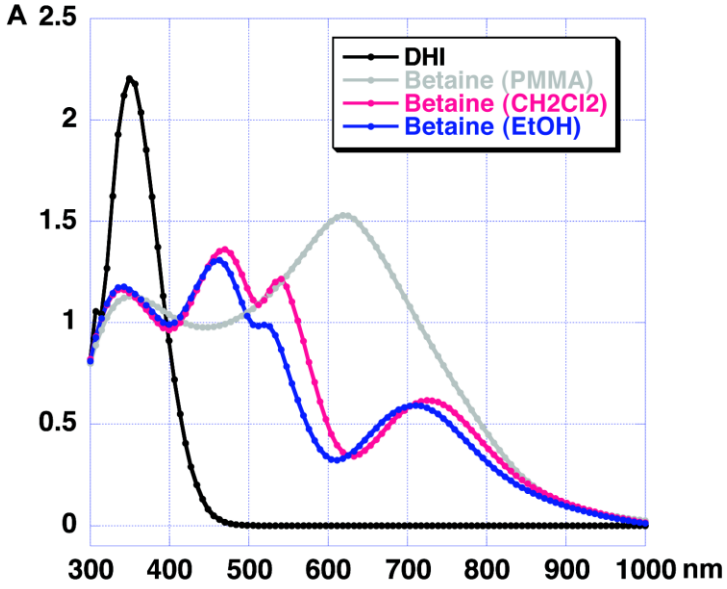

Figure 1.28 UV/Vis-Absorption Spectra of DHI (1, black line) in CH_2Cl_2 c = 1.65 x 10^{-4} M, T = 283 K and mixtures of DHI (1.5.1) and betaine (1.5.2) in PMMA, CH_2Cl_2 and EtOH. The photostationary state at T = 283 K consists of approx. 55±3% DHI and 45±3% betaine.[19]

1.5.2.3 Preparation of the PMMA films

0.058 g of DHI **(1.5.1)** (1.0 x 10-4 M) was dissolved in a solution of 3.0 g polymethylmethacrylate (Aldrich, Mw = 110,000; PDI=1.35) in 100 mL anhydrous CH_2Cl_2 in the dark. The DHI&PMMA containing CH_2Cl_2 was then poured into a crystallization dish. The height of the liquid should be approx. 5 mm prior to evaporation of the solvent at 300 K in the dark. This evaporation process takes up to 12 h. Thus forming a transparent polymeric film, in which the DHI **(1.5.1)** is incorporated and immobilized. Gentle heating up to 340 K allows detaching the PMMA foil from the glass vessel. The average film thickness was approx. 1 mm. The same technique was applied for the preparation of PMMA films containing 1.0 x 10^{-9} M of

DHI **(1.5.1)**, except that this concentration was achieved by dilution of a stock solution of 1.0 x 10^{-4} M DHI **(1.5.1)** in CH_2CH_2.

Interpolation of the $E_T(30)$ values of MMA and PMMA The $E_T(30)$ values for various solvents shown in were obtained from the literature.[25] The data for the determination of the $E_T(30)$ values for MMA and PMMA were obtained from the Ph. D. thesis of Dr. Frahn, who has measured λ_{max} of the solvatochromic dye 1-naphthalene-car-bonitrile, 4-[[1-[4-(2,5-dihydro-2,5-dioxo-1H-pyrrol-1-yl)phenyl]-4-piperidinylidene] methyl]-in various media.[26] **Figure 1.29** shows the linear correlations that were obtained from plots of λ_{max} and the corresponding excited state energies in EV *vs*. $E_T(30)$ (empirical parameters of solvent polarity). [19,25]

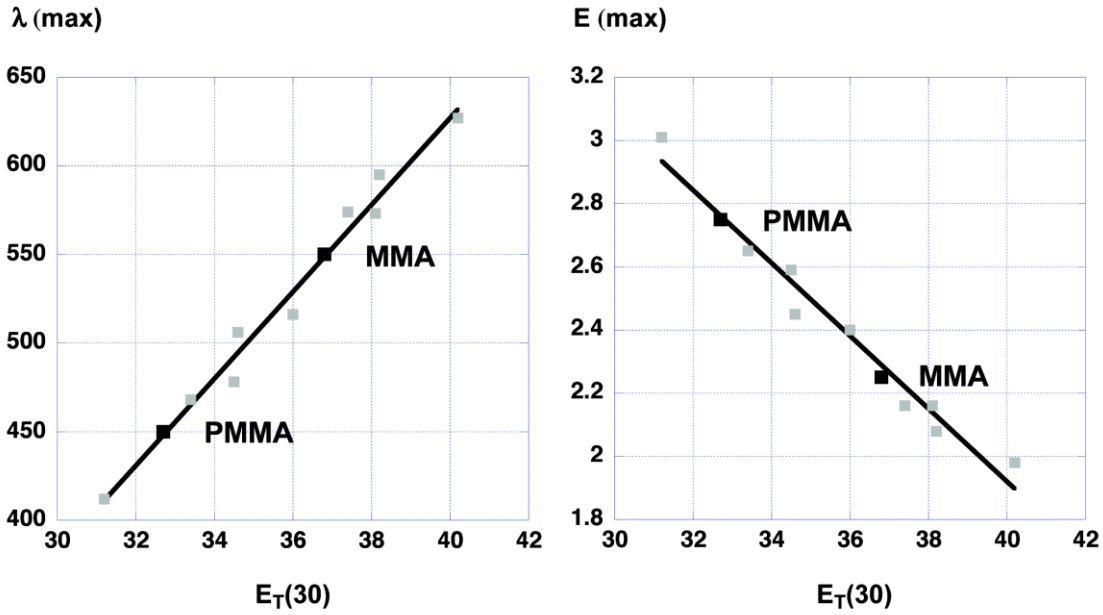

Figure 1.29 λ_{max} and the corresponding excited state energies in EV vs. $E_T(30)$

1.5.2.4 Determination of the Quantum Efficiencies

Rhodamine 6G was used as a reference for the determination of the quantum yields.[27,28] The radiant flux of the incident light was determined by using a ferrioxalateactinometer.[29]

1.5.3 Result and Discussion

1.5.3.1 UV/Vis-Spectra

The UV/Vis-absorption of the novel dimethyl-N,N'-9'-styryl-quinolizidinyldihydroindolizine (DHI **(1.5.1)**) was studied in CH_2Cl_2 (ET(30) = 40.7 kcal mol-1)[30], ethanol (E_T(30) = 51.9 kcal mol-1)[14], and in thin PMMA (E_T(30) = 32.7 kcal mol-1) films. The solvatochromism of styryl-quinolyl functionalized DHI has been reported prior this study.[31] The ET(30) of PMMA has been derived from the data reported in ref. 26 as described in the experimental section. Excitation with UV-light (λ < 400 nm) converts the DHI **(1.5.1)** into the highly colored betaine **(1.5.2)**. The photochemical ring opening of the DHI to the betaines is a conrotatory 1,5 electrocyclic reaction, whereas the thermal ring-closing occurs in the disrotatory mode.[23,32-34] The back reaction can be achieved photochemically as well, however, this reaction is mechanistically not fully understood as of today. For the DHI **(1.5.1)** (λ_{max} in CH_2Cl_2= 355 nm) photochromism has been clearly established by the reversible lightinduced conversion (λ_{EX} < 400 nm) to the violet betaine **(1.5.2)** (CH_2Cl_2: λ_{max1} = 473 nm, λ_{max2} =540 nm, λ_{max3} = 745 nm). In ethanol, λ_{max} remains unchanged at 355 nm, but the three absorption maxima of the betaine **(1.5.2)** have shifted to λ_{max1} = 465 nm, λ_{max2} = 527 nm and λ_{max3} = 730 nm. These data are in excellent agreement with the results of the analogous bisisopropyl ester DHI reported in an earlier paper from the Dürr group.[17] Changing the solvent from dichloromethane to ethanol causes hypsochromic shifts of the VIS-maxima of the betaine **(1.5.2)** of 8 nm (λ_{max1}), 13 nm (λ_{max2}), and 15 nm (λ_{max3}). This solvatochromic effect is in agreement with previous observations on DHI/betaine systems.[31] They were ascribed to Π-Π* transitions in the visible region and charge-transfer transitions in the red and near-IR regions.[31] The betaine **(1.5.2)** features a thermal cyclization half-life time $\tau_{½}$ = 72 ± 4 ms in CH_2Cl_2 and $\tau_{½}$ = 93 ± 5 ms in ethanol at 298 K. Again, this is in very good qualitative agreement with previous results.[17,31]

The DHI **(1.5.1)** in PMMA thin films shows λ_{max} = 354 nm and can be converted with λ_{EX} < 400 nm into the blue betaine **(1.5.2)** (PMMA: λ_{max} = 620 nm). The photostationary state[35] of the DHI **(1.5.1)** betaine **(1.5.2)** system has been determined previously to be 60% of **(1.5.1)** and 40% of **(1.5.2)** at 298 K.[36] (PMMA: λ_{max1} = 482 nm, λ_{max2} = 555 nm, λ_{max3} = 762 nm)

In accordance with numerous previous findings, the thermal betaine **(1.5.2)** →DHI **(1.5.1)** transition does not proceed according to first-order kinetics in a PMMA matrix.[37,38] As it

can be discerned from **Figure 1.30**[19], the observed decay in the betaine absorption at 620 nm can be approximately described as a bi-exponential process. The rate constants for the faster process is k_1 = -4.2±0.2 x 10^{-5} s^{-1} ($\tau_{1/2}$ = 16,500 s (approx. 4.6 h)) and for the slower process k_2 = - 2.4±0.5 x 10^{-6} s^{-1} ($\tau_{½}$ = 288,800 s (80.3h)) at 298K.

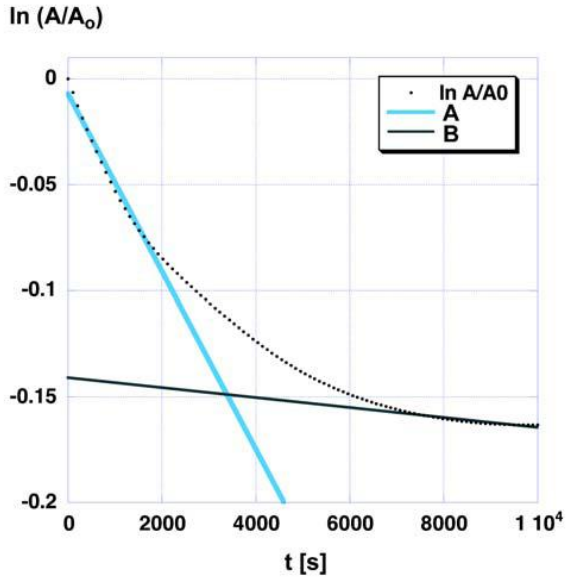

Figure 1.30 Bi-exponential fit of the first-order plot of the absorption data obtained from DHI (1.5.1) in PMMA as a function of time at T = 298K.[19]

1.5.3.2 Fluorescence Studies

Most of the DHIs previously studied exhibit very weak fluorescence at room temperature ($\phi_F \approx 1 \times 10^{-4}$), occurring from an upper state that is not responsible for the observed photochromism.[39,40] The corresponding colored betaines exhibit usually even weaker fluorescence, which is often at the borderline of detection at room temperature. However, at 77 K both the DHI and betaine feature strongly fluorescent bands.

The maximum of the excitation spectrum of DHI **(1.5.1)** in PMMA is λ_{EX} = 381 nm, whereas fluorescence from this (most likely) upper excited state (S_2 or higher) occurs at λ_{EM} = 455 nm. It is noteworthy for the understanding of the Jablonski-diagram of the DHI/betaine system that virtually all DHIs possess fluorescent upper excited states that are not strongly coupled with the S_1-excited state from which the 1,5-electrocyclization reaction to the betaine

occurs.[20,39,40] It is noteworthy that the DHI **(1.5.1)** fluorescence from within the PMMA matrix has a remarkably high quantum yield of emission (Φ_{Fl} = 1.1 x 10^{-2}), which is 100 times bigger than of all known DHIs to date.[40] The betaine (**(1.5.2)** 2) in PMMA possesses the maximum of its excitation spectrum at λ_{EX} = 587 nm. The maximum of the corresponding strong fluorescence (Φ_{Fl} = 2.5 x 10^{-2}) can be detected at λ_{EM} = 645 nm. It is also noteworthy that the NIR-absorption at λ = 745 nm does not lead to a discernible fluorescence band. According to our findings, excitation of the betaine **(1.5.2)** at 587 nm does not lead to a detectable photochemical back reaction. Therefore, this fluorescent band appears to be ideal for a fluorescence read-out of the betaine, which can be achieved without erasing the information that had been deposited by the photochromic reaction DHI **(1.5.1)** → betaine **(1.5.2)**. To the best of our knowledge, this is the first example of a DHI/betaine system, where both constitutional isomers are strongly fluorescent. What are the mechanistic reasons for this remarkable fluorescence enhancement of both the DHI **(1.5.1)** and the betaine **(1.5.2)**?

a) The phenomenon of strong fluorescence can be explained by the presence of a "push-pull system".[41] The dimethyl-amino-phenyl group acts as an intramolecular electron donor D giving rise to the higher fluorescence quantum efficiencies of the DHI **(1.5.1)**, compared to other DHIs. This effect is even more pronounced in the betaine **(1.5.2)**. Here, the dimethylamino-phenyl group and the quinolinium ion constitute a perfect organic push-pull system. Consequently, the fluorescence efficiency of the betaine **(1.5.2)** is further increased! b) The confinement by PMMA causes a dramatic loss of mobility. It is easily discernible that the apparent first-order rate constant for the thermal reaction betaine **(1.5.2)** →DHI **(1.5.1)** increases by a factor of approx. 230,000 when the medium is changed from liquid CH_2Cl_2 to a PMMA film. It is safe to assume that the molecular motion of the DHI **(1.5.1)** / betaine **(1.5.2)** system is greatly reduced, thus decreasing internal conversion and increasing fluorescence. This argument is supported by the low temperature emission spectrum (77 K) of DHI **(1.5.1)** in an ethanol matrix, which is very similar to the fluorescence in PMMA. A summary of the photophysical data is provided in **Table 1.9.**[19]

Table 1.7: **Comparison of the relevant absorption and emission data, Stokes-shifts $\Delta\lambda$, singlet energies E(S1), and fluorescence quantum yields ϕ_F of DHI (1.5.1) and betaine (1.5.2) in PMMA, methylene chloride and ethanol glass.**[19]

Matrix T [K]	**λ_{max} Abs. [nm]**	**λ_{max} Ex. [nm]**	**λ_{max} Em. [nm]**	**Stokes shift $\Delta\lambda$ [nm]**	**$E(S_1)$ [kJ mol^{-1}]**	**ϕ_F**
PMMA, 298 K						
DHI **(31.5.1)**	354	381	455	74	286	$1.1x10^{-2}$
Betaine **(1.5.2)** [a]	620	587[b]	645	58		$2.5x10^{-2}$
CH_2Cl_2 298K						
DHI **(1.5.1)**	355	386	585	199	247	$2.3x10^{-2}$
Betaine **(1.5.2)** [a]	473 539 745					$<10^{-4}$
EtOH 77 K	c	367	451	84	292.5	c

[a] Spectra of betaine **(1.5.2)** are always a superposition of betaine **(1.5.2)** (40%) and DHI **(1.5.1)** (60%) at 298 K. The absorption and excitation bands > 460 nm are, however, discerned unambiguously due to the absence of DHI absorption.

[b] This excitation band induces fluorescence at 645 nm.

[c] has not been studied

1.5.3.3 A Single Mode Optical Switch

The photochemical switching of and the photo-induced back-switching DHI **(1.5.1)** $\xrightarrow{h\nu}$ betaine **(1.5.2)** in PMMA was demonstrated by the following steps:

a) Polychromatic irradiation (λ < 400 nm) of DHI **(1.5.1)** generated the blue betaine **(1.5.2)**, which was fluorescent (λ_F = 645 nm). After 20 min. of irradiation the photostationary state at rooṃ temperature (approx. 40 percent of betaine **(1.5.2)**) was reached and no further

increase of the betaine-fluorescence was observed. The distribution of DHI *vs*. betaine in the photostationary state is strongly temperature-dependent.[32-35]

b) The betaine **(1.5.2)** in PMMA was irradiated by means of a Nd:YAG laser (second harmonic, λ_{EX} = 532 nm). At this wavelength, the photo-induced back reaction of the betaine **(1.5.2)** to the DHI **(1.5.1)** takes place and consequently, the Betaine **(1.5.2)** fluorescence (λ_F = 645 nm) decreased (**Figure 1.31**). After 20 min. of irradiation at λ_{EX} = 532 nm, only traces of Betaine **(1.5.2)** could be discerned.

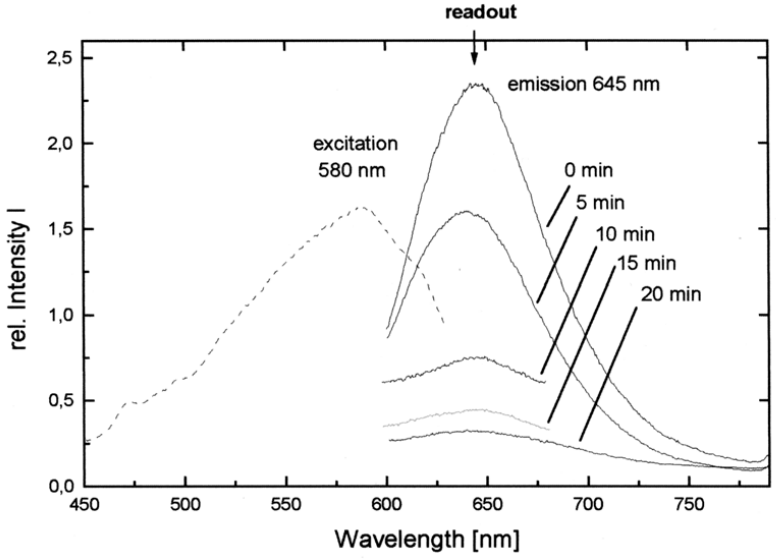

Figure 1.31 Excitation and fluorescence spectra of betaine (1.5.2) in PMMA at 298 K. Irradiation with a 532 nm laser beam causes the photo-induced back reaction betaine (1.5.2) →DHI (1.5.1). Therefore, the emission intensity of betaine (1.5.2) decreases.

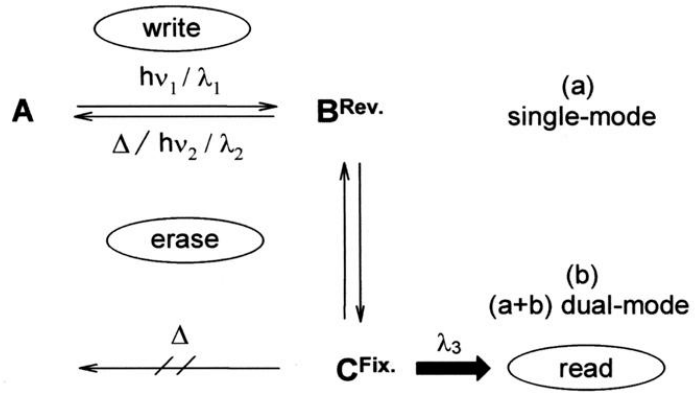

Figure 1.32 Single-mode: λ_1 triggers the DHI (A) →betaine (Brev.) transformation. λ_2 causes the photoinduced back reaction betaine →DHI. Dual-mode: →1 triggers the DHI (A) →betaine ($B^{rev.}$) transformation. $B^{rev.}$ is stabilized by a PMMA matrix (optionally at 77 K) preventing the thermal back reaction to the DHI (A). λ_3 can be employed to readout the stored information (via fluorescence of the stabilized betaine ($C^{FIX.}$)).[19]

The thin film of DHI **(1.5.1)** in PMMA can be used as a read →write system. Writing is achieved applying the third harmonic of the Nd:YAG laser at λ_{EX} = 355 nm. Reading is achieved by exciting the betaine **(1.5.2)** with λ_{EX} = 580 nm and monitoring the fluorescence at λ_F = 645 nm. It is of importance that excitation at λ_{EX} = 580 nm can be performed with low intensity, compared to UV/Vis-measurements, because the fluorescence detection is up to a factor of 1,000 more sensitive than UV/Vis.[42] This contributes remarkably to the stabilization of the betaine **(1.5.2)** against photodecomposition reactions. The quantum efficiency of photobleaching comprising all destructive photochemical reactions that occur by irradiating the betaine in PMMA at room temperature was estimated to Φ_{PB} = 0.001.[36]

Lowering the temperature of the thin film of DHI **(1.5.1)** in PMMA to 77 K has two effects: a) The betaine **(1.5.2)** is protected against virtually any (thermal or photochemical) decomposition reactions, b) Because of the lower temperature, the fraction of the betaine in the photostationary state increases to (almost) 100 %[35]

The practical consequence of lowering the temperature to 77 K is that we have created a truly destruction-free read-out process! The information can be erased by using visible laser light (λ_{EX} = 532 nm). It would also slowly decay thermally at room temperature. However, at 77 K, the half-life time of the thermal 1,5-electrocyclization reaction is practically infinite. The switching process (DHI $\xrightarrow{h\nu_1}$ 1betaine, betaine $\xrightarrow{h\nu_3}$ 3 fluorescence read-out, betaine $\xrightarrow{h\nu_2}$ 2DHI) was repeated six times to demonstrate the feasibility of this approach to information storage (**Figure 1.32**).

The image of a runner (0.5 cm) was recorded in the DHI (**(1.5.1)**, c = 1.0 x 10^{-4} M) in PMMA film by using a 355 nm Nd:YAG laser beam. The runner appears as a blue figure in the colorless film. When exciting with green laser light (532 Nd:YAG, 1 mW), the red fluorescence of the runner occurs (**Figure 1.33**). The orange background results from an orange band-pass

filter, $\lambda > 540$ nm, to exclude light from the excitation source and stray light. Apparently, the fluorescence read-out at $\lambda_F = 654$ nm using $\lambda_{EX} = 532$ nm is competing with the photo-induced back reaction betaine $\xrightarrow{h\nu_2}$ DHI. However, the intensity required for erasing the betaine in the PMMA film is at least a factor of 1,000 higher, thus allowing multiple readouts at this wavelength. When using higher intensities of $\lambda_{EX} = 532$ nm, the runner was completely erased. Six coloration/decoloration cycles of this image were recorded without the apparent loss of fluorescence intensity of betaine **(1.5.2).** The image of the runner in PMMA is discernible for more than 5 h at room temperature. It can be stored indefinitely at 77 K. When raising the temperature to 323 K, the image was erased after 3 h, at 333 K after 1 h. These heating experiments have been carried out in an argon atmosphere to avoid oxidation reactions of the DHI and betaine.

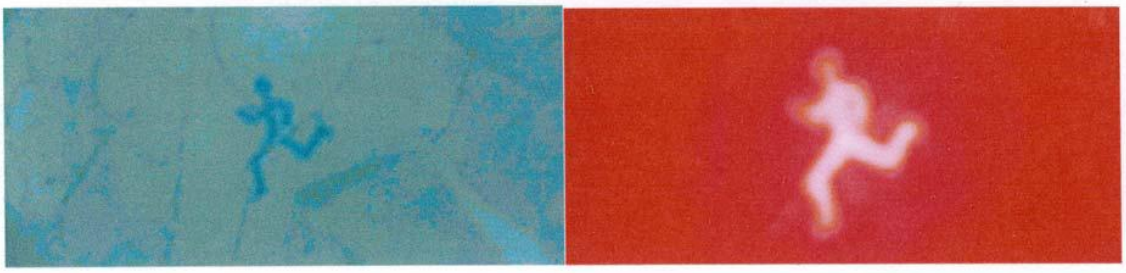

Figure 1.33 Left: VIS-absorption spectrum of the "runner" (DHI (1.5.1) in PMMA after writing with a 355 nm laser beam. Right: Fluorescence spectrum from the "runner", excitation at 532 nm.[19]

1.5.3.4 A Mechanistic Paradigm

On the basis of a recently introduced new paradigm, which was developed for the most simple DHI (*spiro*[9,1'(8'aH)-indolizine]-2',3'-dicarboxylic acid, dimethyl ester), the photochemical and thermal reactivity of the system DHI **(1.5.1)** →betaine **(1.5.2)** can be understood as follows: Upon photoexcitation of DHI with $\lambda < 400$ nm ($h\nu_1$) an adiabatic photoreaction occurs. The excited state-reaction finds the lowest point of the potential-energy surface, which acts as a "sinkhole". As this is the case in many photoreactions[42], the deactivation leads to a "mound", which is the ground-state activation barrier $\Delta G^{\#}$ between the *cisoid* and the

transoid betaine.[20] The exact position of the point where the deactivation funnel hits the mound determines which fraction of the molecules will become *cisoid* and *transoid* betaines.

In the case of DHI **(1.5.1)**, a fluorescent upper excited state can be populated, which does not efficiently deactivate into S1 by internal conversion. Apparently, the exact position of B† with respect to B_{cisoid} and $B_{transoid}$ are not known to date and may strongly depend on the chemical structure of the DHI. As shown in **Figure 1.34B**, *cisoid* and *transoid* pertain to the relative positions of the methyl ester groups at the bond between C_2 and C_3, which is, according to DFT calculations performed by the Ortiz-group, stronger than a single, but weaker than a double bond.[20] According to this mechanistic paradigm, the 1,5-electrocyclization from the DHI to the betaine occurs from the B_{cisoid} state. The ground-state activation barrier $\Delta G^{\#}$ determines the temperature-dependence of the $B_{transoid} \rightarrow B_{cisoid}$ interconversion. It is known that the thermal back reaction of betaine **(1.5.2)** in solvent is complete after <500ms, indicating a very low barrier $\Delta G^{\#}$ and a very fast interconversion of B_{cisoid} and $B_{transoid}$. However, if the medium is changed to PMMA, $\Delta G^{\#}$ increases and, therefore, $B_{transoid}$ is present for several hours! The observed changes of the UV/Vis absorption spectra (**Figure 1.28**) can be attributed to the existence of (mainly) the *cisoid* form of betaine **(1.5.2)** in CH_2Cl_2 and ethanol, whereas in PMMA the *transoid* isomer is predominantly present. The occurrence of at least a bi-exponential decay pattern of betaine **(1.5.2)** in PMMA can be explained by a variety of different polymer environments around the betaine, which hinder the *cisoid/transoid* isomerization more or less. Finally, if betaine **(1.5.2)** is excited with $\lambda_3 = 580$ nm, then betaine-fluorescence, but no photo-induced back reaction to DHI **(1.5.1)** is observed. According to our paradigm, the excited state energy of S_1(betaine) is lower than of B†. However, excitation with $\lambda = 532$ nm, which is higher in energy than B† permits the population of a higher singlet state of betaine **(1.5.2).** In this case, photoinduced isomerization occurs, as well as betaine fluorescence from S_1.

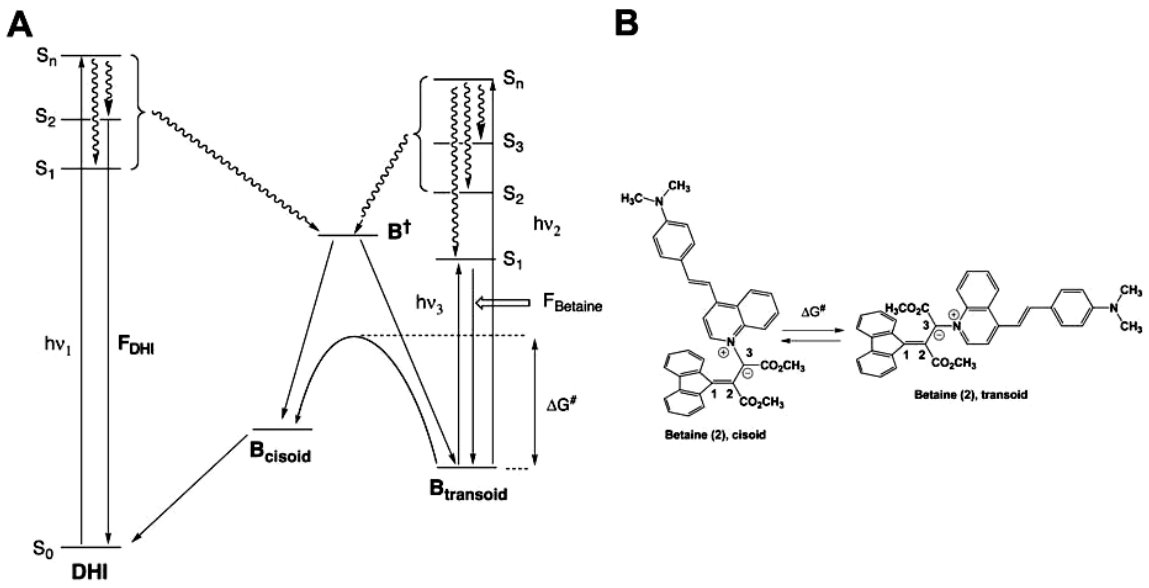

Figure 1.34 A: **Simplified photochemical reactions of the DHI/betaine system showing the generation of *cisoid* and *transoid* betaine following excitation of DHI. The thermal back reaction is fast for *cisoid* betaine, while that for the *transoid* species is slower owing to a large activation barrier to isomerization (f: fluorescence). Further explanations are provided in the text. B: *cisoid -transoid* isomerization of betaine (1.5.2).[19]**

1.5.3.5 Cluster or Single Molecule Spectra

A confocal "raster" microscope was employed to scan films of DHI (**1**, c =1.0 x 10^{-9} M) in PMMA at room temperature. The second harmonic (λ_{EX} = 532 nm) of a Nd:YAG laser was focused through a micro-lens (objective) to a 300 nm spot, permitting the spatially well-defined excitation of the films. Fluorescent light was collected via the same lens, separated from the ingoing light by a dichroitic mirror and detected by a single-photon sensitive avalanche photodiode. Stray light was suppressed by using a notch filter. Piezo-actuators measured the fluorescence of the probe in 62 μm x 62 μm squares (λ_{EX} = 532 nm, 100,000 pulses per second).

A line scan experiment was performed to measure time-dependent fluorescence. Prior to this experiment, DHI **(1.5.1)** in PMMA was converted to the betaine **(1.5.2)** by irradiation with a 300W Hg lamp, which provided sufficient intensity at λ < 400 nm. During the linescan experiment, the PMMA film containing a mixture of DHI **(1.5.1)** and betaine **(1.5.2)** was first

scanned in the *x* and then in the *y* direction by using the collimated 532 nm laser beam. The red bars of **Figure 1.35** correspond to the times when UV-light from the Hg-lamp was applied again.

To measure the time dependence of the fluorescence occurring from single molecules of betaine **(1.5.2)**, one line is repeatedly scanned in the *x*-axis. Fluorescence can be discerned as bright yellow trace on the blue background. The *x*-coordinate represents the location on the probe and the *y*-axis the time. The 532 nm laser induced both fluorescence of betaine **(1.5.2)** and back switching to DHI **(1.5.1)**. Re-coloring with $\lambda > 400$ nm regenerates betaine **(1.5.2)**. After recoloration, new fluorescence traces, as well as fluorescence blinking[40] can be discerned. The discrete disappearance of a fluorescence signal is a clear indication of single molecule fluorescence. The very high dilution ($c < 1.0 \times 10^{-9}$ M) of betaine **(1.5.2)** in PMMA permits the fluorescence of isolated fluorophors. A second type of fluorescence disappears continuously, which is a clear indication of fluorescence occurring from clusters of betaine **(1.5.2)**. The process of fluorescence and fading of betaine **(1.5.2)** has been repeated ten times showing macro-reversible, but not necessarily nano-reversible behavior. Typical results from the linescan experiments are shown in **Figures 1.35 and 1.36.**

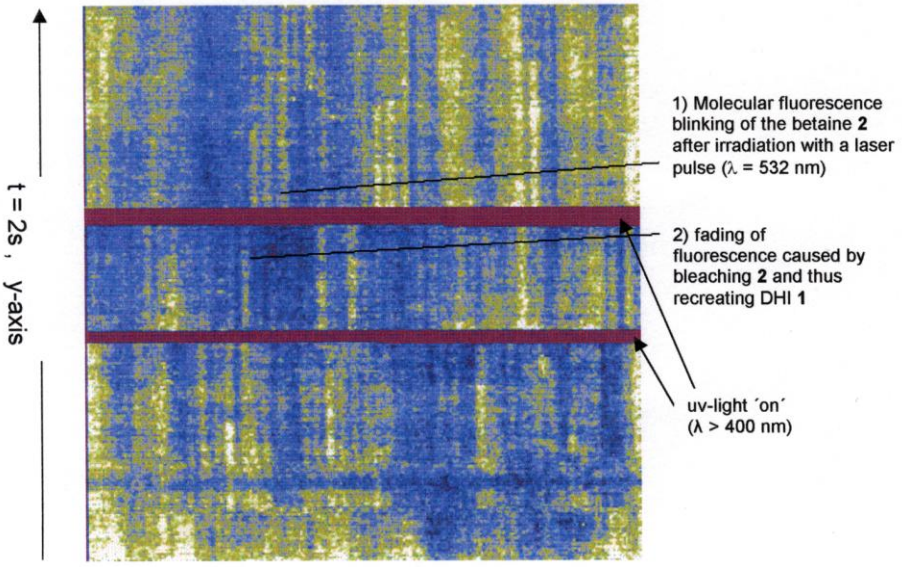

Figure 1.35 Linescan experiment to measure time-dependent fluorescence: A confocal "raster" microscope was employed to scan films of DHI (1, c = 1.0 x 10^{-9}M) in PMMA at room temperature (62 μm x 62 μm square, λ_{EX} = 532 nm, 100,000 pulses per second). The fluorescence intensity increases in the order black/blue/yellow/white.[19]

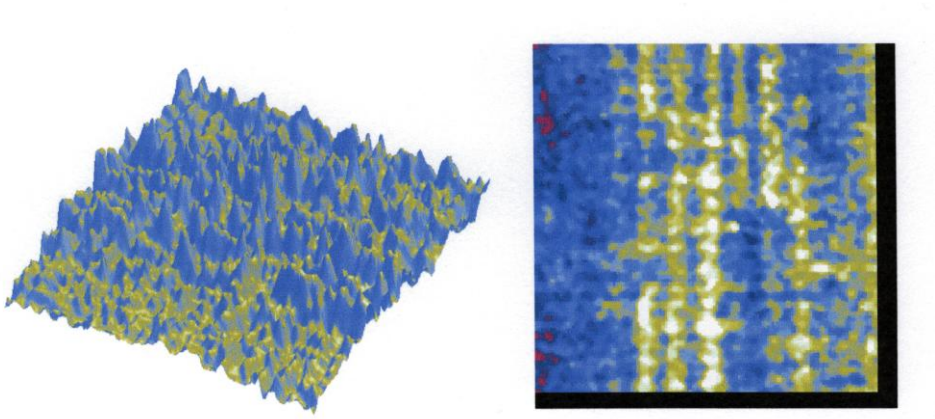

Figure 1.36: Spatially resolved fluorescence intensity (20.8 μm x 20.8 μm, the same experimental conditions as Figure 1.36 apply). Note that the left image has to be turned 100^{o} to the left to achieve superposition.[19]

1.5.4 Conclusion

A new photochromic styryl-quinolyl DHI **(1.5.1)** /(betaine **(1.5.2)** system was synthesized, in which both constitutional isomers show remarkably strong fluorescence. The DHI **(1.5.1)** undergoes a 1,5-electrocyclic reaction to betaine **(1.5.2)** upon irradiation with UVA light (λ < 400 nm). When stabilized in a PMMA matrix, the blue betaine **(1.5.2)** is stable for hours at room temperature and indefinitely stable at 77K against the thermal back reaction to the DHI **(1.5.1)**. However, irradiation of betaine **(1.5.2)** with λ = 532 nm permits the photo-induced back switching process to DHI **(1.5.1)**. The betaine **(1.5.2)** permits its destruction-free read-out at λ = 645 nm when excited with λ = 580 nm. This system has enabled the realization of a prototype for an information recording and storage system. Furthermore, the occurrence of simultaneous cluster and single-molecule fluorescence from a photochromic spirodihydroindolizine (DHI) has been observed for the first time.

1.5.5 References

1. Buncel, E. *Can. J. Chem.* **2000**, *78*, 1251–1271.
2. Akimov, D. A.; Zheltikov, A. M.; Koroteev, N. I.; Magnitskii, S. A.; Naumov, A. N.; Sidorov-Biryukov, D. A.; Sokolyuk, N. T. and Fedotov, A. B. *Laser Phys.* **1997**, *7*, 1242–1252.
3. Lessard, R. A. and Manivannan, G. *Proc. SPIE–Int. Soc. Opt. Eng.* **1998**, *3347*, 11–19.
4. Chapurin, I. V.; Robu, S. V.; Vlad, L. A. Lessard, R. A.; Tork, A.; Lafond, C. and Bolte, M. *Proc. SPIE–Int. Soc. Opt. Eng.* **2001**, *4296*, 337–340.
5. Akimov, D. A.; Fedotov, A. B.; Koroteev, N. I.; Magnitskii, S. A.; Naumov, A. N. Sidorov-Biryukov, D. A.; Sokolyuk; N. T. and Zheltikov, A. M. *Proc. SPIE–Int. Soc. Opt. Eng.* **1998**, *3402*, 137–148.
6 Massimiliano, T.; Deniz, E.; Alvarado, R. J. and Raymo, F. M. *J. Phys. Chem. C* **2008**, *112*, 8038–8045.
7 Massimiliano, T.; Giordani, S. and Raymo, F. M. *Adv. Funct. Mater.* **2005**, *15*, 787–794.
8 Tian, Z.; Wu, W.; Wan, W. and Li, A. D. Q. *J. Am. Chem. Soc.* **2009**, *131*, 4245–4252.
9 Zhu, M.-Q.; Zhu,L.; Han, J. J.; Wu, W.; Hurst, J. K. and Li, A. D. Q. *J. Am. Chem. Soc.* **2006**, *128*, 4303–4309 .
10 Jiang, G.; Song, Y.; Guo, X.; Zhang D. and Zhu, D. *Adv. Mater.* **2008**, *20*, 2888–2898.
11 Kobayashi, N. and Egami, C. *Opt. Lett.* **2005**, *30*, 299–301.
12 Karcher, M.; Rüdt, C.; Elsäßer, C. and Fumagalli, P. *J. Appl. Phys.* **2007**, *102*, 84904–84907.
13 Inada, T.; Uchida S. and Yokoyama, Y. *Chem. Lett.* **1997**, 321–322; Erratum: *Chem. Lett.* **1997**, 961.
14 Irie, M. Diarylethenes for Memories and Switches. *Chem. Rev.* **2000**, *100*, 1685–1716.
15 Siebold, M.; Port, H.; Wolf, H. C. *Molecular Crystals and Liquid Crystals Science and Technology, Section A: Molecular Crystals and Liquid Crystals*, Proceedings of the 7th International Conference on Unconventional Photoactive Systems **1995, 1996**, *283*, 75–80.
16 Walz, J.; Ulrich,K.; Port, H.; Wolf, H. C.; Wonner, J. and Effenberger, F. *Chem. Phys. Lett.* **1993**, *213*, 321–324 .

17 Ahmed, S. A.; Hartmann, T., Huch, V.; Duerr, H. and Abdel-Wahab, A.-M. A. *J. Phys. Org. Chem.* **2000**, *13*, 539–548 .

18 Fernandez-Acebes and Lehn, J.-M. *Chem.Eur. J.* **1999**, *5*, 3285–3292 .

19 Hartmann, T.; Shrestha, T. B.; Bossmann, S. H.; Hübner, C.; Renn, A. and Dürr, H. *Photochem. Photobiol. Sci.* **2009**, 8, 1172-1178.

20 Shrestha, T. B.; Melin, J.; Liu,J.; Dolgounitcheva, O.; Zakrzewski,; V. G. Pokhrel, M. R.; Gogritchiani, E.; Ortiz, J. V.; Turró, C. and Bossmann, S. H. *Photochem. Photobiol. Sci.* **2008**, *7*, 1449–1456.

21 Hess, S. T.; Girirajan,T. P. K. and Mason, M. D. *Biophys. J.* **2006**, *91*, 4258–4272.

22 Betzig, E.; Patterson, G. H.; Sougrat, R.; Lindwasser, O. W.; Olenych, S.; Bonifacino,J. S.; Davidson, M. W.; Lippincott-Schwartz, J. and Hess,H. F. *Science* **2006**, *313*, 1642–1645.

23 Gould, T. J.; Gunewardene, M. S.; Gudheti, M. V.; Verkusha,V. V.; Yin, S.-R.; Gosse, J. A. and Hess, S. T. *Nat. Methods* **2008**, *5*, 1027–1030.

24 Wang, S.-L.; Ho, T.-I.. *J. Photochem. Photobiol. A: Chem.* **2000**, *135*, 119-126.

25 Reichardt, C. *Chem. Rev.* **1994**, *94*, 2319-2358.

26 Frahn, M. S., *Ph.D. thesis*, Technische Universiteit Delft, The Netherlands**, 2003**, page 138.

27 Du, H.; Fuh, R. A.; Li, J.; Corkan, A. and Lindsey, J. S. *Photochem. Photobiol.* **1998**, *68*, 141–142.

28 Kubin, R. F. and Fletcher, A. N. *J. Lumin.* **1982**, *27*, 455–462.

29 Bossmann, S. H.; Oliveros, E.; Goeb, S.; Siegwart, S.; Dahlen, E. P.; Payawan, L. Jr., Straub, M.; Woerner, M. and Braun, A. M. *J. Phys. Chem. A* **1998**, *102*, 5542–5550 .

30 Reichardt, C. *Chem. Rev.* **1994**, *94*, 2319–2358 .

31 Ahmed, S. A.-M. *J. Phys. Org. Chem.* **2002**, *15*, 392–402.

32 (a) Hauck, G. and Duerr, H. *Angew. Chem.* **1979**, *91*, 1010–1011; (b) Gross, H. and Duerr, H. *Angew. Chem.* **1982**, *94*, 204.

33 Duerr, H. *Angew. Chem.* **1989**, *101*, 427–445.

34 Duerr, H. *Pure Appl. Chem.* **1990**, *62*, 1477–1482.

35 Gauglitz, G. and Scheerer, E. *J. Photochem. Photobiol., A: Chem.*, **1993**, *71*, 205–212.

36 Hartmann, T. PhD thesis, University of Saarland, Germany, **2001**.

37 Ahmed, S. A.; Hartmann, T. and Dürr, H. *J. Photochem. Photobiol., A: Chem.* **2008**, *200*, 50–56.

38 Smets, G. *Advances in Polymer Science 50*, Springer, Berlin-Heidelberg, **1983**.

39 Gross, H.; Dürr, H. and Rettig, W. *J. Photochem.* **1984**, *26*, 165–178.

40 Dürr, H. in *Photochromism—Molecules and Systems*, ed. Dürr, H. and Bouas-Lauent, H. Elsevier, Amsterdam, **1990**.

41 Rettig, W.; Majenz, W.; Herter, R.; Letard, J.-F.; Lapouyade, R. *Pure Appl. Chem.* **1993**, *65*, 1699–1704, and references quoted therein.

42 Turro, N. J. *Modern Molecular Photochemistry*, University Science Books, California, USA, **1991**.

1.6 Photogating MspA Porine Channel With Spirodihydroindolizine(DHI)

This research has been conducted in collaboration with Prof. Dr. Michael Niederweis and Mikhail Pavlenok at the University of Alabama at Birmingham, as well as with Prof. Dr. John Tomich in the Department of Biochemistry at Kansas State University.

1.6.1 Introduction

1.6.1.1 MspA Protein Channel

MspA is a very stable homo-octameric membrane protein, located in the outer membrane of *Mycobacterium smegmatis.*[1,2] Each monomer has 184 amino acids and these monomers form 2 consecutive beta barrels: the stem barrel (vestibule) and the base barrel.[1,2] MspA is a funnel-like structure having a single central channel **Figure 1.37**[1,2]. The height of this *porin* is 9.6 nm. The exterior diameter of the channel protein varies from 8.8 nm to 4.9 nm: the external diameter of the vestibule is 8.8 nm and of the base barrel is 4.9 nm. Similarly, the pore diameter of the porin varies from 1 nm to 4.8 nm, depending on the position within the funnel. This porin has a constriction zone ("bottleneck") of 1 nm of inner diameter that is defined by two rings of aspartates in D90 and D91 positions.[1] The exterior surface of MspA is hydrophobic, whereas the interior surface of the porin is hydrophilic.[1] *Mycobacterium smegmatis* uses this protein channel to transport hydrophilic nutrients and to discharge hydrophilic metabolites.[1]

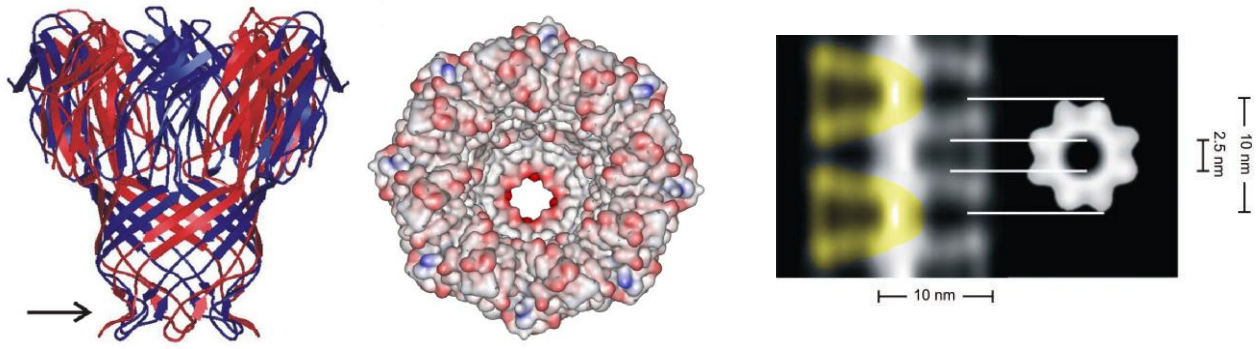

A **B** **C**

Figure 1.37 A: MspA from *Mycobacterium* smegmatis (the arrow indicates the constriction zone), B: top view of MspA, C: Electron microgram of MspA (taken without permission from reference 20,21).[1,2]

1.6.1.2 Photo-Gated Ion Channels

Over several decades, many efforts have been directed towards the goal of generating artificial light-responsive ion channels by modifying naturally occurring protein channels.[3] These systems have in common that they have to be supported by a natural or artificial membrane in order to function properly. Examples for the incorporation of azobenzene-derivatives as optical gates are the Nicotinic Acetylcholine Receptor (nAChR, pentameric transmembrane cation channel)[3,4,5], Gramicidin A (pentadecapeptide, dimer when pore-forming)[6], the family of Synthetic Photoisomerizable Azobenzene Regulated K^+ channels (SPARK, tetrameric ion channels)[7,8] the Ionotropic Glutamate Receptor (homo- or heterotetramers in vivo)[9] and α-Hemolsyin.[10] The main differences between the MspA-based switchable channels that are in development in our groups and the SPARK (synthetic photoisomerizable azobenzene-regulated K^+) channels[11,12] are: a) MspA is the bigger pore, of superior stability and suitable for applications under extreme conditions (up to 100 ^oC or in organic solvents). b) MspA can be used without membrane support. c) The optical switch of MspA is located inside the pore, whereas the SPARK switch is outside. d) MspA is not cation-specific, but can be used for a variety of cations, including H^+ and Ca^{2+}. e) MspA is not suitable for the excitation of neurons, but suitable for the reconstitution within (mammalian) cell membranes. It can be used to reverse gradients (H^+, Na^+, K^+, Ca^{2+}) across cell membranes. Compared to α-Hemolysin, MspA possesses a narrower constriction zone (2.6 nm *vs.* 1.0 nm) and a distinctly higher stability (**Figure 1.38**). Polar and non-polar residues are depicted in green and in yellow, respectively

and the channel lining is shown in black. Black/red: conformation changes during the optical switching process (**Figure 1.38**).[1,10]

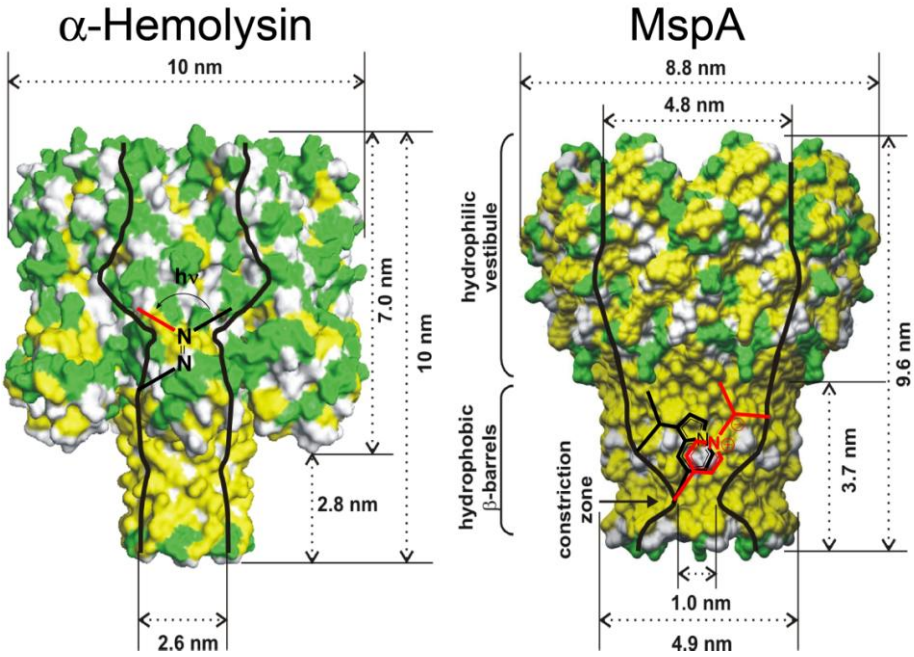

Figure 1.38 Comparison between a-hemolysin (azobenzene-switch, according to ref.[13]) and MspA (structure from ref. [1]) featuring (DHI/ betaine) optical gates at or near their constriction zones.

The use of a photochromic compound of the spiropyran/merocyanine-type as optical gate can be found in the chemically modified MscL-channels (mechanosensitive channel of large conductance).[14,15] A spiropyrane-derivative was chemically linked to a cysteine-mutant of MscL. Irradiation with UVA-light (360-370 nm) caused ring-opening to the significantly more polar merocyanine form.[3] The latter can be switched back when excited with 460-500 nm or reacts thermally via an Arrhenius/Eyring kinetic. Whereas azobenzenes ($\Delta L \leq 0.7$ nm, $\Delta m \leq 3$ D) show pronounced changes in length and geometry[16], but only minor changes in their dipole moments, spiropyranes undergo significant polarity changes, but almost no changes in geometry ($\Delta L \leq 0.2$ nm, $\Delta m \leq 15$ D).[3,17,18] In contrast to azobenzenes, spirodihydroindolizines (DHIs) cannot only be switched by using visible light, but they also show big changes in their dipole moments and their

geometries when reacting to the corresponding betaines (Bs) (up to: $\Delta L \leq 0.8$ nm, $\Delta m \leq 14$ D).[18,19] As already emphasized, MspA is of superior stability to all known protein channels and can readily reconstitute in various environments.[20] The covalent linkage of a series of photochromic spirodihydroindolizines to the constriction zone offers the advantage of fine tuning both the ion-conductivity and the gating time.

Ideally, photo-gated channels should have the following specifications: a) Their diameter and length should be in the low nanometer range. b) The channel must be chemically and thermally stable and resistant to denaturation. c) The channel should function without any support matrix ("*stand-alone-channels*") for applications on surfaces. d) The channel should easily reconstitute in cell membranes for applications in living cells. e) The channel gating must be reversible. Both transitions must be triggered using visible light. f) The "on" and/or "off"-states should be detectable by emission spectroscopy without inducing another switch. g) The molecule used as optical switch should be stable and capable of multiple cycles of activation and deactivation.

The mycobacterial porin MspA (porin A from *Mycobacterium smegmatis*) is especially suited as a channel, because it fulfills all requirements listed above (a-d). [20,21] Photochromic spirodihydroindolizines (DHIs) meet the required photophysical and photochemical properties (e-f) for the optical gate. [22,23] Both components can be combined by linking the tethered DHIs to suitable positions in MspA.

The aim of this research was to demonstrate that the spirodihydroindolizine/betaine system can be successfully used for the optical gating of the mycobacterial channel porin MspA.

1.6.2 Experimental

1.6.2.1 Chemicals, Instrumentation

All chemicals were obtained from Acros Organics and Sigma Aldrich, unless noted otherwise. All solvents were used without distilled unless noted otherwise. 400 MHz and 200 MHz Varian NMR-spectrometer, a Nicolet Protégé 460 FT-IR Spectrometer and Thermo Scientific Nicolet 380 FT-IR (neat sample, Dr Aakeröy Lab KSU) were used in this study. I would like to thank the Analytical Laboratory of Dr. Ruth Welti at KSU for recording the mass

spectra of our compound employing an Applied Biosystems API-4000 triple quadrupole mass spectrometer with electrospray and APCI sources. Lipid bilayer experiments were performed in a home-built bilayer apparatus in Dr. Niederweis Lab in Department of Microbiology, UAB Alabama.

1.6.2.2 Synthesis of Photochromic Compound

1.6.2.2.1 Synthesis of Spiro[9H-fluorene-9,1'(8'aH)-indolizine]-2',3'-dicarboxylic acid, 7'-(4-pyridinyl)-, dimethyl ester (1.6.3)

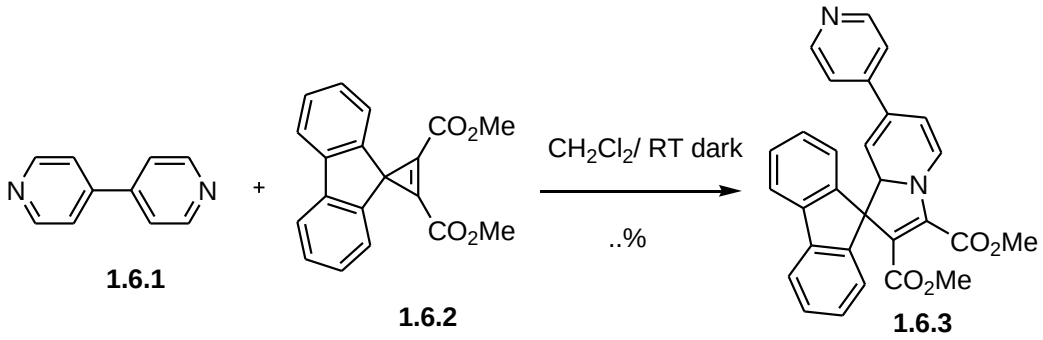

Scheme 1. 20: Synthesis of *Spiro*[9H-fluorene-9,1'(8'aH)-indolizine]-2',3'-dicarboxylic acid, 7'-(4-pyridinyl)-, dimethyl ester (1.6.3)

Synthetic Procedure: *Spiro*[9H-fluorene-9,1'(8'aH)-indolizine]-2',3'-dicarboxylic acid, 7'-(4-pyridinyl)-, dimethyl ester **1.6.3** (molecular formula $C_{29}H_{22}N_2O_4$)**:** Spirocyclopropene **1.6.2** (0.5 g, 1.6 mmol) in 5 mL diethyl ether was added dropwise to 4,4- bipyridine (0.25 g, 1.6 mmol, ACROS Organic) in 30 mL of dry diethyl ether under continuous stirring. The reaction mixture was kept stirring overnight at RT under dark condition. Then the reaction mixture was kept in the refrigerator to yield a dark solid powder, which contained the photochromic product. The filtrate was evaporated and purified by descending column chromatography (stationary phase: SiO_2 mobile phase ethylacetate). The reaction product from the addition of two molecules of spirocyclopropene to 4,4'-bipyridine was obtained first (mainly 332 mg (0.497 mmol) of [7',7'''-*Bispiro*[9H-fluorene-9,1'(8'aH)-indolizine]]-2',2''',3',3'''-tetracarboxylic acid, tetramethyl ester were found, TLC silica R_f = 0.5, *n*-hexane/ethylacetate, 1/1, v/v). The second fraction was the photochromic reaction product **1.6.3**, which crystallized after the removal of the solvent in vacuum as yellowish brown precipitate 0.136 g. (0.296 mmol, 18.5%) R_f = 0.22, 100% EtOAc

as a mobile phase in silica TLC. mp 100 ºCIR (KBr) Wavenumbers cm^{-1} 737, 1137, 1239, 1424, 1547, 1593, 1695, 1746, 2842, 2945, 3047, 3460 (shoulder); ^{1}H NMR ($CDCl_{3,}$ 200 MHz) δ [ppm] 3.2 (s, 3H), 4 (s, 3H), 4.7 (m, 1H), 5.4 (dd, *J* = 7.7 and 1.6 Hz, 1H), 5.58 (d, *J* = 2.2 Hz 1H), 6.6 (d, *J* = 7.7 Hz, 1H), 6.9 (dd, *J* = 4.4 and 1.4 Hz, 2H), 7.18 (td, *J* = 8.5 and 1.5 Hz,1H),7.35 (td, *J* = 7.4 and 1.5 Hz, 2H), 7.47 (d, *J* = 7.7 Hz, 1H), 7.57 (d, 7.3 Hz, 1H), 7.7 (dd, *J* = 7 and 0.7 Hz 2H), 8.4 (dd, *J* = 4.4 and 1.4 Hz, 2H); ^{13}C ($CDCl_{3,}$ 200 MHz) δ [ppm] 51.34, 53.58, 64.5, 69.9, 104.1, 115.9, 120.05, 120.30, 120.38, 123.71, 124.64, 127.38 127.96, 128.48, 128.79, 134.03, 140.55, 141.92, 141.99, 146.05, 147.02, 150.03, 162.13, 163.78; Mass $C_{29}H_{22}N_2O_4$, m/z mass calculated, 462.15 obtained 461.3, 462.3, and 461.3(M-1, M and M+1) also M^+ Na mass 479.4(+23)

1.6.2.2.2 Spiro[9H-fluorene-9,1'(8'aH)-indolizine]-2',3'-dicarboxylic acid, 7'-(N-methyl-4-(4'-pyridyl))-, dimethyl ester (1.6.5)

N-Methyl-4-(4'-pyridyl)pyridinium iodide 1.6.4

Synthetic Procedure: 0.80 g of 4,4′ dipyridyl (4,4'-bipyridine) **1.6.1** (0.0051mol, 98% anhydrous ACROS Organic) and 0.40 mL of methyl iodide (0.0064 mol 99% ACROS Organic) were mixed in 40 mL of dry DCM in a 100 mL RB flask and reflux for 2 hours, adapted from Feng et. al method[25] After 2 hours, a yellow precipitate occurred and the mixture was cooled down to room temperature. The yellow precipitate was separated by filtration, washed twice with ethyl acetate and then was dried in high vacuum (yield of step 1: 0.401g). The filtrate was refluxed again for 15 hours. A yellow precipitate formed again. It was filtered, washed and dried as described (yield of step 2: 0.886 g). Total yield was 1.287g (84%). mp 255 ºC; IR (KBr) wavenumber cm^{-1} 713, 811, 1194, 1222, 1333, 1416., 1547, 1602, 1652, 3025, 3426(shoulder. may be moisture); ^{1}H NMR (400 MHz, DMSO) δ [ppm] 4.3 (s, 3H), 8 (d, *J* = 5.6 Hz, 2H), 8.5 (d, *J* = 6.4 Hz, 2H), 8.8 (d, *J* = 5.6 Hz, 2H), 9 (d, *J* = 6.4 Hz, 2H); ^{13}C NMR (400 MHz, DMSO) δ [ppm] 48.2, 122.5, 125.6, 141.5, 146.8, 151.7, 152.2;

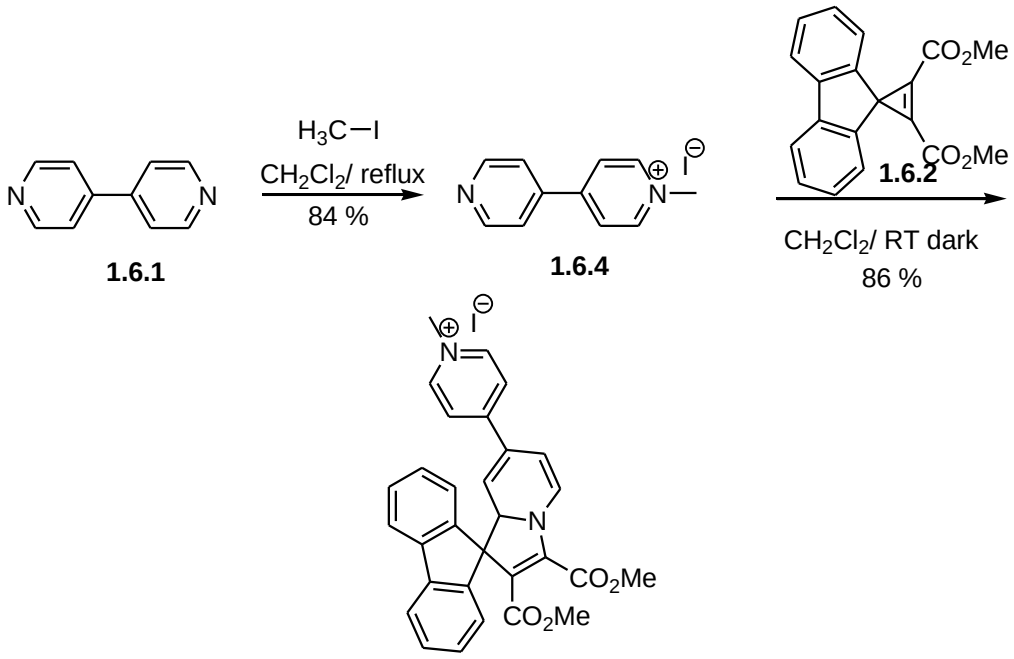

Scheme 1. 21: *Spiro*[9H-fluorene-9,1'(8'aH)-indolizine]-2',3'-dicarboxylic acid, 7'-(N-methyl-4-(4'-pyridyl))-, dimethyl ester (1.6.5)

***Spiro*[9H-fluorene-9,1'(8'aH)-indolizine]-2',3'-dicarboxylic acid, 7'-(N-methyl-4-(4'-pyridyl))-, dimethyl ester 1.6.5 .**

Synthetic Procedure: N-Methyl-4-(4'-pyridyl)pyridinium iodide **1.6.4** (0.016 g, 0.052 mol) and the spirocyclopropene **1.6.2** (0.015 g, 0.05 mol) were mixed in 10 mL of dry dichloromethane in a 50 mL RB flask. The mixture was stirred for 15 hours at room temperature in the dark. After 15 hours of stirring, the solvent was removed and subjected to descending column chromatography (stationary phase: SiO_2). At first 400 mL of DCM was passed through the column to remove unreacted spirocyclopropene. Then eluent was changed to 5% methanol in DCM to obtain *spiro*[9H-fluorene-9,1'(8'aH)-indolizine]-2',3'-dicarboxylic acid, 7'-(N-methyl-4-(4'-pyridyl))-, dimethyl ester methylated DHI **1.6.5** 23 mg. (0.043 mmol, 86% yield). mp: 275 ºC (D); IR (KBr) wave numbers cm^{-1} 748, 1137, 1224, 1378, 1439, 1639, 1741, 2847, 2919, 3446 (shoulder, may be moisture); ^{1}H NMR ($CDCl_3$, 200 MHz,) δ [ppm] 3.2 (s, 3H), 3.9 (s, 3H), 4.4 (s, 3H), 4.8 (s, 1H), 5.4 (d *J* = 7.7 Hz, 1H), 5.5 (d, *J* = 2.2 Hz, 1H), 6.68 (d, *J* = 7.7 Hz, 1H), 7-7.5 (m, 8H), 7.7 (d, *J* = 7.7 Hz, 2H), 8.9 (d, *J* = 6.6 Hz, 2H); ^{13}C ($CDCl_3$, 200 MHz) δ [ppm] 49.02, 51.5, 53.8, 64.4, 69.7, 101.06, 120.4, 120.8, 121.1, 123.7, 123.8, 124.2, 127.7,128.31,

128.37, 128.9, 129.3,132.01, 140.6, 141, 141.8, 145, 145.4, 145.7, 146.1, 161.6, 163.4; MS $C_{30}H_{25}N_2O_4I$ M/z calculated 604.43, found 477.300 (M-I)

1.6.2.2.3 Spiro[9H-fluorene-9,1'(8'aH)-indolizine]-2',3'-dicarboxylic acid, 7'-(N-(1H-Pyrrole-2,5-dione, 1-(3-bromopropyl))-4-(4'-pyridyl))-, dimethyl ester 1.6.7

N-(3-bromopropyl)maleimide-(N- (3-bromopropyl -(1H-Pyrrole-2,5-dione,)) **1.6.8** , (1-(3 N-(1H-Pyrrole-2,5-dione)) 4-(4'-pyridyl)pyridinium bromide **1.6.6** compounds are generously provided by Mausam Kalita.

***Spiro*[9H-fluorene-9,1'(8'aH)-indolizine]-2',3'-dicarboxylic acid, 7'-(N-(1H-Pyrrole-2,5-dione, 1-(3-bromopropyl))-4-(4'-pyridyl))-, dimethyl ester 1.6.7**.

Synthetic Procedure: 20 mg (0.05 mmol) of 1-(3-bromopropyl))-4-(4'-pyridyl)pyridinium bromide **1.6.6** and 20 mg (0.064 mmol) of spirocyclopropene **1.6.2** was dissolved in acetonitrile and stirred overnight (15 h) in the dark at room temperature. The reaction mixture was filtered and the solvent was removed in vacuum. NMR of the crude mixture was taken, ^{1}H NMR (CD_3CN, 400 MHz) δ [ppm] 2.2 (quintet, 2H invisible in CD_3CN, but visible in DMSO) 3.25 (s, 3H), 3.5 (t, *J* = 6 Hz, 2H), 4.1 (s, 3H), 4.8 (t, *J* = 6.5 Hz, 2H), 4.9 (s, 1H), 5.43 (d, *J* = 7.7 Hz, 1H), 5.6 (d, *J* = 3.6 Hz, 1H), 6.69 (s, 2H), 6.74(d, *J* = 7.7 Hz, 1H), 7.2 – 7.8 (m, 10 H), 9.2 (d, *J* = 7 Hz, 2H); ^{13}C NMR (CD_3CN, 200 MHz) δ [ppm] 31.26, 35.20, 52.08, 54.72, 59.62, 65.80, 70.53, 102.37, 118.69, 121.34, 121.80, 122.51, 125.11, 125.33, 127.28, 128.60, 129.21, 129.32, 129.87, 130.19,132.89, 135.80, 142.09, 143.20, 145.67, 147.68, 154.92, 164.26, 172.53 mass: $C_{36}H_{30}BrN_3O_6$ m/z calculated 679.13 found 680.4(M+1) and 600.4(M-Br).

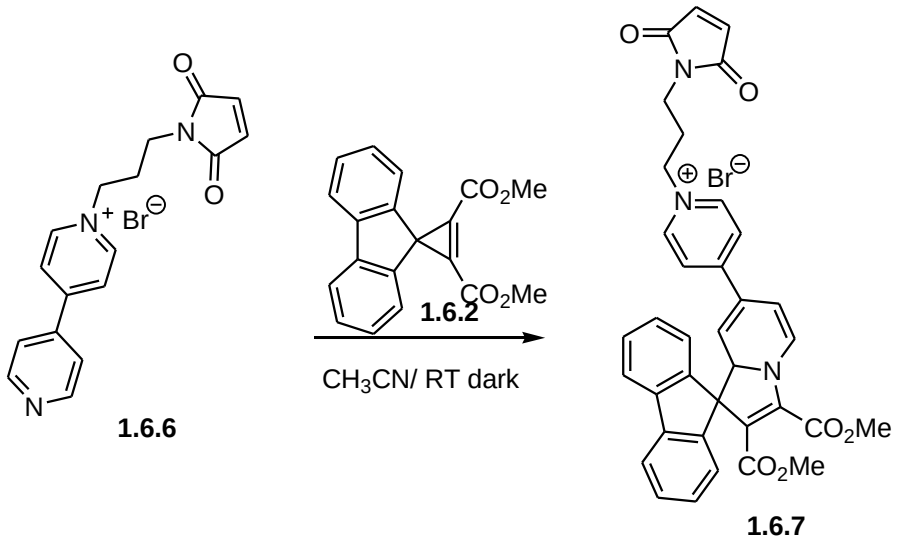

Scheme 1. 22: *Spiro*[9H-fluorene-9,1'(8'aH)-indolizine]-2',3'-dicarboxylic acid, 7'-(N-(1H-Pyrrole-2,5-dione, 1-(3-bromopropyl))-4-(4'-pyridyl))-, dimethyl ester 1.6.7

1.6.2.2.4 4-((E)-2-(pyridinium-4-yl)vinyl)quinolyl spirodihydroindolizinesDHI

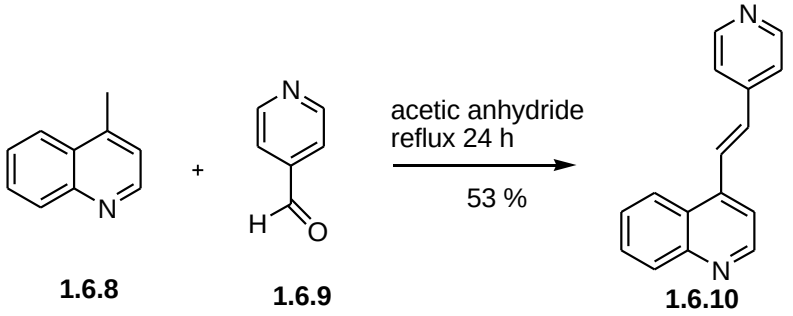

Scheme 1. 23: (E)-2-(pyridinium-4-yl)vinyl)quinol

(E)-2-(pyridinium-4-yl)vinyl)quinol 1.6.10

Synthetic Procedure: Lipidine **1.6.8** (0.5 mL, 3.82 mmol) and 4-carboxyaldehydepyridine **1.6.9** (0.359 mL, 3.82 mmol) were dissolved in 10 mL of acetic anhydride in a 50 mL RB flask. The reaction mixture was refluxed. The reaction progress was monitored by TLC. After two days starting materials was almost over and the reaction mixture was cooled down to RT. The dark brown colored reaction mixture was concentrated to dryness *via* rotary evaporation. The compound 3 was purified by SiO_2 column chromatography. Ethyl acetate was used followed by 5% methanol in ethyl acetate to elute the product **1.6.10**. Single spotted fractions (9-13) were mixed, evaporated and recrystallized in ethyl acetate in hexane to

yield brown crystal, compound **1.6.10** (0.470 g, 2.01 mmol 53 % yield). ^{1}H NMR ($CDCl_{3,}$ 400 MHz) δ [ppm], 8.16–8.209 (t, *J* = 7.8 Hz, 2H), 8.01–8.05 (d, *J* = 16.2 Hz, 1H), 7.76-7.80 (t, *J* = 6.8 Hz, 1H), 7.64-7.66 (t, *J* = 6.8 Hz, 1H), 7.61-7.62 (d, *J* = 4.5 Hz, 1H), 7.49-7.50 (d, *J* = 4.5 Hz, 2H),7.26-7.28 (d, *J* = 16.2 Hz, 1H), 8.68–8.69 (d, *J* = 4.5 Hz, 2H), 8.95 - 8.96(d, *J* = 4.5 Hz, 1H); ^{13}C NMR ($CDCl_{3,}$ 400 MHz) δ [ppm] 117.76, 121.45, 123.42, 126.36, 127.15, 127.80, 129.81, 130.37, 132.68, 142.01, 143.89, 148.77, 150.30, 150.60; MS $C_{16}H_{12}N_2$ m/z [M + 1] 233

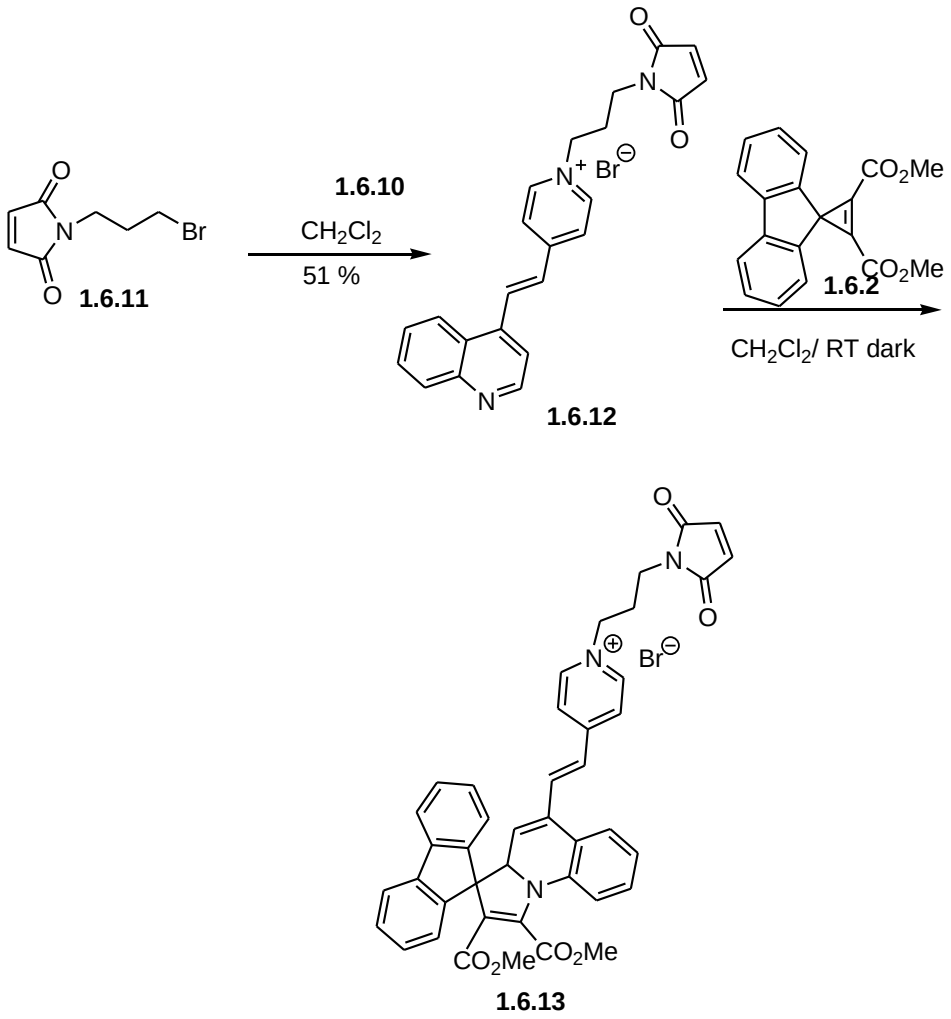

Scheme 1. 24: 4-((E)-2-(pyridinium-4-yl)vinyl)quinolyl spirodihydroindolizinesDHI

4-((E)-*2-(*1'-(3' *N*-(1H-Pyrrole-2,5-dione))pyridinium-4-yl)vinyl)quinolyl bromide 1.6.12

Synthetic Procedure: N-(3-bromopropyl) maleimide **1.6.11** (40 mg, 0.172 mmol) (generously provided by Mausam Kalita) . Compound **1.6.10** (38 mg, 0.174 mmol) were dissolved in 3 mL of dichloromethane in a 10 mL of RB flask. The reaction mixture was refluxed for overnight. The light brown precipitate, formed in next day was filtered and washed with cold dichloromethane to give compound **1.6.12** as brown solids (40 mg, 0.088 mmol, 51% yield) ^{1}H NMR (DMSO, 400 MHz) δ [ppm] 2.21 (t, *J* = 7.4 Hz, 2H),3.51 (t, *J* = 6.4 Hz, 2H), 4.57 (t, *J* = 7.6 Hz, 2H), 7.08 (s, 2H), 7.76 (t, *J* = 7.02 Hz, 2H), 7.83-7.88 (m, 3H), 7.97-7.98 (d, *J* = 4.6 Hz, 1H), 8.02-8.02 (d, *J* = 4.5 Hz, 1H), 8.11 (d, *J* = 8.2 Hz, 1H), 8.54 (d, *J* = 6.6 Hz, 2H),), 8.63 (d, *J* = 8.3 Hz, 1H), 8.80 (d, *J* = 16.2 Hz, 1H), 9.08 (d, *J* = 6.6 Hz, 2H); ^{13}C NMR (DMSO, 400 MHz) δ [ppm] 30.55, 34.67, 58.34, 118.55, 124.84, 125.71, 126.24, 127.92, 130.24, 130.60, 135.21, 135.36, 135.38, 140.83, 145.43, 148.91, 151.005, 152.55, 171.82; MS $C_{23}H_{20}N_3O_2$ Br calculated 450.33 found 370.300 (M-Br)

((E)-2-(pyridinium-4-yl)vinyl)quinolyl spirodihydroindolizinesDHI

Synthetic Procedure: Compound **1.6.12** (23 mg, 0.049 mmol) and spirocyclopropene **1.6.2** (15 mg, 0.049 mmol) were dissolved in 5 mL of DMSO and stirred overnight (24 h) in the dark at room temperature. After the completion of reaction DMSO was removed in high vacuum at 50 ^{o}C. NMRs were recorded as crude. ^{1}H NMR (DMSO-d_6, 400 MHz) δ [ppm] 2.11 (quintet, *J* = 7.6, 2H), 3.18 (s, 3 H), 3.5 (t, imbedded in water pick), 4.01 (s, 3H), 4.45 (t, *J* = 7.4 Hz, 2H) 5.24 (s,1 H), 5.707 (s, 1H), 6.88 (d, 12.5 Hz, 1H), 7.01-7.16 (m, 4 H), 7.22-7.54 (m, 9 H, 7.74 (m, 2H, 7.90 (d, *J* = 7.7Hz, 2H), 8.12 (d, *J* = 6.2, 2H), 8.87 (d, *J* = 6.2, 2H); MS $C_{42}H_{34}BrN_3O_6$ Calculated 756.64, found 676.300(M-Br)

1.6.2.3 Photo-gating of wt MspA/DHI complexes in lipid bilayer experiments

Lipid bilayer experiments were performed in a self-made lipid bilayer apparatus as described.[26] These experiments were carried out in artificial membranes made from diphytanoyl phosphatidyl-choline in 0.5 M KCl/5 mM HEPES at pH 7.0.[26] Current traces were recorded using an applied voltage of 10 mV and an amplification factor of 10^9 by both, a chart recorder on paper and by a data acquisition computer at a sampling rate of 100 Hz. The baseline current was

recorded with diphytanoyl phosphatidyl-chloride membrane without any channel protein. Unmodified wild-type MspA (50 ng) was added as a positive control. The pre-formed MspA-DHI-complex (500 ng) was added to the electrolyte and current traces were recorded a) without light and b) during polychromatic irradiation of the membrane light λ = 230-450 nm (Fiber Lite 180, Doilan-Jenner Industries equipped with a water filter and a 450 nm-cutoff filter). The black arrows indicate either the addition of protein or the beginning or the end of irradiation. It should be noted that the current traces in panels **A, B, C** and **E (Figure 1.39)** are complete current traces taken from the same experiment. The employed current data acquisition software (Testpoint macro) needs to be modified to allow higher sampling frequencies up to 100,000 Hz and a digital recording of the DHI-induced photo-switch of MspA. One experiment consisted of five consecutive recordings of approximately 10 min each.

1.6.3 Results and Discussion

Photochromism of the *Spiro*[9H-fluorene-9,1'(8'aH)-indolizine]-2',3'-dicarboxylic acid, 7'-(N-methyl-4-(4'-pyridyl))-, dimethyl ester (methylated DHI) **1.6.5** is given in **Scheme 1.23** . Upon irradiation of UV light (λ = 230- 450 nm) it undergoes a ring opening reaction to yield the isomeric *cisoid* and *transoid* Betaines. The *transoid* Betaine, if it is formed in the rather narrow MspA channel, undergoes ring closing to the DHI via the *cisoid* isomer. However, the relevant lifetime for the channel-triggering process is most likely for the disrotatory 1,5-electrocyclization from the *cisoid* betaine to the DHI. From laser-absorption experiments, which were conducted in the group of Prof. Dr. Claudia Turro at Ohio State University in Columbus/OH, we know that this lifetime is of the order of 35 μs at 293K. This time window is apparently sufficient to trigger the flow of ions through the lipid bilayer membrane via the channel protein MspA.

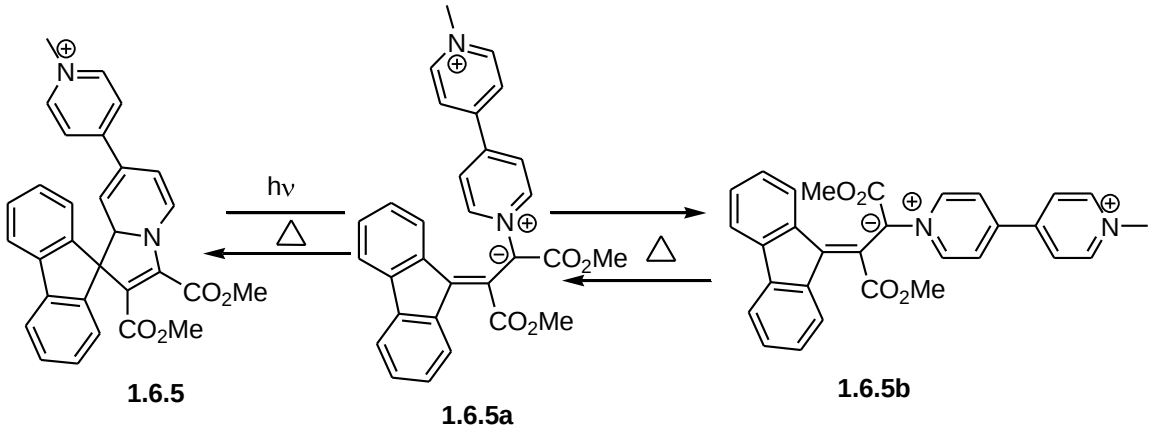

Scheme 1. 25: Photochromism of the *Spiro*[9H-fluorene-9,1'(8'aH)-indolizine]-2',3'-dicarboxylic acid, 7'-(N-methyl-4-(4'-pyridyl))-, dimethyl ester.

The current trace in the lipid bilayer experiments did not show any deviation from the baseline indicating that the lipid membrane was stable and all components in the system were free of channel-forming activity (**Figure 1.39A**). No channel activity was recorded (**Figure 1.39B**) with the MspA-DHI complex without irradiation, but the channeling activity increased significantly within minutes after the continuous irradiation with polychromatic light (λ = 230 – 450 nm) had begun. Those spikes, observed after irradiation, were caused by short-lived channel openings (**1.39 C and D**). These spikes were faster than 10 ms, because they were not recorded by a data acquisition computer operating at a sampling frequency of 100 Hz. Very few or no spikes were observed after the light was turned off (**Figure 1.39E**). As a positive control for the quality of the membrane, 50 ng of fresh MspA was added to the same membrane. After incubation time of a few minutes a rapid insertion of stable MspA pores into the membrane was observed **(Figure 1.39F**). **G.** Analysis of conductance steps of wt MspA in 0.5 M KCl as shown in panel **F**. A total of 65 putative insertions in two membranes were analyzed. **H.** Analysis of current spikes as shown in **C** and **D** in 0.5 M KCl. A total of 75 spikes in three membranes were analyzed.

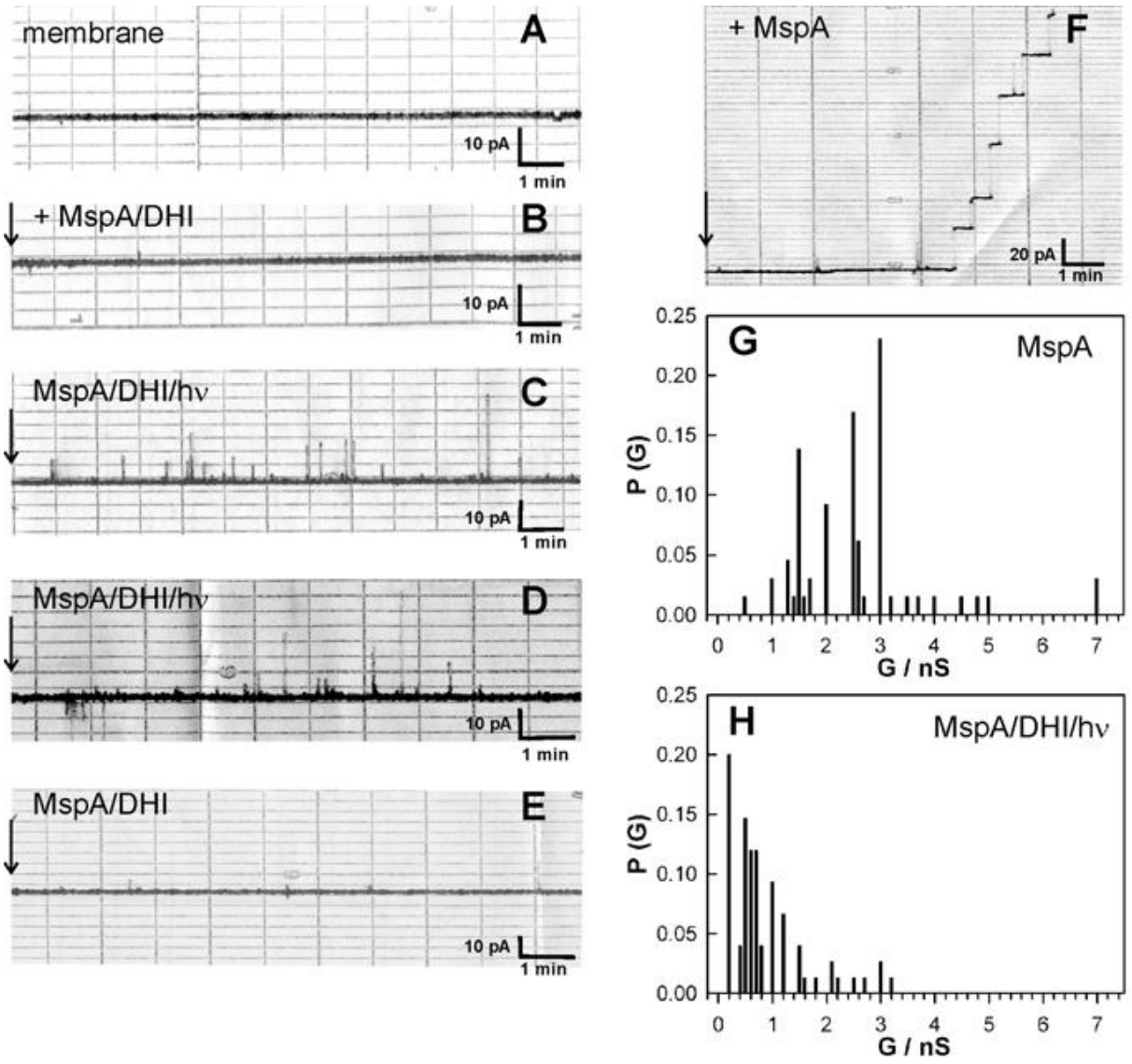

Figure 1.39 Analysis of the photo-gating of MspA-DHI complexes in lipid bilayer experiments.

Three experiments with the same results were performed (**Figure 1.39D**). These results demonstrate that binding of the DHI to MspA completely blocks the channel. Since this was not due to the absence of MspA protein from the membrane as shown in **Figure 1.39 C** and **D**, we

have concluded that the DHI binds in the channel interior of MspA. Secondly, irradiation at the wavelengths, which specifically trigger the isomerization of the DHI to the betaine, induced rapid and transient channel openings of the MspA/DHI complex. This demonstrated that the DHI is photoactive inside MspA and the photo-induced switch temporarily opens the MspA pore. While the main single-channel conductance of MspA was approximately 3 nS in 0.5 M KCl (**Figure 1.39G**), the main conductance of the light-triggered channel openings of the MspA/DHI complex under the same conditions was 0.2 nS (**Figure 1.39H**). Only very few full channel openings were observed. It is likely that the positively charged DHI binds to the highly negatively charged constriction zone inside the MspA pores.

To improve the stability of the MspA/DHI complex, DHIs were modified with a maleimide linker **1.6.7**. The thiol group of the cysteine-modified MspA will be able to bind with covalently maleimide-tethered DHIs inside the MspA pore. Styrylquinline-DHI with a maleimide linker was also synthesized **1.6.13**. In addition, confocal microscopy, as well as Atomic Force Microscopy will be able to locate the position of the DHI inside the MspA protein channel. Furthermore, triggering the channel activity of MspA will undoubtedly prove this concept. Unfortunately, technical difficulties arose in the group of Prof. Dr. Niederweis at UAB that have prevented me from finishing these experiments. However, they will be continued.

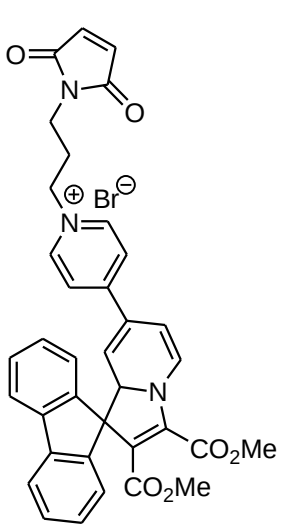

1.6.7

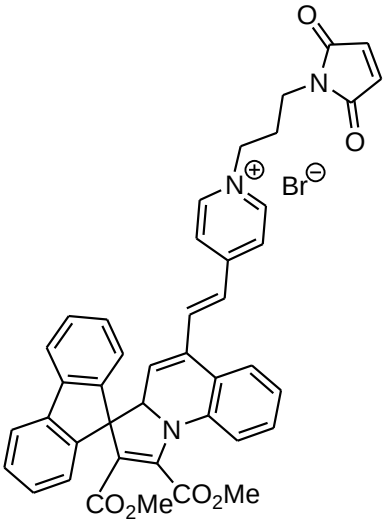

1.6.13

Figure 1.40 Maleimide linked DHIs

1.6.4 Conclusion

The flow of ions through an otherwise impermeable lipid bilayer membrane of diphytanoyl phosphatidyl-choline can be controlled by light. This can be achieved by reconstituting the mycobacterial channel porin MspA, which forms a supramolecular complex with a photochromic DHI/Betaine-system, within the membrane (DHI: spirodihydroindolizine). This system undergoes the DHI to Betaine isomerization when irradiated with UV or blue light and acts as a molecular gate. In the absence of UV/blue- irradiation, the photochromic compound is in its closed and uncharged form, which is able to close the constriction zone (bottleneck) of MspA. Therefore, there is no flow of ions observable. Irradiation of UV/blue-light causes the DHI to isomerize into the betaine (open zwitterionic form). Spikes in the resulting current are the indication of electrolyte flow though the MspA channel. It is likely that the positively charged DHI binds to the highly negatively charged constriction zone inside the MspA pores, which is made of a double-ring of eight aspartates each.

1.6.5 References

1. Faller, M.; Neiderweis, M.; Schulz, G. E. *Science* **2004**, *303*, 1189-1192.
2. Engelhardt, H.; Christian Heinz, C.; Niederweis, M. *J. Biol Chem*. **2002**, *277*, 37567–37572.
3. Banghart, M. R.; Volgraf, M.; Trauner, D. *Biochem.* **2006**, *45*, 15129-15141.
4. Bartels, E.; Wasserman, N. H.; Erlanger, B. F. *Proc. Natl. Acad. Sci. U. S. A.* **1971**, *68*, 1820-1823.
5. Silman, I.; Karlin, A. *Science* **1969**, *164*, 1420-1421.
6. Stankovich, C. J.; Heinemann, S. H.; Schreiber, S. L. *Biochim. Biophys. Acta.* **1991**, *1061*, 163-170.

7. Banghart, M.; Borges, K.; Isacoff, E.; Trauner, D.; Kramer, R. H. *Nat. Neurosci.* **2004**, *7,* 1381-1386.
8. Chambers, J. J.; Banghart, M. R.; Trauner, D.; Kramer, R. H. *J. Neurophysiol* **2006**, *96,* 2792-2796.
9. Volgraf, M.; Gorostiza, P.; Numano, R.; Kramer, R. H.; Isacoff, E. Y.; Trauner, D. *Nat. Chem. Biol.* **2006**, *2,* 47-52.
10. Song, L. Z.; Hobough, M. R.; Shustak, M. R.; Cheley, S.; Bayley, H.; Gouaux, J. E. *Science* **1996**, *274,* 1859-1866.
11. Isacoff, E. Y.; Kramer, R. H.; Trauner, D.; Banghart, M. R.; Volgraf, M.; Langa, P.; Gorostiza, I. *U. S. Pat. Appl. Publ.* **2007**, 92pp.
12. Gorostiza, P.; Isacoff, E. *Mol.BioSyst.* **2007**, *3,* 686-704.
13. Kocer, A.; Walko, M.; Meijberg, W.; Feringa, B. L. *Science* **2005**, *309,* 755-758.
14. Kocer, A.; Walko, M.; Feringa, B. L. *Nature Protocols* **2007**, *2,* 1426-1437.
15. Rau, H. in *Azo Compounds*; Eds: Duerr, H. Bouas-Laurent, H.; *Photochromism: Molecular Systems:* Elsevier, Amsterdam, Netherlands, **1990**, 165-192.
16. Guglielmetti, R. in *4n + 2 Systems: Spiropyrans*; Eds: Duerr, H. Bouas-Laurent, H.; *Photochromism: Molecular Systems*; Elsevier, Amsterdam, The Netherlands, **1990**, 314-466.
17. Duerr, H. in *The 4n + 2 Systems Based on 1,5-Electrocyclization*; Eds.: Duerr, H. Bouas-Laurent, H.; *Photochromism: Molecular Systems*; Elsevier, Amsterdam, The Netherlands, **1990**, 210-269.
18. Shrestha, T. B.; Melin, J.; Liu,J.; Dolgounitcheva, O.; Zakrzewski, V. G.; Pokhrel, M. R.; Gogritchiani, E.; Ortiz, J. V.; Turró, C. and Bossmann, S. H. *Photochem. Photobiol. Sci.* **2008**, *7,* 1449–1456.
19. Niederweis, M.; Bossmann, S. H. *Encyclopedia of Nanoscience and Nanotechnology* **2004**, 851-867.
20. Niederweis, M.; Ehrt, S.; Heinz, C.; Klöcker, U.; Karosi, S.; Swiderek, K. M.; Riley, L.; Benz, R. *Mol. Microbiol.* **1999**, *33,* 933-945.
21. Heinz, C.; Engelhardt, H.; Niederweis, M. *J. Biol. Chem.* **2003**, *278,* 8678-8685.
22. Duerr, H. *Pure Appl. Chem.* **1990**, *62,* 1477-1482.

23. (a) Duerr, H. *Pure Appl. Chem.* **1990**, *62*, 1477-1482. (b) Spang, P.; Duerr, H. *Angewandte Chemie* **1984**, *96*, 227-9.
24. Duerr, H. *Organic Photochromic and Thermochromic Compounds* **1999**, 223-266.
25. Feng,Dai-Jun; Li, Xiao-Qiang; Wang, Xiao Zhong; Jiang, Xi-Kui; Li, Zhan-Ting *Tetrahedron*, **2004,** *60*, 6137- 6144.
26. Engelhardt, H.; Heinz, C.; Niederweis, M. *J. Biol. Chem.* **2002**, *277*, 37567-37572.

CHAPTER 2 - Synthesis of Coelenterazine

2.1 Introduction

Photodynamic therapy (PDT) has been successful in treating non-hypoxic tumors, which were conveniently located to permit high doses of incident light.[1]To date, the U. S. Food and Drug Administration (FDA) has approved the photo-sensitizing agent called porfimer sodium (Photofrin®), for use in PDT for the treatment of esophageal cancer[2], non small cell lung cancer[2] and of precancerous lesions in patients with Barrett's esophagus (a condition that can lead to esophageal cancer). However, the main obstacle to a prevalent application of PDT is not the enrichment of photodynamic drugs within tumors, but the availability of light sources that provide sufficiently high doses in the appropriate excitation windows for mono-photonic and bi/multiphotonic excitation. Numerous strategies for enhanced irradiation of tumors that are located within the human or mammalian body are discussed in the literature.[3]Among these approaches is the use of high-energy lasers instead of lamps[2], laser diodes[1], fiber-optical devices for the in-situ irradiation of the interstitium[5], the use of gold nanoshells and nanocages as high absorption & scattering materials[6] and bi- and multi-photon excitation of suitable chromophores.[7] Whereas laser-light sources can certainly be regarded as an improvement in comparison to lamps, their very narrow bandwidth excitation requires the use of an appropriate laser-source for virtually each PDT agent. Bi- and multiphoton absorption offers the advantage of spatially resolved irradiation and higher selectivity than mono-photonic excitation, especially when femtosecond pulses are used.[6] However, the light intensities required for the simultaneous absorption of two or several photons are very hard to achieve when treating tumors within the human/mammalian body, because the two- and three photon absorption cross-sections are too low.[6]Therefore, generation of light deep inside tissue is very important for PDT.

The recent advances in life-science and bioengineering permit the transfection, cellular expression, and real-time imaging of lightemitting proteins, such as *Renilla* luciferase (Ruc), bacterial luciferase (Lux), firefly luciferase (Luc), green fluorescent protein (GFP), or Ruc-GFP fusion protein.[8] All of these marker proteins, which generate their fluorescence

(bioluminescence) by chemical processes[8], have been successfully employed for tumor detection. These marker proteins can be used in-situ-photodynamic therapy for treatment of tumor deep inside the tissue by using appropriate bioluminescent substrate.

Coelenterazine , 2-(4-hydroxybenzyl)-6- (4-hydroxyphenyl)-8-(phenylmethyl)imidazo [1,2-a]pyrazin-3(7H)-one, is a bioluminescent compound found in different marine organism *Aequorea victoria* jellyfish[9,10], *Renilla reniformis* sea pansy[11,12] and *Watasenia scintillans* squid[13,14]. This bioluminescent compound forms blue fluorescence protein (BFP) in the presence of molecular oxygen in jellyfish which emits blue light with aid of calcium ion[9,10]. Like other chemoluminescent compounds (luciferins), coelentrazine emits blue light (λ_{max} = 480 nm) in the presence of an enzyme (*Renilla luciferase*) outside the biological system without ATP. [15] The molecular basis of the chemoluminescence of coelenterazine is shown in **Scheme 2.1**.[10] Since no excitation light is required, there is no background fluorescence and, consequently, a much improved signal to noise ratio in imaging experiments. Furthermore, light of blue wavelength is better suited to excite potent photodynamic agents, such as porphyrins and ruthenium(II)polypyridyl -complexes. It must be noted that blue light from *renilla* luminescence has a very low penetration in human tissue (1-2 mm), so that external irradiation in photodynamic treatment is very difficult. Therefore, our chemoluminescent system has a significant advantage, because it allows in-situ-photodynamic therapy.

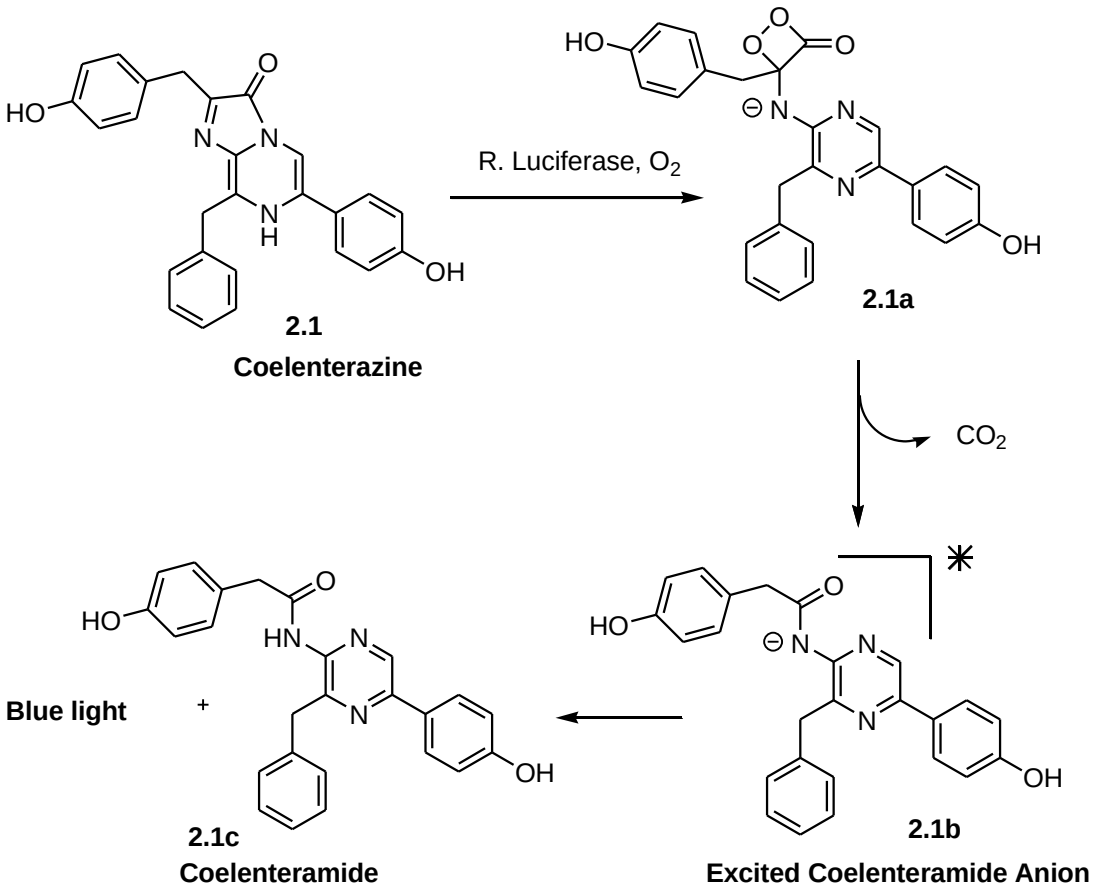

Scheme 2. 1: Chemoluminescence of Coelenterazine[10]

The total synthesis of this bioluminescent compound was first reported by Inoue et al. in 1975[13]. Since then many methods for the synthesis of coelenterazine have evolved .[16-25] Although coelenterazine is commercially available, it is very expensive and not long-term stable. Therefore, my goal was to modify the existing methods for the synthesis of coelenterazine to provide it highly pure and in large quantities (gram scale) from inexpensive starting materials.

2.2 Experimental

2.2.1 Chemicals and Instrumentation

All chemicals were obtained from Acros Organics and Sigma Aldrich, unless noted otherwise. Tetrahydrofuran (THF) was distilled over sodium in presence of benzophenone in argon atmosphere. N,N-dimethyl acetamide (DMA) was distilled over calcium hydride in an

argon atmosphere. All other solvents were used without distillation unless otherwise noted. 400 MHz and 200 MHz Varian NMR-spectrometer, Thermo Scientific Nicolet 380 FT-IR (neat sample, thanks to Prof. Dr Aakeröy, Department of Chemistry at KSU) were used in this study. I would like to thank the Analytical Laboratory of Dr. Ruth Welti at KSU for recording the mass spectra of our compound employing an Applied Biosystems API-4000 triple quadrupole mass spectrometer with electrospray and APCI sources.

2.2.2 Synthesis of Coelenterazine

2.2.2.1 3,5-dibromo-2-aminopyrazine (molecular formula $C_4H_3Br_2N_3$).

Synthetic procedure: 3,5-dibromo-2-aminopyrazine **2.3** was synthesized by modifying the bromination procedure of aminopyrazine.[26] First, aminopyrazine **2.2**(1.00 g, 10.5 mmol,1.0 eq) was completely dissolved in 75 mL dichloromethane (DCM) in an argon flushed 500 mL RB flask, and then N-bromosuccinimide (NBS) (4.683 g, 26.3 mmol, 2.5 eq) was added at once. The reaction mixture was stirred for 2 hours at room temperature (RT). The reaction was completed within 2 hours, which was confirmed by TLC. Reaction mixture was poured in 500 mL of 5% Na_2CO_3 and extracted with dichloromethane (3* 100 mL) and washed with water (3* 100 mL). The organic layer was dried using sodium sulfate and concentrated *via* rotary evaporation. Finally the dibromo- aminopyrazine was purified by descending silica gel column chromatography with 1:2 ethyl acetate: hexane as eluent. A pale yellow needle shaped crystalline compound was obtained **2.3** (1.555 g, 6.17 mmol, 62% yield). R_f value of the compound on SiO_2 thin layer chromatography (TLC) using 2:1 hexane: ethylacetate as mobile phase is 0.46. Melting point (MP) of the compound is 115-116 °C. IR (neat) wavenumber (υ) cm^{-1} 635, 877, 907,1040, 1096,1133,1314, 1450, 1506, 1548, 1620, 3150, 3168, 3280, 3448; ^{1}H NMR ($CDCl_3$, 400 MHz) δ [ppm] 5.105 (b s, 2H, NH_2) 8.04 (s, 1H, Ar-H); ^{13}C NMR ($CDCl_3$, 400 M Hz) δ [ppm] 123.87, 124.15, 143.38, 152.11; MS $C_4H_3Br_2N_3$, m/z calculated 250, found 251.1(M^+)

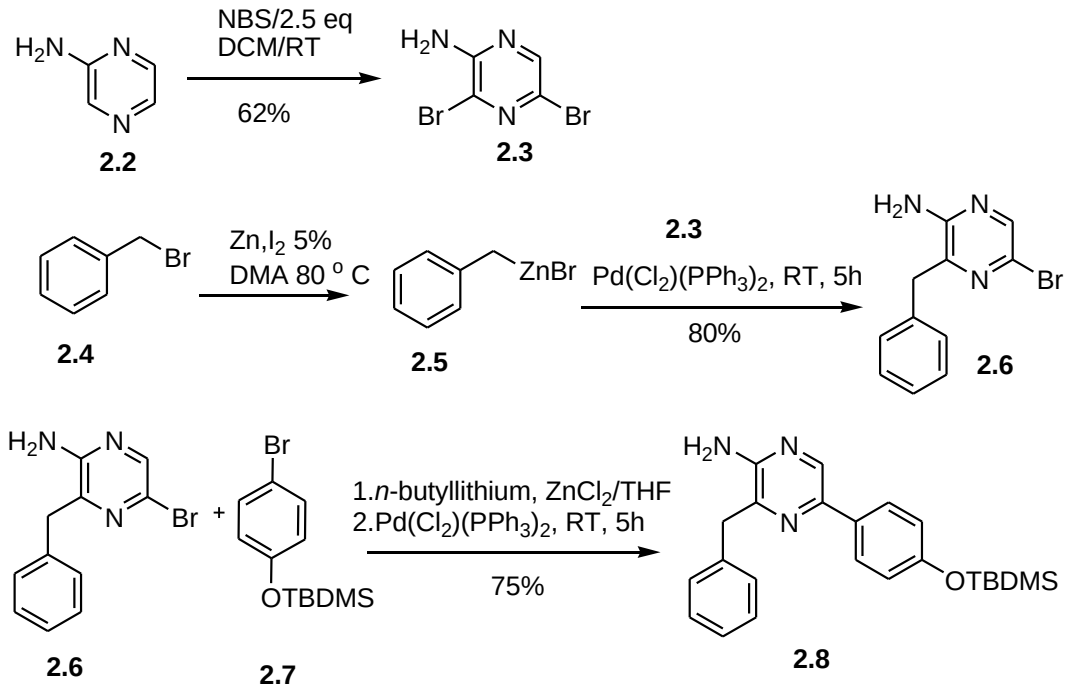

Scheme 2. 2: 3-benzyl-5-(4-tert-butyldimethylsilyloxyphenyl)-2-pyrazineamine(2.8)

2.2.2.2 3-Benzyl-5-bromo-2-amino-pyrazine 2.6.

Synthetic procedure: The Huo modification of the Negishi coupling reaction was adapted for this reaction.[27] Zn dust (1140 mg, 8.71 mmol , 3.5 eq.) and I_2 (216 mg, 5% of Zn) were given in a dry 25 mL two- necked round bottom flask under argon atmosphere. 5 mL of anhydrous dimethylacetamide (DMA), freshly distilled over calcium hydride, was added by using a syringe. The mixture was stirred at RT until the brown color of I_2 disappeared. Then freshly distilled benzyl bromide (1526 mg, 4.46 mmol, 2.5 eq) was added by using a syringe and the reaction mixture was stirred at 80 ºC for 3 hours. After insertion of Zn, the reaction mixture was cooled to RT and the suspension of dibromoaminopyrazine **2.3** (900 mg, 3.571 mmol, 1 eq.) and $PdCl_2(PPh_3)_2$ (126 mg, 0.178 mmol, 5% of pyrazine) in 6 mL of DMA was added. The reaction mixture was continuously stirred for 5.5 hours. Then the mixture was poured in 25 mL of water and extracted with ethyl acetate (3*25 mL). The organic fractions were combined and dried over anhydrous sodium sulfate and then concentrated on a rotary evaporator. Compound **2.6** (830 mg, 1.4 mmol, 88 % yield) brown viscous oil was purified by silica gel descending column chromatography using 2/1, *n*-hexane/etylacetate(v/v) as an eluent. TLC (silica, mobile phase: *n*-hexane/ethyl acetate 2/1 v/v, R_f = 0.35). IR (neat) wavenumber (υ) cm^{-1} 633, 923, 1072, 1118,

1220, 1388, 1423, 1604, 2921, 3023, 3060, 3203, 3317, 3438; ^{1}H NMR ($CDCl_3$, 400 MHz) δ [ppm] 4.065(s, 2H, CH_2) 4.449 (br s, 2H, NH_2), 7.198-7.317 (m, 5H, Ar-H), 8.012 (s, 1H, Ar-H); ^{13}C NMR ($CDCl_3$, 200 MHz) δ [ppm] 41.11,126.428, 127.503128.592, 129.304, 135.837, 141.909, 142.635, 152.253, MS $C_{11}H_{10}BrN_3$, m/z calculated 264, found 264 (M+), 265 (M+ 1)

2.2.2.3 3-Benzyl-5-(4-tert-butyldimethylsilyloxyphenyl)-2-pyrazineamine(2.8).[4]

Synthetic procedure: This procedure is a modification of the Buchwald variant of a Negishi-type cross coupling reaction between aryl halides.[28] A 25 mL round-bottom flask was dried overnight at 150 ºC, allowed to cool down to RT under argon atmosphere and then filled with (4-bromop-phenoxy)-*tert*-butyldimethylsilane **2.7** (1.984 g, 6.908 mmol, 2.2 eq) and 12 mL tetrahydrofuran (THF) (distilled over sodium in presence of benzophenone). A septum was used to block the influx of air. The mixture was cooled to -78 ^{o}C, then *n*-butyl-lithium from a 2.8 molar solution in hexane (3.03 mL, 8.792 mmol, 2.8 eq) was added drop-wise by means of a syringe. The resulting solution was stirred at -78 ºC for one hour. $ZnCl_2$ (1.283mg, 9.42 mmol in 10 mL THF, 3 eq) was added via syringe through the septum. Again, the reaction mixture was stirred for 0.5 hours at -78 ºC. Then the reaction mixture was allowed to warm up to RT and the solution was further stirred for one additional hour at RT. A suspension of $PdCl_2(PPh_3)_2$ (110 mg, 0.157 mmol, 5% mol) and pyrazine **2.6** (830 mg, 3.14 mmol, 1eq) in 10 mL of THF was added and stirred at RT. The reaction progress was monitored by TLC (silica, mobile phase: *n*-hexane/ethyl acetate 2/1 v/v, R_f values for starting material, product and by-product(s) are 0.4, 0.29 and 0.55 respectively). There was some starting material discernible after five hours of reaction, but after 15 hours there was no more starting material. There was a minor fraction of by-product, which was identified as the product from the "unwanted coupling reaction" (R_f = 0.29, silica, mobile phase: *n*-hexane/ethyl acetate 2/1 v/v), but the main fraction consisted of the product (R_f = 0.55, silica, mobile phase: *n*-hexane/ethyl acetate 2/1 v/v). The reaction mixture was poured into 50 mL of water, extracted with ethyl acetate (3*50 mL) and dried over anhydrous sodium sulfate. After drying the organic fraction, ethyl acetate was removed by using a rotary evaporator. The product **2.8,** yellow solid (897 mg, 2.294 mmol, 73 %), was purified by descending silica gel column chromatography by using 2/1 hexane/ethylacetate. IR (neat) wavenumber (υ) cm^{-1} 728, 834, 918, 1170, 1237, 1251, 1454, 1519, 1609, 2851, 2933, 3145, 3284, 3485; ^{1}H NMR ($CDCl_3$, 400 MHz) δ [ppm] 0.22 (s, 6H, $2CH_3$), 1.005 (s, 9H, *tert*-butyl),

4.17 (s, 2H, CH_2), 4.37 (br s 2H, NH_2), 6.92 (d, *J*= 8.59 Hz 2H), 7.25-7.32(m, 5H), 7.81, (d, *J*= 8.59 Hz, 2H), 8.32 (s, 1H, Ar-H); ^{13}C NMR ($CDCl_3$, 400 MHz) δ [ppm] -4.1, 18.48, 25.9, 41.4, 120.7, 127.1, 127.2, 128.7, 129.1, 130.8,137,137.1,140.6, 142.9, 151.6, 156.2, MS $C_{23}H_{29}N_3OSi$, m/z calculated 291.58, found 391.8 (M^+), 392.8 (M+1)

2.2.2.4 (4-bromo-phenoxy)-tert-butyl-dimethyl-silane (2.7)

Synthetic procedure: 4-bromophenol **2.9** (2g, 11.56 mmol, 1eq) and 4-DMAP(0.141 g, 1.156 mmol) were dissolved in 30 mL DCM in a 100 mL round-bottom flask at 0 ºC. After 15 min imidazole (1.18 g 17.34 mmol, 1.5 eq) and TBDMS-Cl (2.613 g, 17.34 mmol, and 1.5 eq) were added and stirred at 0 ºC for one additional hour. DCM was removed by using a rotary evaporator and the resulting solid was dissolved in 25 mL of diethyl ether. The diethyl ether solution was first washed with concentrated ammonium solution (2*50 mL), followed by water (2* 50 mL), and finally brine solution (2*50 mL). Diethyl ether was removed *via* rotary evaporation to leave compound **2.7** behind, which was obtained as a colorless liquid (3.293 g, 11.46 mmol, 99% yield). ^{1}H NMR ($CDCl_3$, 400 MHz) δ [ppm] 0.16 (s, 6H), 0.95 (s, 9H), 6.69 (d, *J* = 8 8.78, 2H), 7.29 (d, *J* = 8.78 Hz, 2H); ^{13}C NMR ($CDCl_3$, 400MHz) δ [ppm] -4.2618.42, 25.85, 113.83, , 122.13, 132.51,155.07

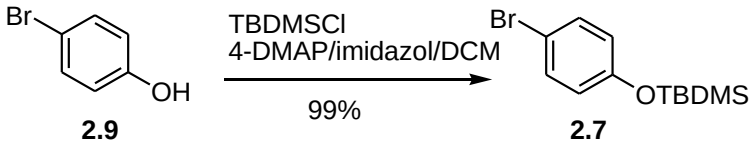

2.9 **2.7**

Scheme 2. 3: *tert*-butyldimethylsilyl(TBDMS) protection of 4-bromophenol

2.2.2.5 4-benzyloxybenzylalcohol (2.12)

Synthetic procedure: 2.0 g (16.11 mmol) of 4-hydroxybenzyl alcohol **2.10** and 11.132 g (80.5 mmol, 5 eq) of anhydrous potassium carbonate were dissolved in 40 mL dry DMF in a 100 mL round-bottom flask. The suspension of the mixture was purged with argon and stirred for 30 minutes at room temperature. Then 6.886 g (40.02 mmol, 2.5 eq) of benzyl bromide was added by means of a syringe to the suspension and stirred for 24 hours at RT. Then reaction mixture was filtered through celite and the celite cake was washed with 50 mL of diethyl ether. The filtered solution was washed with water (3 * 30 mL), followed by concentrated brine solution (2

*25 mL). The diethyl ether solution was dried over anhydrous sodium sulfate and the solvent was evaporated by using a rotary evaporator and then further in a high *vacuum.* This experimental procedure yielded a white solid 3.12 g (15.58 mmol, 96 % yield) of pure 4-benzyloxybenzylalcohol **2.12.** R_f value of the compound is 0.75, 1/1 ethyl acetate/ *n*-hexane, v/v as mobile phase in pre coated SiO_2 thin layer chromatography (TLC). MP 73-75 °C IR (neat) wavenumber cm^{-1} 612, 694, 739, 810, 994, 1237, 1380, 1509, 1585, 1605, 1723, 1171, 2864, 2913, 3051, 3060, 3321 ^{1}H NMR ($CDCl_3$, 400 MHz) δ [ppm] 4.63(d, *J* = 5.86 Hz, 2H), 5.08 (s, 2H), 6.98 (d, *J* = 8.7 Hz, 2H), 7.30(d, *J* = 8.7 Hz, 2H), 7.43-7.37 (m 5H); ^{13}C NMR ($CDCl_3$, 400 MHz) δ [ppm] 65.28, 70.28, 115.20, 127.67, 128.20, 128.89, 129.43, 133.61, 137.17, 158.65.

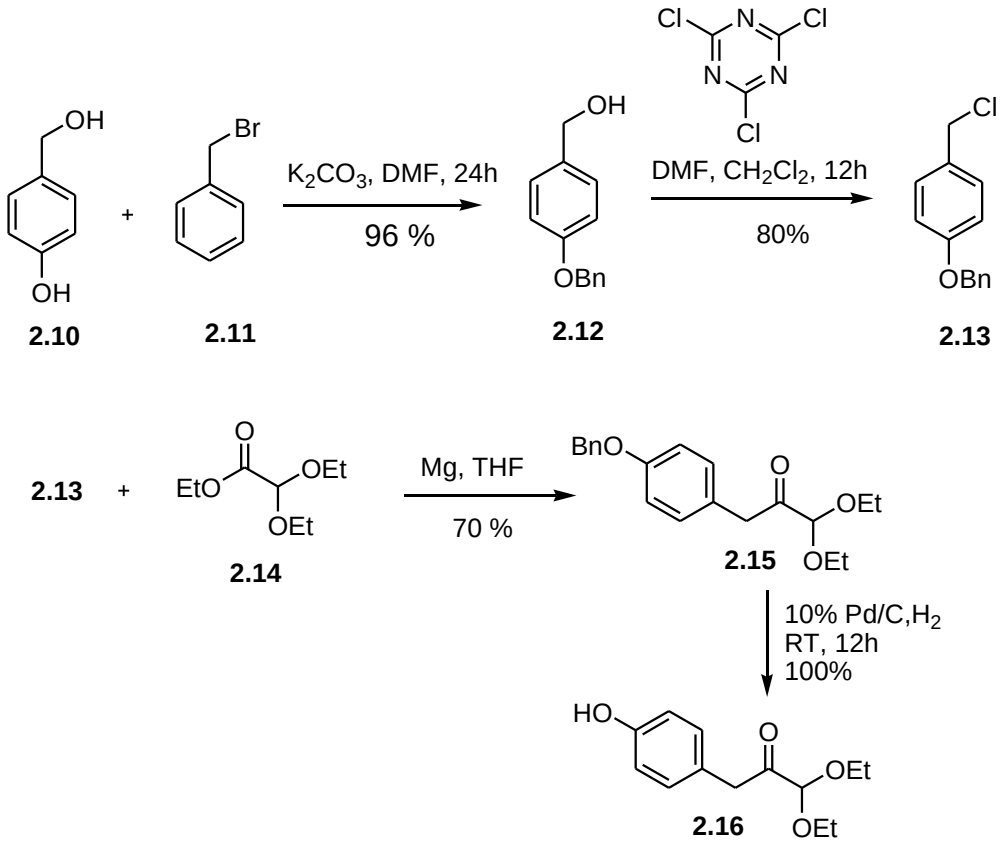

Scheme 2. 4: **Synthesis of 2-Propanone, 1,1-diethoxy-3-(4-benyloxyphenyl)-** ***(2.16)***

2.2.2.6 4-Benzyloxybenzylchloride (2.13)

Synthetic procedure: Surprisingly, the chlorination of benzyl alcohol turned out to be very problematic. The best experimental approach is described here: The chlorination of benzyl alcohol **2.12** was efficiently carried out by employing the cyanuric chloride(2,4,6-trichloro[1,3,5]triazine) and *N*,*N*-dimethyl formamide complexation method (CTC/DMF).[29] 0.369 g (1.997 mmol) of cyanuric chloride was dissolved in 1.0 mL of dry DMF in a two-necked 50 mL round-bottom flask,. The solution was stirred at room temperature under argon atmosphere. After 30 minutes of stirring at RT, the white solid of the cyanuric chloride/ DMF complex was formed. Then 0.40 g (1.997 mmol) of **2.12** (4-benzyloxybenzylalcohol) solution in 10 mL dichloromethane was added at once by means of a syringe to the white solid. The mixture was then stirred at room temperature. Reaction progress was monitored by TLC (silica, mobile phase: *n*-hexane/ethyl acetate, 10/1 v/v, R_f values for starting material, product are 0.09 and 0.63 respectively). The chlorination of benzyl alcohol was completed after 4 hours. After the completion of the reaction the reaction mixture was diluted to 20 mL by DCM. The white turbid suspension was filtered through celite, followed by washing the celite cake with 20 mL DCM. The solvent of the filtered solution was removed *via* rotary evaporation. This procedure yielded a white solid. The white solid was subjected to descending SiO_2 column chromatography by using 10 % ethylacetate in hexane and yielded a fluffy white solid **7.13** 0.31g (1.417 mmol, 70.95 %) MP 74-76 °C. IR (neat) wavenumber(υ) cm^{-1} 609, 660, 741, 834, 1004, 1171, 1241, 1380, 1512, 1580, 1609, 2868, 696, 2933, 3027; ^{1}H NMR ($CDCl_3$,400 MHz) δ [ppm] 4.57 (s, 2H) 5.08 (s, 2H), 6.96 (d, *J* = 8.7 Hz, 2H), 7.32 (d, *J* = 8.7 Hz, 2H), 7.43-7.37 (m 5H); ^{13}C NMR ($CDCl_3$,400 M Hz) δ [ppm] 46.48, 70.28, 115.29, 127.67, 128.27, 128.84, 130.30, 136.97, 159.108.

2.2.2.7 2-Propanone, 1,1-diethoxy-3-(4-benyloxyphenyl)- (2.15)

Synthetic procedure: This method is modified form of Adamczyks method.[20] 236 mg (10.289 mmol, 2.5 eq.) of magnesium was suspended in 3 mL of freshly distilled tetrahydrofuran (THF) in an argon flushed 50 mL two- necked round-bottom flask. Dibromoethane (0.10 mL) was added to activate the magnesium. After 20 minutes of activation, a solution of 0.90 g (4.115 mmol) of **2.13** in THF was added and stirred at RT for 30 minutes. Then reaction mixture was

further refluxed for one hour to complete the reaction. The pale yellow Grignard reagent was allowed to cool to RT and then kept on an ice bath. Then 906 mg (5.143 mmol, 1.25 eq) of ethyldiethoxyacetate **2.14** was dissolved in 10 mL THF in a separate 50 mL round- bottom flask under argon atmosphere and cooled to –78 ºC. The Grignard reagent was transferred drop-wise into the cooled flask during 10 minutes. The reaction mixture was then stirred for 1.5 hours at –78 ºC. Then reaction was quenched by 50 mL water and further diluted by 100 mL of ethylacetate. The ethylacetate layer was washed with water (2*50 mL), followed by saturated brine solution (2*50 mL). The organic layer was dried over anhydrous sodium sulfate and the solvent was evaporated by rotary evaporation. The viscous Grignard product was further purified by descending SiO_2 column chromatography 10% ethyl acetate in *n*-hexene(v/v) as an eluent. This procedure yielded 0.95 g (2.49 mmol, 70 % yield) of the oily colorless compound **2.15.** R_f =0.4 (TLC, silica, mobile phase: *n*-hexane/ethyl acetate 10/1 v/v) ^{1}H NMR ($CDCl_3$, 400 MHz) δ [ppm] 1.25 (t, *J* = 7.3 Hz, 6H) 3.57 (m, 2H), 3.69 (m, 2H), 3.84(s, 2H), 4.64(s, 1H), 5.05(s, 2H), 6.94 (d, *J* = 8.4 Hz, 2H), 7.14 (d, *J* = 8.4 Hz, 2H), 7.43-7.35 (m 5H); ^{13}C NMR ($CDCl_3$,400 MHz) δ [ppm] 15.35 42.99, 63.53, 70.17, 115.5, 126.17, 127.66, 128.12, 128.76, 130.96, 132.007, 137.21, 157.94, 203.73,

2.2.2.8 2-Propanone, 1,1-diethoxy-3-(4-hydroxyphenyl)-(2.16)

Synthetic procedure: The deprotection of the benzyl group of compound **2.15** was carried out by reduction using hydrogen on a palladium/carbon catalyst. 0.90 g (mmol 4.115) of compound **2.15** was dissolved in 50 mL of methanol in a 100 mL round-bottom flask. 100 mg of 10% palladium on carbon was added. At first the resulting suspension was put under vacuum and then hydrogen gas was passed into the RB flask from a balloon of hydrogen gas. The reaction mixture was stirred for 24 hours under hydrogen atmosphere. TLC (silica, mobile phase: *n*-hexane/ethyl acetate 1/10 v/v, R_f values for starting material, product were 0.4 and 0.16 respectively) was used to confirm the completeness of the deprotection of the benzyl group. The black suspension was filtered and the solvent was removed by using a rotary evaporator. The deprotected product **2.16** was further purified by SiO_2 column chromatography using 50 % ethylacetate in hexane, yielding 0.570 mg (2.392 mmol, 58 %) colorless oil **2.16**. ^{1}H NMR ($CDCl_3$, 400 MHz) δ [ppm] 1.25(t, *J* = 7.03 Hz, 6H) 3.55 (m, 2H), 3.71(m, 2H), 3.82 (s, 2H), 4.64 (s, 1H), 5.11 (br s, 1H), 6.77 (d, *J* = 8.59 Hz, 2H), 7.07 (d, *J* = 8.59 Hz, 2H); ^{13}C NMR

($CDCl_3$, 400 MHz) δ [ppm] 15.36, 43.08, 63.61, 102.42, 115.65, 125.86, 131.14, 154.83, 204.06,MS, m/z $C_{13}H_{18}O_4$ calculated 238.28, found 261.3 (M + Na)

2.2.2.8 Coelenterazine (2.1)

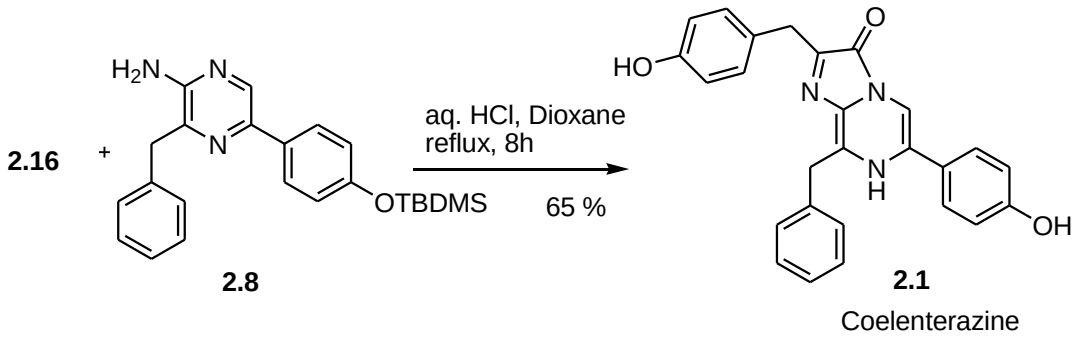

Scheme 2. 5: Final condensation step of synthesis of coelenterazine

Synthetic procedure: The final condensation step was adapted from a published method.[13,23] **2.16** 200 mg (0.839 mg) of compound was dissolved in 4.0 mL of degassed 1,4-dioxane (N_2, Ar, freeze-pump-and thaw) in a 50 mL two-necked flask. Then 0.60 mL of conc. HCl (38%) was dissolved in 2.0 mL of dioxane and added into the flask. Finally, a solution of **2.8** (328 mg 0.891 mmol) in 4.0 mL of dioxane was added into the mixture, which was then refluxed for 8 hours under argon atmosphere. After 8 hours of reflux, a dark brown solution was obtained, which was allowed to cool down to room temperature. The solvent was then removed by rotary evaporation. The resulting dark brown solid was subjected to descending SiO_2 column chromatography using 10 % methanol in dichloromethane as eluent, yielding **15**, coelenterazine (0.543 mmol, 65%). R_f = 0.42 (TLC silica, mobile phase: dichloromethane/methanol, 10/1, v/v), IR (neat) wavenumber cm^{-1} 631, 695, 834, 1031, 1099, 1170, 1233, 1339,1368, 1451, 1508, 1552, 1610, 2851, 2917, 3056, 3170; ^1H NMR (CD_3OD-d_4) δ [ppm] 4.06 (s, 2H) 4.39 (s, 2H), 6.68 (d, *J* = 8.58 Hz, 2H), 6.86 (d, *J* = 8.59 Hz, 2H), 7.14 (d, *J* = 8.39 Hz, 2H), 7.18-7.22(m, 2H), 7.29-7.25 (m, 2H), 7.38 (d, *J* = 7.41 Hz, 2H), 7.48 (d, *J* = 8.78 Hz, 2H), 7.62(s, 1H); MS: m/z $C_{26}H_{21}N_3O_3$ calculated 423.15, found 424.3 (M + H), 446.3 (M + Na)

2.3 Discussion

Reddy et al. had synthesized coelenterazine by the following sequence of reactions, which are summarized in Scheme **2.6** and **2.8**.[23] Over-all yield of this approach was (48%), if calculated the yield on the basis of 3,5-dibro-2-aminopyrazine only. However, the disadvantages of this approach were expensive starting materials, costly catalysts. Since coelenterazine is only metastable in aqueous buffers, it is of great importance that the substance is clean. Otherwise, impurities are able to catalyze the decomposition of coelenterazine, thus reducing is lifetime in PBS (phosphate-buffered saline) from 72 h to less than 1 h. (Basel, Shrestha, Bossmann, Troyer, unpublished results.)

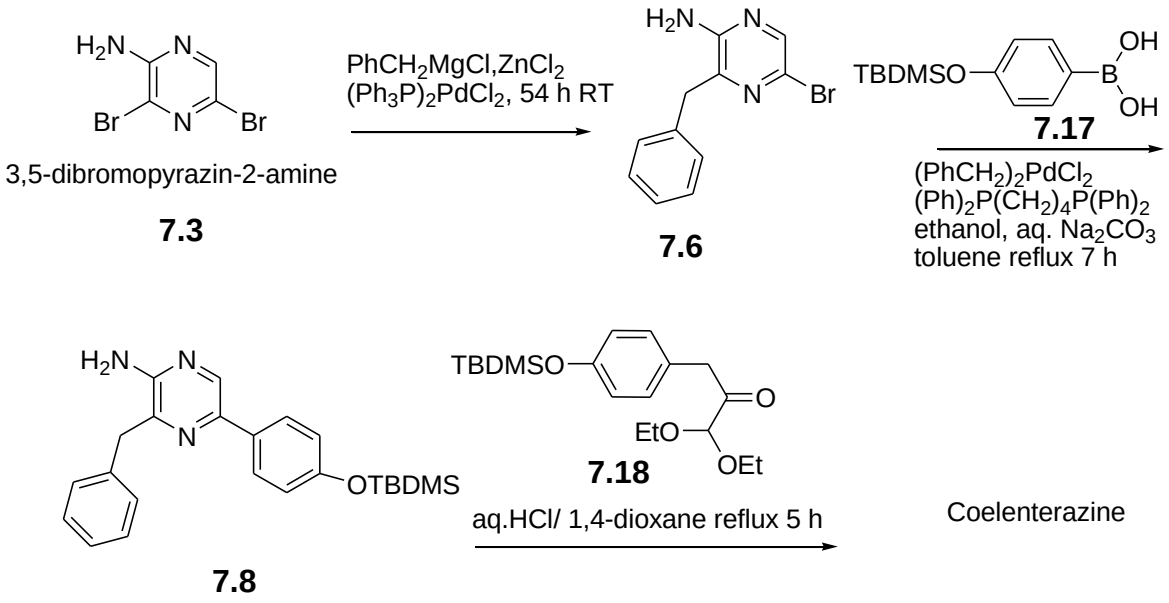

Scheme 2. 6: Reddy's synthetic scheme of coelenterazine [23]

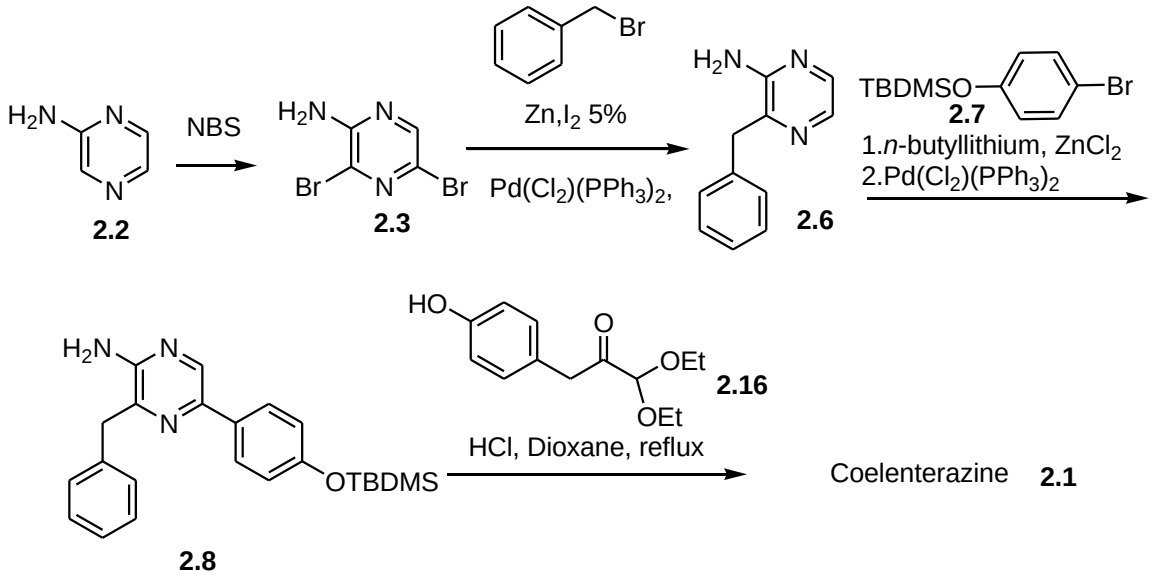

Scheme 2. 7: **Improved synthesis of coelenterazine**

The starting material of the modified method is aminopyrazine. The sequence of reactions is summarized in **Scheme 2.7** and **Scheme 2.9.** The first reaction was started with aminopyrazine **2.2**, because it is cheaper than 3,5-dibromo-2-aminopyrazine **2.3** and the bromination of aminopyrazine **2.2** with 2. 5 eq. NBS is an easy reaction with an excellent yield (**Scheme 2.3)**.[26] In addition, side product obtained during the bromination reaction is monobromo aminopyrazizne which can subsequently converted into dibromoaminopyrazine.

The next change concerned the introduction of the zinc atom. Instead of the zincation of the previously formed Grignard reagent, phenyl magnesium chloride, with $ZnCl_2$ for the Negishi coupling reaction (**Scheme 2.6**), direct zinc insertion approach was used, inspired by Huo's method **Scheme 2.7**.[27] Zn was inserted directly into the C-Br bond of benzyl bromide to make the alkylzinc reagent, followed by a Negishi cross-coupling reaction using bistriphenylphosphinepalladium(II)chloride catalyst. This coupling reaction produced a very high yield: more than 80 mol% of product, which was isolated after column chromatography, in addition to some bis-coupling product (less than 10 mol%). There was no evidence of homocoupling indicating that the Zn insertion was quantitative even when commercial zinc powder (not activated zinc) was used. 5 mol % of I_2 was used to activate the zinc surface. I_2 can create a reactive zinc surface by oxidizing Zn into Zn^{2+} and reduce itself to I^-.[27] I^- can further

facilitate the oxidative zinc insertion by converting benzyl bromide into more reactive benzyl iodide.

The next step was another cross-coupling reaction to obtain compound **2.8**. Adamczyk et al. have used the Suzuki-Miyaura coupling reaction, using a different Pd catalyst with an expensive ligand 1,4-Bis(diphenylphosphino)butane, which shown given in **Scheme 2.6**.[23] The main aim was to make the same Negishi cross-coupling reaction using the same palladium catalyst, but avoiding the boron-compound. Direct insertion of zinc in aryl bromide using the zinc powder did not work. This is understandable, because the substrate is an aryl halide but a benzyl halide or alkyl halide (as they have been described in the literature) (a cation intermediate is stabilized in the benzylic position and a little stabilized by the inductive effects in alkyl halides, but not in aromatic halides, where it has an angle 90 degree with respect to the aromatic ring system (= no overlap). This problem was solved using Buchwald's and Milne's approach to zincation **Scheme 2.7**.[28] First, TBDMS protected bromophenol was treated with *n*-butyl lithium to create the phenyl lithium organometallic compound in situ. Second, the phenyl lithium compound was treated with anhydrous zinc chloride to create the phenyl zinc chloride. Finally, this aryl zinc chloride was cross-coupled with the aryl bromide **2.6 (**containing the pyrazine moiety)**,** using bistriphenylphosphinepalladium(II)chloride.

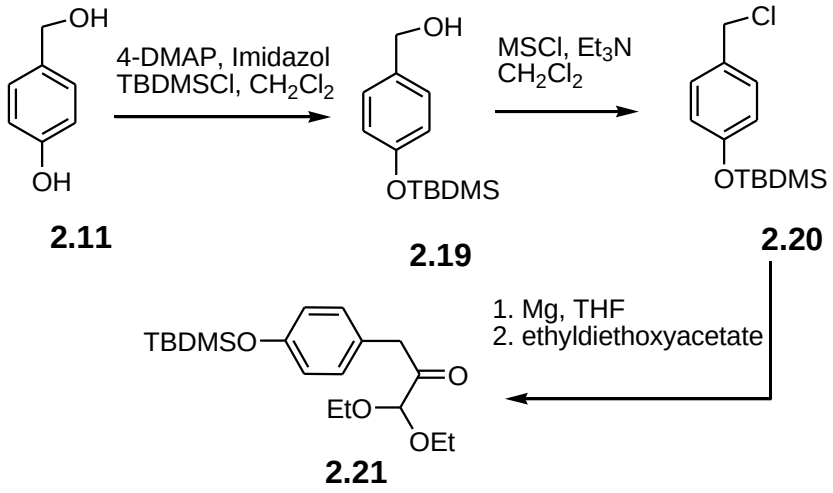

Scheme 2. 8: **Reddy's approach to make2-Propanone, 1,1-diethoxy-3-(4-*t*-butyldimethylsiloxy*phenyl*)-** 2.21[23]

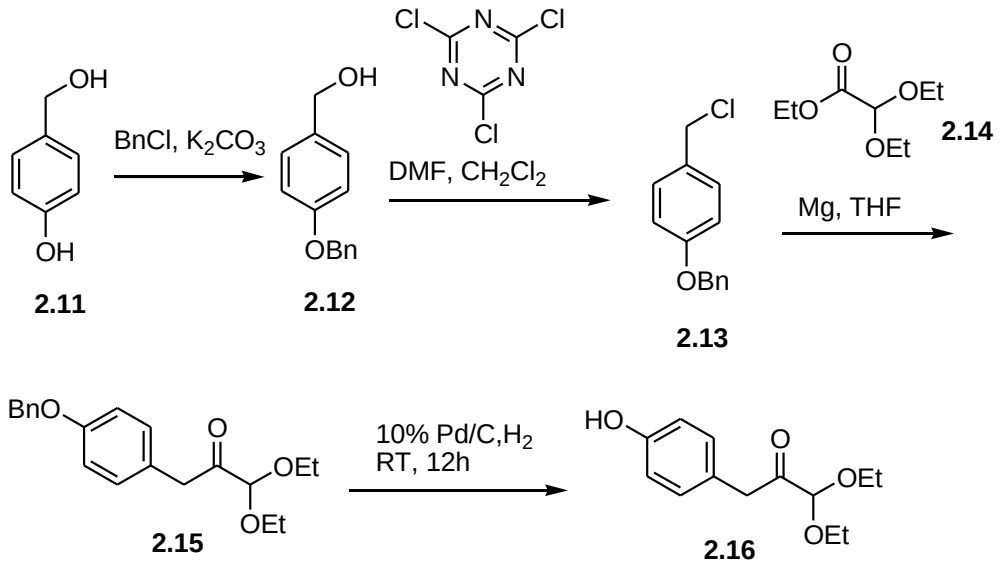

Scheme 2. 9: **Improved synthesis of 2-Propanone, 1,1-diethoxy-3-(4-benyloxyphenyl)- 2.16**

The other component, which is required for the final condensation step to form coelenterazine, is an acetal protected carbonyl compound (**2.21**).[23] TBDMS protection of 4-hydroxybenzyl alcohol 2.11 was not a problem, but the halogenation of the protected benzyl alcohol appeared to be very problematic: The bromo compound is very unstable as mentioned in the literature [18] and the chloro compound is volatile and hard to dry. Both, chlorination by using methanesulfonyl chloride (MsCl) and bromination by using CBr_4/PPh_3, did not work in this case, even though both are published methods.[18,20] In the first case, I did not get any product, and in the second case there was product, but the bromo compound decomposed very fast during work up and purification.[18] I also tried a chlorination reaction by using conc. HCl and thionyl chloride, but both of them were found to be useless for this reaction, because a water-free chloroorganic compound could not be obtained. The cyanuric chloride/DMF(CTC/DMF)[29] complex was found to be very helpful for this chlorination, but the yield of this reaction was low (15 %) and the chloro compound was still very volatile. Changing the protection group of 4-hydroxy benzyl alcohol form TBDMS to the benzyl group came out very successful (**Scheme 2.9)**. Benyzl protection has some advantages: both benzyl protection and deprotection were quantitative and easy to carry out, the benzyl protected compound is solid and easy to dry and benzyl ether is stable during chlorination reaction. Furthermore, chlorination of *p*-benzyloxy benzyl alcohol **2.12** by CTC/DMF was very good even when performed in the gram scale.[29] In addition, the benzyl chloride **2.13** is easy to dry, which is required for subsequent Grignard reaction, because

this compound is a solid and has a much lower vapor pressure. The benzyl group was removed via catalytic hydrogenation before the final condensation step, because the phenolic group is not a problem in acidic condensation reactions.

2.4 Conclusion

A new method of synthesis of coelenterazine has been developed. This synthetic route is able to deliver extremely pure coelenterazine on the gram scale. It uses inexpensive starting materials and catalysts. Aminopyrazine is used as a building block for introducing the pyrazine moiety of coelenterazine. Negishi-type coupling reactions are used to couple two different aromatic rings to the pyrazine moiety. The final condensation reaction to form coelenterazine had a very high yield and produced very pure materials, which is required for in-vivo applications in the in-situ photodynamic therapy of cancer using *Renilla* luciferase as light-generating enzyme.

2.5. References

1. Dolmans, D. E. J. G. J.; Fukumura, D.; Jain, R. K. *Nature Reviews Cancer* **2003**, *3,* 380-387.
2. U.S. Food and Drug Administration (December 2003). Approved claims for palliative line therapy. Retrieved December 29, **2003**, from: http://www.accessdata.fda.gov
3. Haedersdal, M.; Togsverd-Bo, K.; Wulf, H. C. *JEADV* **2008**, *22,* 267-78.
4. Schmidt, M. H.; Bajic, D. M.; Reichert, K. W. 2.; Martin, T. S.; Meyer, G. A.; Whelan, H. T. *Neurosurgery* **1996**, *38,* 552-7.
5. van den Bergh, H.; Mizeret, J.; Theumann, J.-F.; Woodtli, A.; Bays, R.; Robert, D.; Thielen, P.; Philippoz, J.-M.; Braichotte, D., *Proceedings of SPIE-The International Society for Optical Engineering* **1995**, *2631,* 173-98
6. Melancon, M. P.; Lu, W.; Yang, Z.; Zhang, R.; Cheng, Z.; Elliot, A. M.; Stafford, J.; Olson, T.; Zhang, J. Z.; Li, C. *Molecular Cancer Therapeutics* **2008**, *7,* 1730-1739
7. Ogawa, K.; Kobuke, Y. *Anti-Cancer Agents in Medicinal Chemistry* **2008**, *8,* 269-279.

8. Yu, Y. A.; Timiryasova, T.; Zhang, Q.; Beltz, R.; Szalay, A. A. *Anal. Bioanal. Chem.* **2003**, *377,* 964-972.
9. Shimomura, O.; Johnson, F. H. *Tetrahedron Lett.* **1973**, 2963-6.
10. Shimomura, O.; Johnson, F. H. *Proc. Natl. Acad. Sci. U. S. A.* **1978**, *75*, 2611-15.
11. Hori, K.; Cormier, M. J. *Proc. Natl. Acad. Sci. U. S. A.* **1973**, *70*, 120-3.
12. Hori, K.; Charbonneau, H.; Hart, R. C.; Cormier, M. J. Structure of native Renilla reniformis luciferin. *Proc. Natl. Acad. Sci. U. S. A.* **1977**, *74*.
13. Inoue, S.; Sugiura, S.; Kakoi, H.; Hasizume, K.; Goto, T.; Iio, H. *Chem. Lett.* **1975**, 141-4.
14. Inoue, S.; Kakoi, H.; Goto, T. *Tetrahedron Lett.* **1976**, 2971-4.
15. Loening, A. M.; Fenn, T. D.; Wu, A. M.; Gambhir, S. S. *Protein Engineering, Design and Selection* **2006**, *19,* 391-400.
16. Teranishi, K.; Goto, T. *Bull. Chem. Soc. Jpn.* **1990**, *6311*, 3132-40.
17. Gonzalez-Trueba, G.; Paradisi, C.; Zoratti, M. *Analytical Biochemistry* **1996**, 240, 308-310.
18. Hirano, T.; Negishi, R.; Yamaguchi, M.; Chen, F. Q.; Ohmiya, Y.; Tsuji, F. I.; Ohashi, M.. *Tetrahedron* **1997**, *53*, 12903-12916.
19. Keenan, M.; Jones, K.; Hibbert, F. *Chem. Commun.* **1997**, 323-324.
20. Adamczyk, M.; Johnson, D. D.; Mattingly, P. G.; Pan, Y.; Reddy, R. E. *Organic Preparations and Procedures International* **2001**, *33*, 477-485.
21. Kakoi, H. *Chem. Pharm. Bull.* **2002**, *50*, 301-302.
22. Devillers, I.; Arrault, A.; Olive, G.; Marchand-Brynaert, J. *Tetrahedron Lett.* **2002**, *43*, 3161-3164.
23. Adamczyk, M.; Akireddy, S. R.; Johnson, D. D.; Mattingly, P. G.; Pan, Y.; Reddy, R. E. *Tetrahedron* **2003**, *59*, 8129-8142.
24. Makarasen, A.; Kuse, M.; Nishikawa, T.; Isobe, M. *Bull. Chem. Soc. Jpn.* **2009**, *82*, 870-878.
25. Mosrin, M.; Bresser, T.; Knochel, P. *Org. Lett.* **2009**, *11*, 3406-3409.
26. Zimmermann, P. J.; Brehm, C.; Buhr, W.; Palmer, A. M.; Volz, J.; Simon, W. A. *Bioorg. Med. Chem.* **2008**, *16*, 536-541.
27. Hou, *S. Org Lett*, **2003**, *5*, 423-425

28. Milne, J. E.; Buchwald, S. L. *J. Am. Chem. Soc.* **2004**, *126*, 13028-13032.
29. De Luca, L.; Giacomelli, G.; Porcheddu, A. *Org. Lett.* **2002**, *4*, 553-555.

Appendix A - ^{1}H and ^{13}C NMR and Mass Spectra

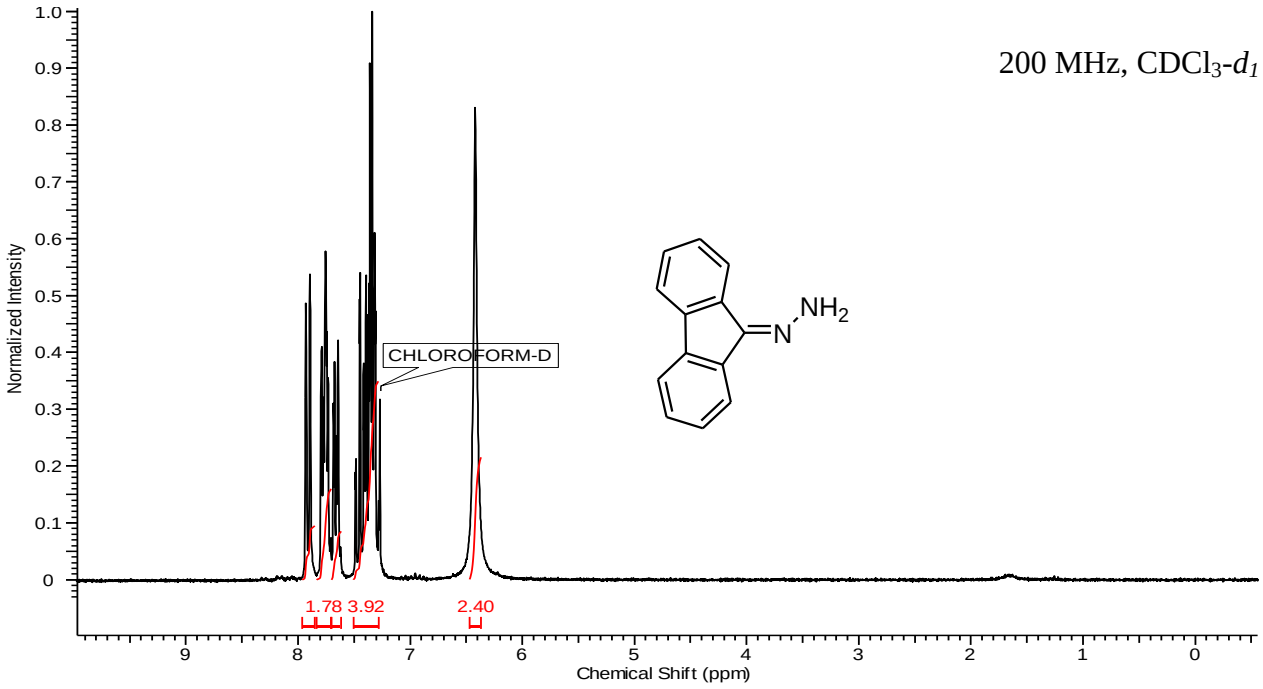

(a)

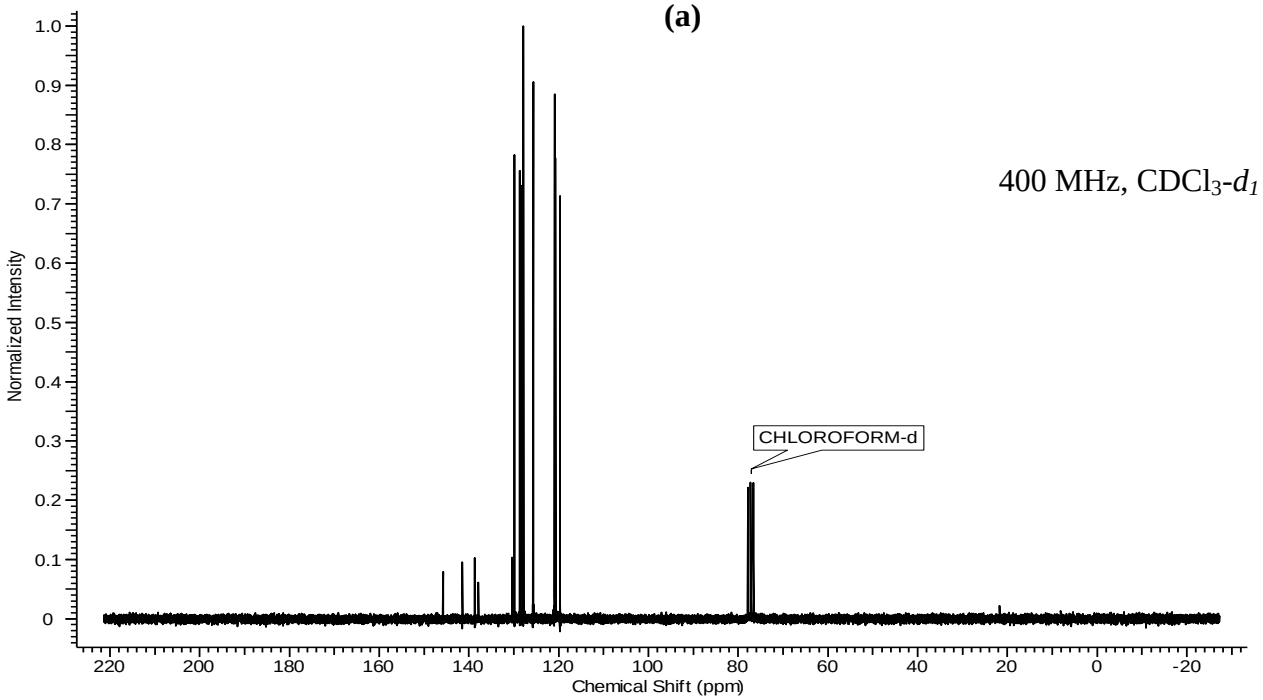

(b)

Figure A.1 (a) 1H and (b) 13C NMR of 1.2.2

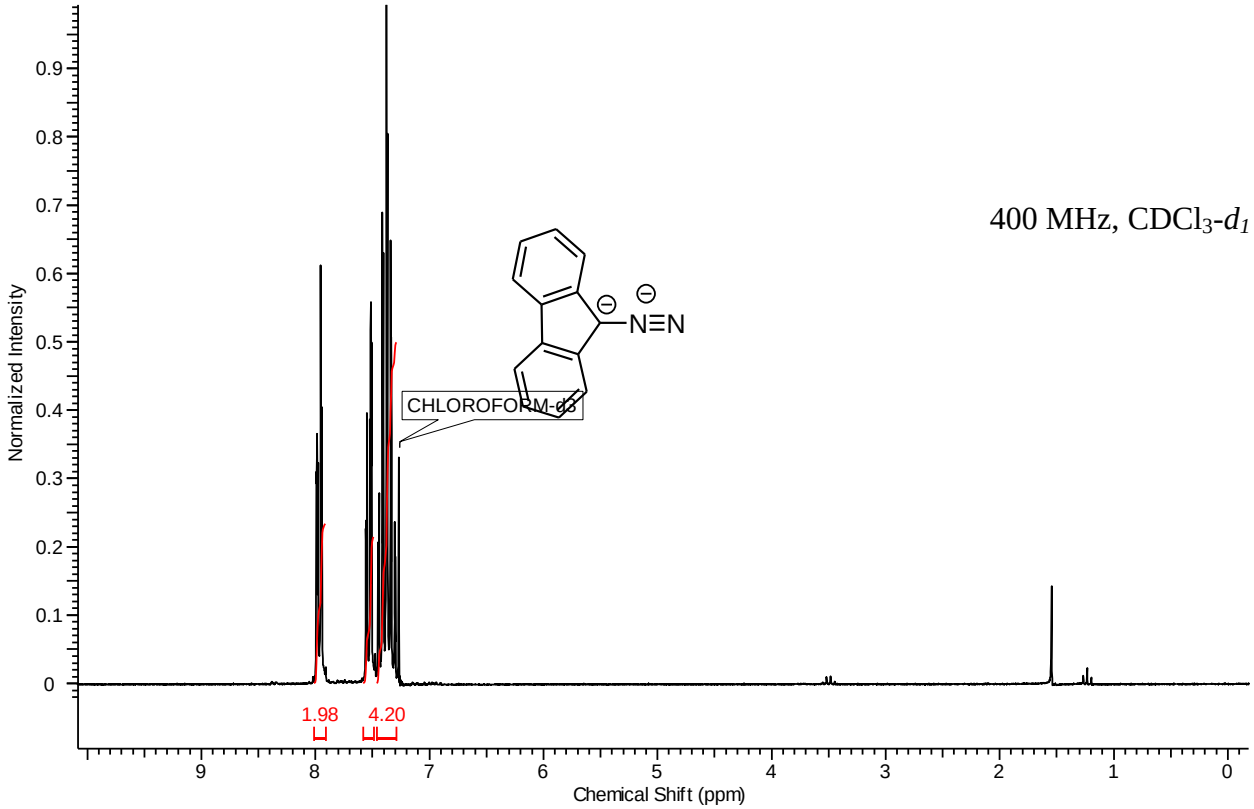

(a)

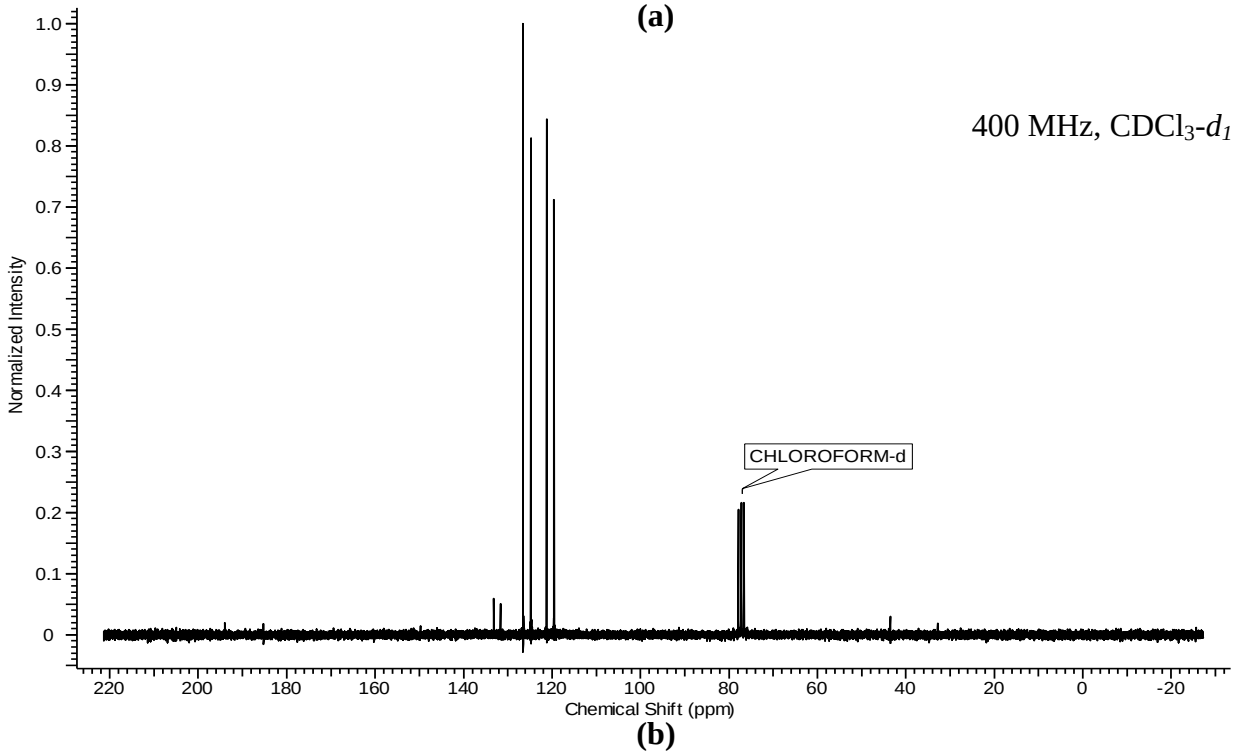

(b)

Figure A.2 (a) ^{1}H and (b) ^{13}C NMR of 1.2.3(a)

400 MHz, $CDCl_3$-d_1

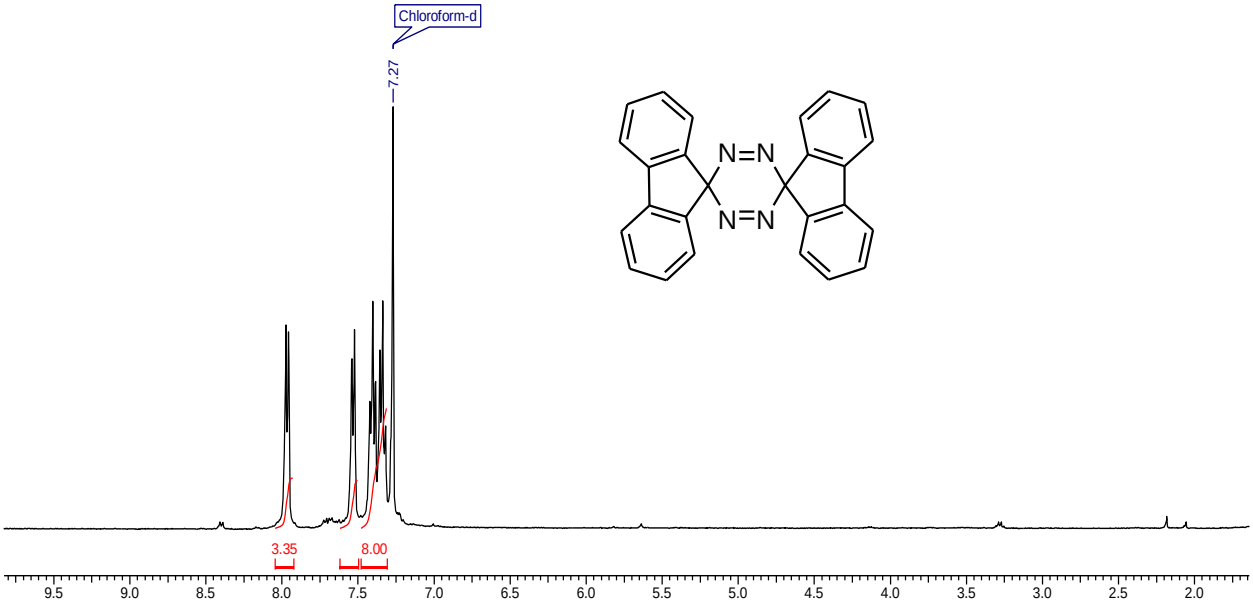

(a)

200 MHz, $CDCl_3$-d_1

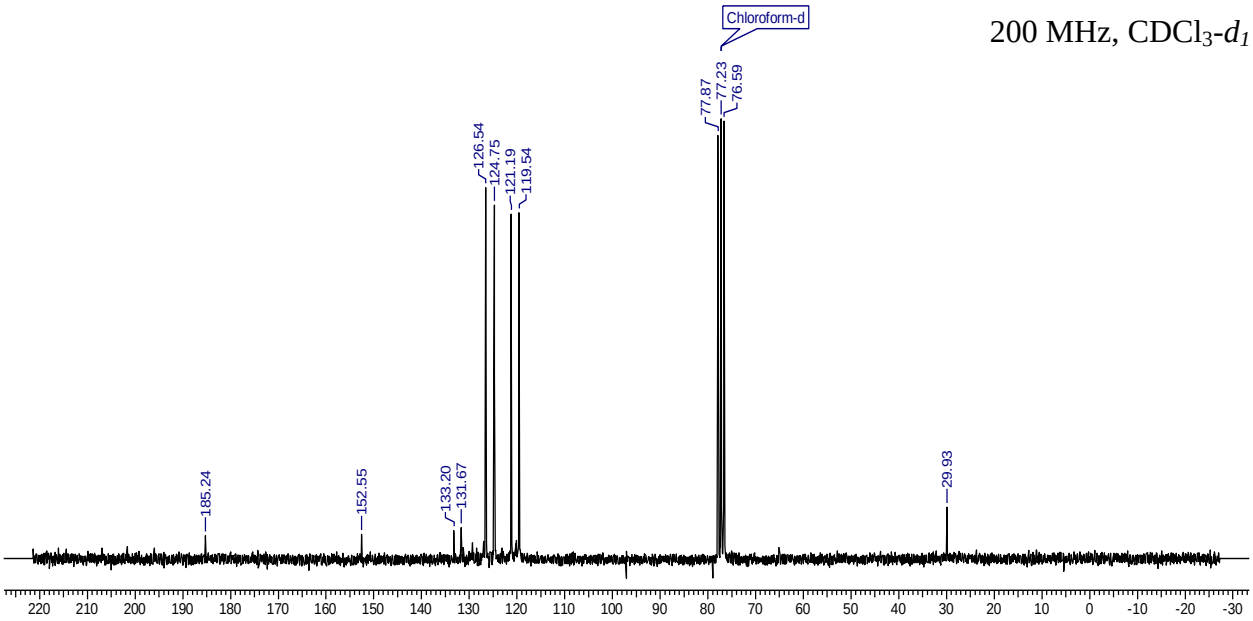

(b)

Figure A.3 (a) ^{1}H and (b) ^{13}C NMR of 1.2.3(b)

400 MHz, $CDCl_3$-d_1

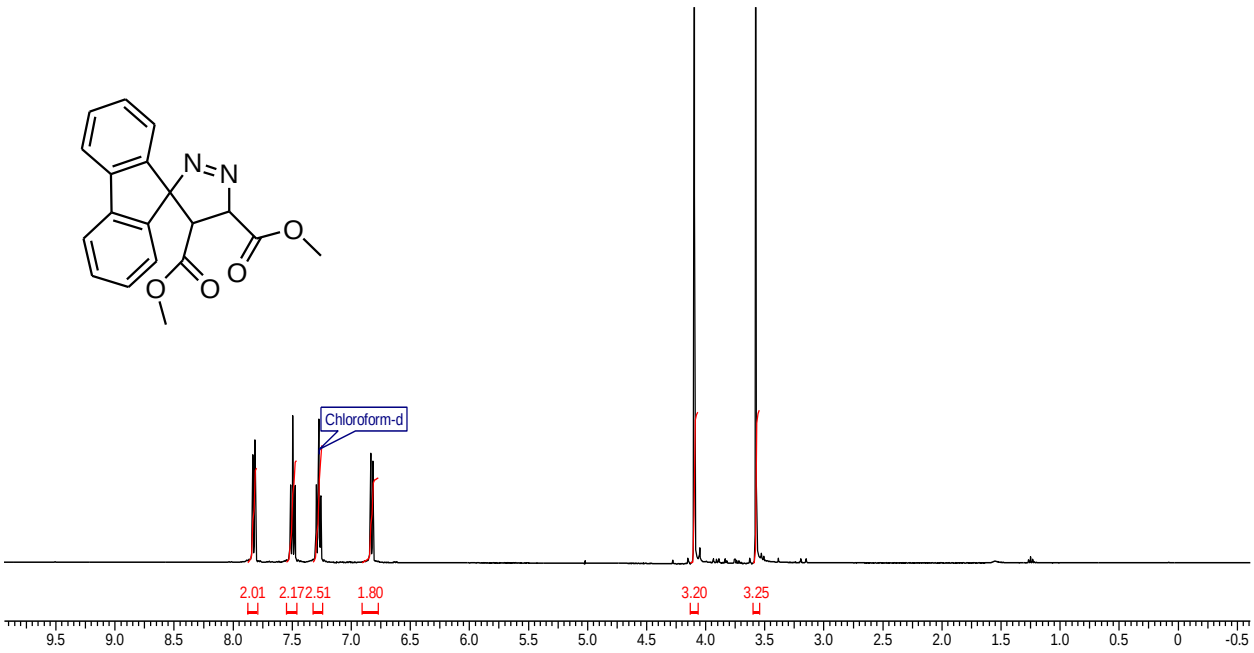

(a)

400 MHz, $CDCl_3$-d_1

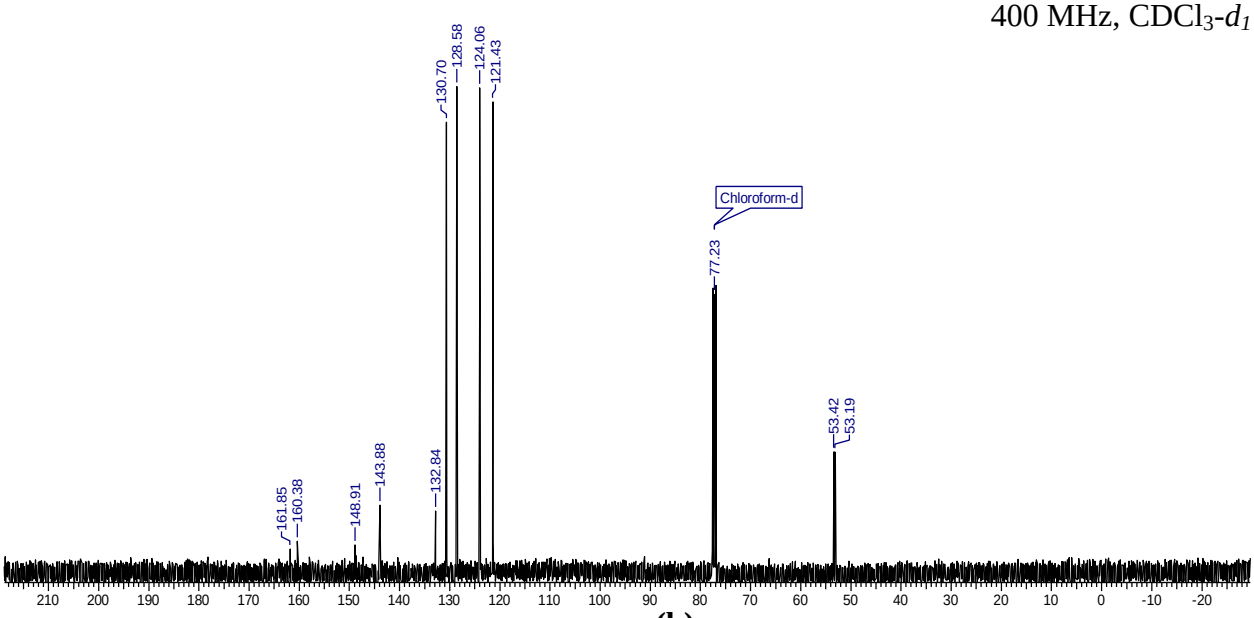

(b)

Figure A.4 (a) ^{1}H and (b) ^{13}C NMR of 1.2.5

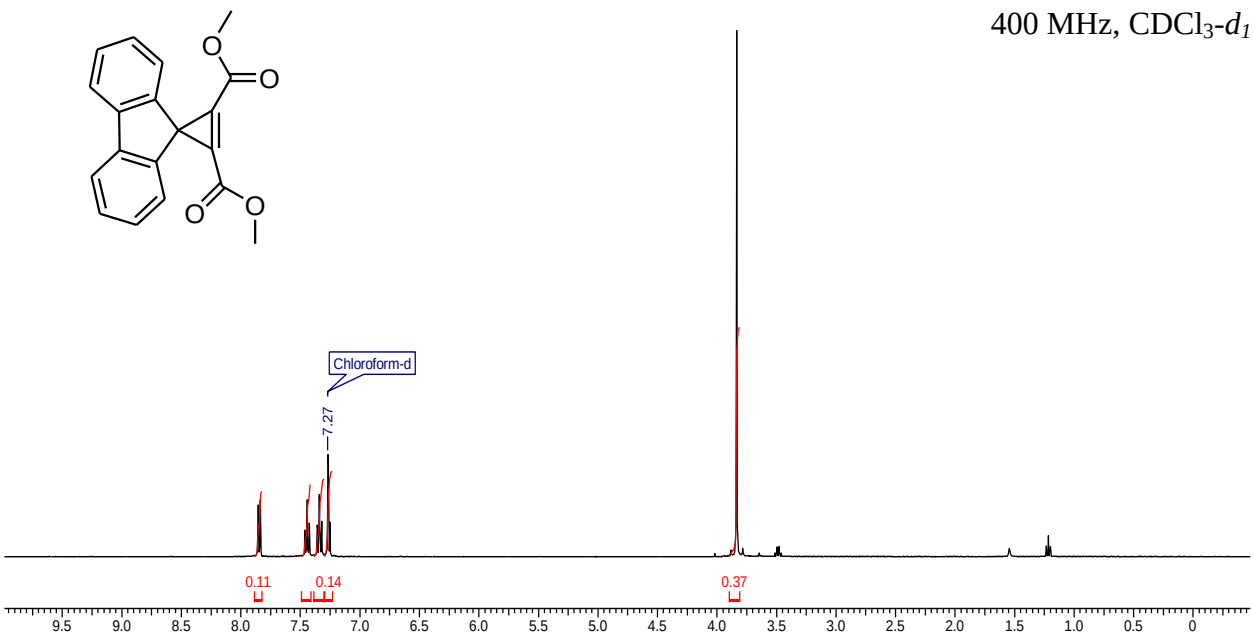

(a)

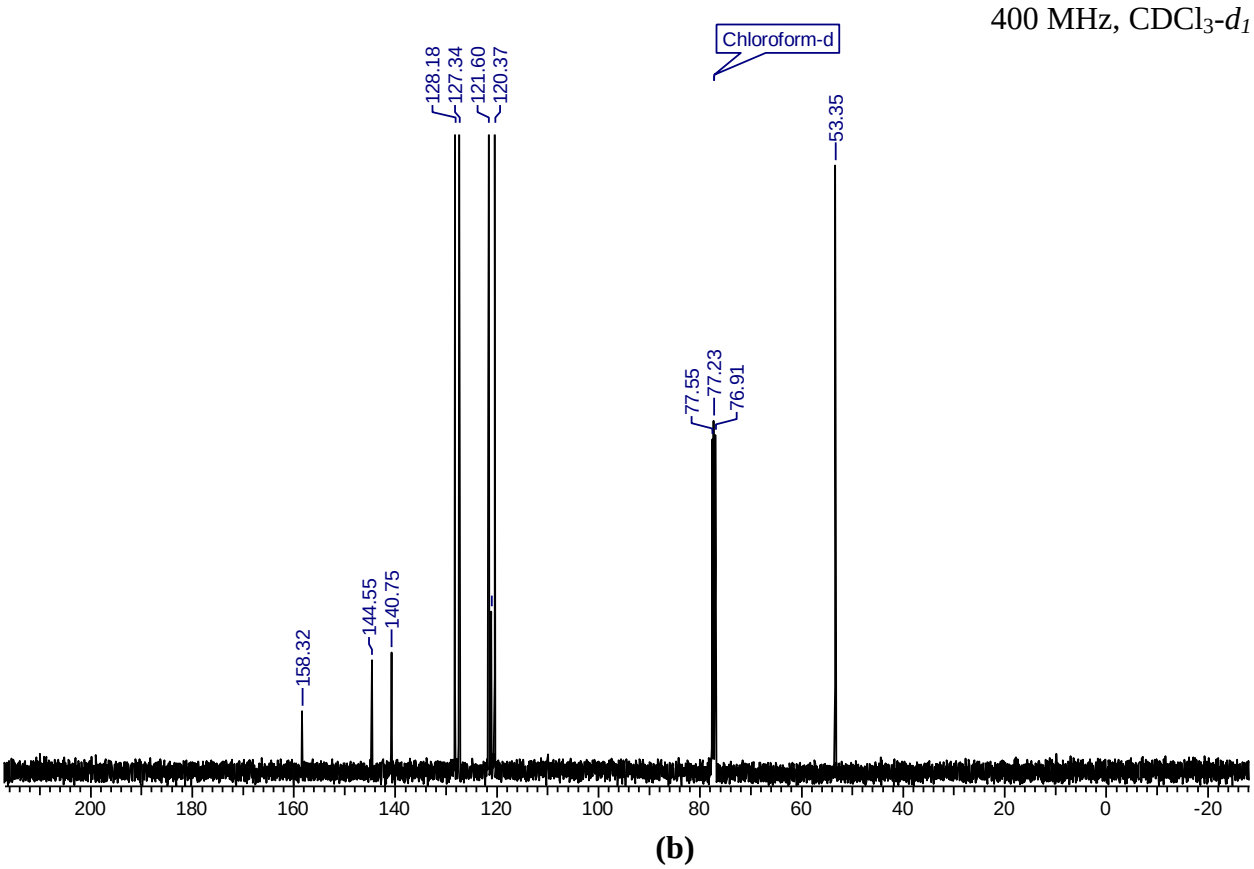

(b)

Figure A.5 (a) ^{1}H and (b) ^{13}C NMR of 1.2.6

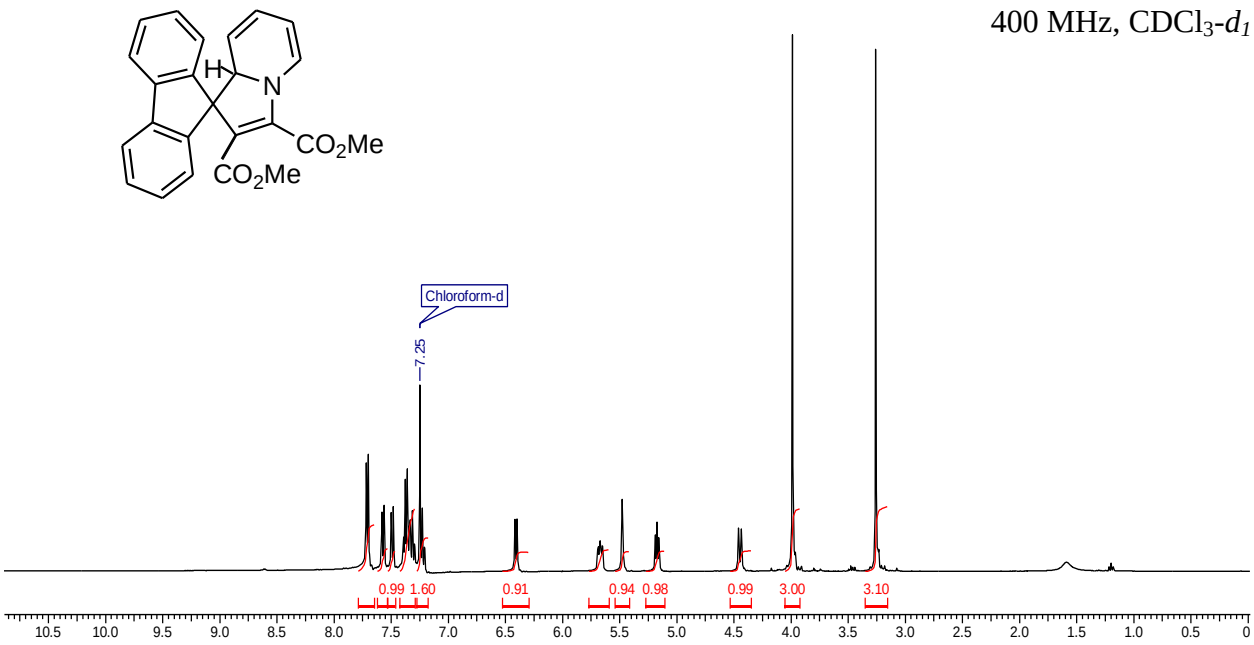

(a)

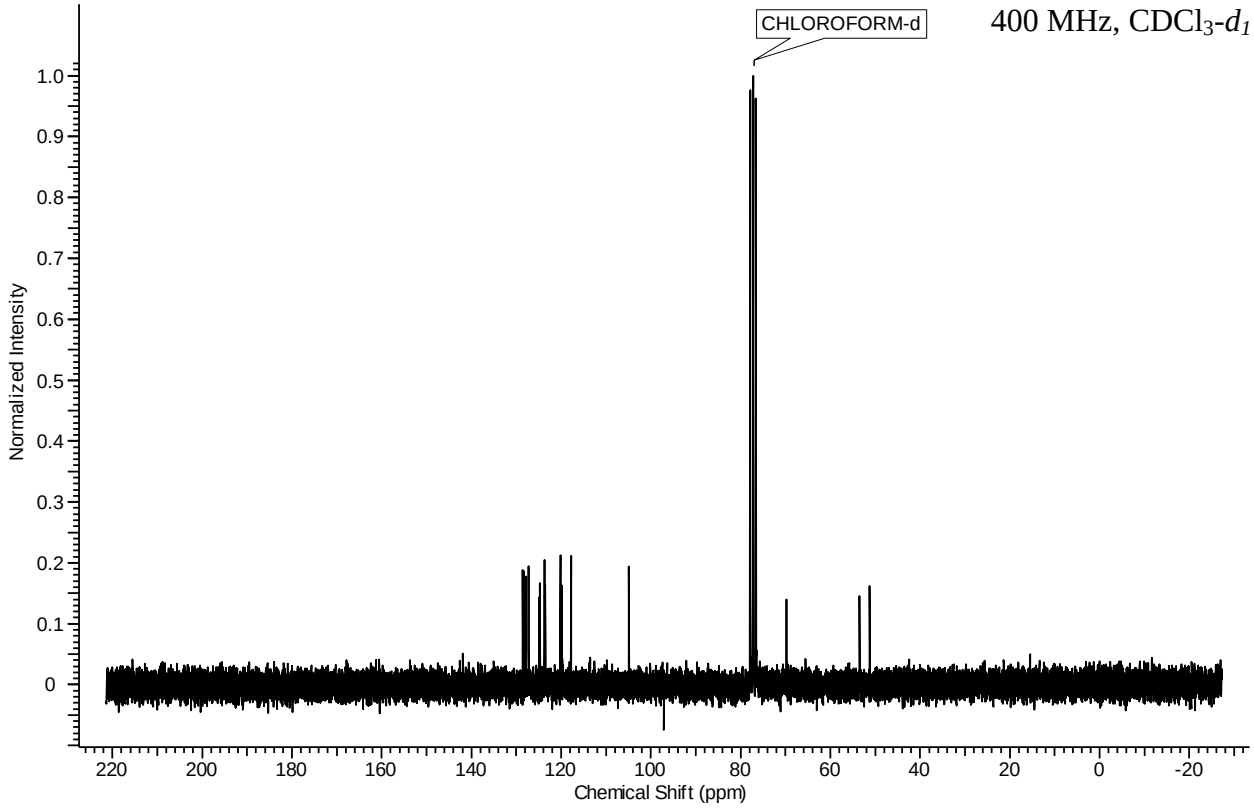

(b)

Figure A.6 (a) ^{1}H and (b) ^{13}C NMR of 1.2.1a

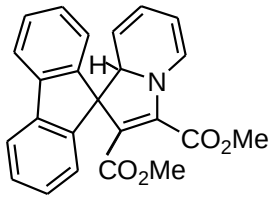

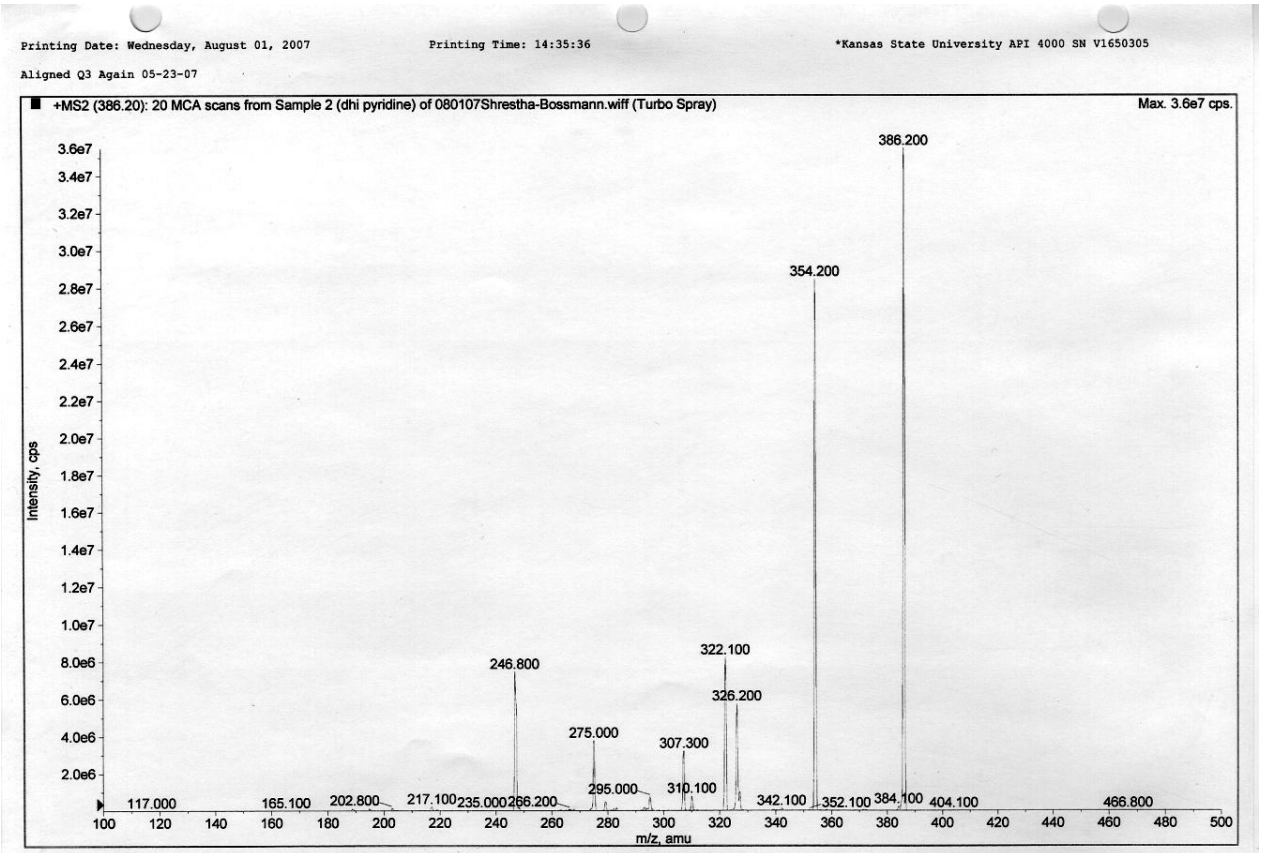

Figure A.7 Mass 1.2.1a

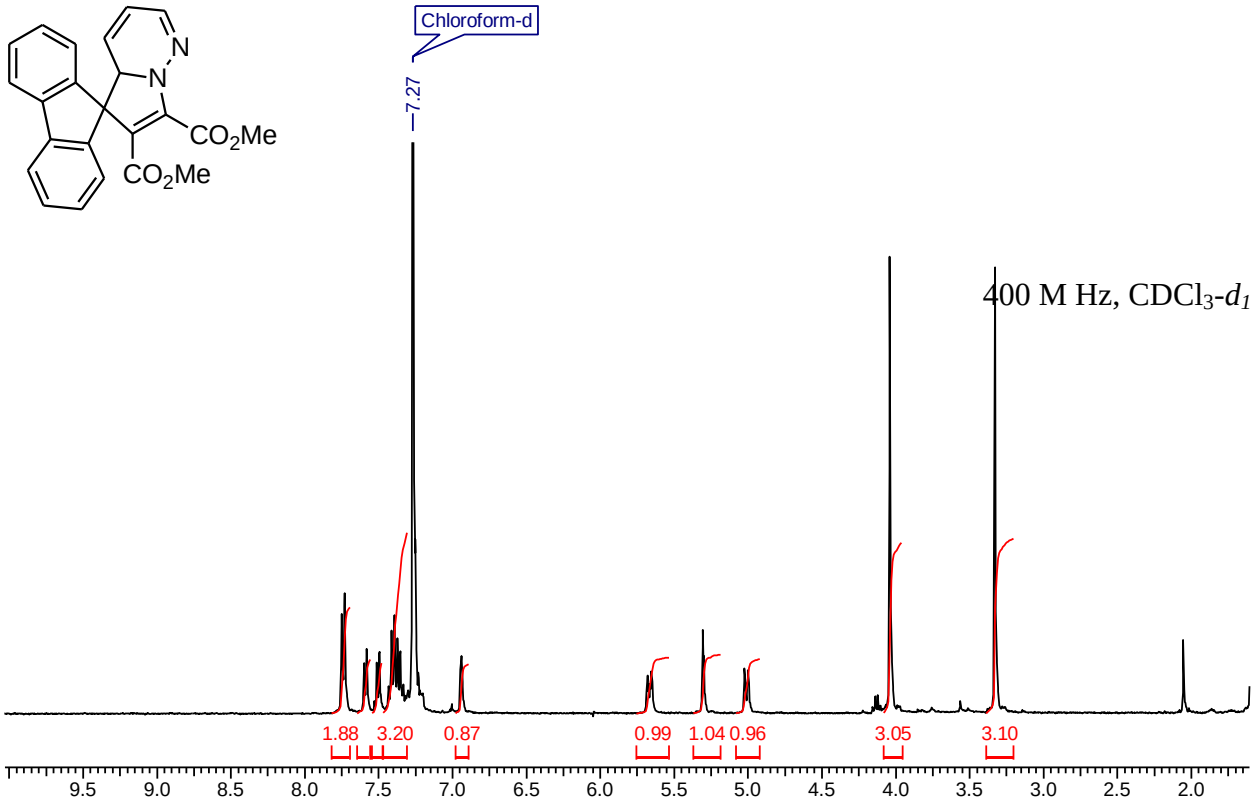

(a)

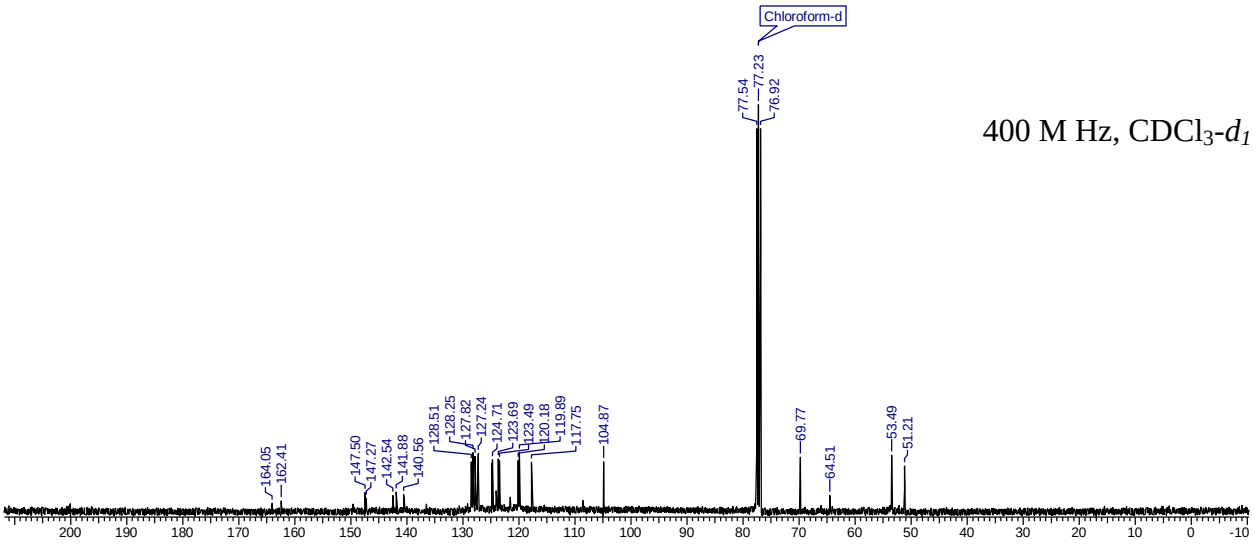

(b)

Figure A.8 ^{1}H (a), ^{13}C (b) NMR of 1.3.1a

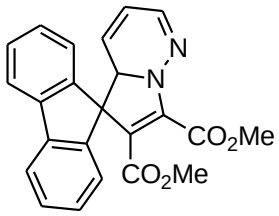

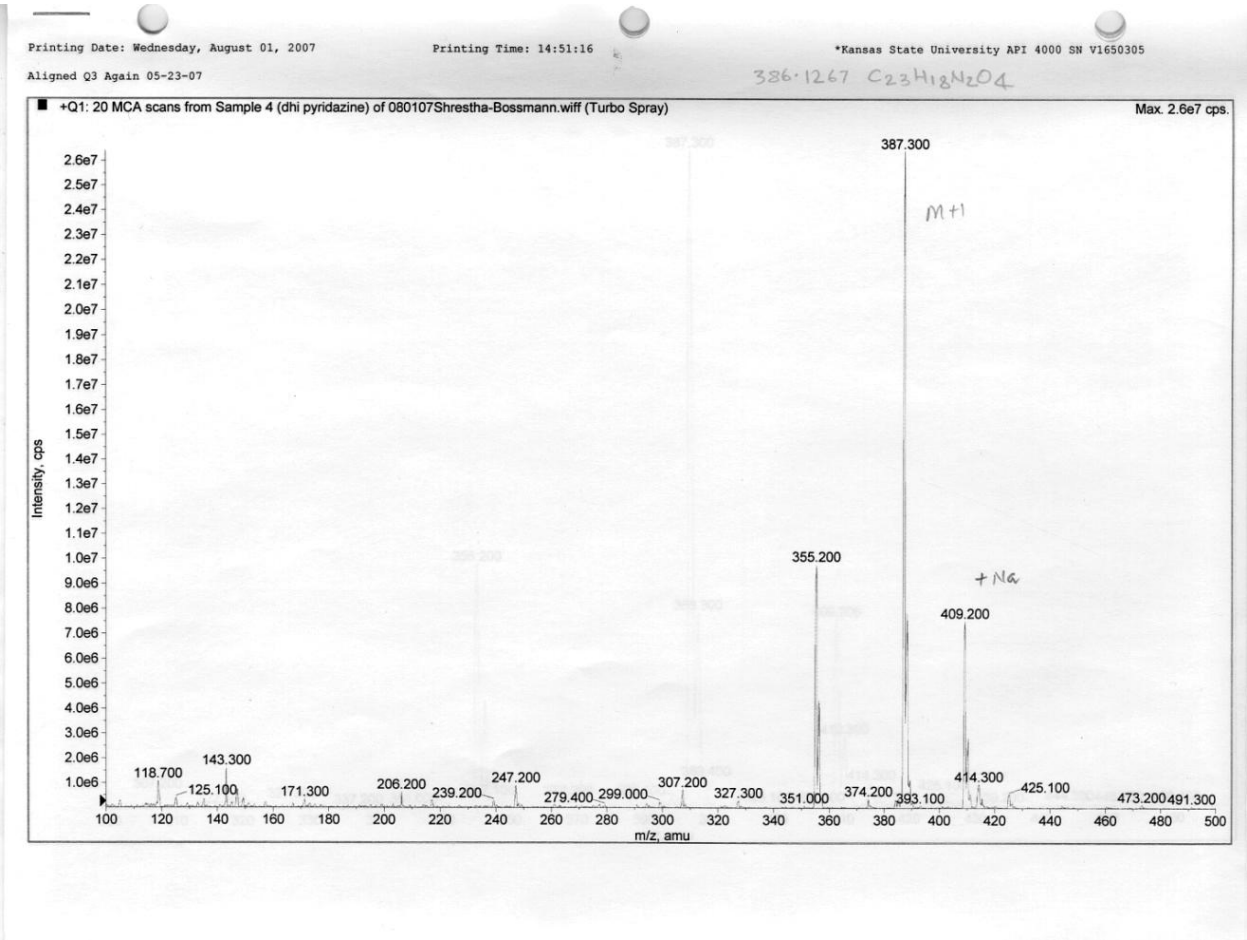

Figure A.9 Mass Spectrum of 1.3.1a

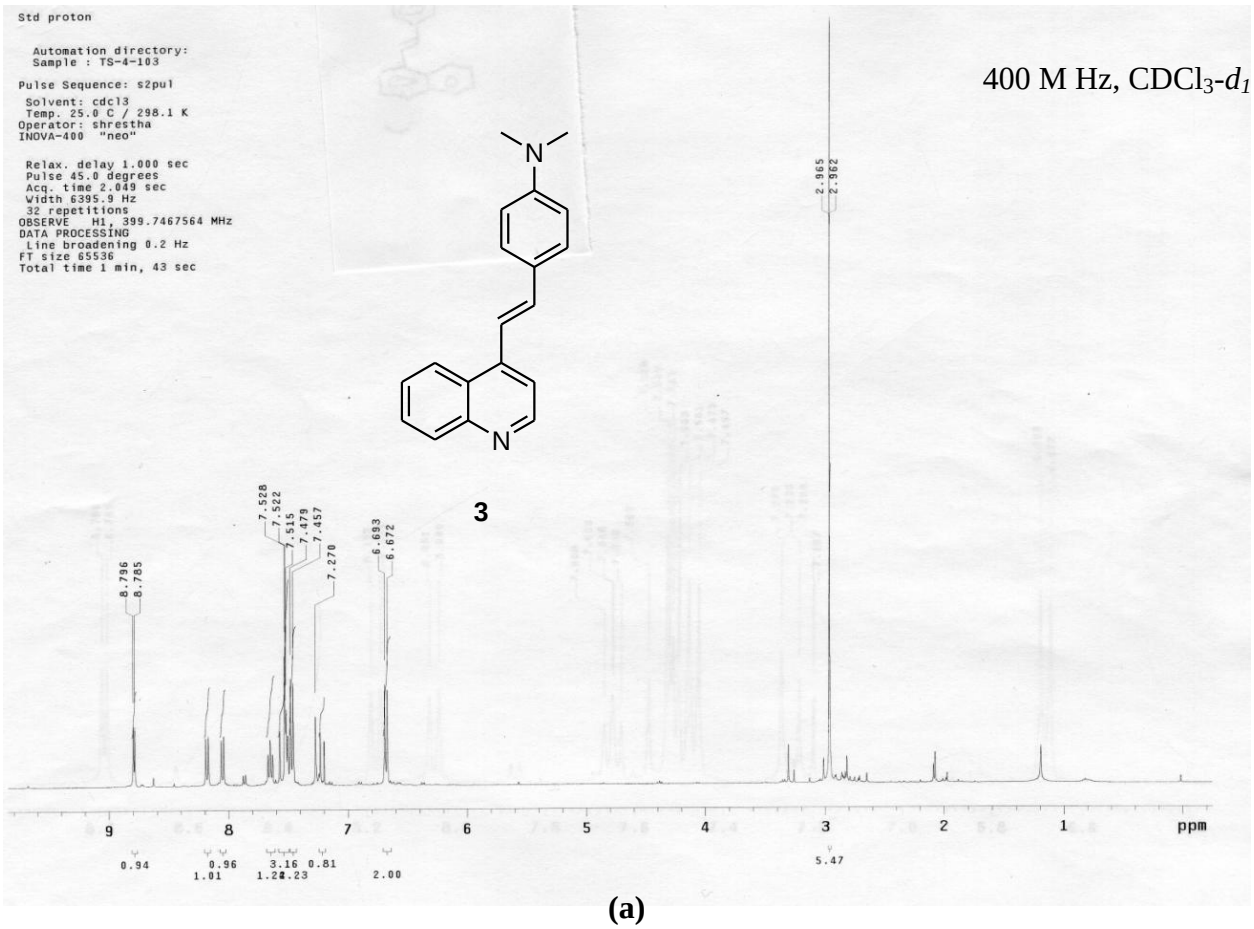

(a)

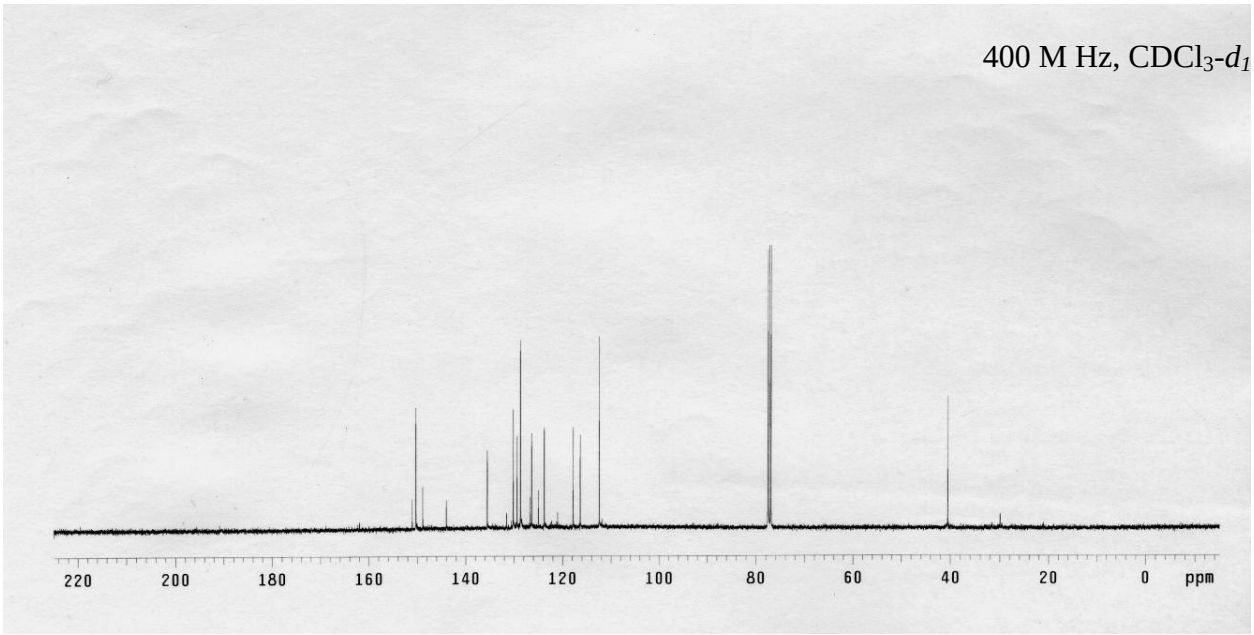

(b)

Figure A.10 ^{1}H (a), ^{13}C (b) NMR of 1.5.4

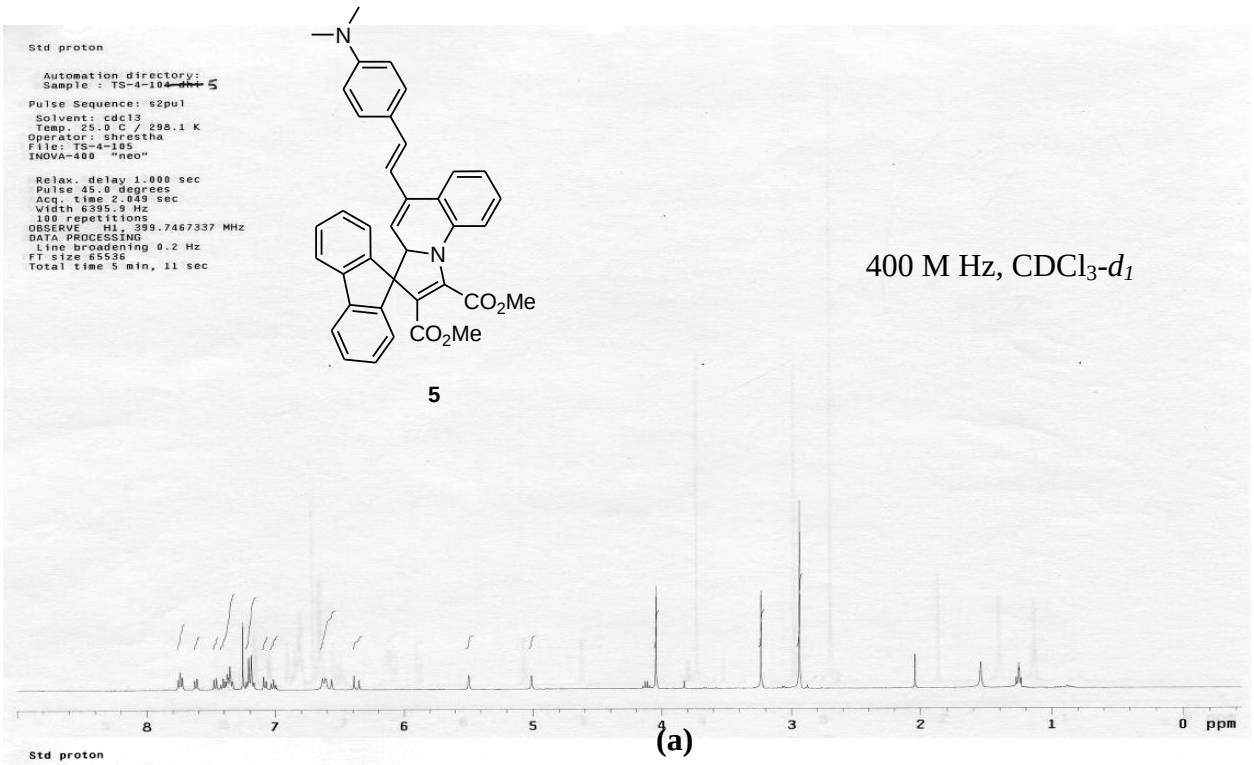

5

(a)

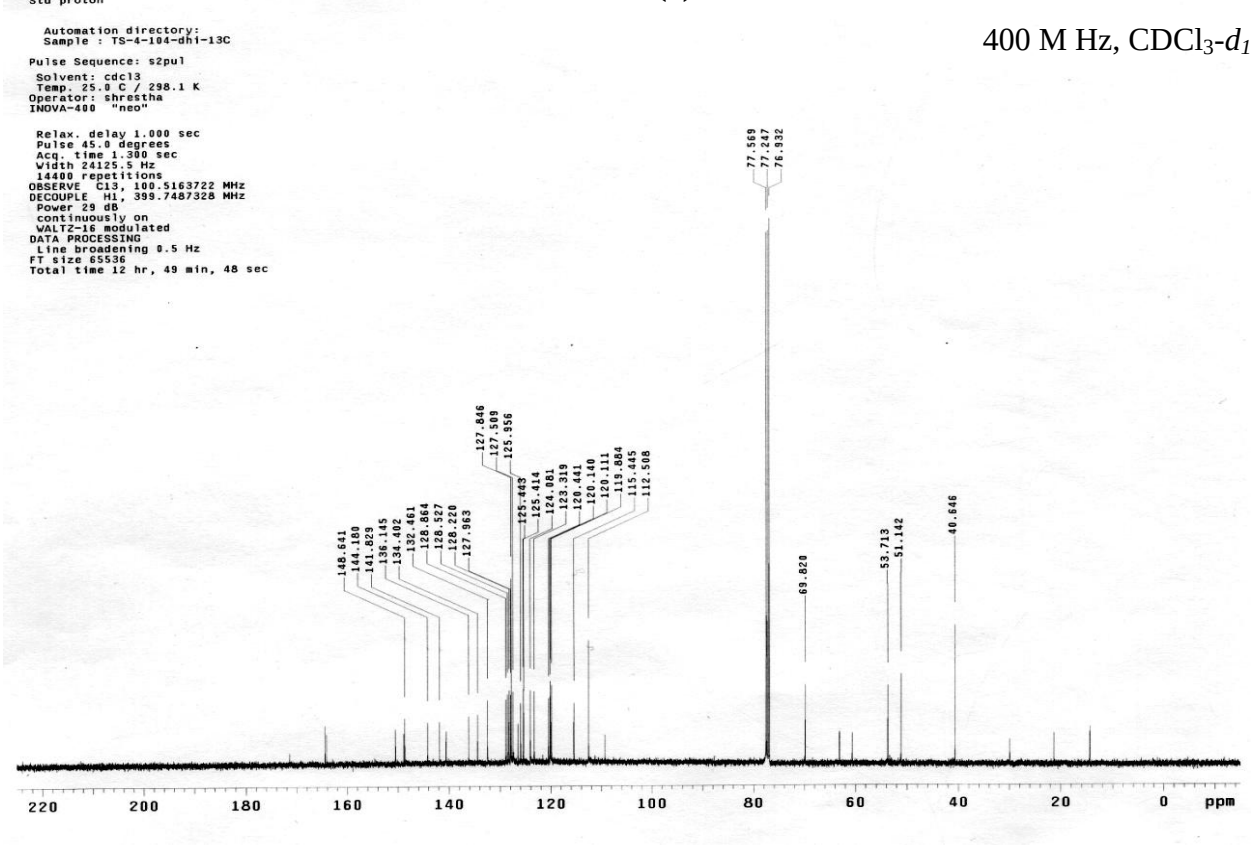

(b)

Figure A.11 ^{1}H (a), ^{13}C (b) NMR of 1.5.1

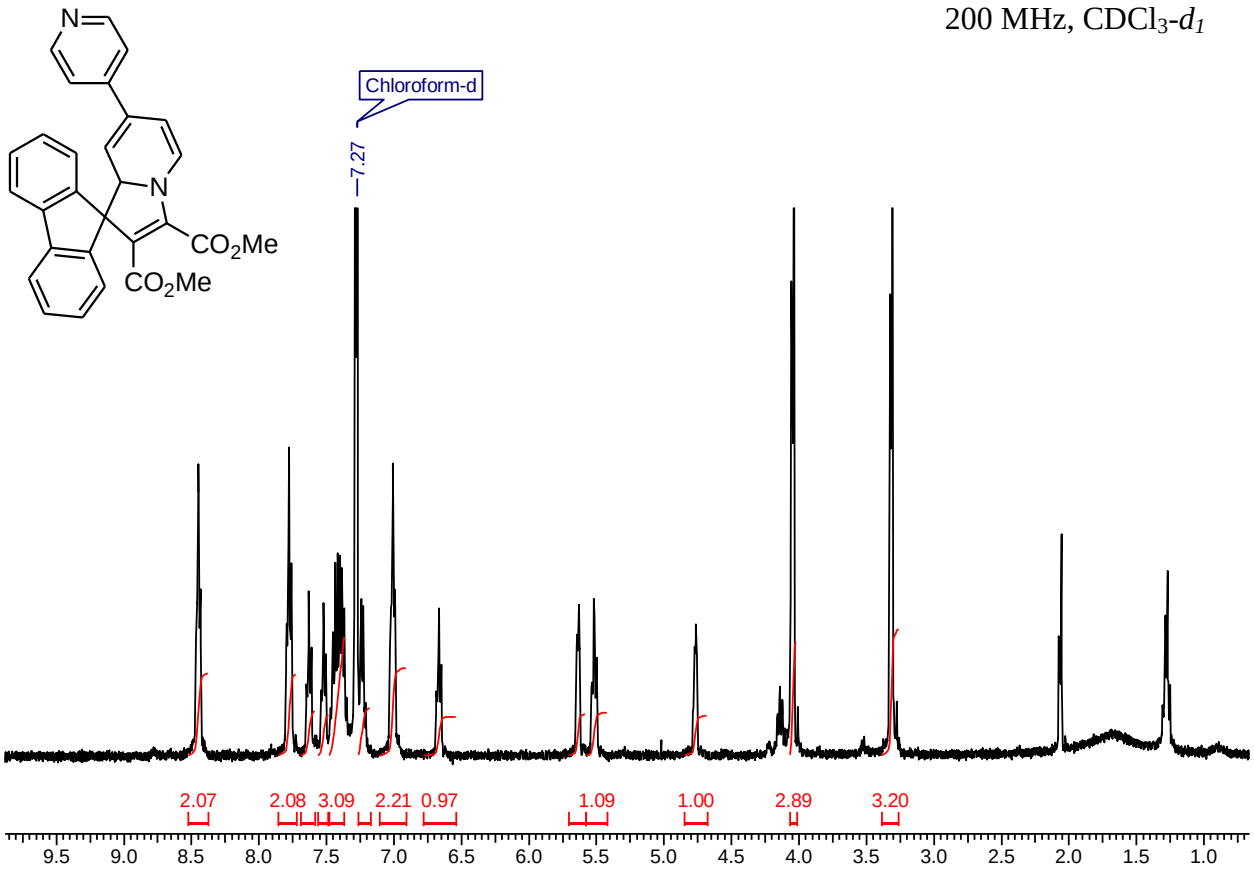

(a)

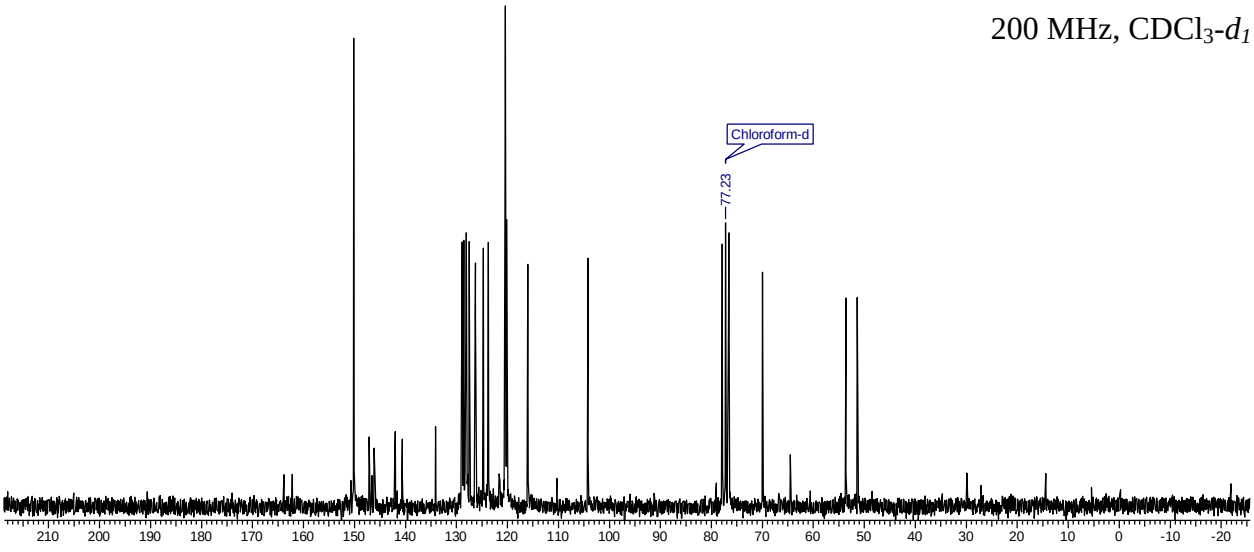

(b)

Figure A.12 (a) ^{1}H and (b) ^{13}C NMR of 1.6.3

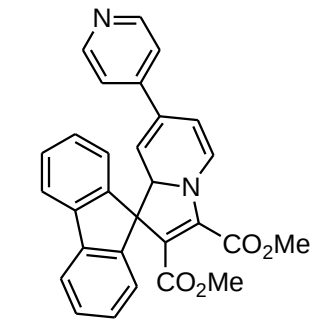

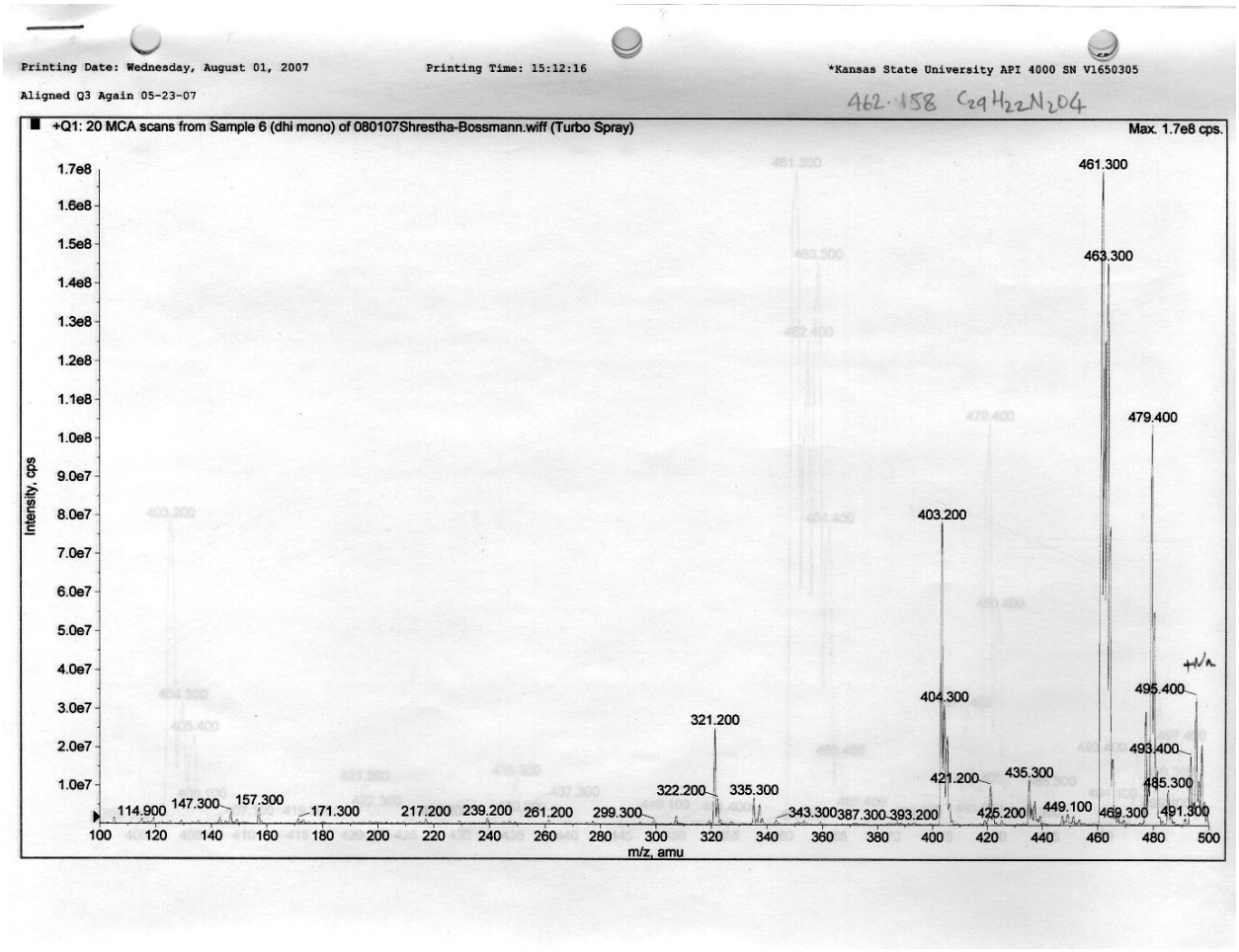

Figure A.13 Mass of 1.6.3

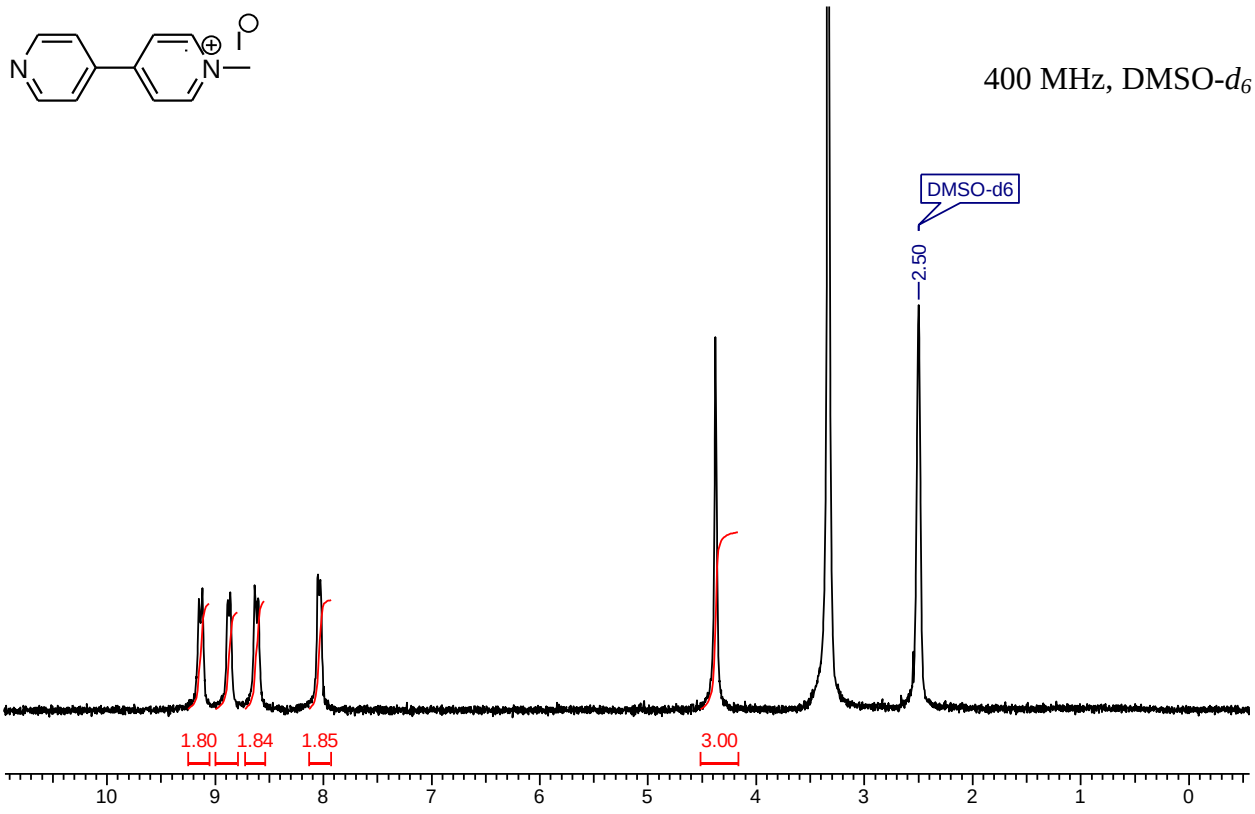

(a)

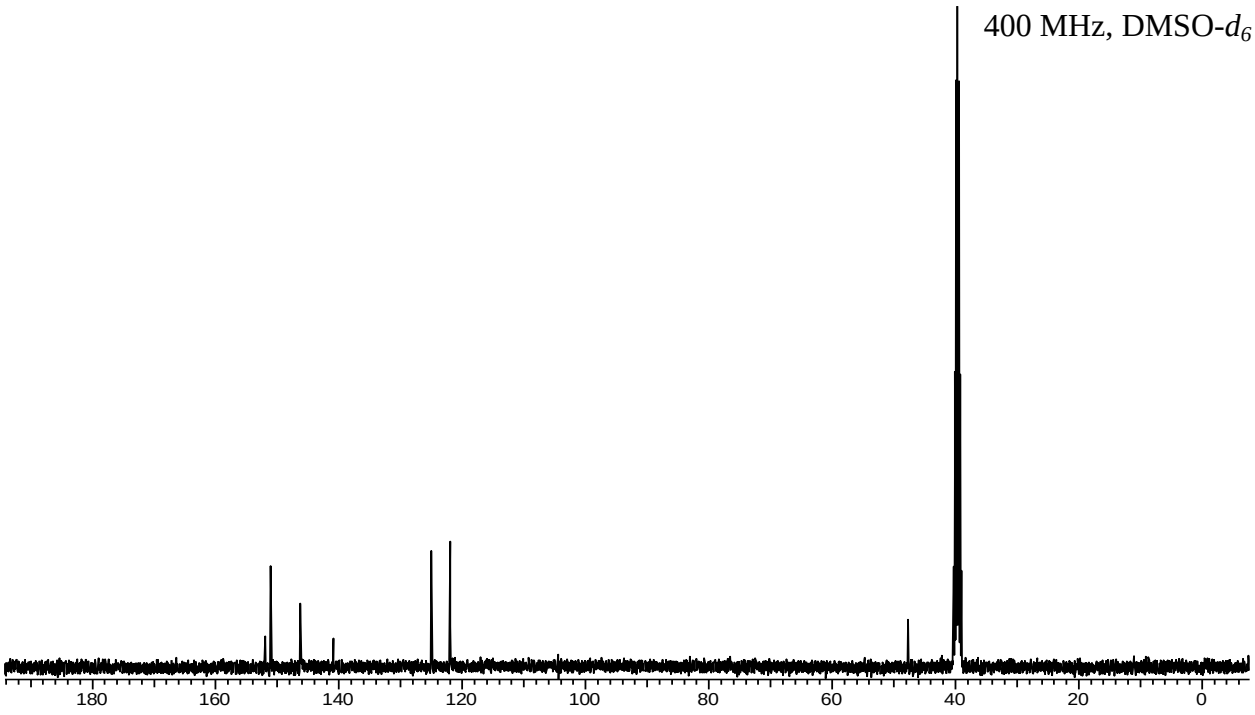

(b)

Figure A.14 (a) ^{1}H and (b) ^{13}C NMR of 1.6.4

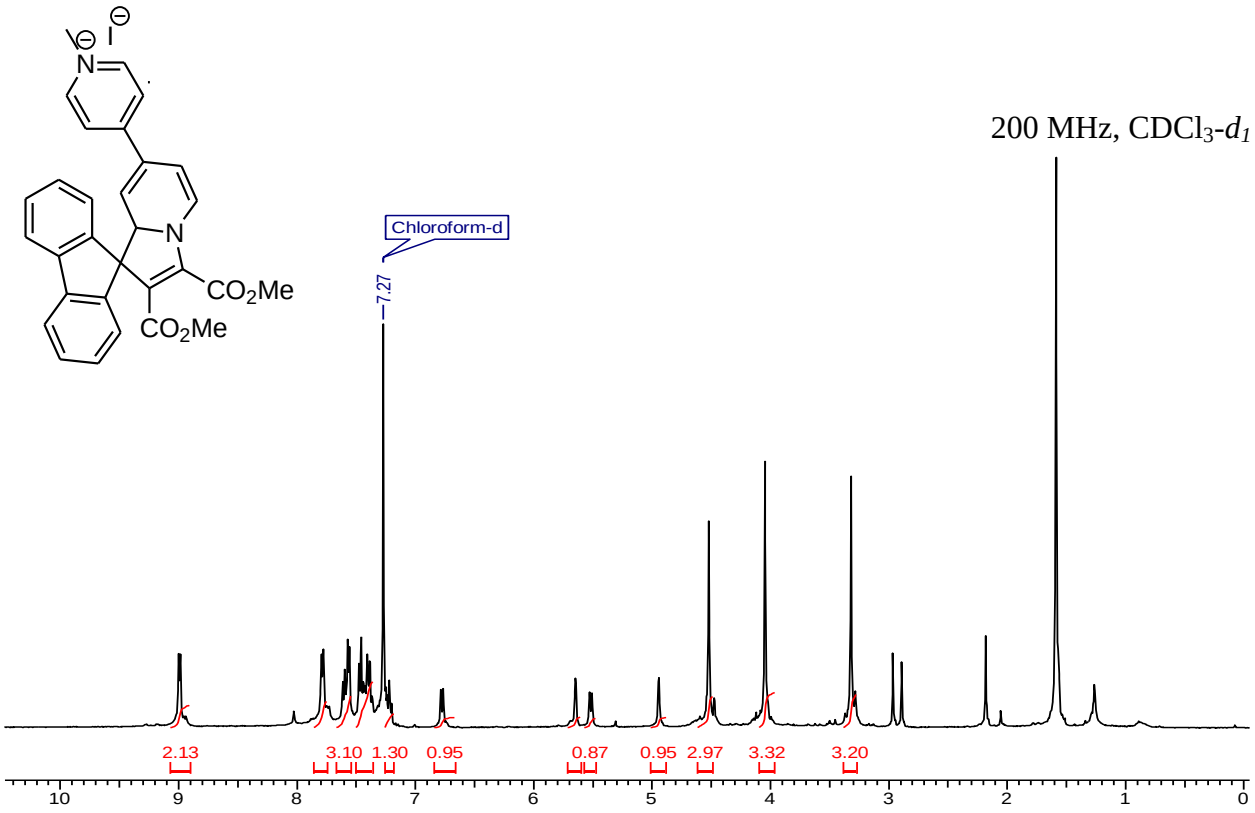

(a)

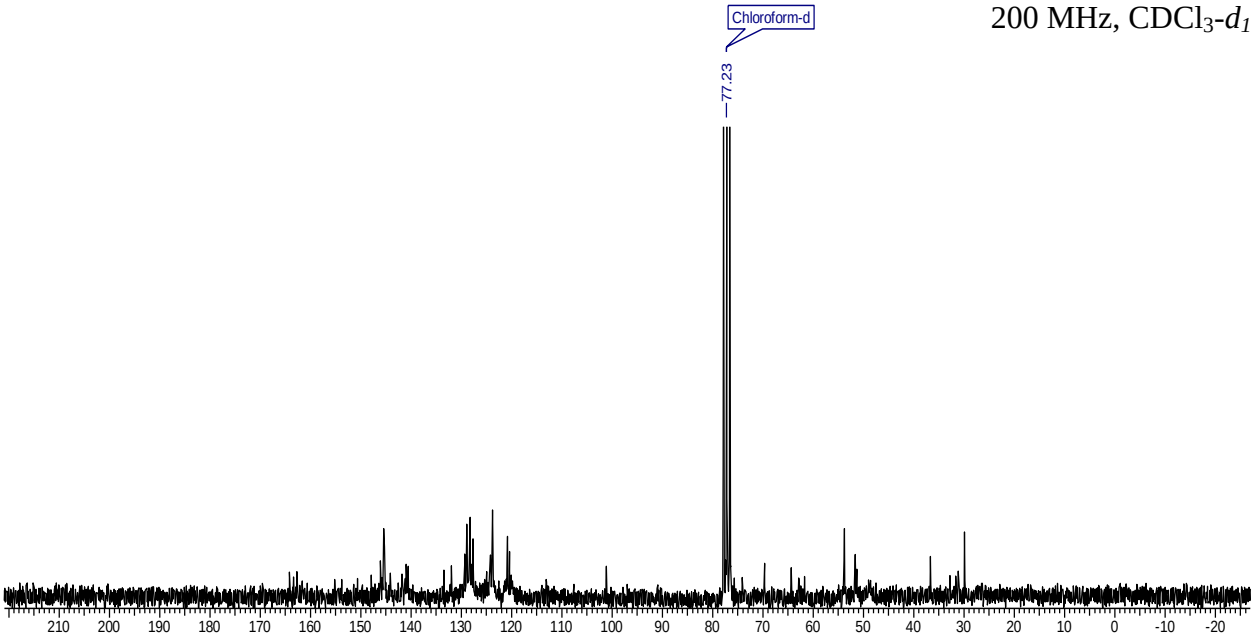

(b)

Figure A.15 (a) ^{1}H and (b) ^{13}C NMR of 1.6.5

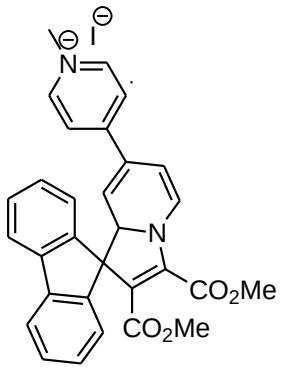

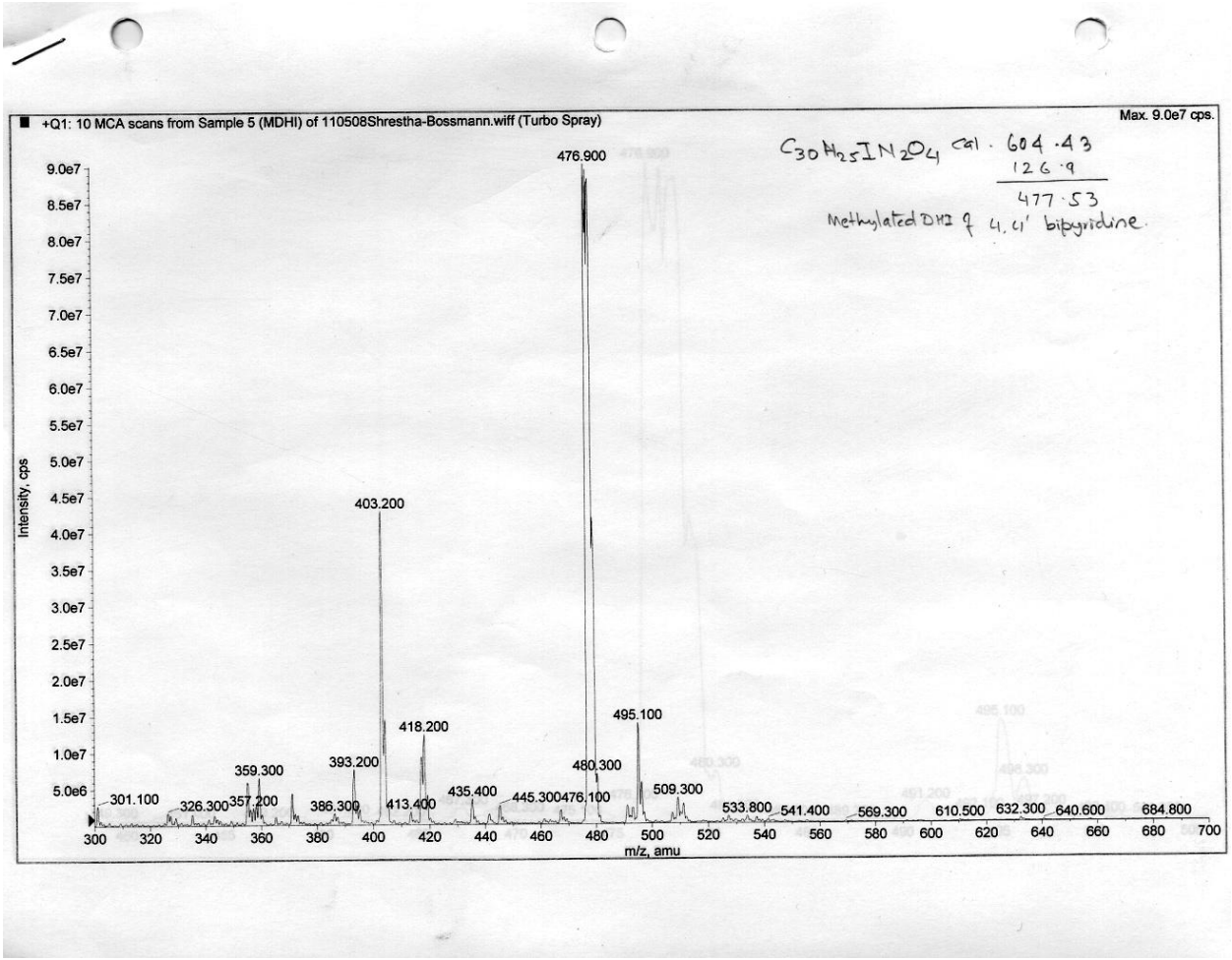

Figure A.16 Mass 1.6.5

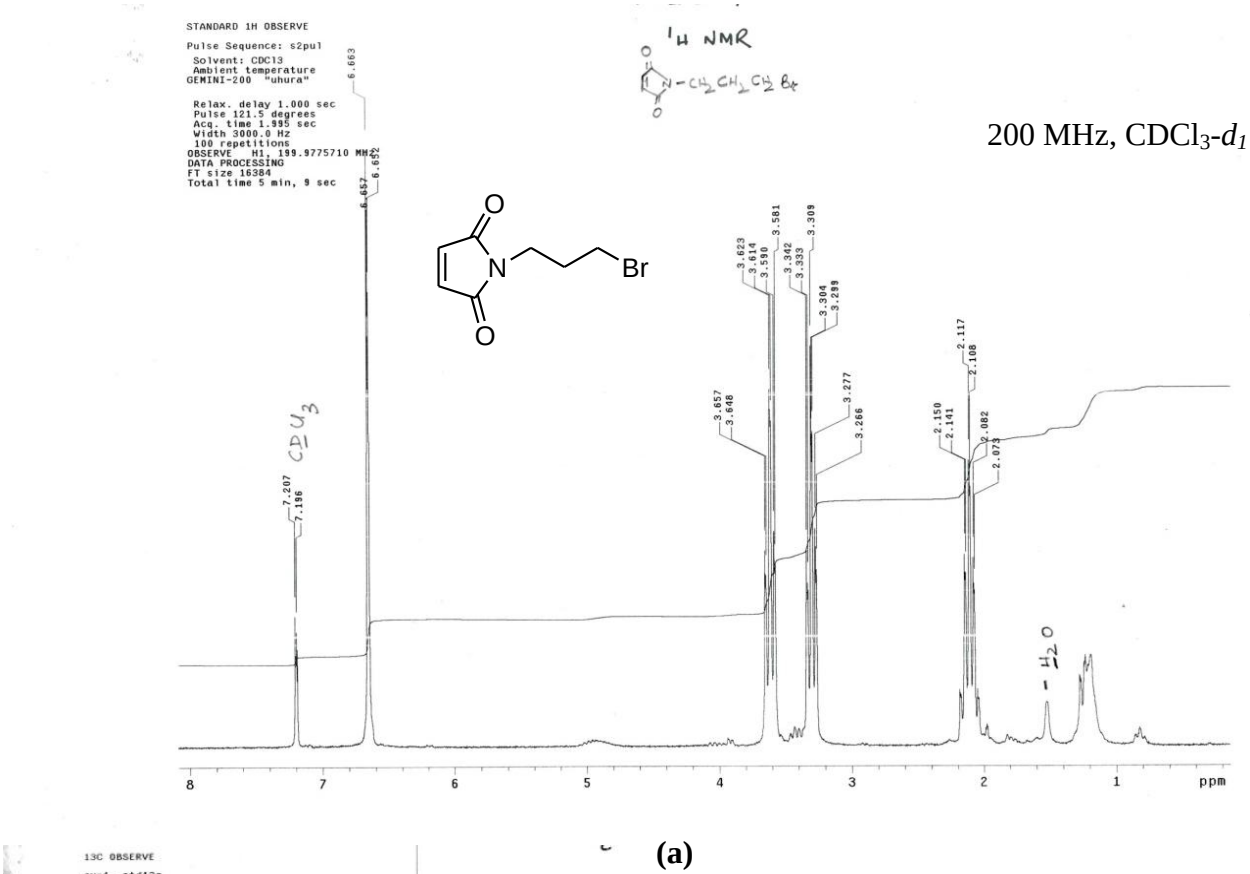

(a)

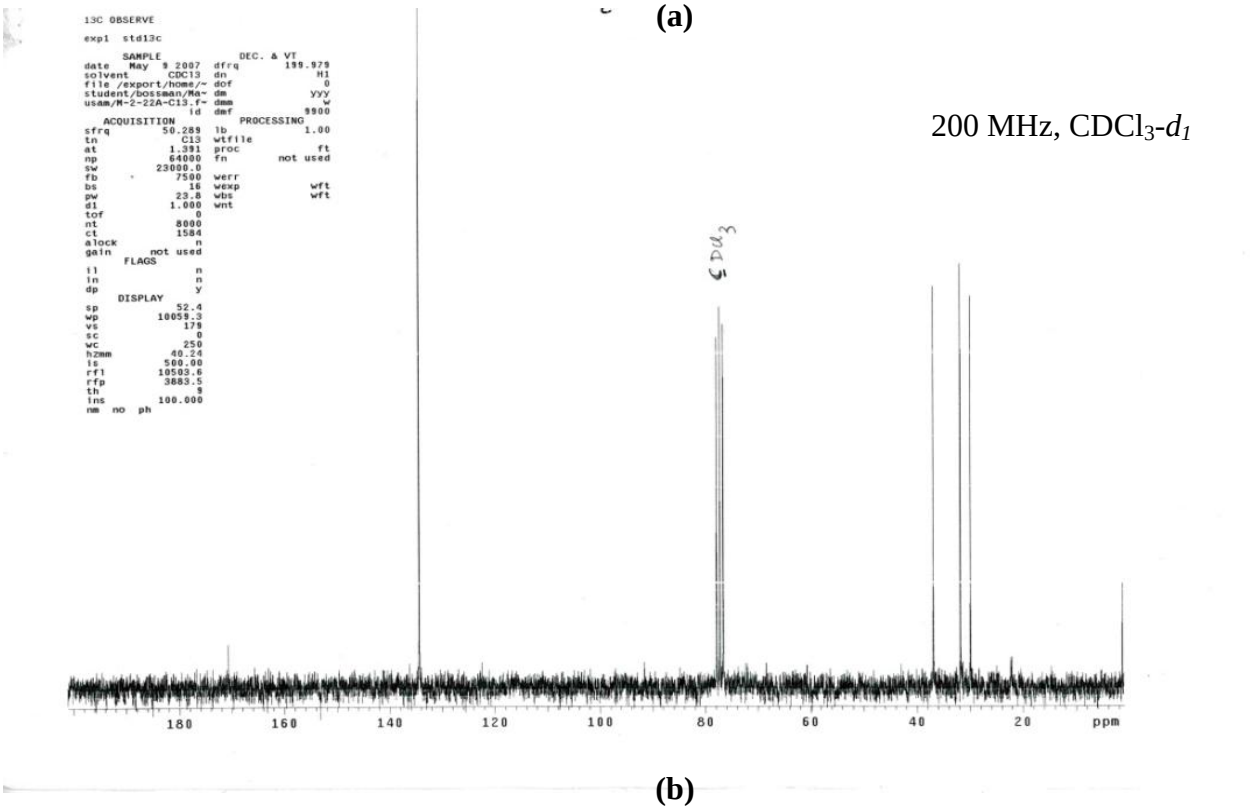

(b)

Figure A.17 (a) ^{1}H and (b) ^{13}C NMR of 1.6.11

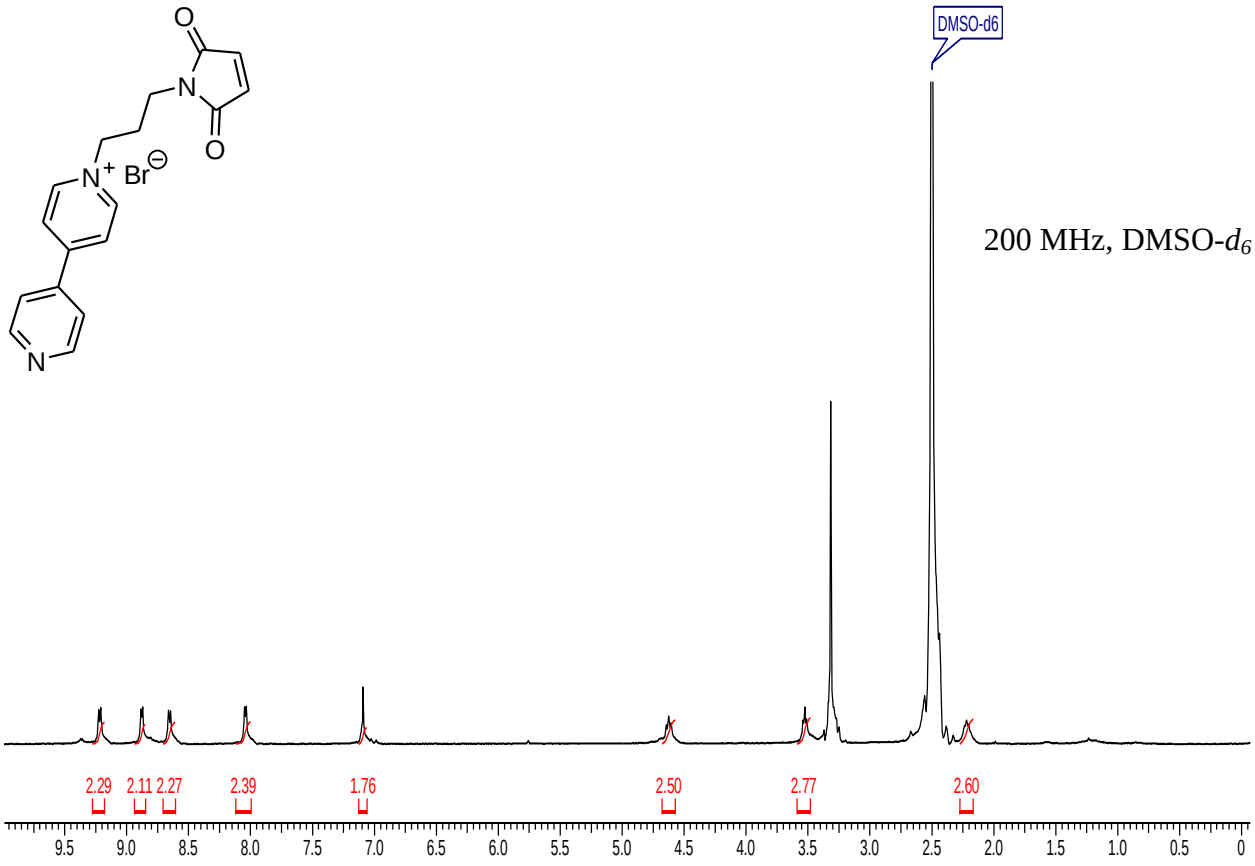

(a)

Figure A.18 (a) ^{1}H and of 1.6.6

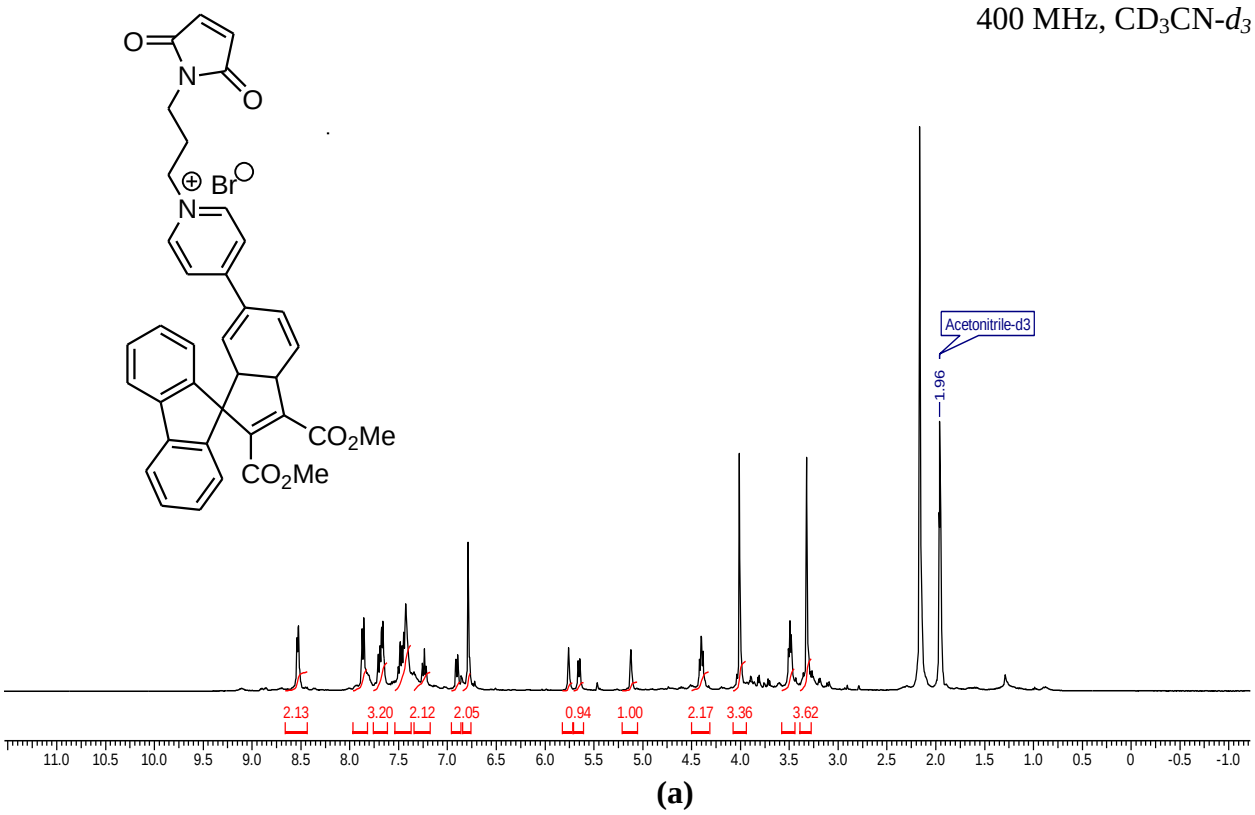

Figure A.19 (a) ^{1}H and (b) ^{13}C NMR of 1.5.7

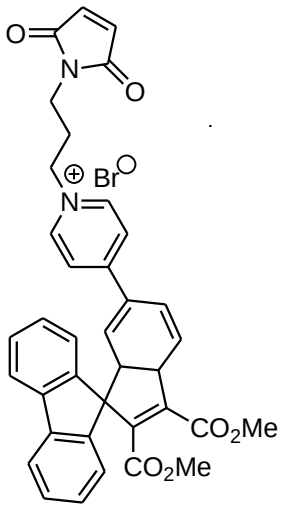

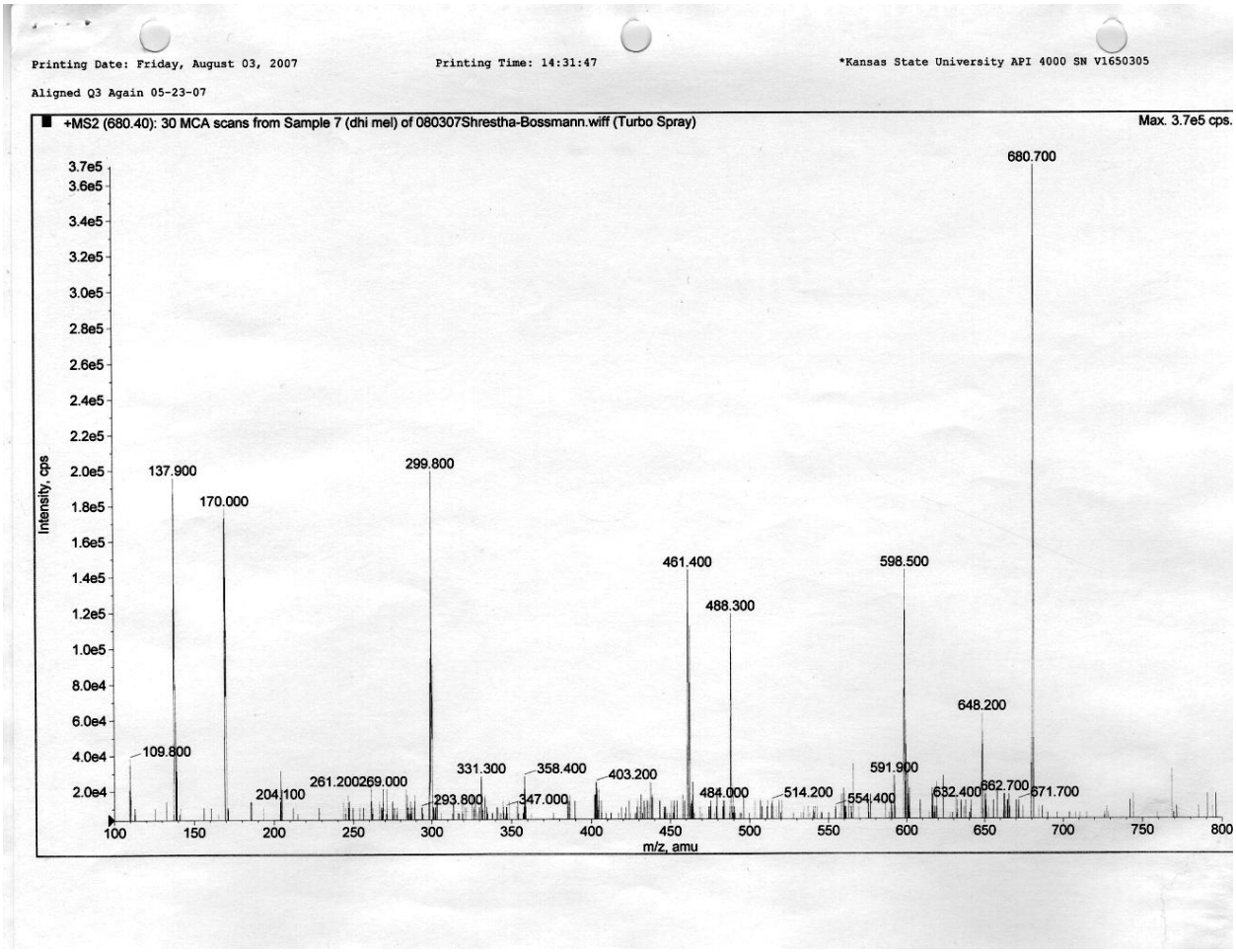

Figure A.20 Mass 1.5.7

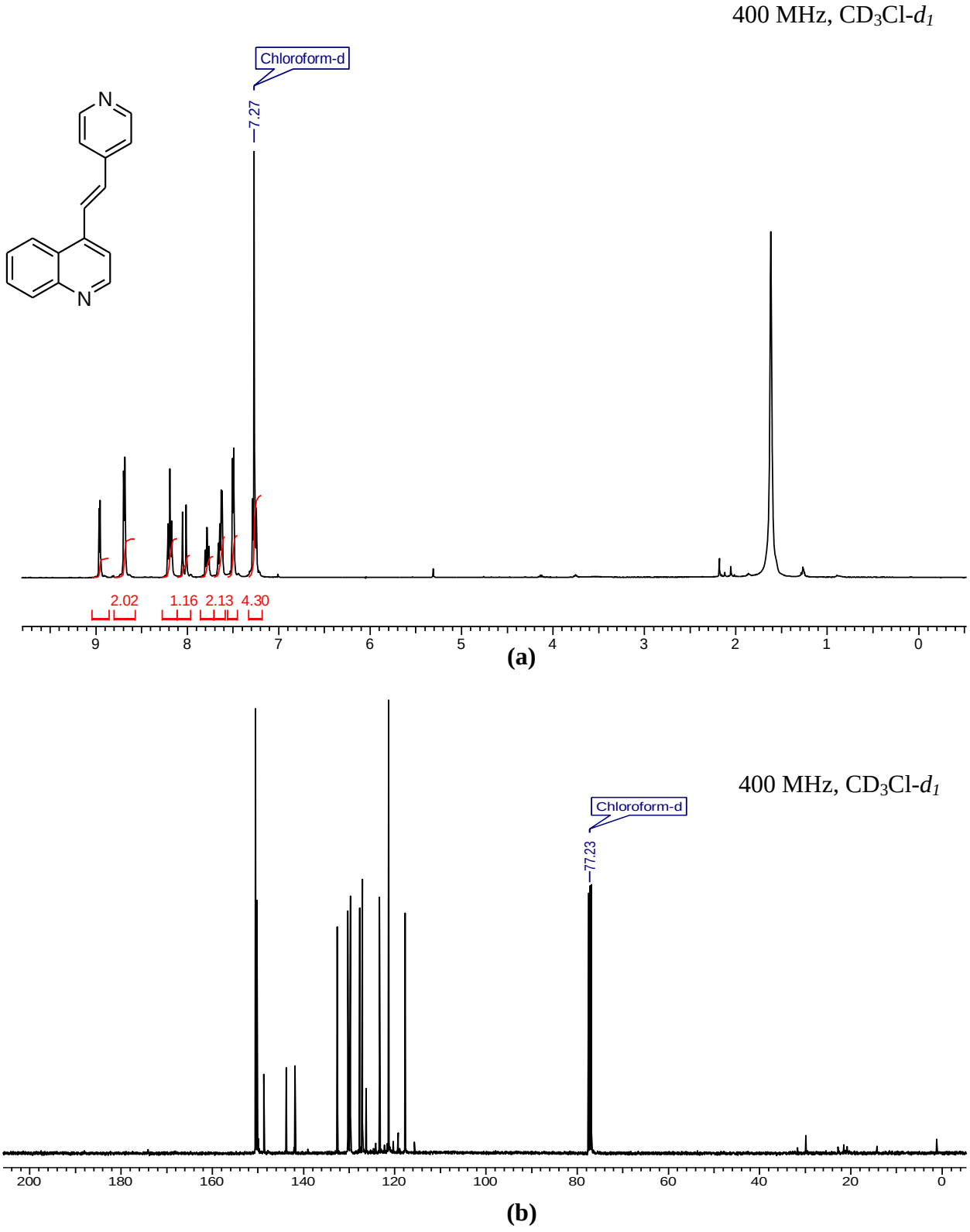

Figure A.21 (a) ^{1}H and (b) ^{13}C NMR of 1.6.10

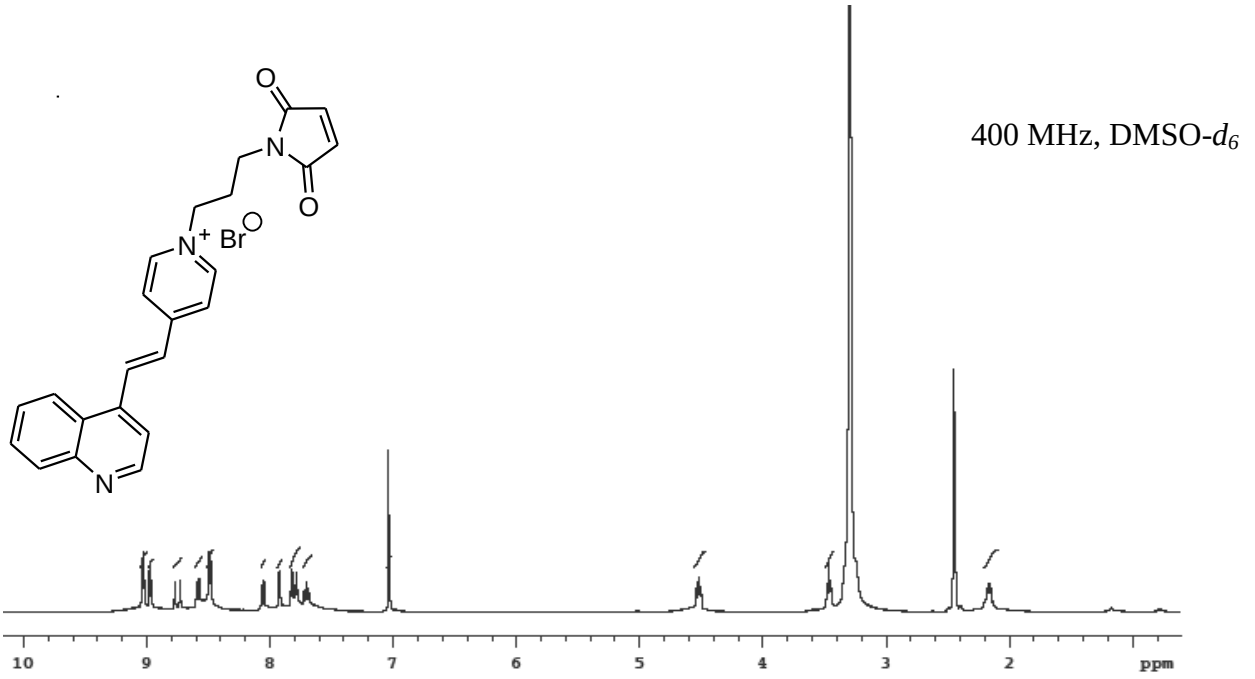

(a)

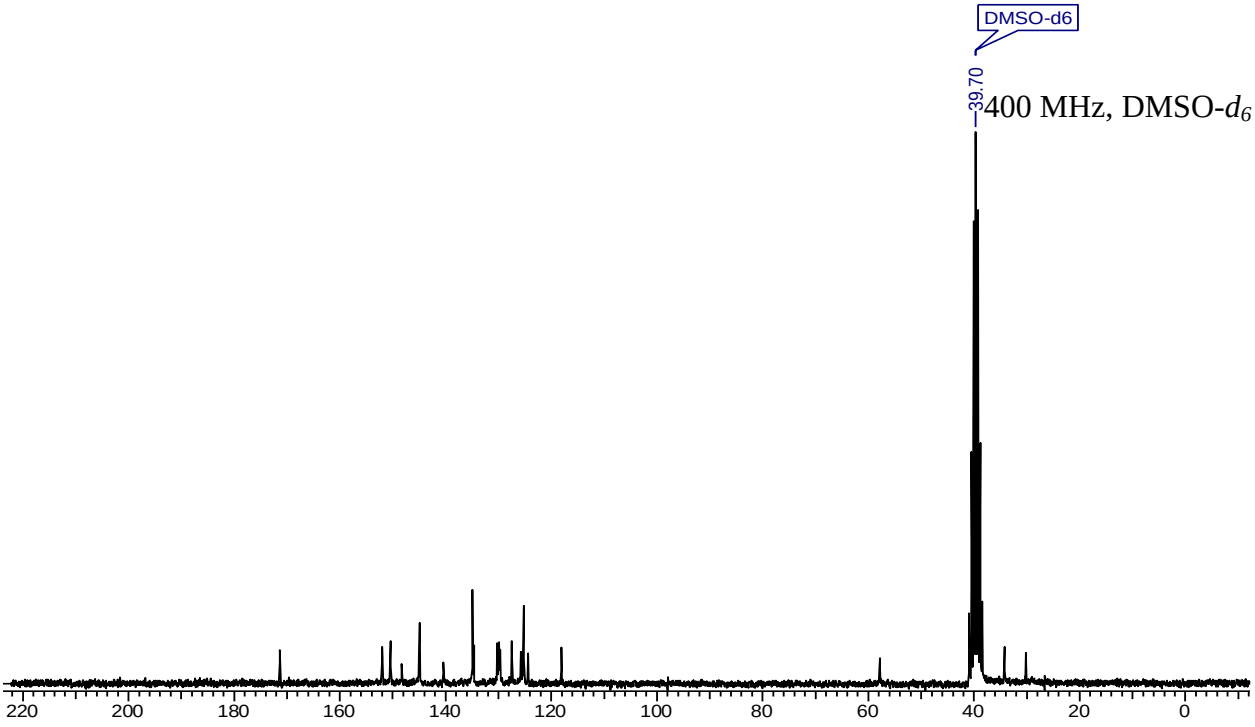

(b)

Figure A.22 (a) ^{1}H and (b) ^{13}C NMR of 1.6.12

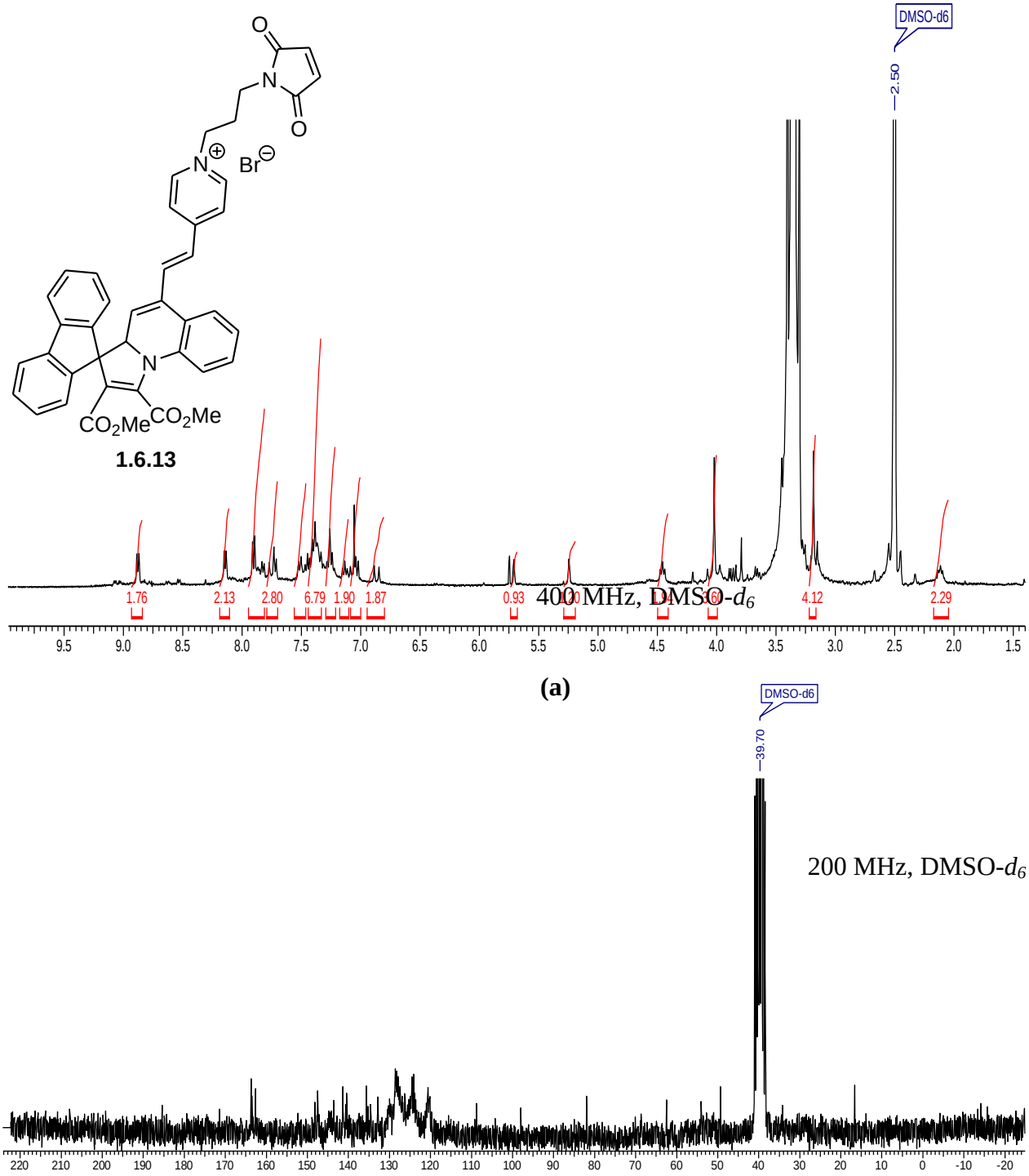

1.6.13

Figure A.23 (a) ^{1}H and (b) ^{13}C NMR of 1.6.13

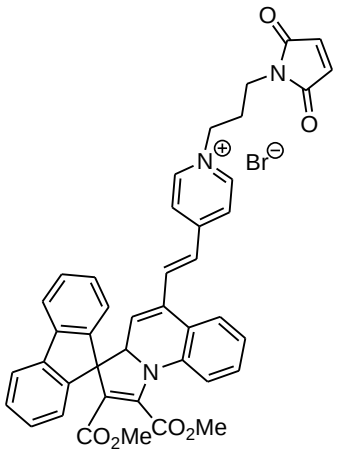

1.6.13

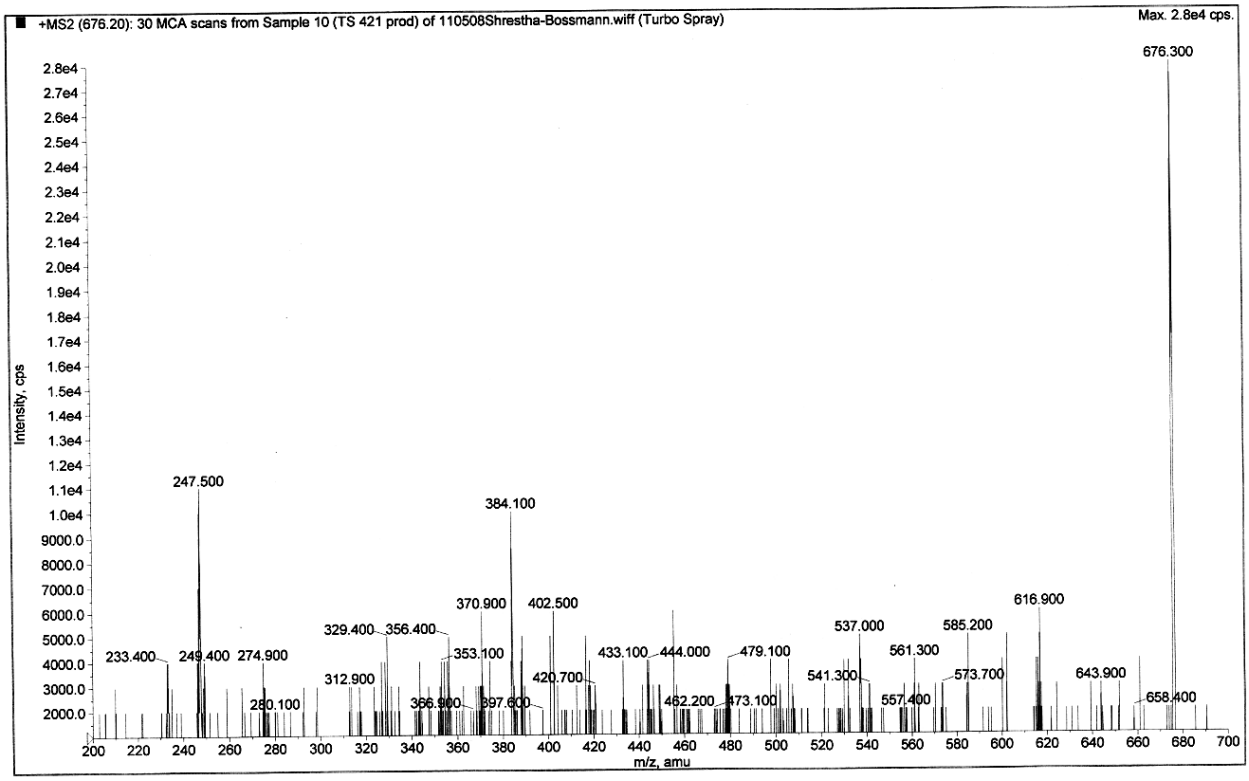

Figure A.24 Mass of 1.6.1

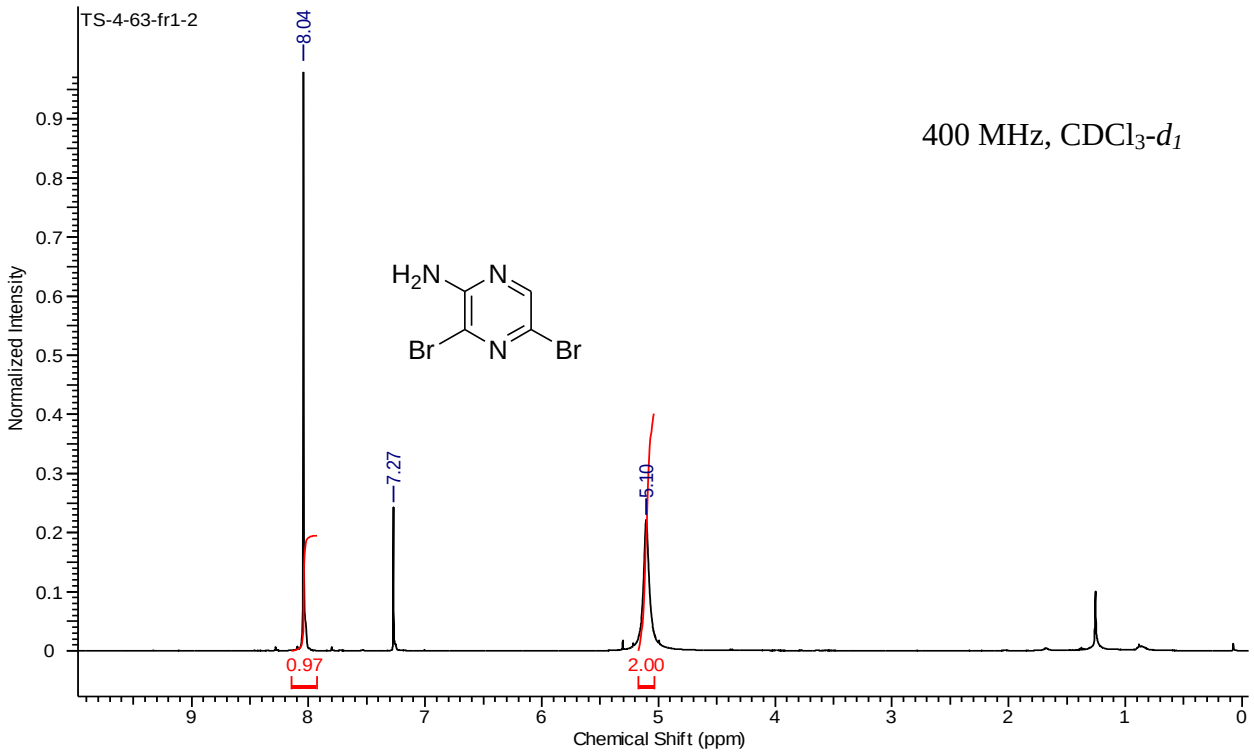

(a)

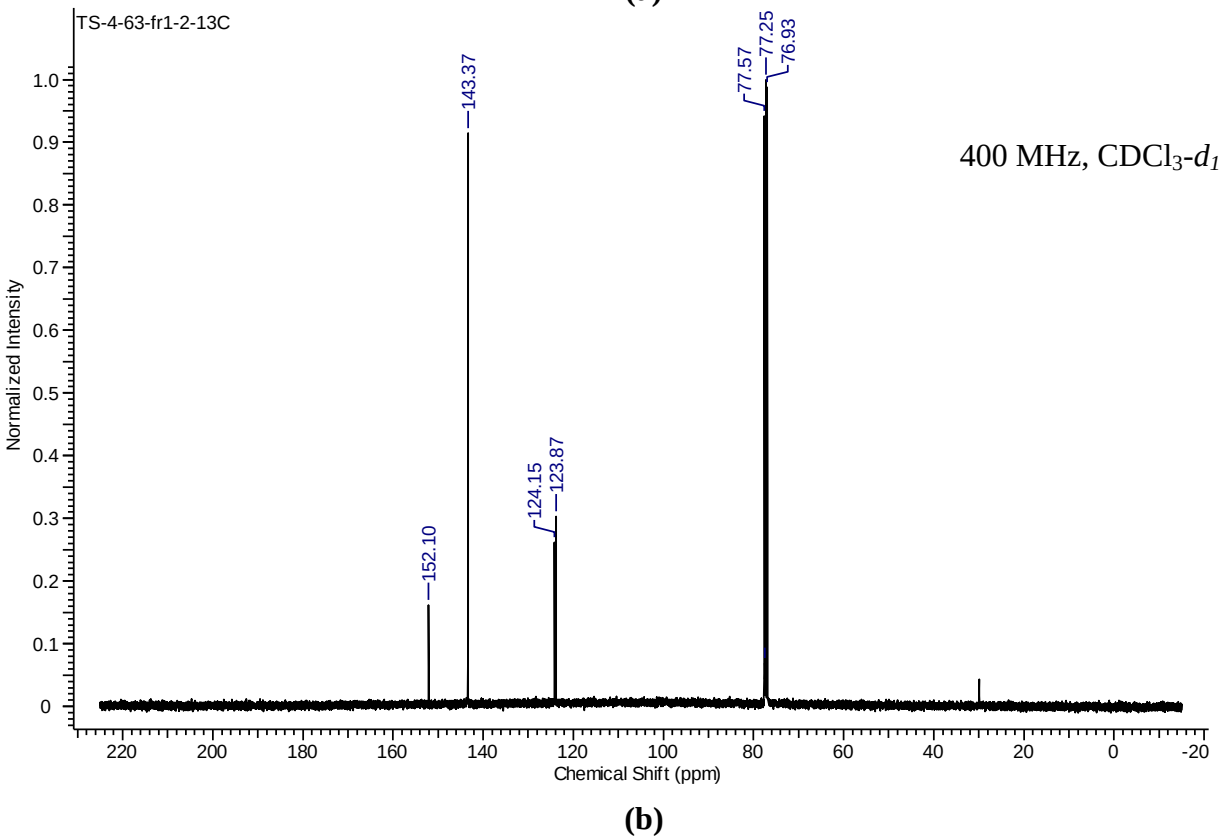

(b)

Figure A.25 (a) ^{1}H and (b) ^{13}C NMR of 2.3

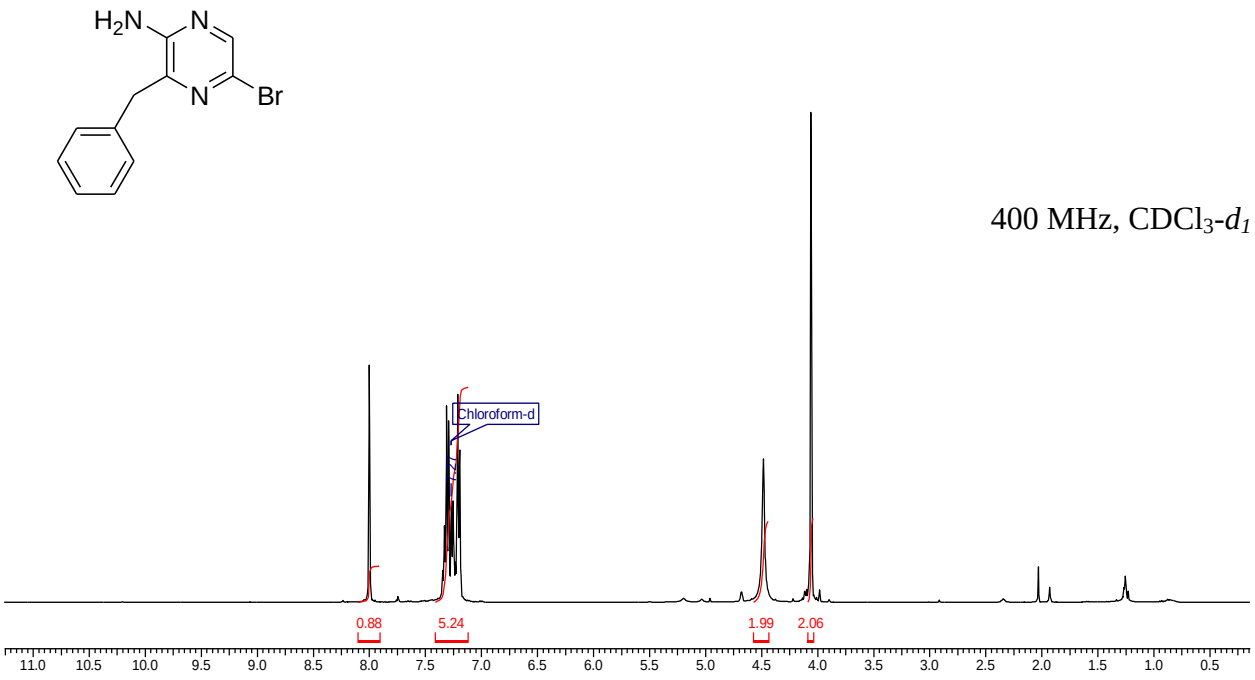

(a)

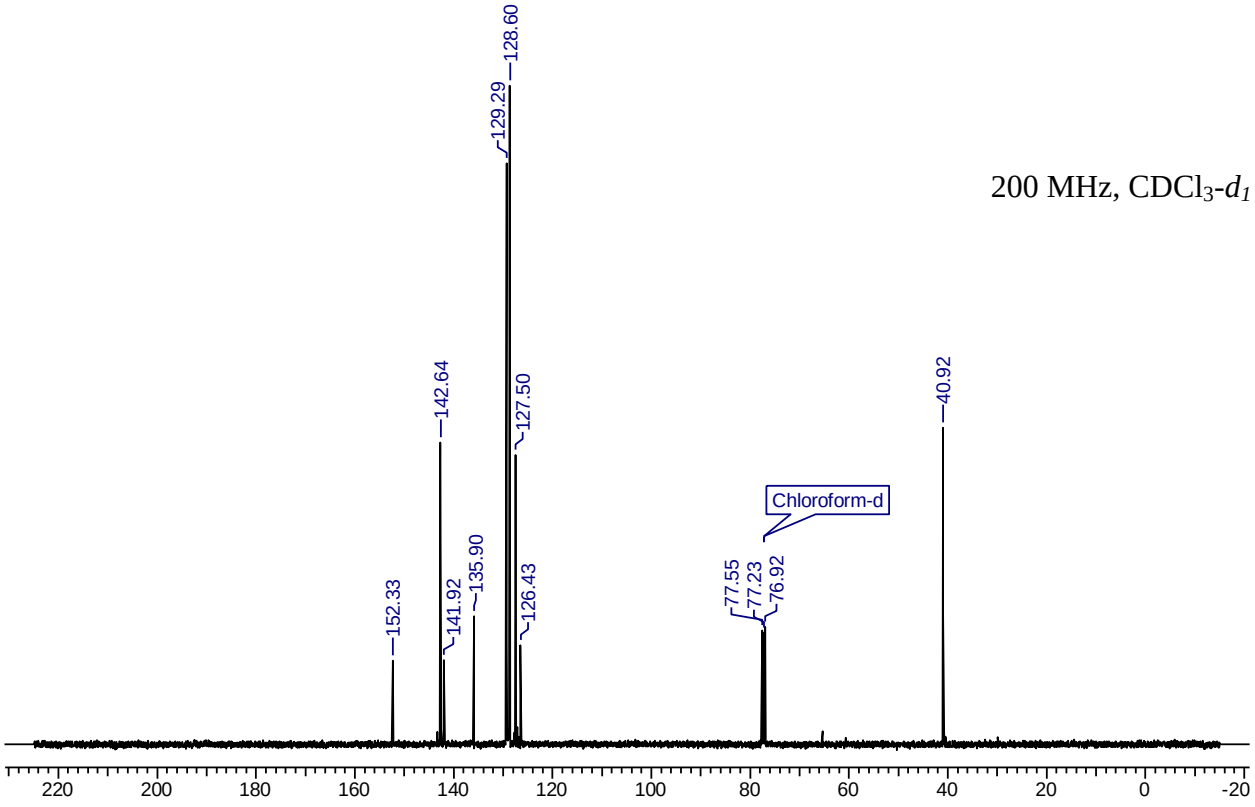

(b)

Figure A.26 (a) ^{1}H and (b) ^{13}C NMR of 2.6

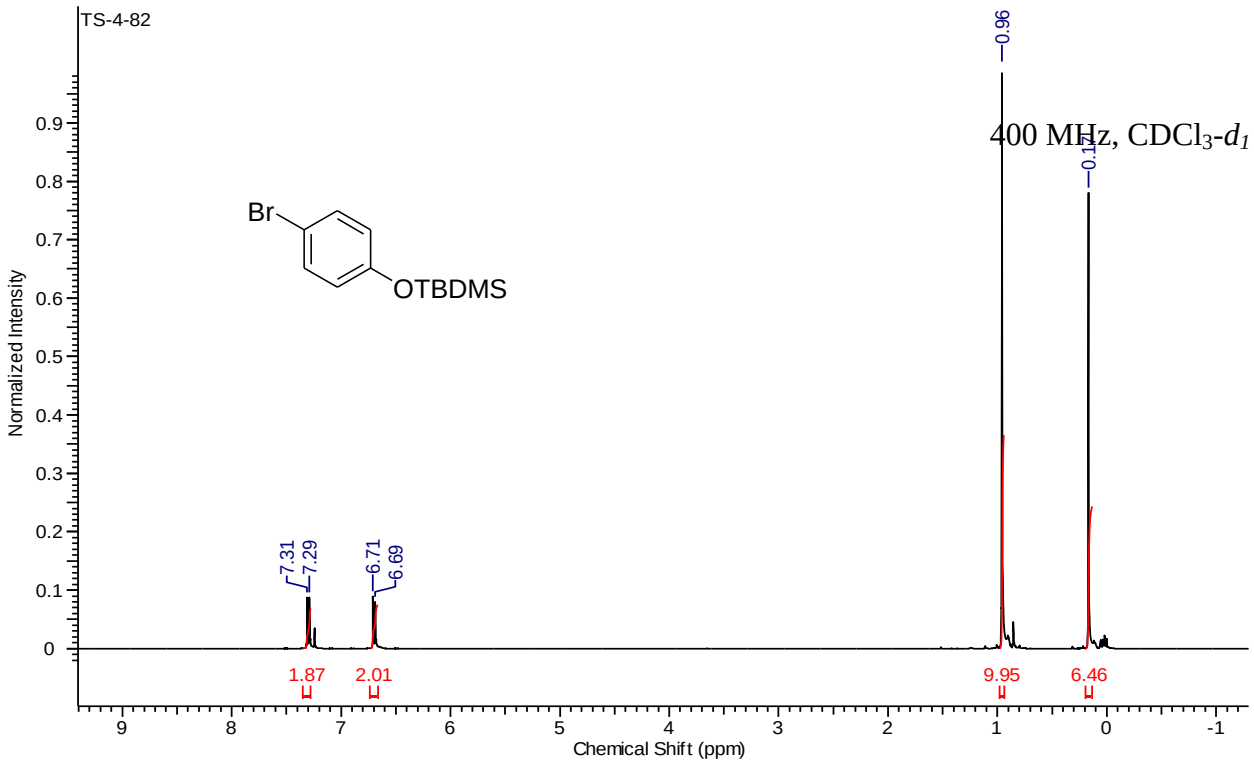

(a)

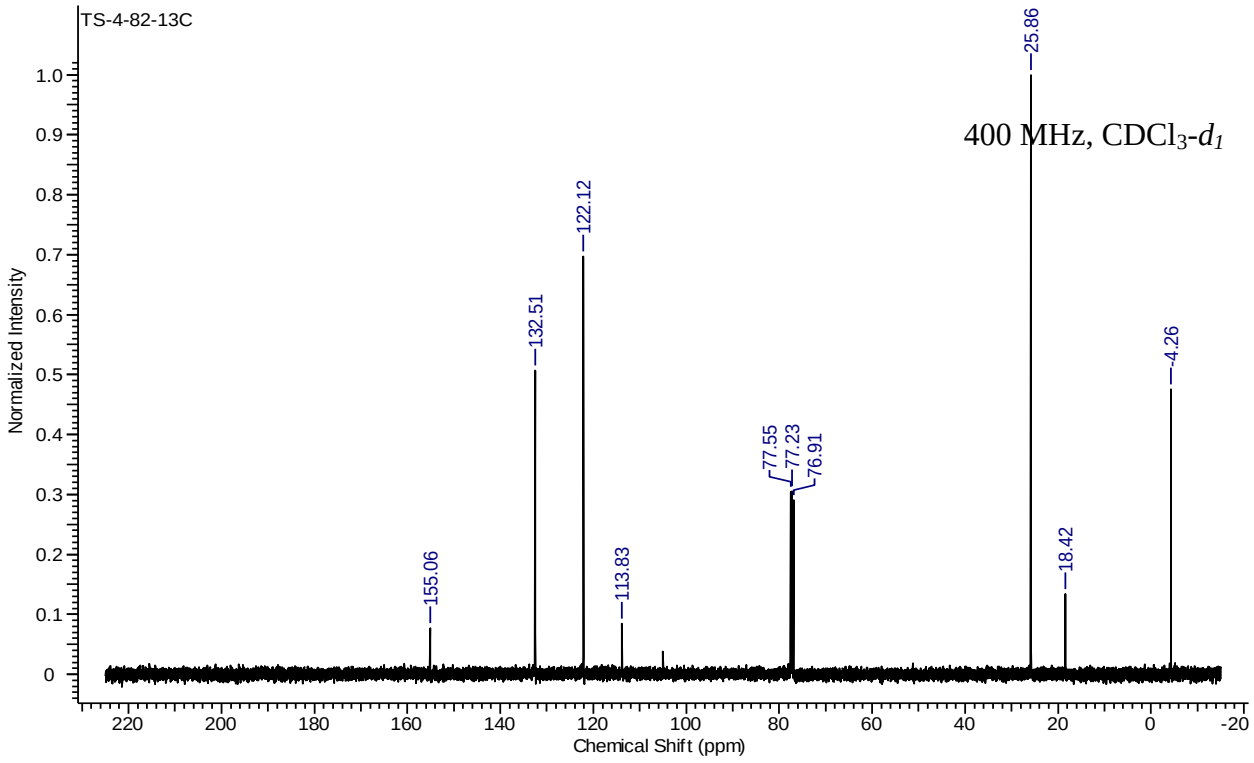

(b)

Figure A.27 (a) ^{1}H and (b) ^{13}C NMR of 2.7

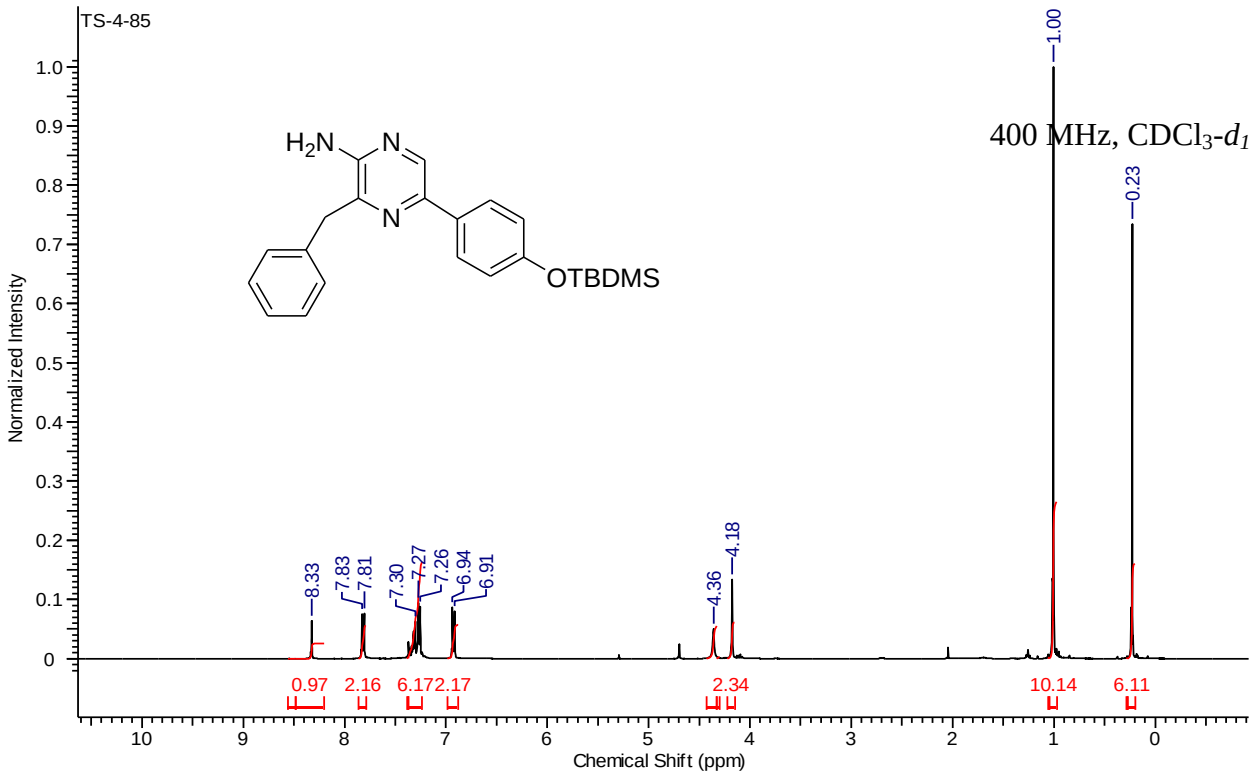

(a)

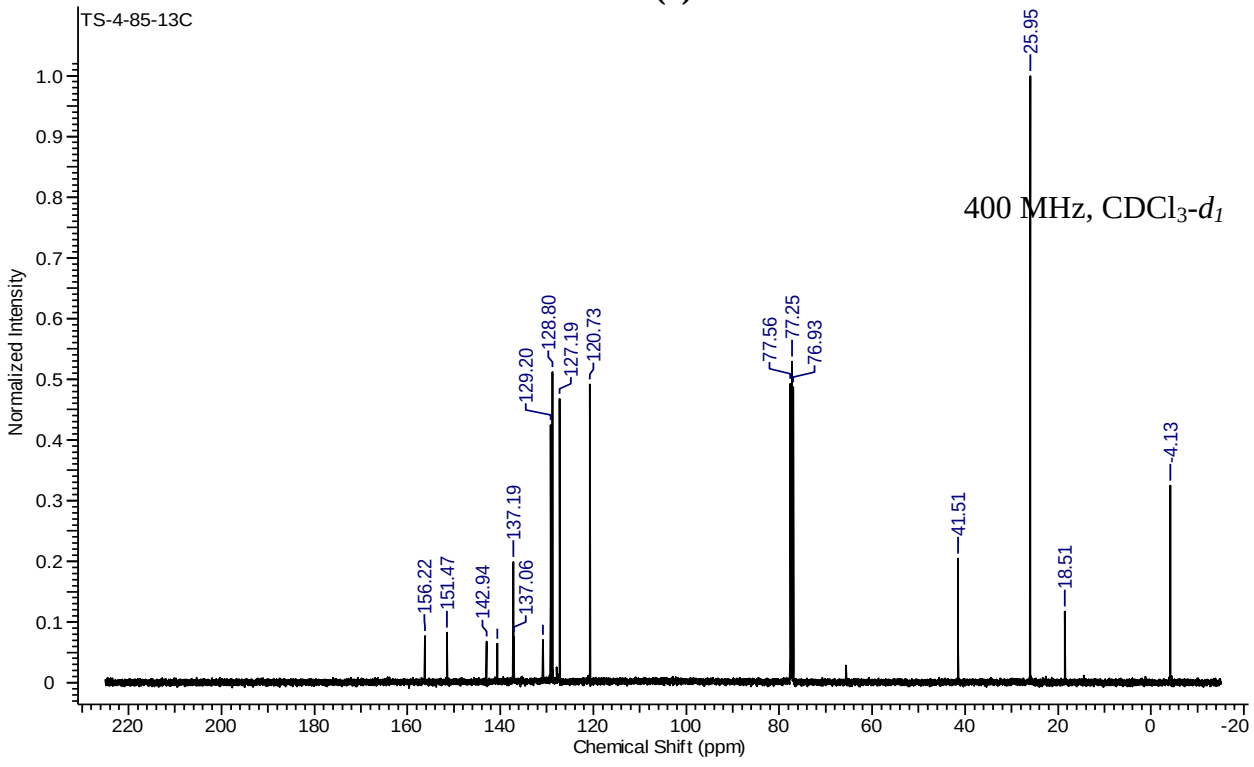

(b)

Figure A.28 (a) ^{1}H and (b) ^{13}C NMR of 2.8

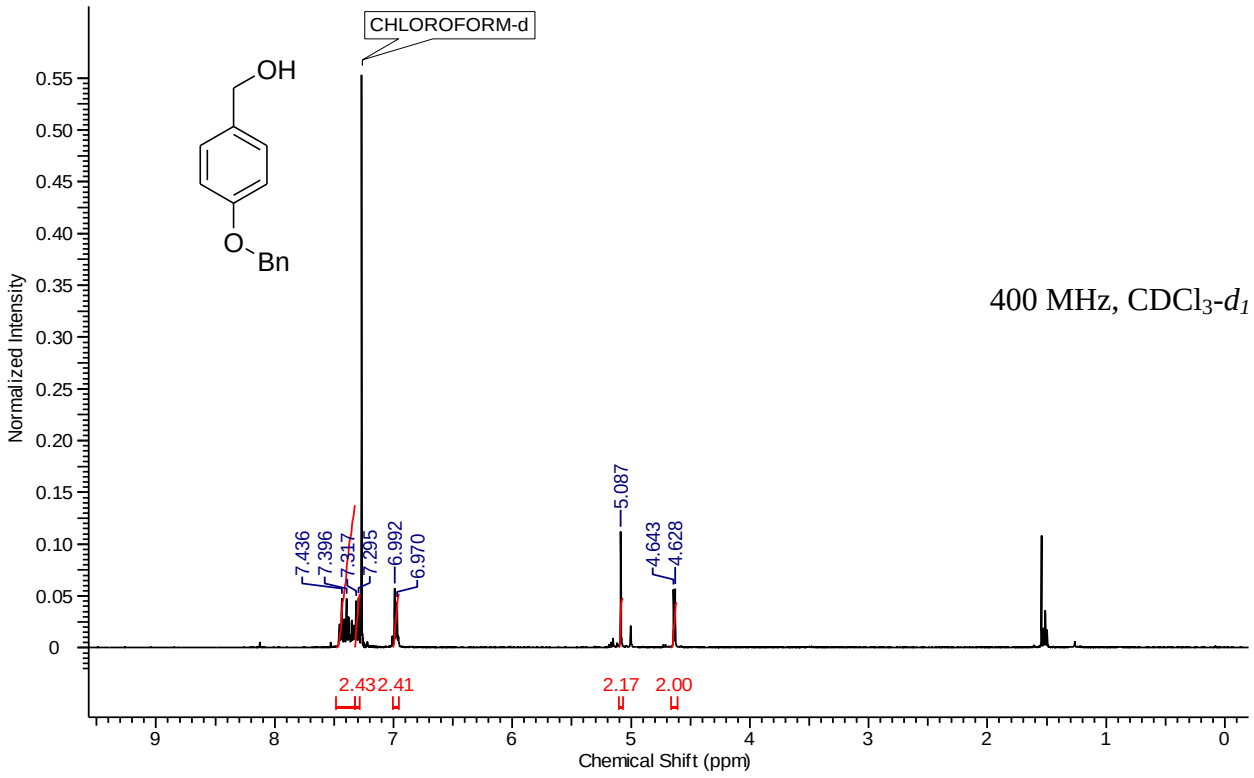

(a)

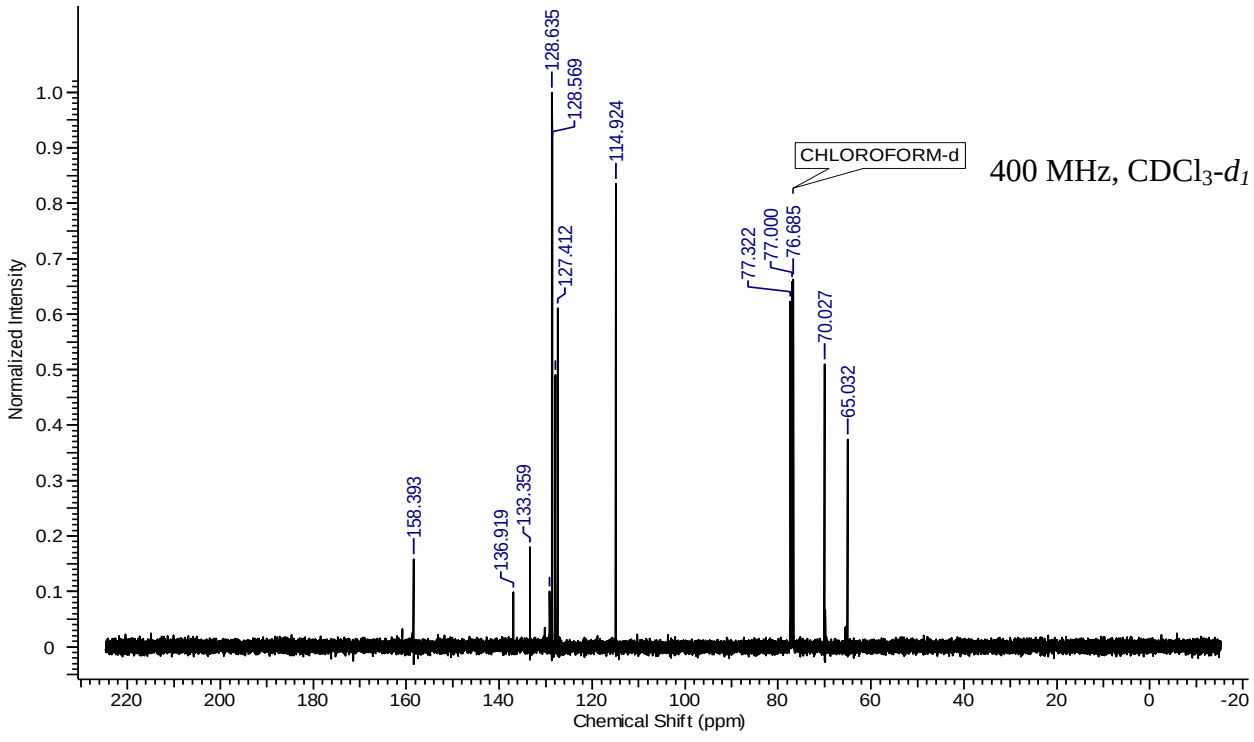

(b)

Figure A.29 (a) ^{1}H and (b) ^{13}C NMR of 2.12

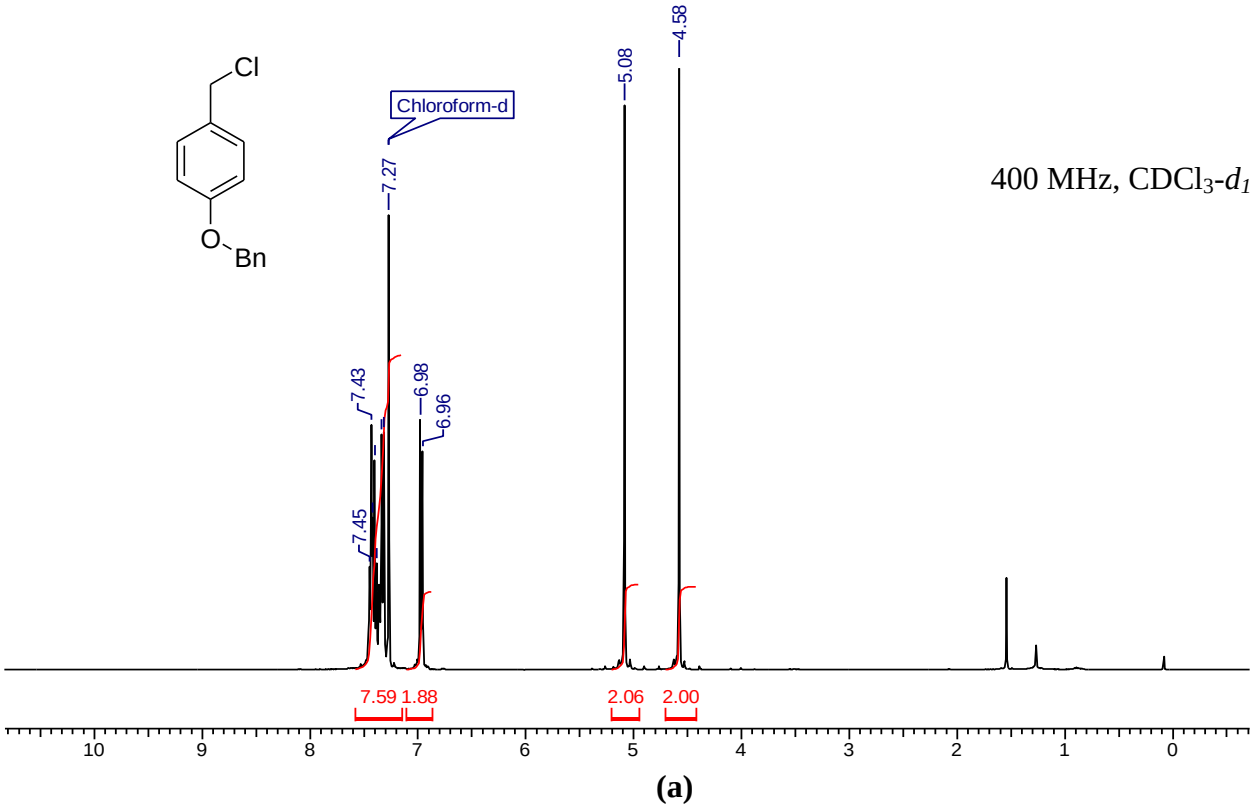

(a)

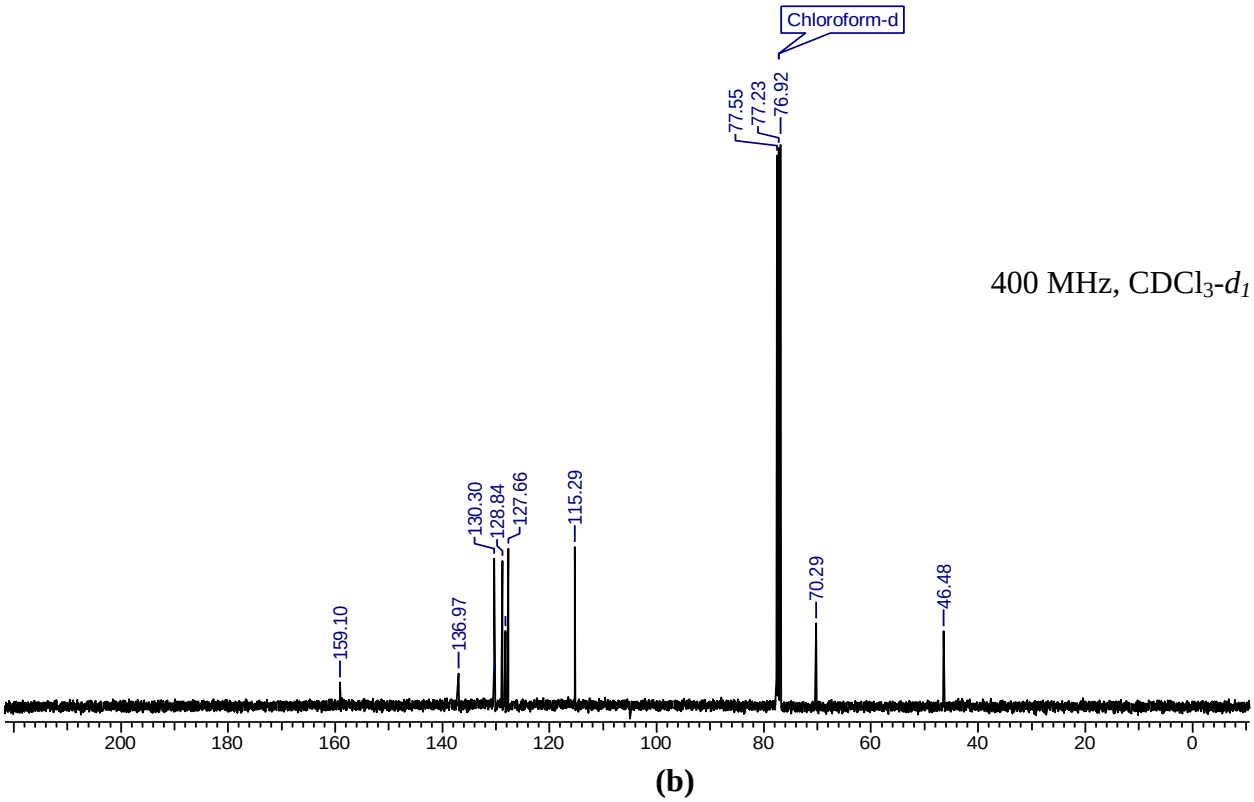

(b)

Figure A.30 (a) ^{1}H and (b) ^{13}C NMR of 2.13

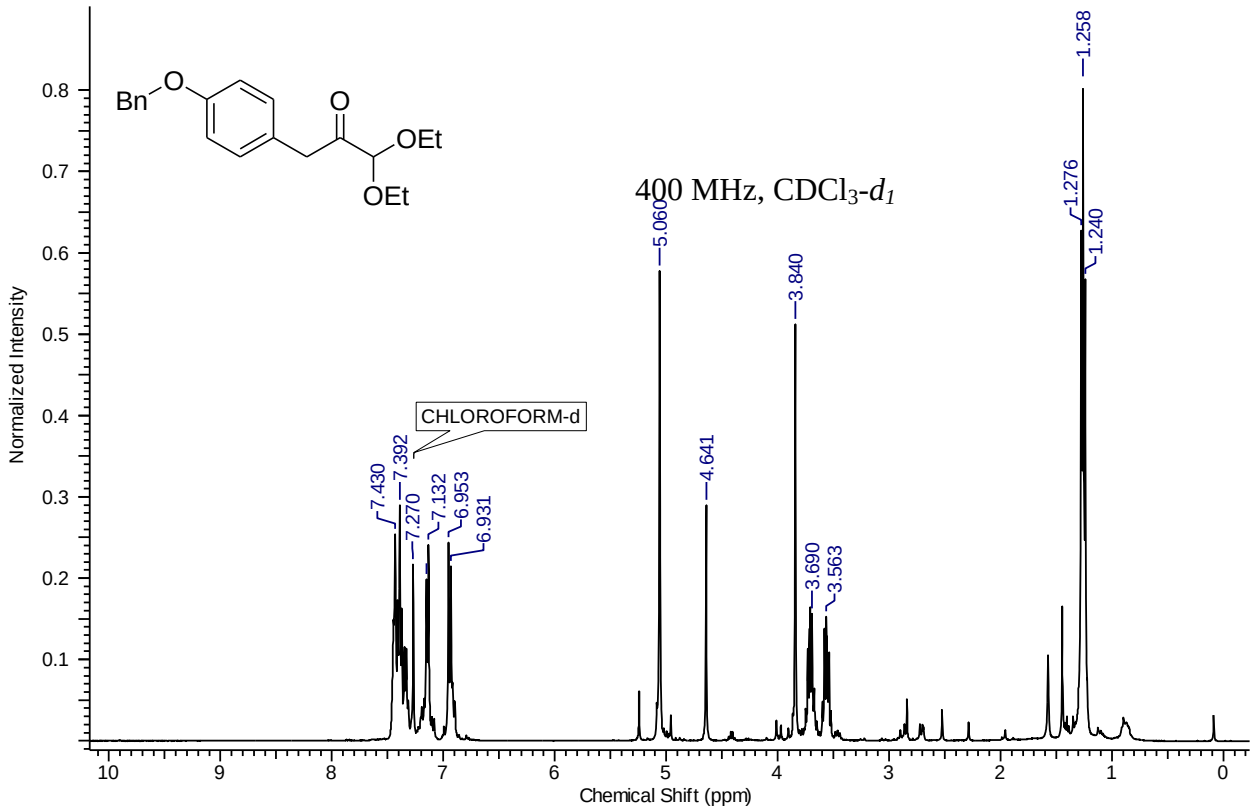

(a)

200 MHz, $CDCl_3$-d_1

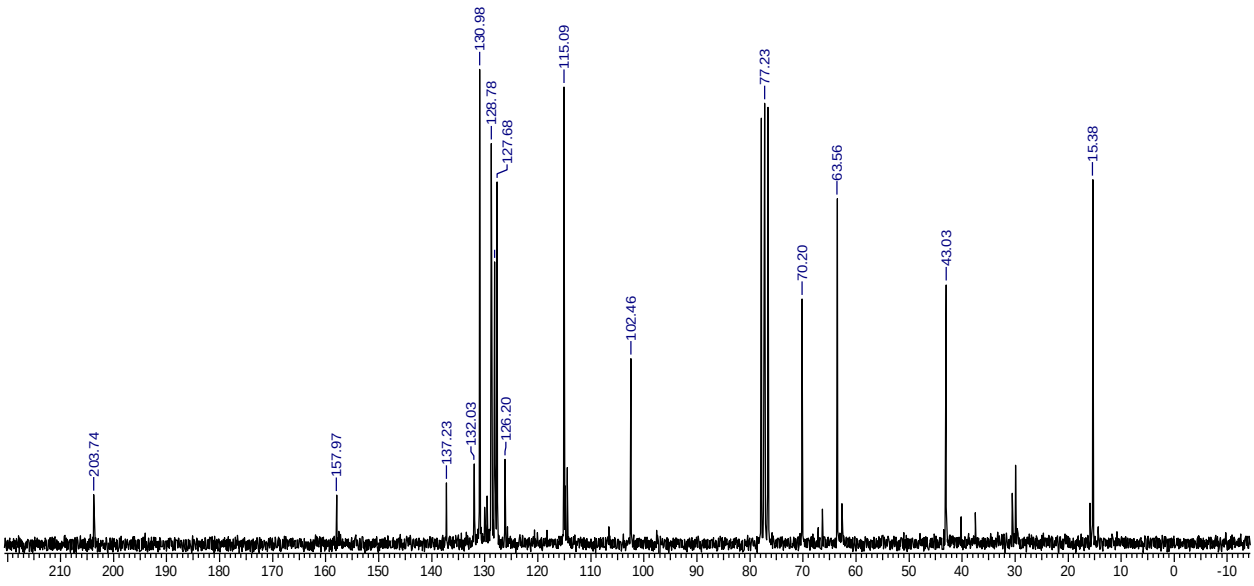

(b)

Figure A.31 (a) ^{1}H and (b) ^{13}C NMR of 2.15

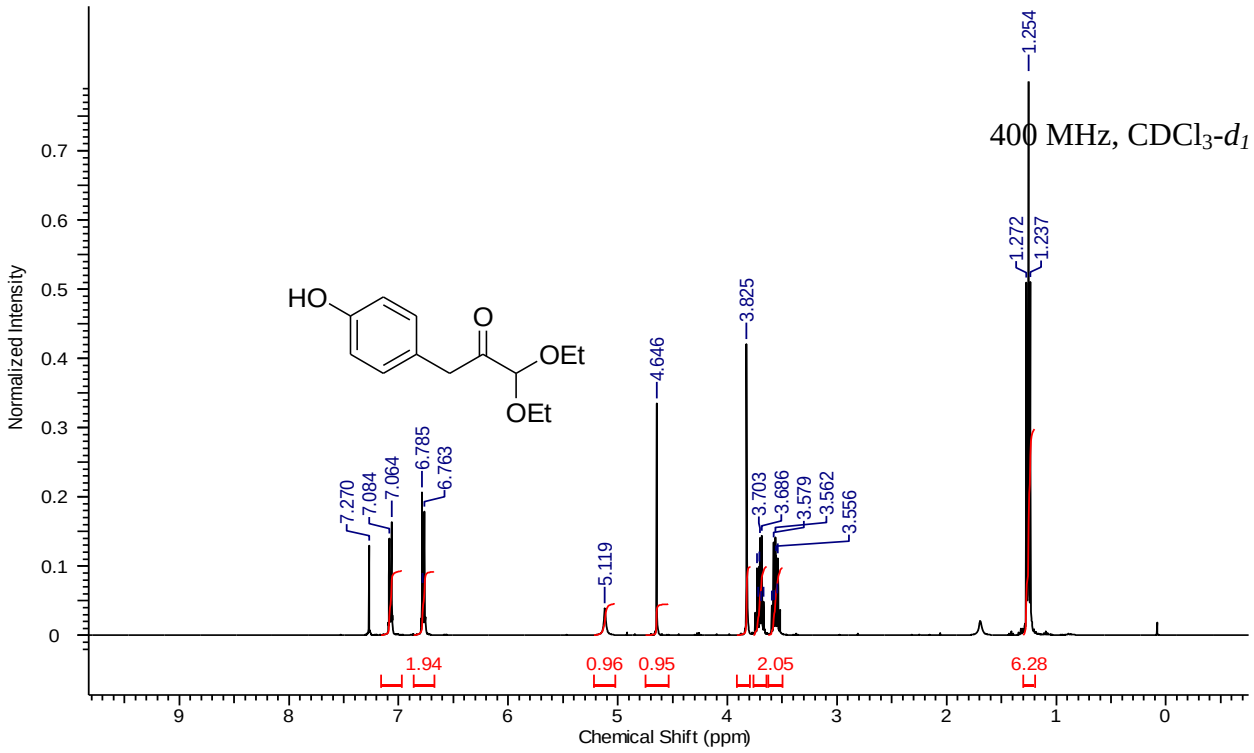

(a)

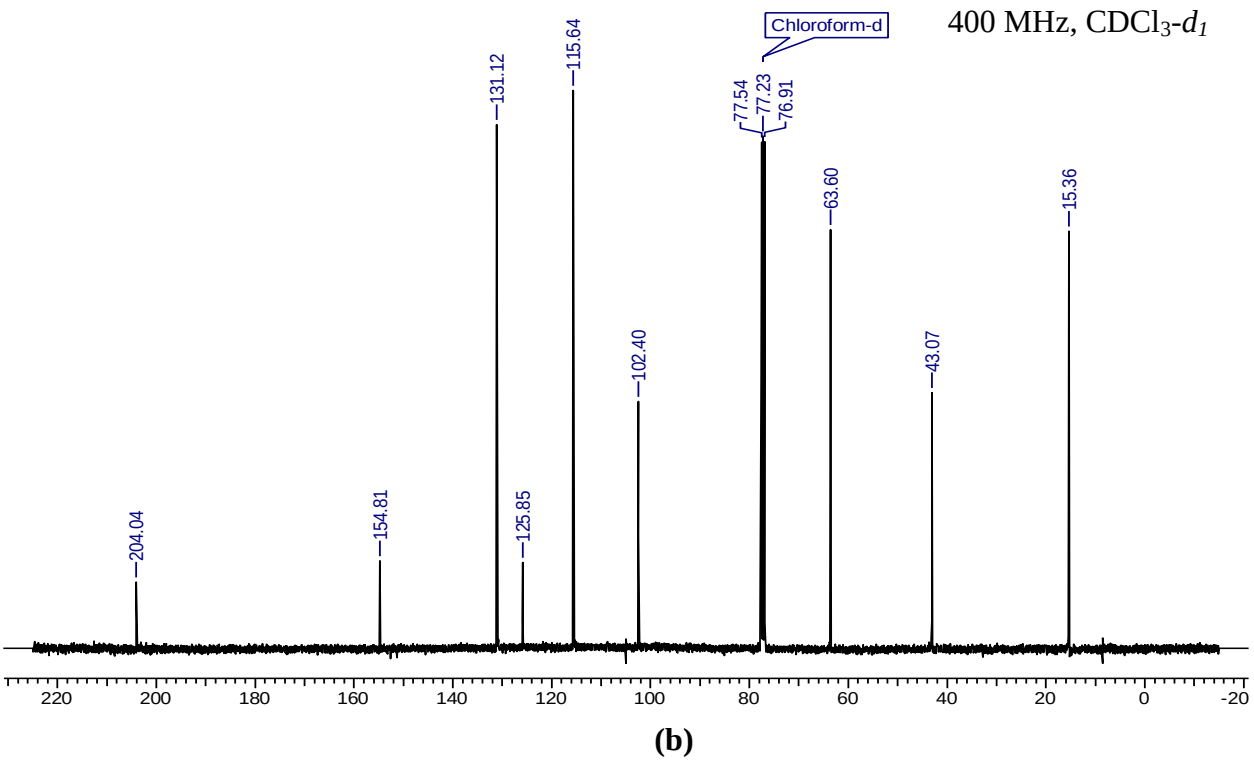

(b)

Figure A.32 (a)^{1}H and (b) ^{13}C NMR of 2.16

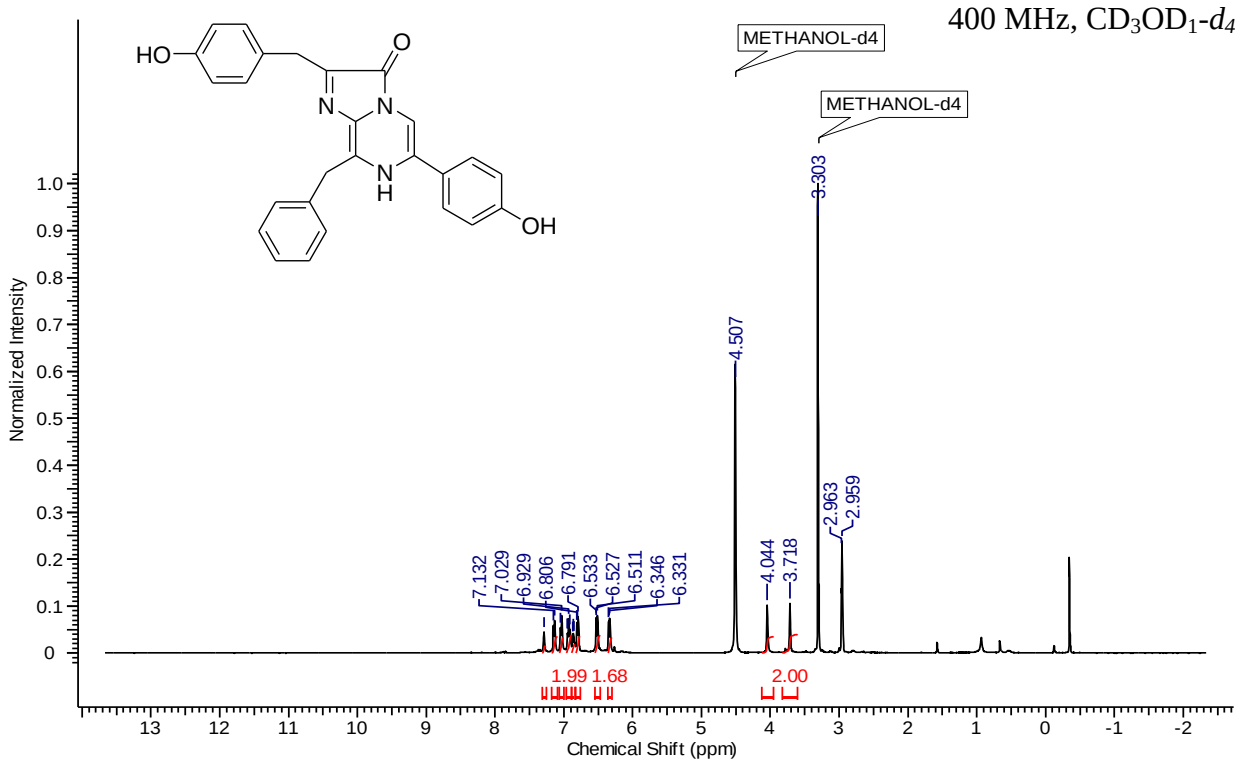

(a)

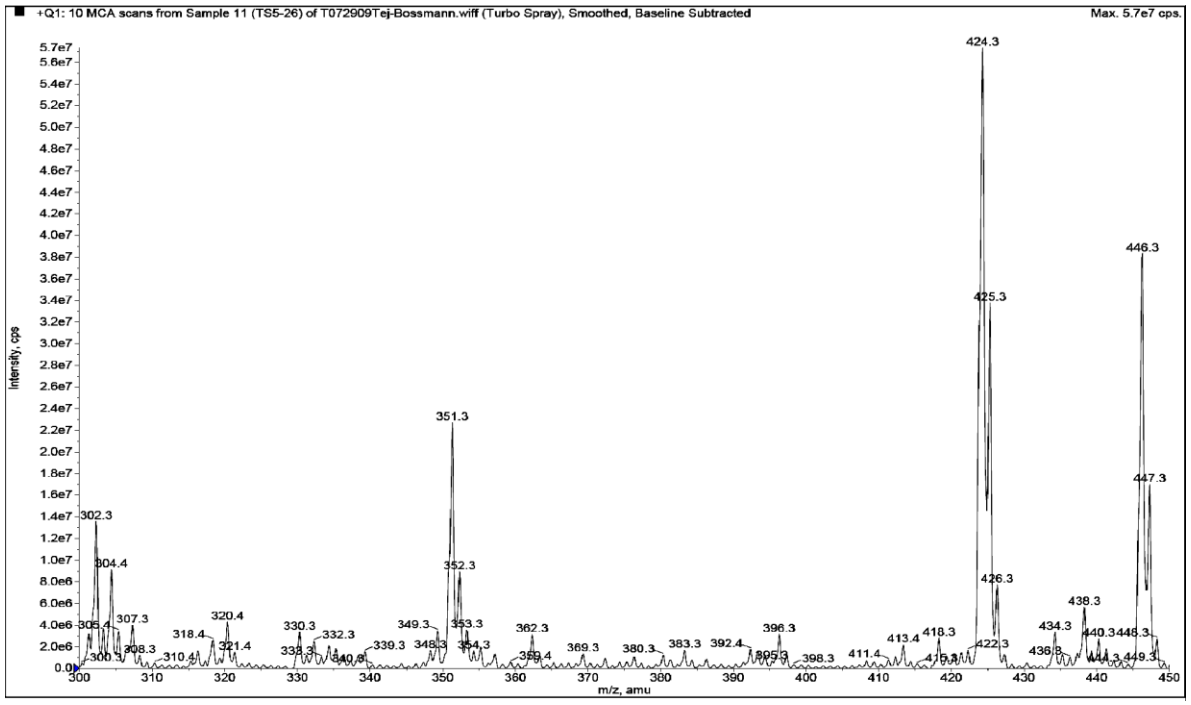

(b)

Figure A.33 (a) ^{1}H and (b) Mass of 2.1